

WATER LEVEL CHANGES AND RELATED SEDIMENTARY ENVIRONMENTS AT LAKE DONGGI CONA, NORTH-EASTERN TIBETAN PLATEAU, CHINA

ELISABETH DIETZE



中国青藏高原东北部冬给措纳湖面变化及相关沉积环境研究

Dissertation at the Department of Geoscience, Free University Berlin
August, 2012

**Water level changes and related sedimentary environments at Lake
Donggi Cona, north-eastern Tibetan Plateau, China**

Seespiegelschwankungen und assoziierte Sedimentationsumgebungen am Donggi
Cona See, nordöstliches Tibet-Plateau, China

Dissertation
zur Erlangung des akademischen Grades
Doktor der Naturwissenschaften (Dr. rer. nat.)
im Fach Geographie

am Fachbereich Geowissenschaften
der Freien Universität Berlin

vorgelegt von

Elisabeth Dietze

Berlin, 2012

BETREUER:

Prof. Dr. Bernd Wünnemann

Institut für Geographische Wissenschaften, Interdisciplinary Center of Ecosystem
Dynamics of Central Asia (EDCA), Freie Universität Berlin

TAG DER VERTEIDIGUNG:

5. November, 2012

EIDESSTATTLICHE ERKLÄRUNG

Hiermit erkläre ich, dass ich die vorgelegte Arbeit selbständig und ohne fremde Hilfe verfasst und andere als die angegebenen Hilfsmittel nicht benutzt habe. Die Beiträge der Co-Autoren der wissenschaftlichen Veröffentlichungen sind in Kapitel 1.2 dargelegt. Ich erkläre, dass ich die Arbeit erstmalig und nur am Fachbereich Geowissenschaften der Freien Universität Berlin eingereicht habe und keinen entsprechenden Doktorgrad besitze. Der Inhalt der dem Verfahren zugrunde liegenden Promotionsordnung ist mir bekannt.

Dipl.-Geogr. Elisabeth Dietze

Berlin, den 13. August, 2012

POR MI HIJO MARAVILLOSO

TABLE OF CONTENTS

| | |
|--|----|
| List of figures | 5 |
| List of tables | 7 |
| List of abbreviations..... | 7 |
| Abstract..... | 9 |
| Kurzfassung | 12 |
| 1. Introduction..... | 15 |
| 1.1 Motivation | 15 |
| 1.2 Objectives, approach and outline..... | 17 |
| 1.3 State-of-the-Art | 20 |
| 1.3.1 Study area | 20 |
| 1.3.2 Geological and tectonic constraints | 21 |
| 1.3.3 Climatic constraints..... | 22 |
| 1.3.4 Anthropogenic constraints..... | 23 |
| 1.3.5 Components of a Tibetan sediment cascade..... | 24 |
| 2. Basin morphology and seismic stratigraphy of Lake Donggi Cona | 29 |
| Abstract..... | 29 |
| 2.1 Introduction..... | 29 |
| 2.2 Regional setting | 31 |
| 2.3 Data and Methods | 34 |
| 2.4 Results | 35 |
| 2.4.1 Basin morphometry..... | 35 |
| 2.4.2 Fault pattern | 37 |
| 2.4.3 Seismo-depositional units | 38 |
| Unit I..... | 38 |
| Unit II | 41 |

| | |
|--|----|
| Unit III | 41 |
| 2.5 Basin and lake development..... | 43 |
| 2.5.1 Tectonic basin structures | 43 |
| 2.5.2 Origin of depositional units | 44 |
| 2.5.3 Depositional history and lake level fluctuations..... | 46 |
| 2.6 Conclusions and Outlook | 49 |
| Acknowledgements..... | 50 |
| 3. An end-member algorithm for the decomposition of grain-size distributions | 51 |
| Abstract..... | 51 |
| 3.1 Introduction..... | 52 |
| 3.2 Background of end-member modelling analysis..... | 54 |
| 3.2.1 Mathematical concept of eigenspace analysis | 54 |
| 3.2.2 Application of eigenspace analysis in environmental research..... | 56 |
| 3.3 Geographical Setting..... | 58 |
| 3.4 Material and methods..... | 59 |
| 3.4.1 Field and laboratory analyses | 59 |
| 3.4.2 End-member modelling analysis (EMMA) of grain-size distributions | 60 |
| 3.5 Results | 63 |
| 3.5.1 General characterisation of lake sediments and EMMA | 63 |
| 3.5.2 The optimal end-member model..... | 65 |
| 3.5.3 The robust end-member model | 66 |
| 3.6 Interpretation and Discussion | 69 |
| 3.6.1 Evaluation of the end-member modelling algorithm..... | 69 |
| 3.6.2 Detrital processes within Lake Donggi Cona | 70 |
| 3.7 Conclusion and Outlook..... | 72 |
| Acknowledgements..... | 73 |

| | |
|--|-----|
| 4. Higher than present lake stands at Lake Donggi Cona | 75 |
| 4.1 Onshore lake terraces..... | 75 |
| 4.2 Lake high-stand sediments | 76 |
| Abstract..... | 76 |
| 4.2.1 Introduction..... | 76 |
| 4.2.2 Study area..... | 76 |
| 4.2.3 Methods | 79 |
| 4.2.3.1 Field methods..... | 79 |
| 4.2.3.2 Laboratory methods..... | 79 |
| 4.2.3.3 Statistical methods..... | 79 |
| 4.2.3.4 Radiocarbon dating | 80 |
| 4.2.4 Results and interpretation..... | 81 |
| 4.2.4.1 Sediment sections and radiocarbon dating..... | 81 |
| 4.2.4.2 Classification of depositional environments | 83 |
| 4.2.4.3 Detrital grain-size end-members..... | 86 |
| 4.2.4.4 Lake level reconstruction from sediment facies..... | 90 |
| 4.2.5 Discussion..... | 90 |
| 4.2.5.1 Chronology of lake level changes | 91 |
| 4.2.5.2 Synthesis | 93 |
| 4.2.6 Conclusions | 96 |
| Acknowledgements..... | 98 |
| 5. Synthesis | 100 |
| 5.1 Landscape sensitivity and the local driving forces..... | 100 |
| 5.1.1 Basin morphology and the littoral zone | 100 |
| 5.1.2 Impacts from the catchment..... | 101 |
| 5.1.3 Tectonic impact..... | 104 |

| | |
|--|-----|
| 5.2 Hydrological variations at Lake Donggi Cona..... | 105 |
| 6. Conclusions | 110 |
| 7. Acknowledgements..... | 112 |
| 8. Overall references..... | 114 |
| 9. Appendix | 128 |
| 9.1 End-member modeling script for Matlab | 128 |
| 9.2 List of publications and presentations..... | 131 |
| Publications in peer-reviewed journals..... | 131 |
| Oral presentations | 131 |
| Poster Presentations | 132 |
| 9.3 List of original grain size data sets..... | 133 |

LIST OF FIGURES

| | |
|---|-----|
| Figure 1.1: Sediment and water pathways along a sediment cascade..... | 16 |
| Figure 1.2: Location of Lake Donggi Cona at the north-eastern Tibetan Plateau | 20 |
| Figure 2.1: Location of Donggi Cona lake basin and its catchment | 32 |
| Figure 2.2: Bathymetry of Lake Donggi Cona | 36 |
| Figure 2.3: Relative and cumulated hypsometric depth distribution | 37 |
| Figure 2.4: Seismic transects in a West-East-longitudinal profile | 40 |
| Figure 2.5: North-south seismic transects at Lake Donggi Cona..... | 42 |
| Figure 2.6: Characteristics of seismo-depositional units | 44 |
| Figure 2.7: Interpretation of seismo-depositional units | 47 |
| Figure 3.1: Map of Lake Donggi Cona and sampling sites | 58 |
| Figure 3.2: Individual grain-size distributions | 63 |
| Figure 3.3: Different EMMA percentile weight transformations | 64 |
| Figure 3.4: Results of the optimal end-member model | 66 |
| Figure 3.5: Results of the robust end-member model | 68 |
| Figure 3.6: End-member scores of the robust end-members | 69 |
| Figure 4.1: Onshore terrace heights (after Lockot, 2010) | 75 |
| Figure 4.2: Donggi Cona lake basin and its catchment | 78 |
| Figure 4.3: Sites of onshore lake high-stand sediment sections | 81 |
| Figure 4.4: Corrected and calibrated ages of high-stand sediments | 83 |
| Figure 4.5: Generalized stratigraphic descriptions of high-stand sediments | 84 |
| Figure 4.6: Examples for strata of different sediment facies | 85 |
| Figure 4.7: End-member loadings of high-stand sediments | 87 |
| Figure 4.8: End-member scores, EM_{diff} , and their relation to field stratigraphy | 88 |
| Figure 4.9: Higher than present lake level phases at Lake Donggi Cona | 95 |
| Figure 5.1: Extents of Lake Donggi Cona and associated processes | 108 |

LIST OF TABLES

| | |
|--|----|
| Table 1.1: Published and submitted manuscripts of this dissertation ... | 19 |
| Table 4.1: General characteristics of onshore high-stand sediment sections ... | 82 |
| Table 4.2: Dating of high-stand sediments of Lake Donggi Cona ... | 82 |
| Table 10.1: Grain size data sets ... | 82 |

LIST OF ABBREVIATIONS

| | |
|----------|--|
| a.p.l.l. | above present lake level |
| a.s.l. | above sea level |
| b.l.l. | below present lake level |
| cal. | calibrated |
| corr. | hard-water corrected (cf. Chapter 4.2.3.4) |
| CRN | cosmogenic radio nuclides |
| ka BP | 1000 years before 1950 |
| MIS | marine oxygen-isotope stage |
| OSL | optical stimulated luminescence |
| TP | Tibetan Plateau |

ABSTRACT

The world's largest mountain plateau, the Tibetan Plateau, not only plays an important role in supplying water to more than a third of world's population, but its unique characteristics also influence global climate. Different circulation systems interact there, including the Asian monsoons and the westerlies, though the past variability of the circulation patterns is still under debate. Sediments and landforms of different process-environments along a catchment-wide sediment cascade can be used to infer landscape evolution and past environmental conditions, e.g., climatic changes. More than 1000 lake catchments on the Tibetan Plateau receive water mainly from Asian summer monsoon precipitation and from glacial melt. Although the extent of past glaciers is still under discussion, it can be assumed that most Tibetan catchments were affected by glaciers in the past, and may still be today. At the glacial/periglacial zone, sediment transfer starts via the fluvial and the aeolian system towards the local end of a sediment cascade: the lake. However, sedimentation and geomorphological dynamics are not always triggered by climate alone. Tectonic activity is a further important driver of landscape evolution, as uplift and accommodation of the Indo-Eurasian collision is still ongoing and many lakes have formed in extensional basins. Human impact also started to significantly affect sedimentation dynamics via grazing during at least the last 2000 years.

This study focuses on the reconstruction of past hydrological changes at Lake Donggi Cona ($35^{\circ}18'N$, $98^{\circ}32'E$, 4090 m a.s.l.), in Qinghai province, on the north-eastern Tibetan Plateau. The lake is situated along the Kunlun fault, at the northern limit of the Asian summer monsoons. Lake level changes were assessed from landforms and sediments along the littoral zone of the lake. Basin morphology and depositional stratigraphy below the present lake level were studied with echo depth sounding and shallow seismic sub-bottom profiling. A flexible end-member modelling algorithm based on eigenspace analysis was developed and applied to the detrital, multi-modal grain-size components of lacustrine surface sediment samples to quantify transport processes that contribute sediments to the lake. High-stand sediments in nine sections from lake terraces above the present lake level (a.p.l.l.) were studied stratigraphically and end-member modelling was applied to their grain size distributions. Lake level changes were interpreted from submersed terraces and delta sediments, as well as from lake shorelines and high-stand sediments. The sensitivity of the lake basin and littoral zone to climatic change depends on the basin and shore morphology, as well as on the contribution of sediment and water from the catchment. Finally, the involved driving forces, i.e., climate, geomorphological processes, tectonics and human impact are discussed in a broader context.

The basin morphology and seismic survey confirm the evolution of the pull-apart basin. The basin can be divided into an up to 92 m deep graben in the western part and a flat eastern part of the lake. The in-lake continuation of the Kunlun fault could be tentatively traced along the graben rims, below ~30 m of draping sediments of three depositional units. Several morphological levels were found at 24, 39 and 57 m water depth, as well as associated delta systems that point to past lower lake stands.

End-member modelling of grain size distributions from modern lake surface sediments helped to distinguish and quantify five sediment transport processes. A clay end-member represents fluvial/alluvial suspension load, three end-members in the fine sand to medium silt domains represent local to remote aeolian processes, and a multimodal end-member represents the highly variable fluvial and littoral input that reached the deeper lake. The two finest-grained end-members are robust grain size components of the lake and represent sedimentation in deep, calm water.

Stratigraphies and grain size end-members of past high-stand sediments were used to reconstruct the interaction of different sedimentary environments at the littoral zone (i.e., fluvial/alluvial, littoral, and lacustrine) during recorded higher than present lake stands. After a lake level rise with intense fluctuations from ~11.5 cal. ka BP onwards, the highest lake stand was reached at ~16.5 m a.p.l.l., i.e., the level of the T4 onshore terrace, at ~9.1 cal. ka BP. After a short-term lake level decline at ~8.5 cal. ka BP, as indicated by a lack of lacustrine high-stand sedimentation, a phase of post-depositional cryoturbation, and potential floodplain sedimentation at the second largest inflow, the lake rose again to ~10.1 m a.p.l.l., i.e., the level of the T3 onshore terrace, at ~7.5 cal. ka BP. The lake changed from a closed to an open system at ~6.8 cal. ka BP and stabilized at the height of T2 terrace at ~6.1 m a.p.l.l. afterwards. A further lake level decline to ~3.5 m a.p.l.l. (T1 terrace), with some fluctuations, happened after ~4.3 cal. ka BP, parallel with a change in lake stratification. No high-stand sediments were deposited thereafter.

In general, lake high-stand sedimentation and lake level changes responded to the overall changes in Asian monsoon variability. Lake low stands occurred during the cold and dry phases of the Pleistocene, though only the lake stand at -24 m could be dated to ~20 cal. ka BP. The increase in monsoon-related precipitation caused the lake to rise during the early to mid-Holocene, with a short-term reduction at the time of the global centennial cooling and drying phase at 8.5 cal. ka BP. The end of the subsequent high-stand sedimentation marks the shift to a dry and cool period during the late Holocene. However, the fluctuations at the beginning and end of high-stand sedimentation, as well as the opening of the lake at ~6.8 cal. ka BP, are instead a response to local geomorphological and tectonic dynamics. Ero-

sional processes and tectonics may have affected the lake's spillway at the western shore, independent of climatic change, and could have exerted a strong control on past hydrological changes.

The geological and geomorphological heterogeneity of the lake basin, littoral zone, and sub-catchment complicates sediment facies interpretations and lake level reconstructions from granulometric data, and probably also affected the uncertainty in radiocarbon dating (i.e., reservoir and hard-water effect). However, the lake responded very sensitively to past hydrological changes, as recorded, for instance, in unique high-stand sediment sections, and quantitative estimations of past lake volumes could be derived, even though the lake is an artificially controlled freshwater lake system in modern times.

KURZFASSUNG

Das größte Gebirgsplateau der Welt, das Tibet-Plateau, spielt nicht nur eine wichtige Rolle für die Versorgung von über einem Dritteln der Weltbevölkerung mit Wasser, sondern es beeinflusst mit seinen Eigenheiten auch das globale Klima. Verschiedene Zirkulationssysteme interagieren dort: die Asiatischen Monsune und die Westwindzirkulation, deren Muster und Variabilität in der Vergangenheit noch immer diskutiert werden. Sedimente und geomorphologische Formen aus verschiedenen Prozessregimen entlang einer Sedimentkaskade können verwendet werden um die Landschaftsentwicklung und frühere Umwelt- und insbesondere Klimabedingungen abzuleiten. Über 1000 tibetische Seeeinzugsgebiete erhalten Wasser vorwiegend aus dem Niederschlag der Asiatischen Sommermonsune und von Gletscherschmelze. Obwohl die damalige Ausdehnung der Gletscher noch diskutiert wird, kann davon ausgegangen werden, dass die meisten tibetischen Einzugsgebiete von Gletschern beeinflusst wurden und werden. In der glazialen und periglazialen Zone beginnt der Sedimenttransfer über das fluviale und äolische System in Richtung des lokalen Endglieds einer Sedimentkaskade: dem See. Jedoch werden sedimentologische und geomorphologische Prozesse nicht allein vom Klima bestimmt. Tektonische Aktivität ist eine weitere wichtige Steuergröße für die Landschaftsentwicklung, da die Hebung und Anpassung an die Indo-Eurasische Kollision anhält und viele Seen Extensionsbecken füllen. Menschlicher Einfluss, d.h. Beweidung, begann zudem die Sedimentationsdynamiken seit mindestens den letzten 2000 Jahren zu beeinflussen.

Diese Arbeit konzentriert sich auf die Rekonstruktion der hydrologischen Veränderungen am Donggi Cona See ($35^{\circ}18'N$, $98^{\circ}32'E$, 4090 m ü.d.M.), in der chinesischen Provinz Qinghai, auf dem nordöstlichen Tibet Plateau. Der See liegt an der Kunlunverwerfung und im Bereich der nördlichen Grenze der Asiatischen Sommermonsune. Seespiegelschwankungen wurden an geomorphologischen Formen und Sedimenten entlang der litoralen Zone des Sees abgeleitet. Die Beckenmorphologie und Sedimentstratigraphie unterhalb des aktuellen Seespiegels wurde über Echolotungen und Flachseismik untersucht. Um Transportprozesse zu quantifizieren, die zur Sedimentation im See beitragen wurde ein flexibler Endmember-Modellierungsalgorithmus entwickelt, basierend auf den Prinzipien der Eigenaumanalyse, und auf die detritischen, multi-modalen Korngrößenverteilungen lakustriner Oberflächensedimentproben angewendet. Hochstandssedimente von neun Profilen in Seeterrassen über dem aktuellen Seespiegel (a.p.l.l.) wurden stratigraphisch und durch Endmember-Modellierung ihrer Korngrößenverteilungen untersucht. Seespiegelschwankungen wurden aus subaquatischen Terrassen und Deltasedimenten sowie aus Strandlinien und Hochstandssedimenten abgeleitet. Die Sensitivität des Seebeckens und

des Strandbereichs gegenüber klimatischen Veränderungen ist sowohl abhängig von der Becken- und Strandmorphologie, als auch von Sediment- und Wasserzustrom aus dem Einzugsgebiet. Die beeinflussenden Steuergrößen, Klima, geomorphologische Prozesse, Tektonik und Mensch, wurden schließlich in einem größeren Kontext diskutiert.

Die Beckenmorphologie und seismische Erkundung bestätigt die Entwicklung des Sees in einem „pull-apart“-Becken. Das Becken ist gegliedert in einen bis zu 92 m tiefen Graben im westlichen Teilbecken und in ein flaches östliches Teilbecken. Die Fortsetzung der Kunlunverwerfung im See konnte entlang der Grabenstruktur unter einer ~30 m Sedimentschicht, bestehend aus drei Sedimenteinheiten, vermutet werden. Mehrere geomorphologische Niveaus in 24, 39 und 57 m Wassertiefe und damit assoziierte Deltasysteme weisen auf tiefere Seestände hin.

Die Endmember-Modellierung der Korngrößenverteilungen moderner Seesedimente half fünf Sedimenttransportprozesse zu identifizieren und zu quantifizieren. Ein Ton-Endmember repräsentiert fluviale/alluviale Suspensionsfracht, drei Endmember in den Feinsand- bis Mittelschlufffraktionen repräsentieren äolischen Nah- und Ferntransport und ein multimodaler Endmember repräsentiert den hochvariablen Fluss- und Strandbeitrag, der auch tiefere Seebereiche erreichen kann. Die beiden feinsten Endmember sind dabei die robustesten Korngrößenbestandteile des Sees und repräsentieren die Sedimentation im ruhigen, tiefen Wasser.

Die Stratigraphien und Korngrößen-Endmember der Hochstandssedimente halfen, die Interaktion der verschiedenen (d.h. fluvialen/alluvialen, littoralen und lakustrinen) Sedimentationsprozesse im Strandbereich während höherer Seephäsen zu rekonstruieren. Nach einem Seespiegelanstieg mit starken Schwankungen beginnend um 11.5 cal. ka BP wurde der höchste Seestand bei ~16.5 m a.p.l.l. (das Niveau der T4-Strandterrasse), um 9.1 cal. ka BP erreicht. Nach einem kurzen Rückgang um ~8.5 cal. ka BP, angedeutet durch fehlendes lakustrines Hochstandssediment, einer Phase der nachträglichen Kryoturbation und einer potentiellen Hochflutsedimentation am zweitgrößten Zufluss, stieg der See um 7.5 cal. ka BP wieder auf ~10.1 m a.p.l.l., was dem Niveau der T3-Strandterrasse entspricht. Der See öffnete sich um 6.8 cal. ka BP und stabilisierte sich danach auf Höhe der T2-Terrasse (~6.1 m a.p.l.l.). Ein weiterer Seespiegelrückgang auf ~3.5 m a.p.l.l. (T1-Terrasse) fand nach ~4.3 cal. ka BP statt, parallel mit einem Wechsel in der Seeschichtung. Danach wurden keine weiteren lakustrinen Hochstandssedimente mehr abgelagert.

Im Allgemeinen folgten die Seehochstandsedimentation und die Seespiegelschwankungen den Hauptveränderungen in der Monsundynamik. Seetiefstände fanden während der

kalten, trockenen Phasen des Pleistozäns statt, auch wenn nur der drittiefste Seestand bei -24 m auf ~20 cal. ka BP datiert werden konnte. Die Intensivierung der Monsunniederschläge verursachte den Seeanstieg im frühen und mittleren Holozän, mit einem kurzen Rückgang zur Zeit einer globalen, hundertjährigen Kalt- und Trockenheitsphase um 8.5 cal. ka BP. Das Ende der Hochstandssedimentation korreliert mit dem Übergang zu einer trockneren und kühleren Phase im späten Holozän. Allerdings waren die Fluktuationen zu Beginn und Ende der Hochstandsphase sowie die Seeöffnung eher durch lokale geomorphologische und tektonische Dynamiken verursacht. Erosions- und tektonische Prozesse könnten den Überlauf am westlichen Strand beeinflusst haben, unabhängig von klimatischen Veränderungen, und könnten eine starke Kontrolle auf die früheren hydrologischen Schwankungen ausgeübt haben.

Die geologische und geomorphologische Heterogenität des Seebeckens, des Litorals und der Teileinzugsgebiete komplizieren die Auswertung der Sedimentfazien und die Rekonstruktion der Seespiegelschwankungen aus Korngrößendaten. Sie beeinflussen sicherlich auch die Unsicherheiten in der Radiokohlenstoffdatierung (z.B. Reservoireffekt). Allerdings reagierte der See sehr sensibel auf vergangene hydrologische Schwankungen, dokumentiert u.a. in einzigartigen Hochstandssedimentprofilen, und es konnten frühere Seevolumina quantifiziert werden, obwohl der Frischwassersee heute künstlich reguliert wird.

1. INTRODUCTION

1.1 MOTIVATION

The Tibetan Plateau has unique characteristics that call for (palaeo-) environmental research. It is the world's largest mountain plateau with an average elevation above 4300 m a.s.l., and is bordered by some of the highest mountain ranges in the world (e.g., Himalaya, Karakorum, Tian Shan). Outside of the Polar Regions, the Tibetan Plateau represents the largest glaciated region on the planet. Acting as a “water tower” that supplies more than a third of the world's population with drinking and industrial water (e.g., Bolch et al., 2012) – it is the source of some of the world's largest rivers, such as the Brahmaputra, Mekong, Yangtze, and Huanghe (Yellow River) (Huang et al., 2008; Qiu, 2008) and hosts more than 1000 lakes (Hou et al., 2012). The Plateau exhibits a high sensitivity to anthropogenic global climate change that is similar to Antarctica and the Arctic (Qiu, 2008). However, future scenarios on water availability and how climate change is affecting the Tibetan Plateau are contradictory (Thompson et al., 1993; Liu et al., 2009; Bolch et al., 2012) and often draw conclusions from a poor database (Bräuning and Mantwill, 2004). Current trends conflictingly suggest either a reduction (Wang and Ding, 2006) or an increase in precipitation (Wu et al., 2006), whereas Tibetan lakes predominantly show a declining trend over the last two decades (Colman et al., 2007; Xin, 2008). Hence, a major aim of many projects is to reconstruct hydrological processes on the Tibetan Plateau.

In 2008, the priority programme 1372 of the German Research Foundation (DFG) on “Tibetan Plateau: Formation – Climate – Ecosystems” started its research. With its focus set on late Cenozoic climate evolution, a team consisting of geographers and geologists from RWTH Aachen, AWI Potsdam and FU Berlin started its work on “Landscape and lake system response to Late Quaternary monsoon dynamics on the Tibetan Plateau – Northern Transect” in summer 2008. The study reconstructs land forming processes from different archives along catchment-wide sediment cascades in well-defined lake catchments that are influenced by monsoonal dynamics.

A *sediment cascade* is the path of sediments, which spans a wide range of geomorphological and sedimentological process-dynamics. The concept of a sediment cascade refers to several sedimentary environments that are characterized by specific processes of sediment erosion, transport and storage. These processes are related in space and time. For example, fluvial/alluvial processes connect all components of a sediment cascade, from the upper catchments (where glacial and periglacial processes may dominate) to the local base level (e.g., a lake as the final depocentre, where littoral and lacustrine processes dominate).

Hence, sediment eroded from the upper catchments may be found accumulated in a sediment archive in the lower catchment. Aeolian processes, in contrast, may recycle and distribute sediment in all directions and across watersheds (Figure 1.1). Reconstructing past sedimentary conditions related to hydrological conditions, for example, is possible from sedimentary archives and related landforms. Studies of the manifold components of a local or regional sediment cascade (Figure 1.1) have revealed different ways of reconstructing past environmental conditions, e.g., using lake sediments (Cohen, 2003; Jones and Jordan, 2007), glacial deposits (Kirkbride and Winkler, 2012), or loess-palaeosol-sequences (Pye, 1995; Muhs, 2007). However, the idea of studying the different components of a single catchment-wide sediment cascade and connecting the different archives along it is unique to the Northern Transect project.

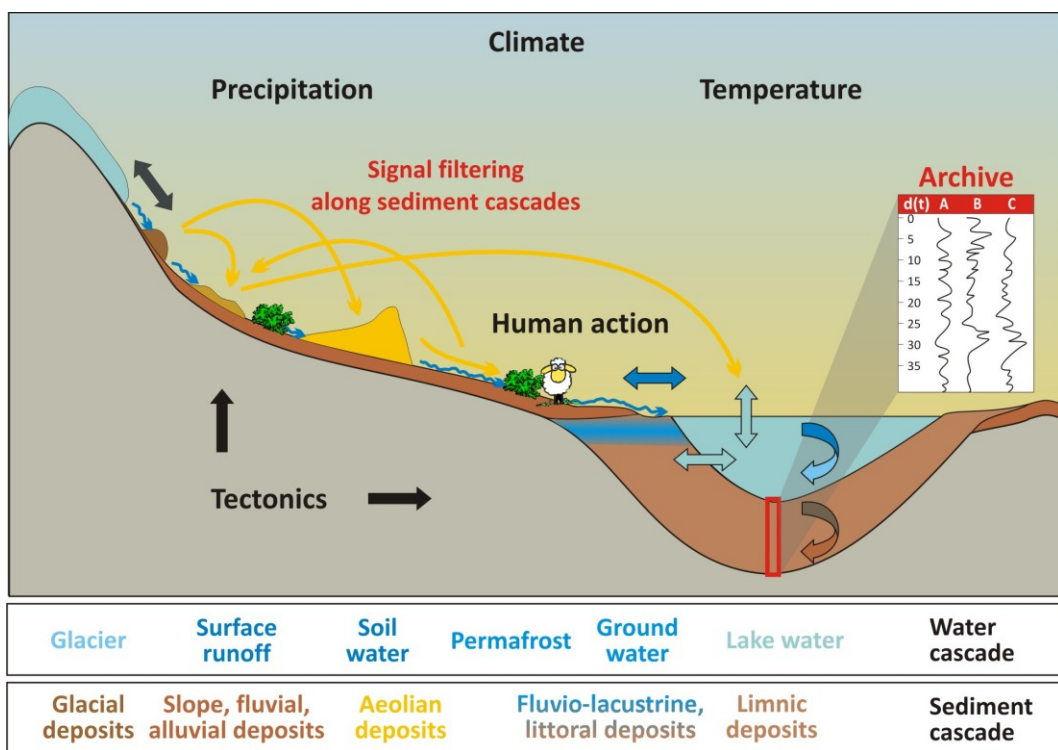


Figure 1.1: Sediment and water pathways along a sediment cascade in a lake catchment, including the main drivers of environmental change that integrate in a sediment archive.

However, reconstruction of hydrological processes using sedimentological and geomorphological approaches can be a very complex task, since *climate* is only one of the driving factors that control sedimentation and morphology. In some regions climate may even be of minor importance (Slaymaker et al., 2009), when *tectonic* movements, for example, come into play. They shape landscapes, alter sedimentation and overprint sediments post-depositionally at different spatial and temporal scales. Also, *human* activity can affect land cover, alter water pathways and storage (lakes and reservoirs), and can even remove water from a landscape system (see summaries in Slaymaker et al., 2009). Considering these three

main *drivers* is an important precondition for a valid sedimentological and geomorphological analysis. An archive or landscape can be regarded as *sensitive*, when small-scale alterations of climatic or non-climatic change leave a distinct fingerprint in the sediment archive.

Different temporal and spatial scales have to be considered, as environmental and especially hydrological signals can be filtered and buffered in multiple ways along a sediment cascade (Figure 1.1). Minor filters and buffers, related to the major drivers of environmental change, are long- and short-term storage, reworking, and alteration of sediment by physical and geochemical processes (e.g., pedogenesis, permafrost). The larger the catchment, the more it integrates long-term alterations caused by the driving factors. In contrast, small catchments are rather prone to small-scale, local disturbances (Slaymaker et al., 2009). Hence, it is important to characterize the lake basin and catchment configuration to determine the sensitivity of the sediment cascade, and also the potential buffering systems associated with the evolution of the lake. As a consequence, methods are needed to distinguish the relevant signals in sediments from random noise, as well as to allow a characterization of the depositional environments (glacial, fluvial/alluvial, aeolian, littoral, and lacustrine), especially along the transition zone between land and lake.

1.2 OBJECTIVES, APPROACH AND OUTLINE

During field campaigns in 2006 and 2007, morphological indications of higher lake stands at Lake Donggi Cona on the north-eastern Tibetan Plateau suggested considerable water level variations in the past, although the studied lake is currently an open system. The dissertation presented here comprises most of the work performed on the sedimentary environments of the littoral zone and the lake basin morphology. It represents a connecting study between the research groups of the Northern Transect project, because it considers both lake and catchment response to Late Quaternary climate change by using sediments and landforms of lacustrine and terrestrial origin.

Two general questions are the focus of this thesis:

- How sensitive is the Lake Donggi Cona basin and its sediment cascade to climatic changes, and what further driving forces of environmental change play a role in the catchment?
- How did lake levels at Lake Donggi Cona vary in the past and what were the responsible driving mechanisms?

To answer these questions, morphological and sedimentological characteristics of the transition zone between land and lake have been studied. First, a characterization of the

basin morphology and sediment architecture of Lake Donggi Cona aimed to decipher how the lake and its basin evolved. To differentiate the depositional environments that respond to lake level changes, sediment transport signals needed to be separated in sedimentological data (especially in grain size data). As a consequence, the detrital sediment composition of modern and fossil lake sediments was studied. Finally, lake level changes were reconstructed quantitatively and compared with other hydrological reconstructions in the area to decipher the main driving mechanisms, and assess the transferability of the results in space and time.

In Chapter 1.3, I provide an overview of our current knowledge regarding the reconstruction of hydrological processes on the Tibetan Plateau using sedimentological and geomorphological methods. First, I introduce the main drivers of hydrological processes, i.e., climate, tectonics and human activity, and their general importance for the Tibetan Plateau. Then, the role of these drivers is discussed with respect to different components of a typical Tibetan sediment cascade.

In Chapters 2 through 4, I present the results in the same order and way they were prepared for submission to international, peer-reviewed journals (Table 1.1). Chapter 2 presents detailed descriptions of the basin morphology and sediment architecture of Lake Donggi Cona, which gives first implications for the climatic sensitivity of the lake and its catchment and allows the reconstruction of lake evolution and lower-than-present water level changes. In Chapter 3, I present an algorithm on end-member modelling analysis (EMMA) of grain size data that has been applied to modern surface samples of Lake Donggi Cona. The developed EMMA algorithm is a flexible tool for studying the signals of sediment sorting processes in many types of depositional settings, and allows robust and quantitative grain size studies, including estimations of uncertainty (see Chapter 9 for Matlab-code and further references where EMMA has been successfully used).

Chapter 4 summarizes the major findings from field work at Lake Donggi Cona in May and August/September, 2009. Chapter 4.1, contains a short summary of the investigations of four onshore terraces that encircle the lake. These terraces contain high-stand sediments of lacustrine, littoral, near-shore, and fluvial/alluvial origin. Their stratigraphies were studied, and EMMA was applied to the grain size data to characterize past depositional changes in the onshore terrace sediments. Using a combination of high-stand sediment stratigraphy and granulometry, I was able to reconstruct lake level changes above the present level, as well as to discuss the driving forces involved in these changes (Chapter 4.2).

Following the main objectives, Chapter 5 integrates and discusses the all the results of this thesis. An overall reference list, including also the references of the already published articles can be found in Chapter 8.

| Chapter | Publication | Status in August 2012 |
|---------|---|---|
| 2 | Basin morphology and seismic stratigraphy of Lake Donggi Cona, north-eastern Tibetan Plateau, China by Dietze, E., Wünnemann, B., Diekmann, B., Aichner, B., Hartmann, K., Herzschuh, U., Ijmker, J., Jin, H., Kopsch, C., Lehmkuhl, F., Li, S., Mischke, S., Niessen, F., Opitz, S., Stauch, G., Yang, S. http://www.sciencedirect.com/science/article/pii/S1040618209004418 | published in May, 2010 Quaternary International 218, 131-142 (submitted in February, 2009) |
| 3 | An end-member algorithm for deciphering modern detrital processes from lake sediments of Lake Donggi Cona, north-eastern Tibetan Plateau, China by Dietze, E., Hartmann, K., Diekmann, B., Ijmker, J., Lehmkuhl, F., Opitz, S., Stauch, G., Wünnemann, B., Borchers, A. http://www.sciencedirect.com/science/article/pii/S003707381100265X | published in January, 2012 Sedimentary Geology 243-244, 169-180 (submitted in September, 2010) |
| 4.2 | Early to mid-Holocene lake high-stand sediments at Lake Donggi Cona, north-eastern Tibetan Plateau, China by Dietze, E., Wünnemann, B., Hartmann, K., Diekmann, B., Jin, H., Stauch, G., Yang, S., Lehmkuhl, F. http://dx.doi.org/10.1016/j.yqres.2012.12.008 | accepted 18 th December, 2012, Quaternary Research (submitted in August, 2012) |

Table 1.1: Published and submitted manuscripts and the chapters in this dissertation, where they are presented.

All included manuscripts (Table 1.1) were entirely structured and prepared by myself. I performed all of the revisions after the already published articles were peer-reviewed. The results of Chapter 2 are based on field work conducted in summer 2006 (bathymetric and seismic work done by B. Wünnemann, B. Diekmann, and S. Yang). C. Kopsch and F. Niessen helped with processing and interpreting the seismic data. S. Mischke, U. Herzschuh, B. Aichner and S. Opitz provided the core data. The other co-authors participated in the project and revised the initial version of the manuscript.

The article presented in Chapter 3 is based on lake surface samples collected in summer 2006 by B. Wünnemann, B. Diekmann, and S. Mischke. Grain sizes were measured by B. Diekmann. EMMA was developed by me, along with K. Hartmann and A. Borchers, and I applied it to the grain size data. The other co-authors revised the initial manuscript.

For the manuscript comprising Chapter 4.2, I did more than 80% of the field work (profile descriptions and sampling) and half of the laboratory work, helped in the field by B. Wünnemann, K. Hartmann, H. Jin, S. Yang and the students mentioned in the acknowledgements. I interpreted the data and wrote all of the manuscript. F. Lehmkühl, G. Stauch and B. Diekmann helped in revising the initial version of the manuscript.

1.3 STATE-OF-THE-ART

1.3.1 STUDY AREA

Lake Donggi Cona is situated at 35°18'N and 98°32'E at an elevation of 4090 m a.s.l., in Qinghai province on the north-eastern Tibetan Plateau, China (Figure 1.2). The Donggi Cona catchment is influenced by Asian monsoon systems that interact with the westerlies (Domrös and Peng, 1988). Moisture to the catchment is mainly provided by the summer monsoons (Figure 1.2). Because the lake fills the western half of a pull-apart basin situated at the Kunlun fault (Van der Woerd et al., 2002), tectonic movements must be considered as an active driver of morphological and sedimentological dynamics. The configuration of the semi-arid catchment (area: 3174 km²) is very heterogeneous, including a major fault zone, different rock types, mountain ranges up to 5300 m a.s.l., moraines, episodic and perennial fluvial systems, aeolian deposits, wetlands associated with discontinuous permafrost, and the currently 229 km² freshwater Lake Donggi Cona (see below for details).

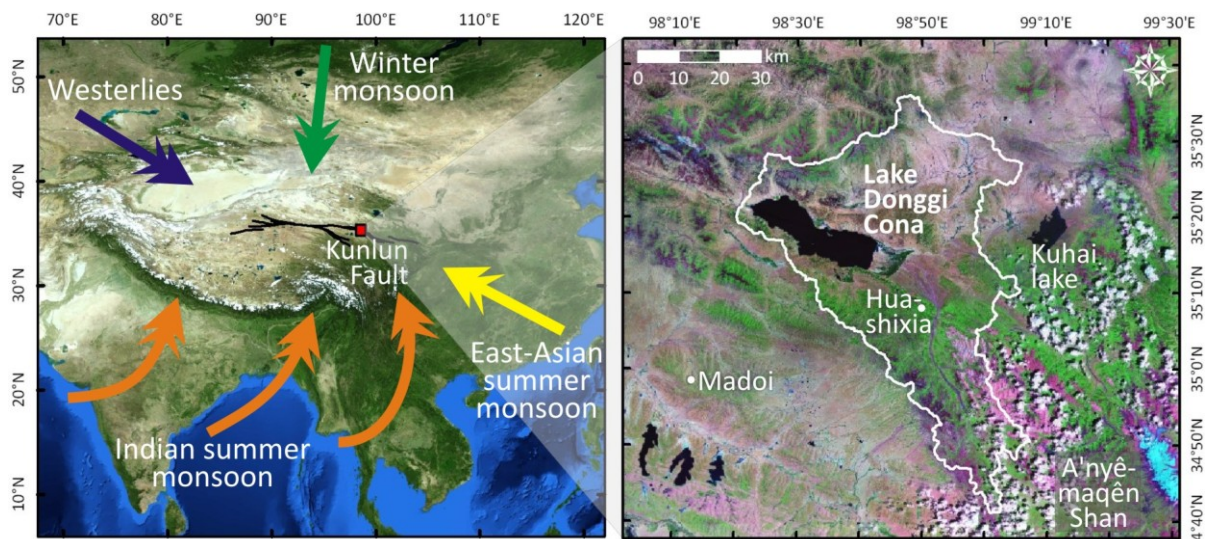


Figure 1.2: Location of Lake Donggi Cona at the north-eastern Tibetan Plateau. Arrows (left) indicate interacting air masses at the Tibetan Plateau, black lines mark the dominant course of the Kunlun

fault (after Fu et al., 2005). The white line in the right figure delineates the Donggi Cona catchment including some sites referred to in the text.

The Donggi Cona area is populated by Golog Tibetan nomads, who use the areas close to the lake as winter dwelling regions and move to higher areas during summers. The national road G214 crosses the catchment in the east connecting the towns of Gonghe in the north with Madoi in the southwest. The small settlement of Huashixia has around 1500 inhabitants and has probably existed as a town since the 1970s (S. Yang, personal communication, May 2009; Figure 1.2).

1.3.2 GEOLOGICAL AND TECTONIC CONSTRAINTS

Tibetan Plateau uplift started around 50 Ma ago from the active continent-continent collision of the Indian plate with the Eurasian plate, where several ophiolite melange zones, island arc-basins, and asynchronously rifted blocks formed a compound orogenic system. Intracontinental convergence, uplift and northeastward movement of the Tibetan crust are ongoing and are accommodated by long, strike-slip faults (Chen et al., 2004; Royden et al., 2008; Pan et al., 2012). Though there is still debate on when, how and where this collision started, and why this plateau kept so flat (Nelson et al., 1996; Yin and Harrison, 2000; Tapponier et al., 2001; Ding et al., 2005), it is widely accepted that the formation of the plateau happened in several uplift phases that were associated with the evolution of the Asian monsoon system (An et al., 2001; Qiang et al., 2001; Harris, 2006), possibly also via an uplift-erosion feedback (Wobus et al., 2006; Whipple, 2009).

When studying sedimentary palaeoenvironmental archives on the Tibetan Plateau, it is important to consider that most of the catchment and lake systems are influenced by this collision in some way. Many formed along the major fault systems that accommodate the collision stress, which opened deep lakes in places. Some of the lakes might even represent the remnants of separate oceanic basins that were amalgamated in suture zones during collision (e.g., Nam Co basin, Pan et al., 2012). The Donggi Cona catchment belongs geologically to the Burhan Buda ophiolite melange zone and the Buqingshan–Maduo–Maqin accretionary complex of the Kangxiwar–Muzitagh–Maqin–Mianxian suture system (Pan et al., 2012).

The main tectonic boundary in this suture zone is the left-lateral Kunlun fault, where the ongoing collision stress has been accommodated since at least the Pliocene/early Pleistocene (Zheng et al., 2000; Wu et al., 2001). Offsets, calculated along alluvial terraces at six sites along 600 km of the Kunlun fault, indicate uniform left-lateral slip rates of at least 11.5 mm/year during the last 40 ka (Van der Woerd et al., 2002). At the Dongxi Co segment,

which Lake Donggi Cona belongs to, Van der Woerd et al. (2000, 2002) found a vertical slip component ten times smaller than the horizontal component. The well-known earthquake of M~7.5 ruptured the Kunlun fault along the Donggi Cona segment in 1937, leaving characteristic mole tracks, e.g., those found north of the modern lake outlet (Figure 4.3A). In comparison with sites further west, similar seismic slip events appear to have smaller magnitudes and shorter recurrence intervals (M~7.5 every 420 years at the Donggi Cona segment *versus* M~8 every 900 years at the Xidatan-Dongdatan-segment, Van der Woerd et al., 2002). Between 1973 and July 2012, the USGS/NEIC earthquake database recorded 24 seismic events between 96°E and 100°E along the Kunlun fault, at depths ranging from 10 to 33 km. Five events had a magnitude of M \geq 5, 15 events with M~3.8 to M~4.7, and four events of unknown magnitude also took place. According to the seismic hazard map of China, the Donggi Cona area is exposed to a medium seismic risk (USGS/NEIC, 2012; cf. Chapter 2.5.1, 4.2.5.2, and 5.1.3 for further discussion of past tectonic activity at the lake).

1.3.3 CLIMATIC CONSTRAINTS

Although the evolution of the Tibetan topographic relief is primarily linked to collision and the resulting geological pattern, it is further driven by large-scale climatic changes that have triggered glacial and fluvial erosion (Harris, 2006; Stroeve et al., 2009). Northern hemisphere glaciations have played an important role in shaping the Tibetan Plateau. For example, glacial advances and the associated blockage of large valleys by moraine dams were responsible for preserving the prominent edges of the plateau (Korup and Montgomery, 2008).

The main climatic system on the Tibetan Plateau consists of different interplaying circulation systems (Figure 1.2) that are primarily affected by the large and high extent of the Tibetan Plateau (Böhner, 2006). The most important circulation system is the Asian monsoon, which can be divided into the dry winter component driven by the large Siberian anticyclone, and the wet Indian and East Asian summer monsoons. The summer monsoons result from the temperature difference between the Tibetan Plateau and the large Eurasian landmass, and the Indian and Pacific oceans. These oceans are the main moisture source for the Tibetan Plateau. However, westerlies may also bring some moisture from the North Atlantic region, especially to the western part of the Tibetan Plateau and northern forelands (Böhner, 2006; Wünnemann et al., 2007) – this is probably a major moisture delivery mechanism during cooler periods (e.g., Little Ice Age, Chen et al., 2010).

The onset of the Asian monsoon is dated back to around 8 Ma, with an intensification phase about 3.6-2.6 Ma ago, followed by an increase in variability and the establishment of

the modern summer and winter monsoon relationship around 2.6 Ma (An et al., 2001). However, the mechanisms behind, and variability of monsoon intensity and teleconnections are still the subject of debate. The effects of solar insolation changes (e.g., Fleitmann et al., 2003; Dykoski et al., 2005; Wang et al., 2010) and Greenland temperatures on the Asian monsoons seem well-established. The latter may be associated with a teleconnection between North Atlantic deep water formation and snowfall on the Tibetan Plateau (Dykoski et al., 2005). Though the northern hemisphere climate seems to be the main trigger of the Asian monsoons, influences from the southern hemisphere via the position of the ITCZ and the state of El Niño-Southern Oscillation are also possible (Morrill et al., 2003; An et al., 2011; Shi et al., 2012). The possible southern hemisphere influences may explain the connection of the Asian monsoons with the African and South American monsoon systems (Morrill et al., 2003; Dykoski et al., 2005). Changes in the general patterns of the Asian monsoons and especially global cooling events seem to be synchronous for the Holocene (Dykoski et al., 2005; Wang et al., 2010). The most abrupt changes in the Asian monsoons occurred at 11.5 cal. ka (the onset of the Holocene and intensification of the Asian monsoons), at 4.5 to 5.0 cal. ka (overall weakening of the monsoon) and 1300 AD (increase in heterogeneity of the monsoon) in accordance with global climate variability (Morrill et al., 2003).

The Donggi Cona catchment is situated at the modern northern boundary of where the wet East Asian and Indian summer monsoon interact with the dry winter monsoon and westerlies (Figure 1.2). However, the extents of the modern monsoon differ strongly between publications, as the Asian monsoons have a strong intra- and interannual variability (Shi et al., 2012). Hence, its current extent is better described as a zone of different probabilities that would require further study to accurately map. Further, it is not yet clear which monsoon system (Indian or East Asian) is (or was) the most dominant control of summer precipitation in the Donggi Cona area. The answer to the above question seems to depend on the time-scale considered (Xu et al., 2007). Hence, the phrase “the Asian summer monsoons” is used here to integrate these considerations.

1.3.4 ANTHROPOGENIC CONSTRAINTS

The Tibetan population is very small compared to Tibetan Plateau’s large area of around 2.2 million km². Tibetan people are primarily nomads that rear yaks and sheep. There is still debate regarding when the Tibetan Plateau was inhabited permanently and how nomadic grazing systems have influenced landscape dynamics. Miehe et al. (2006) and Schlütz and Lehmkühl (2009) determined nomads were present since around 8000 years ago, and that the so-called nomadic “Anthropocene” had already started around 6000 years

ago, when *Kobresia*-pastures became dominant and began affecting slope stabilities. Modern grazing systems were established around 2200 years ago (Schlütz and Lehmkuhl, 2009; Miehe et al., 2011) leading to an increase in sediment reworking along the slopes. Other authors suggest that humans have only made a minor contribution to vegetation changes, starting around 2000 years ago at the earliest. They attribute vegetation changes to climate, especially monsoon dynamics that correlate with global climate variations in the Holocene (Herzschnuh, 2006; Zhao and Yu, 2012). The climate and grazing impact led to wet tundra with mainly alpine steppe vegetation in the Donggi Cona area (Kürschner et al., 2005).

1.3.5 COMPONENTS OF A TIBETAN SEDIMENT CASCADE

The Tibetan Plateau hosts a large area of currently glaciated upper catchments (Qiu, 2008), which is where hydrological conditions start to affect sediment transfer. Glaciers or glacial remains (e.g., cirques, moraines) indicate present or past conditions that are sufficiently cold and moist enough to accumulate and preserve ice. Glaciers are an important archive of past atmospheric conditions, including records of environmental changes in dust, chemistry, stable isotopes, and net accumulation. High-mountain glaciers are very sensitive to small-scale climatic changes (Thompson et al., 1993). Hence, considering past glaciations is an important requirement for hydrological studies, as they a) are driven primarily by climate and relief (Bolch et al., 2012), independent of tectonic movements; b) may respond with some site-specific time delay (Kirkbride and Winkler, 2012); and c) can contribute an important amount of meltwater to a lake causing lake levels to rise independently of precipitation (Wünnemann et al., 2007, 2010). During transitions to warmer periods, high amounts of meltwater are produced that can significantly contribute to the water balance of a lake.

The extent and timing of glaciations in Tibet is still under debate (e.g., Kuhle, 2003, 2011 *versus*, e.g., Owen et al., 2003; Owen, 2009; Heyman et al., 2011). Tibetan glaciations are primarily driven by moisture availability and often advanced most during wetter early glacial periods (such as MIS 3, i.e., local LGM; Owen, 2009). CRN-dating of the moraines of the A'nyêmaqên Shan, some 70 km southeast of Lake Donggi Cona, indicate a maximum glacial advance during MIS 3, and probably smaller MIS 2 and early Holocene advances (Owen et al., 2003). In contrast, glaciations only occurred until 40 ka in the Bayan Har mountains, 170 km southwest of the lake (Heyman et al., 2011).

The *periglacial* component of a Tibetan sediment cascade has been studied mainly on the western Tibetan Plateau. Many studies were focused along the Golmud-Lhasa-Highway and concerned engineering topics and only few integrating studies are available (Jin et al., 2007). Periglacial dynamics include all sediment production, transport and storage process-

es, as well as landforms that are connected to permafrost and active layer mixing (e.g., cryoturbation, gelifluction, thermokarst evolution). Periglacial processes depend primarily on temperature and relief. In the past, permafrost affected sediments over large areas of the Tibetan Plateau. Today, the permafrost distribution differs between the western, central and eastern part of the plateau, depending on regional climate and relief. The modern lower limit of alpine permafrost is at 4000-4050 m and continuous permafrost occurs above 4500 m a.s.l. in the study area (i.e., A'nyêmaqên Shan, Jin et al., 2007). Mixing from permafrost dynamics can be regarded as an important buffer in a sediment cascade, overprinting sediment post-depositionally. Periglacial processes may even “reduce” the past environmental information recorded in sediment archives (Wünnemann et al., 2009).

Another buffer that can overprint deposited sediment is soil formation. However, only a few pedological studies investigated local soil forming processes so far, mainly in relation to the *Kobresia*-grasslands (Kaiser et al., 2007; Miehe et al., 2008), which occur only on wetlands of the large alluvial plain east of Lake Donggi Cona. Although in principal all types of soil could form at the altitude and under the climate of the Donggi Cona area (K. Kaiser, personal communication, June 2012), the soils expected on the dry steppe slopes may mainly be of Kastanozem and/or Cambisol character (cf. plot 16 in Miehe et al., 2008).

Intensification of the local *aeolian sediment* cycle due to climatic change is mostly associated with sediment mobilisation in dryer and cooler times, e.g., when sufficient material from glacial and periglacial weathering was provided, vegetation cover was reduced, and/or when lake levels lowered exposing lake sediments that acted as a sediment source (Lehmkuhl and Haselein, 2000; IJmker et al., 2012b). Modern aeolian sediment transport on the Tibetan Plateau happens mostly during the winter, when vegetation cover reduces and air masses associated with the dry winter monsoon and westerlies prevail (Sun et al., 2002, 2007; IJmker et al., 2012a, b). However, for at least the last 2000 years (Schlütz and Lehmkuhl, 2009; Miehe et al., 2011), the impact of grazing herds owned by Tibetan nomads has to be considered as a mechanism for the mobilisation of sediment along the slopes. Tectonic movements may be of minor importance in the aeolian cycle.

A further important component of a catchment-wide sediment cascade is the *fluvial system* that connects all the components of it. Rivers are the transport medium to distribute the large amounts of sediment that are produced by intense frost weathering. Fluvial processes are mainly driven by precipitation and relief, with the latter being very prone to alteration by tectonic movements. Fluvial processes probably bring most of the water and sediment to the lake, especially in large catchments (in contrast to direct precipitation offshore). They are activated primarily by direct precipitation and, in catchments with connections to glaci-

ers, by meltwater that can generate significant amounts of runoff (e.g., around 40% in the Hala Hu catchment, B. Wünnemann, personal communication, July 2012). Incision and the formation of fluvial terraces happen when sediment supply and/or runoff is reduced, and/or when base level changes (cf. Stokes et al., 2012). Lakes often form the local base level, so prominent water level changes can also be reflected in fluvial terrace formation.

On the Tibetan Plateau, as in other mountainous areas of the world, alluvial fan aggradation is high when sediment produced by glacial and periglacial weathering can be transported, i.e., during the transitions between dry and wet phases, also depending on tectonic uplift phases (Chen et al., 2011). However, the role of precipitation and the timing of terrace aggradation and incision is still debated (Pan et al., 2009; Vandenbergh et al. 2011). Periods of aggradation have been dated predominantly to the Pleistocene (Lehmkuhl and Haselein, 2000), whereas incision is often correlated with warmer and moister interglacials (e.g., mid-Holocene in the Karakorum, Brown et al., 2003). In contrast, Wang et al. (2009) correlated terrace formation, i.e., incision along the eastern Kunlun range, with dry periods, whereas aggradation took place under phases of high precipitation.

Lakes form the local depocentre of a catchment-wide sediment cascade (Figure 1.1). Hence, they integrate and record most of the sedimentary processes within a catchment, often more continuously than terrestrial archives. An overview of the multiple palaeoenvironmental proxies lake sediments can provide is given in Cohen (2003), for example. At lakes, characteristic littoral land forms (terraces, beach ridges, shorelines, and deltas) and sedimentological variations (e.g., grain size fining off-shore) indicate changes in the position of the lake level (e.g., Jones and Jordan, 2007; Abu Ghazleh and Kempe, 2009). In closed lake systems these variations can be related to changes in the precipitation-evaporation ratio (Street-Perrott and Harrison, 1985). In open lake systems, sedimentological variations and the study of sediment core transects, spanning from the shore to the lake centre, provide suitable approaches to infer hydrological variations (Harrison and Digerfeldt, 1993), whereas typical littoral landforms are sparse, since a higher water input generally increases outflow, rather than the lake level (Jones and Jordan, 2007). Submersed landforms of littoral genesis can be detected by bathymetric and seismic studies. The latter also help to distinguish distorted, faulted or slumped sediment strata (e.g., Charlet et al., 2005 for Lake Baikal; Chapter 2.4).

On the Tibetan Plateau, lake level studies are one of the main tools to investigate past hydrological conditions (Yu et al., 2001; Herzschuh, 2006; Wang et al., 2010). According to some studies, maximum lake levels were reached at many places on the Tibetan Plateau, and its northern foreland, during MIS 5 and MIS 3 as response to the most intense phase of

the monsoon system (e.g., Herzschuh, 2006; Madsen et al., 2008; Liu et al., 2010; Kong et al., 2011) – though this association is still under debate (especially the extraordinary wet phase during MIS 3, Colman et al., 2007). Lake low stands, in contrast, were associated with the cool and dry phases of the Pleistocene (e.g., Lister et al., 1991). Further, lake high-stands are reported for the early and mid-Holocene (Chapter 4.2.5.2). However, interpretations often rely on single lake sediment cores and, therefore, information on local catchment conditions (e.g., the presence of glaciers, perennial streams, basin morphology) is often not well discussed. A study by Wünnemann et al. (2007), conducted in the northern foreland of the Tibetan Plateau, yielded considerably different lake status and moisture reconstructions when they considered sites with and without any glaciers in their upper catchments, separately.

Different methods were used to reveal past water level changes at the littoral zone of Lake Donggi Cona. Submersed landforms and sediments (Chapter 2) were studied using bathymetric and seismic methods. An end-member modelling algorithm (EMMA) was developed to evaluate the distribution of grain sizes in a robust way using modern lake surface sediments, as well as to study the association between water depth and grain size composition (Chapter 3). Fossil high-stand sediments in onshore lake terraces (Chapter 4.1) were studied using field stratigraphies and the application of EMMA – including the suggestion of a new proxy for water level changes (EM_{diff} , Chapter 4.2). The synthesis provides a robust reconstruction of water level changes at Lake Donggi Cona for the Late Quaternary by considering the lake basin sensitivity, the driving forces of environmental change and the influence of signal transfer along the Donggi Cona catchment-wide sediment cascade.

2. BASIN MORPHOLOGY AND SEISMIC STRATIGRAPHY OF LAKE DONGGI CONA

This chapter appeared as an internationally peer-reviewed research article in the special volume of Quaternary International “Climate Evolution and Environmental Response on the Tibetan Plateau” in 2010 with the title “Basin morphology and seismic stratigraphy of Lake Donggi Cona, north-eastern Tibetan Plateau, China”.
(<http://www.sciencedirect.com/science/article/pii/S1040618209004418>).

ABSTRACT

Basin morphology and depositional stratigraphy of Lake Donggi Cona on the north-eastern Tibetan Plateau has been studied with echo depth sounding and shallow seismic sub-bottom profiling. The basin is a pull-apart structure situated at the highly active Kunlun fault. It is characterised by a 92 m deep graben structure in the western part of the lake basin, and a shallow eastern lake part, the latter filled up with fluvial sediments from a large alluvial plain. We identified three prominent morphological levels at 24 m, 39 m and 57 m below present lake level. They were partly created by basin subsidence, while the deposition of prograding delta sediments primarily formed the morphological steps. The inherited tectonic structures control ongoing neotectonic activity, which seems to have only minor influence on present basin morphology. The basin is filled by sediments of at least 30 m thickness in the depocentre. Three major depositional units can be distinguished. In comparison with lithological changes in a sediment core, they give evidence of pronounced lake-level fluctuations and dramatic changes in lake volume. An absolute age datum of ~19 cal ka BP at the base of the sediment core allows a tentative reconstruction of Late Glacial to Holocene lake development. A very low base level preceded a time of delta formation during higher lake level, i.e. ~26 m lower than present during Last Glacial Maximum, creating a lake of only 18 % of its present size. At the transition to Holocene the lake level rose very quickly changing to a deep lake environment. Thus, main transgression may have promoted maximum lake stands.

2.1 INTRODUCTION

Intramontane lake basins such as the Donggi Cona Basin on the north-eastern Tibetan Plateau, China, are believed to be excellent archives for studies on interlinked dynamic processes that have influenced environmental changes through time. Most studies of the past decade dealt with proxy records from sediment sequences of lakes and other terrestrial deposits to infer climatic and/or environmental history related to monsoon dynamics (e.g.

Chen et al., 2003; Chen et al., 2001, 2006; Herzschuh et al., 2004; Ji et al., 2005; Peng et al., 2005; Shen et al., 2005; Wu et al., 2006).

A key approach is the reconstruction of moisture availability, which evolved regionally asynchronous throughout the Holocene and Late Pleistocene (< 50 ka), as available palaeoclimate records from Central Asia indicate (e.g. An, 2000; Herzschuh, 2006; Wünnemann et al., 2007a; Chen et al., 2008, Hartmann and Wünnemann, 2009). The boundary between westerly and monsoonal air masses, both controlling moisture transport over Central China, has fluctuated during Quaternary time, mainly in concert with global climate shifts driven by insolation and millennial-scale circulation patterns (An, 2000).

Lake records from the northern foreland of the Tibetan Plateau show that lake-water balances are closely linked to changes of the circulation patterns (Wünnemann et al., 2007b, Chen et al., 2008), which also affected glacier development on the Tibetan Plateau (Owen, 2008; Owen et al., 2008). However, water budgets as a result of regional hydrological cycles as well as sediment architecture and sediment components in a lake basin strongly depend on local catchment characteristics within their tectonic setting and on regional precipitation-temperature relationships as well (Blais and Kalff, 1995; Holmes et al., 2007).

Previous palaeoclimate reconstructions based on multi-proxy analyses of lake sediments from several sites in Central Asia (e.g. Wünnemann et al., 1998, 2006, 2007a, 2007b, Zhang et al., 2000, 2002) indicate that the complex relationship between various climatic and non-climatic processes (e.g. tectonic or human impact) affecting landscape dynamics induce spatially and temporally variable responses of different magnitude and frequency. This has not been considered consequently, which might be one reason that reported high-resolution palaeoclimate records are rather heterogeneous and partly incomparable.

To enable the connection between the various information from terrestrial and lacustrine archives, spatial and temporal palaeo-environmental information such as path and dynamics along the sediment cascade need to be considered. Within a lake, the development of its basin morphology is mainly determined by non-climatic processes (e.g. tectonic). However, climatic influences may alter basin development, e.g. by glacial dynamics and lake level fluctuations, as well. As lake basins are depocentres for catchment-wide eroded and sedimented particles, they integrate terrestrial landscape dynamics and lacustrine processes over long periods of time.

Basin-morphology studies are essential to understand internal lake system dynamics such as seasonal temperature variation, water stratification pattern, biological activity and spatial distribution of sediments. Additionally, they provide information on lake evolution

and -in combination with seismic stratigraphy- help to decipher the climatic sensitivity of specific basins. The application of seismic stratigraphy in lake-basins is well-suited to infer the depositional history of glacial and post-glacial sedimentation, lake level fluctuations and/or neotectonic impact (Niessen et al., 1999; Colman et al., 2002; D'Agostino et al., 2002; Brooks et al., 2005; Anselmetti et al., 2006; Colman, 2006; Hofmann et al., 2006; Beres et al., 2008; Wagner et al., 2008). However, little is known about basin morphology and the spatial distribution of sediments in Tibetan lakes, apart from Qinghai Lake (Lister et al., 1991; Henderson et al., 2003; Shen et al., 2005) and Nam Co (Daut et al., this volume).

With our study at Lake Donggi Cona, we follow a comprehensive geomorphological and limnogeological approach to improve our understanding of interlinked dynamic land-forming processes governed by climatic and non-climatic factors on catchment scale. Here, we present hitherto unknown morphological and seismic data from Lake Donggi Cona derived from echo depth sounding and shallow seismic sub-bottom profiling that help to identify i) morphological features in the lake basin, ii) spatial sediment architecture and causes of its variability, and iii) appropriate locations for representative sediment coring. We describe the present basin morphology and general sediment stratigraphy using a bathymetric model and selected seismic key sections. Furthermore, we compare the inferred sediment sequences with a sediment core from Lake Donggi Cona and discuss the potential range of former lake level fluctuations during the last 20 ka BP. This work is part of a Sino-German multidisciplinary research program that aims at reconstructing the formation, climate and ecosystem development on the Tibetan Plateau (<http://www.tip.uni-tuebingen.de/>).

2.2 REGIONAL SETTING

Lake Donggi Cona, also referred to as Dongxi Co (Van der Woerd et al., 2002) or Tuosu Hu (Fu and Awata, 2007), is situated on the northeastern margin of the Tibetan Plateau in Qinghai-Province, China (35°18'N, 98°32'E, 4090 m a.s.l., Figure 2.1), northwest and east of the A'nyêmaqên and Kunlun mountain ranges, respectively. Lake Donggi Cona belongs to a series of pull-apart basins along the Kunlun Fault with the A'nyêmaqên Shan, whose peaks exceed 6000 m a.s.l., representing the respective push-up ridge southeast of the lake catchment (Van der Woerd et al., 2002; Fu and Awata, 2007).

The Kunlun Fault accommodates convergence of the ongoing Indo-Asian collision. An open question concerns the timing of initiation of its left-lateral strike-slip movement, and thus, the origin of Donggi Cona basin, which either started during the Middle to Late Triassic (Xu et al., 1997 cited in Fu and Awata, 2007) or during the Pliocene to Early Pleistocene

(Zheng et al., 2000; Wu et al., 2001). There are also uncertainties in regard to mean vertical offset and exact slip-rates along the Kunlun Fault and its role in accommodating displacement, especially at its eastern termination (Kirby et al., 2007).

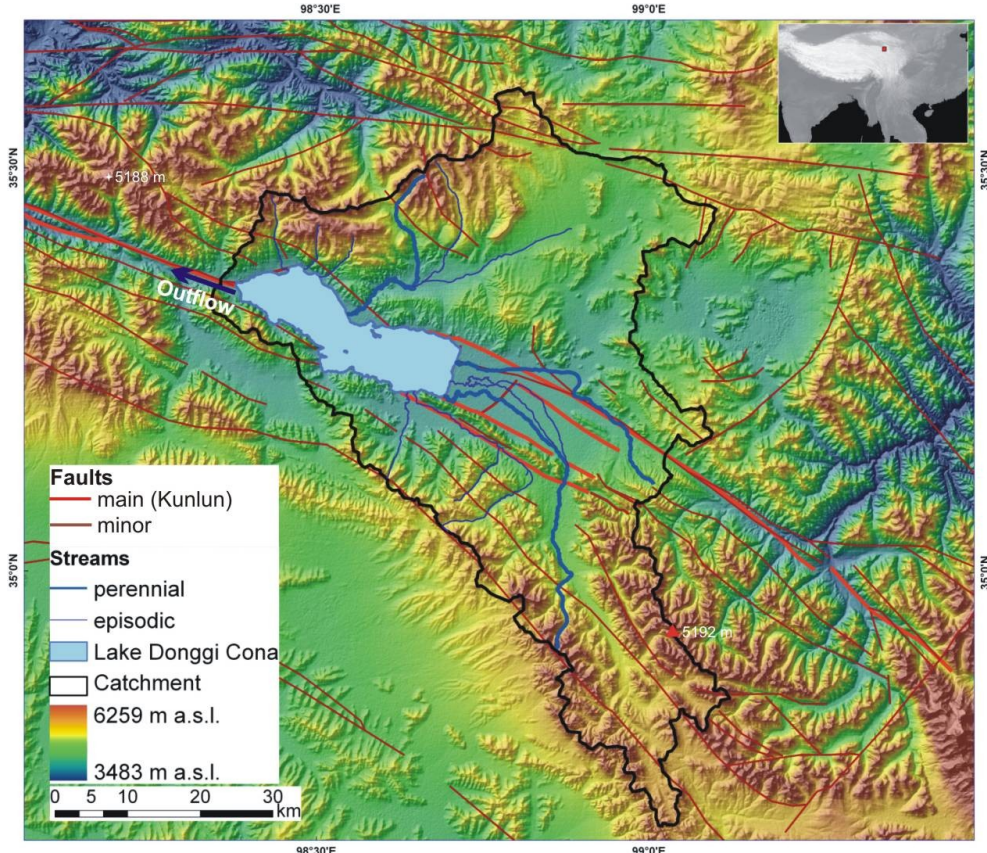


Figure 2.1: Location of Donggi Cona lake basin and its catchment on the north-eastern Tibetan Plateau. Main Kunlun fault after Van der Woerd et al. (2002), minor faults after Geological Map of the Qinghai-Xizang (Tibet) Plateau and Adjacent Areas (1:1 500 000; Chengdu Institute of Geology and Mineral Resources, China Geological Survey, 1988).

The main Kunlun Fault intersects the Donggi Cona and its catchment from WNW to ESE with an angle of $\sim N115^\circ E$ (Figure 2.1). Detailed tectono-geomorphic investigations by Van der Woerd et al. (2002) and Fu et al. (2005) along several parts of the fault indicated mean neotectonic annual slip rates along the Donggi Cona segment between 98.0° and $99.5^\circ E$ to be around 10.3 mm/a. There, the main fault ruptured in the 1937-earthquake with $M=7.5$ between $96^\circ E$ and $99^\circ E$ with mean sinistral and vertical offsets of 4.4 to 8.0 m and 0.4 to 3.5 m at two locations, respectively (Van der Woerd et al., 2000). Recurrence intervals of similarly strong earthquakes were estimated to be 420 years (Van der Woerd et al., 2000, 2002) or 640 years (Li et al., 2005). Other minor faults related to the Kunlun system within the Donggi Cona catchment have not been studied in detail, though most of them do not seem to be active anymore.

Lake Donggi Cona fills the western half of the 60 km long to 20 km wide pull-apart basin, with a catchment of 3174 km² (Figure 2.1). The northern catchment area consists of dissected series of Early and Middle Triassic lime- and sandstones (Wang et al., 2001; Wang and Yang, 2004) faulted against Triassic quartzite and black to green shales. These rifted blocks are unconformably overlain by reddish Neogene conglomerates and sandstones (similar to those described in Zheng et al., 2000). In the south, the basin is bound by an uplifted elongated mountain ridge composed of Middle Permian limestone. The catchment area is characterised by high relief gradients in its north and southeast. There, fluvial incision is forming V-shaped valleys, while lateral moraines and U-shaped valleys, indicating former glaciations, are also present, though they did not directly affect the lake basin itself. Lower mountains with gently inclining slopes characterise the southern and north-eastern catchment.

The lake is fed by a perennial and some episodic inflows (Figure 2.1). At the northern shore the inflows form three major prograding arcuate delta systems. There, the only perennial stream originates from a flat basin connected to Lake Donggi Cona by a transverse valley. However, major perennial inflow with varying intra-annual discharge enters the lake from the east along two channels (Figure 2.1). A large alluvial plain with very gentle slopes forms a bay delta restricted by the steeper northern and southern shore. It drains the western A'nyêmaqên Shan and fills this part of the pull-apart basin with fluvial sediments conserving various terrace generations. Numerous short episodic inflows encircle the rest of the basin with smaller alluvial cones.

Drainage of the lake is currently directed through an artificial channel at the western lake margin towards the endorheic Qaidam Basin, ca. 200 km northwest of the lake. At present, outflow is controlled by a gauge station set up during the 1970s. However, morphological features such as palaeo-shorelines, ancient on-shore terraces, and lake sediments exposed above the present lake level can be found in the vicinity of the lake, indicating former high lake levels. At present the lake is an oligotrophic, freshwater lake (electrical conductivity: 0.635 mS/cm) with oxygen supply down to the lake bottom, a mean pH-value of 8.6 and a maximum Secchi depth of 12 m (Mischke et al., 2010a). The lake is frozen from November to April (observations since 2006) and did not show a distinct stratification during the unfrozen period (three month field trips in 2006 and 2009) due to full circulation.

Climate is controlled both by the monsoon system and the extra-tropical westerlies, as the lake basin is located close to the western limit of the East Asian Summer Monsoon trajectories (Domrös and Peng, 1988; An et al., 2001). Local climate conditions can be deduced from the climate station at Madoi at 4272 m a.s.l., some 50 km southeast of the lake (data

from 1958-2007, Chinese Central Meteorological Office, 2008). Mean annual precipitation is 304 mm and mean annual air temperature -4.1°C. Mean relative humidity, relative sunshine hours, total pan evaporation and wind velocity are 59%, 61 %, 1375 mm and 3.4 m/s, respectively. At this high elevation site, climate and grazing impact lead to a vegetation of alpine meadows and steppes dominated by Kobresia, Artemisia, and Poaceae (Kürschner et al., 2005). It is well-developed on top of loess-like sediments covering most of the slopes in the northern and eastern catchment. While dunes in the eastern part of the large alluvial plain are often grown by Salix spec. Frozen ground appears as discontinuous permafrost in the flat and water-saturated supralittoral zones around the lake up to around 5 m above the present lake level. Permafrost features comprise hummocky land surfaces and the presence of small thermokarst depressions, especially along the western part of the large alluvial plain.

2.3 DATA AND METHODS

Echo depth sounding of 3977 points all over the lake has been carried out in summer 2006 using a Dual-Beam Garmin fishfinder, coupled with GPS. At the same time, acoustic sub-bottom profiling was conducted with a mean boat speed of 5 km/h using a single-channel GeoPulse 3.5-kHz Profiler system (Geoacoustics) along 16 transects with a total length of 144 km (Figure 2.2). Most transects are oriented as cross-sections perpendicular to the main WNW to ESE extension of the lake. The seismic trigger rate was 1 s. Acoustic pulses allow a penetration of the upper lake sediments down to a maximum of 50 m below the lake floor. As far as possible, seismic and echo- sounded depth profiles obtained at the same time have been spatially synchronized, though due to some technical problems a GPS-coupling of the GeoPulse profiles, and thus, an absolute comparison with the echo sounding data was not possible. Raw seismic transducer signals from an 80° x 80° wide acoustic cone were recorded on Sony Premium 60P data cartridges with a Sony 4-channel data recorder PC204Ax. The raw data were then digitized and converted to the internationally common SEGY-format with an analogue-digital converter (EAQ Pad 6052E, 16bit, National Instruments) and a converting software written in LabView 7.1 by C. Kopsch (AWI Potsdam). Processing was done afterwards using Reflex-Win Version 5.0 by Sandmeier Software. Two-way travel times of sound have been transformed to depth assuming a mean sound velocity of 1490 m/s in accordance to fresh lake water temperature. Theoretical object resolution depends on the signal-to-noise ratio and is assumed to be around 30 cm at most.

An ordinary kriging approach was applied by ArcGIS 9.2 software to create a bathymetric map using the depth points achieved from echo sounding, a point shape of the present shoreline from Landsat7 ETM+ multispectral images (GLCF, 2008), and the 3''-DEM of the

Shuttle Radar Topography Mission (SRTM3) heights of the two islands within the lake. This method yielded low interpolation errors (RMS of 3.3 m) and turned out to be the most suitable interpolation with least artefacts from linear boat transects in comparison to e.g. spline interpolation and triangular irregular network (TIN) approaches.

SRTM elevations were corrected by +6 m to account for the orthometric height of 4090 m a.s.l. of the present shoreline as measured by differential GPS in summer 2006. All described morphological and sedimentological features are interpreted relative to lake level in summer 2006.

Seismic stratigraphy was determined by mapping seismic reflection changes (unconformities like onlap structures), geometry, and linearity following standardized methods (Miall, 1984; Van Wagoner et al., 1990; Catuneanu et al., 2009), which allows a distinction of several depositional units throughout the basin. Sigmoidal clinoforms indicating delta sediments and potential vertical fault lines were mapped with special attention, though only few transects are presented here (Figure 2.2).

At a representative site with well-stratified sediments identified from seismic sub-bottom profiling, sediment coring has been conducted from ice with an UWITEC piston-corer system in winter 2007 gaining the 4.84 m long sediment core PG1790 (35°20'N, 98°26'W, 35 m water depth, Figure 2.2). The upper 15 cm got lost by recovering. Seismic reflections of the upper lake bottom sediments were generally compared with the lithologic characteristics of the core.

Nine AMS-¹⁴C ages derived from bulk organic material (total organic carbon fraction, TOC) measured at Poznań Radiocarbon Laboratory are preliminarily presented in Figure 2.6. They were preliminarily corrected for a potential lake water reservoir effect (modern TOC: 1983 years, unpubl. data) and calibrated using CALIB (online version 5.1.beta, Reimer, 2004). Thus, tentative age estimation for the upper depositional units could be determined. However, further analyses of the core and still on-going age analysis will be presented elsewhere.

2.4 RESULTS

2.4.1 BASIN MORPHOMETRY

Lake Donggi Cona shows the typical rhombic shape of a pull-apart basin. The lake basin consists of a western and an eastern part (Figure 2.2). The western part includes an asymmetric graben structure with a maximum lake depth of 92 m. The graben is characterised by

a ca. 30 km², mainly northward inclined lake floor with up to 26° steep slopes at its northern rim and southern shore, respectively. North of the graben, the lake floor exhibits relative gentle slopes of less than 5° that pass over to the northern and north-western lake shore. The eastern part of the lake basin is characterised by a gently west- to northward dipping flat lake floor with slopes generally inclined less than 2°. It represents the drowned continuation of the large alluvial plain, which occupies the eastern sub-aerial part of the pull-apart basin. The mean present water depth of the eastern part is 38 to 40 m below present lake level (b.l.l.; 95% confidence level) (Figure 2.2). The two parts of the lake basin are separated by an approximately northeast-southwest striking step including a small arcuate northern island and a steeper southern island. There, local compressions seem to mark the basin's accommodation zone (*sensu* Cohen, 2003).

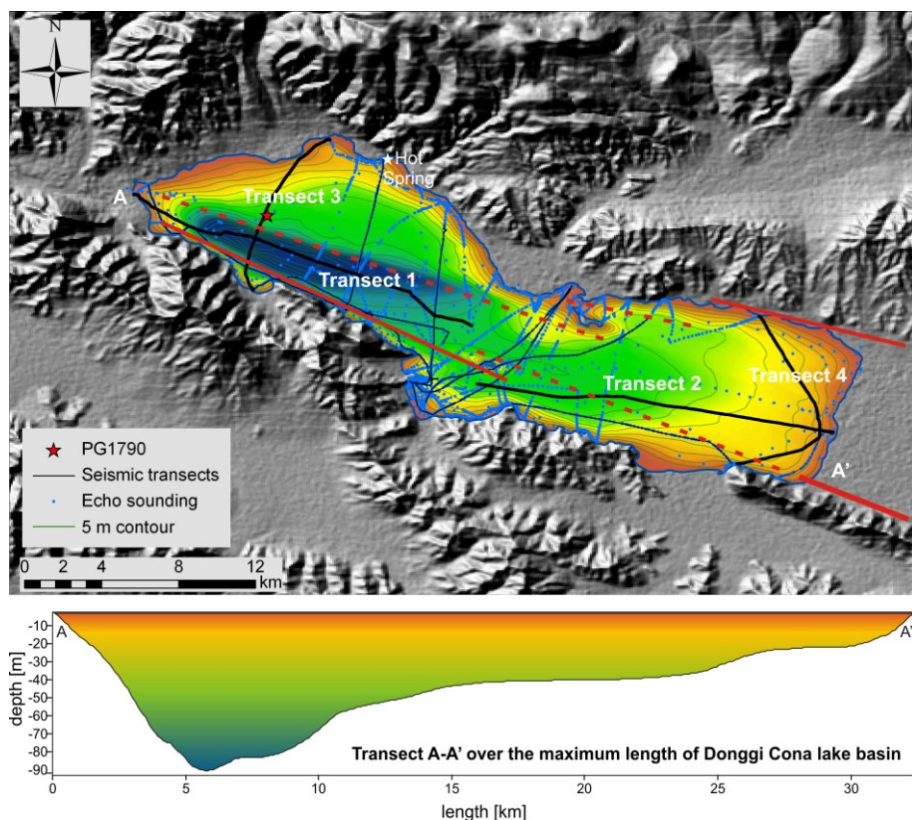


Figure 2.2: Bathymetry of Lake Donggi Cona from echo depth sounding relative to the lake level in 2006 bedded in SRTM3-hillshade; seismic transects, site of sediment core PG1790 and longitudinal profile at the maximum fetch of the lake basin between A and A'. Seismic transects marked with bold lines are presented in Figure 2.4 and 2.5. Suggested faults in red; dashed red line uncertain faults.

The lake has a surface of 229 km² (excluding the two small islands of 0.4 km²) and a maximum WNW to ESE fetch of 32.7 km. The maximum width is 9.5 km in the eastern part of the lake. The present shoreline has a length of 94.7 km (Landsat ETM+ 2001, scale 1:100,000). Bathymetry reveals a current lake volume of 6.8 km³.

Hypsometric depth distribution gives a weighted mean depth of 30.3 m with a weighted standard deviation of 2.7 m (Figure 2.3). It displays four modes at -39 m, -32 m, -24 m, and -3 m below lake level (b.l.l.), which represent major morphological levels. These morphological levels are visible in the lake bathymetry as well as in seismic profiles. Most prominent levels are -24 m and -39 m b.l.l., which are present in the entire lake basin creating subaqueous terraces. The -3 m level represents the continuation of the present flat shores of the basin and their submerged platform. An additional level at about -57 m water depth can be recognized only in the deeper areas of the western part as displayed in a longitudinal bathymetric and seismic section (Figure 2.2, 2.4B).

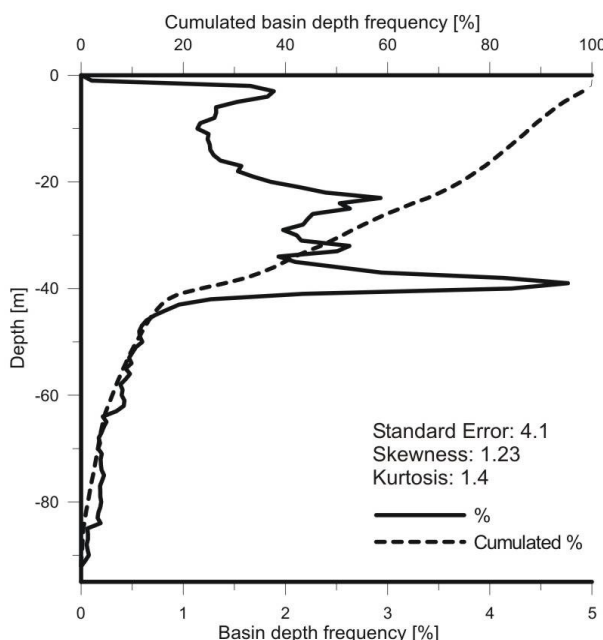


Figure 2.3: Relative and cumulated hypsometric depth distribution of Donggi Cona lake basin and some descriptive statistic parameters of the relative hypsometric depth distribution.

2.4.2 FAULT PATTERN

Major fault lines bound the northern and southern shore of the Donggi Cona basin, respectively, and are already visible in the morphology of the lake basin. Below the lake bottom, fault lines are identified either by distinct morphological steps or slight reflection offsets in the seismic images.

Fault lines are distributed throughout the basin with two major fault lines striking WNW to ESE and NW to SE, clearly marking the northern and southern graben rims in the western sub-basin, respectively (Figure 2.2). These fault lines converge at the western outflow creating the deepest parts of the basin with the southern graben shore representing the escarpment margin of the basin (*sensu* Cohen, 2003). It probably experiences the highest

rates of subsidence and accumulation, as also indicated by the systematic northward deepening of the graben floor along its longitudinal axis. Especially at the northern and western margin of the graben, they are accompanied by several step faults (Figure 2.4A). As part of the accommodation zone of the basin, we found a fault affecting and partly contorting the depositional units by a slight block rotation or sediment compaction (Figure 2.4A, right). Faults are also located north and south of the southern island and west of the northern island. Additionally, sediment relocation is prominent along the steep southern shore (Figure 2.5A) and southern island (not shown).

However, most faults are only visible in connection to basin morphology and downward from about 5 m below the lake floor. Thus, the upper drape onlaps on most tectonic structures like on the step faults at the graben margins as they seem to affect only the lowermost sedimentary unit (Figure 2.4, right).

2.4.3 SEISMO-DEPOSITIONAL UNITS

In most of the seismic transects three main depositional units can be identified, which are assigned as units I to III in ascending stratigraphic order from old to young. At the eastern margin of the lake, however, gas appearance masks a lot of the original stratigraphy (transects 2, 4; Figures 4B, 5B). Differences in depositional thickness and acoustic reflection features mainly depend on their position relative to the basin margins, and vary with the dominant morphological levels at -24 m, -39 m, as well as in the graben below around -43 m. Above around -14 m, there is no sediment penetration due to total acoustic reflection at the sediment surface leading to strong amplitude lake-bottom multiples (Figure 2.4, 2.5). The characterization of the two upper depositional units (II, III) is aided by the lithological information and preliminary age data from sediment core PG1790 that was retrieved at the -39 m level in the north-western part of the lake (Figure 2.6).

UNIT I

The lowermost visible depositional sequence (Unit I) is present at most of the seismic transects throughout the basin and constitutes the main basin infill. It shows a basinward prograding clinoform package of relatively low backscatter (low impedance contrasts, Figure 2.4A, 2.5A). In the eastern part and the northern shore of the lake, Unit I could only tentatively be defined as the lowermost depositional unit. Thus, at the northern lake shore more parallel reflections of low impedance contrast grading upwards into distinctly higher impedance appear on top of a slightly hummocky reflector and compose an up to 10 m thick deposit (Figure 2.5A). It thins out towards the morphological step between the -24 and

-39 m level. However, closer to the depocentre in the western sub-basin some reflection patterns even allow a distinction of two sub-units (Figure 2.4A, 2.5A). Sub-unit Ia consists of several stacked sigmoidal features characteristic for prograding delta systems, which are marked by slight gradual or abrupt reflection changes (Figure 2.5A). They cannot be identified throughout the basin and seem to be restricted to the western part of the lake basin. Below the -39 m level sub-unit Ia reaches thicknesses of at least 30 m. Sub-unit Ib onlaps on sub-unit Ia along the graben margins, where its sediment reaches thicknesses of at least 15 m. It shows more pronounced prograding reflections and an irregular geometry. Its progradation towards the graben seems to be responsible for a steepening of the graben margins (Figure 2.5A). Especially at the eastern margin of the graben (transect 1, Figure 2.4A), sub-unit Ia shows less impedance contrasts and more parallel reflections than sub-unit Ib. Here, a sigmoidal clinoform wedge is visible in Unit Ib with toplaps at around -68 m b.l.l. (Figure 2.4A). It creates the morphological step at -57 m b.l.l. in transect 1 and may be slightly distorted by fault movement and/or post-depositional sediment compaction (Figure 2.4A). Unit Ib thickens towards the graben centre, where it might not be distinguished any more from lowermost sub-unit Ia.

The upper boundary of Unit I has a mainly massive, dark appearance (i.e. strong changes between high and low acoustic impedance) of distinctly higher backscatter and shows hummocky and densely spaced reflections of an erosional surface, unconformably truncating both sub-units everywhere in the basin. However, below -43 m b.l.l. a more parallel reflector marks the boundary towards the upper unit (Figure 2.4A, 2.5A).

An exact estimation of geometry and thickness of Unit I is not possible as reflection multiples and diffractions mask its basal reflector. It cannot be further characterised as it was not recovered in a sediment core.

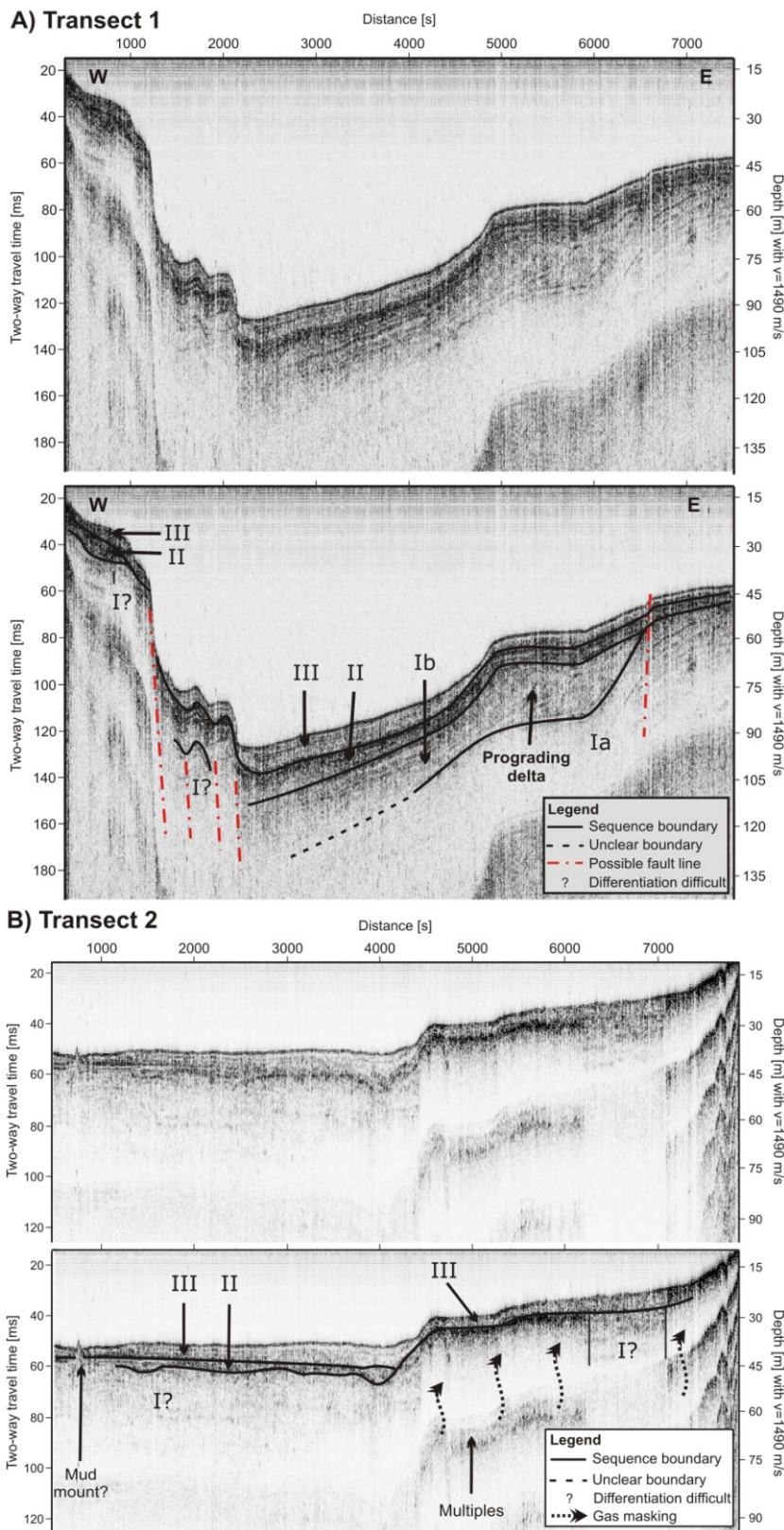


Figure 2.4: Seismic transects in a West-East-longitudinal profile show several morphological levels, depositional units and fault lines interpreted in the lower part. A) Transect 1 is situated at the western sub-basin. B) Transect 2 (eastern part of the lake) has a slight offset of the starting point towards the south (see location in Figure 2.2).

UNIT II

Unit II shows an asymmetric geometry throughout the basin. It could not be distinguished in water depth less than 30 m. Below the -39 m level and towards the basin margins, Unit II displays dark, parallel reflections of high acoustic impedance contrasts. Below the -24 m level, reflection clinoforms of low impedance contrast and varying thickness with a simple sigmoidal (eastern part and accommodation zone) or sigmoidal-oblique (western part) character can be observed (Figure 2.4A, 2.5A). They are interpreted as delta wedges with relatively homogenous sediments of up to 16 m thickness. They display more or less consistent toplaps at -26 to -29 m b.l.l., lense out towards the shore- and thins basinward becoming thicker again in the deepest part of the lake. There, Unit II may reach maximum thicknesses of more than 20 m within the depocentre, where a distinct lower boundary is not detected (Figure 2.5A). The upper boundary of Unit II within the graben is marked by a change to less intense impedance contrasts of the upper Unit III (Figure 2.5A). However, in areas shallower than 39 m water depth, a much more intense reflector of high acoustic impedance shows a sharp boundary towards Unit III. We suggest a drastic change in the depositional environment from prograding to hemipelagic sedimentation in a rapidly rising water body. Thus, the Unit II-III boundary can be interpreted in terms of a maximum flooding surface (MFS). No truncation of Unit II is recognizable, except in areas shallower than 30 m water depth, where Unit II thins out and Unit I appears to be overlain unconformably by Unit III (Figure 2.4B, 2.5B). At the -39 m level, the top of Unit II has been recovered by PG1790 core and consists of unlaminated, silty-sand (Figure 2.6). According to the basal age of the sediment core, the upper part of Unit II has a preliminary age of ~19 cal ka BP.

UNIT III

The uppermost Unit III drapes the lower units everywhere in the Donggi Cona basin onlapping at the basin margins at least from a depth of ca. 14 m b.l.l. This unit displays a more or less constant thickness of 5 m throughout the basin. It shows slightly thicker deposits in the graben, where it consists of a relatively homogenous and parallel reflection sequence of low impedance contrasts (Figure 2.5A). Above 24 m water depth, Unit III shows a relatively diffuse low-frequent reflection pattern. It grades upwards into parallel reflections of very little impedance contrast along the -39 m level. There, Unit III consists of silty-sandy to silty-clayey laminae with higher carbonate contents in the upper parts (Figure 2.6). Unit III is of Late Pleistocene and Holocene age (Figure 2.6). A sharp, very intense, i.e. high-amplitude reflection change masking the uppermost meter of sediment marks the sediment-water interface.

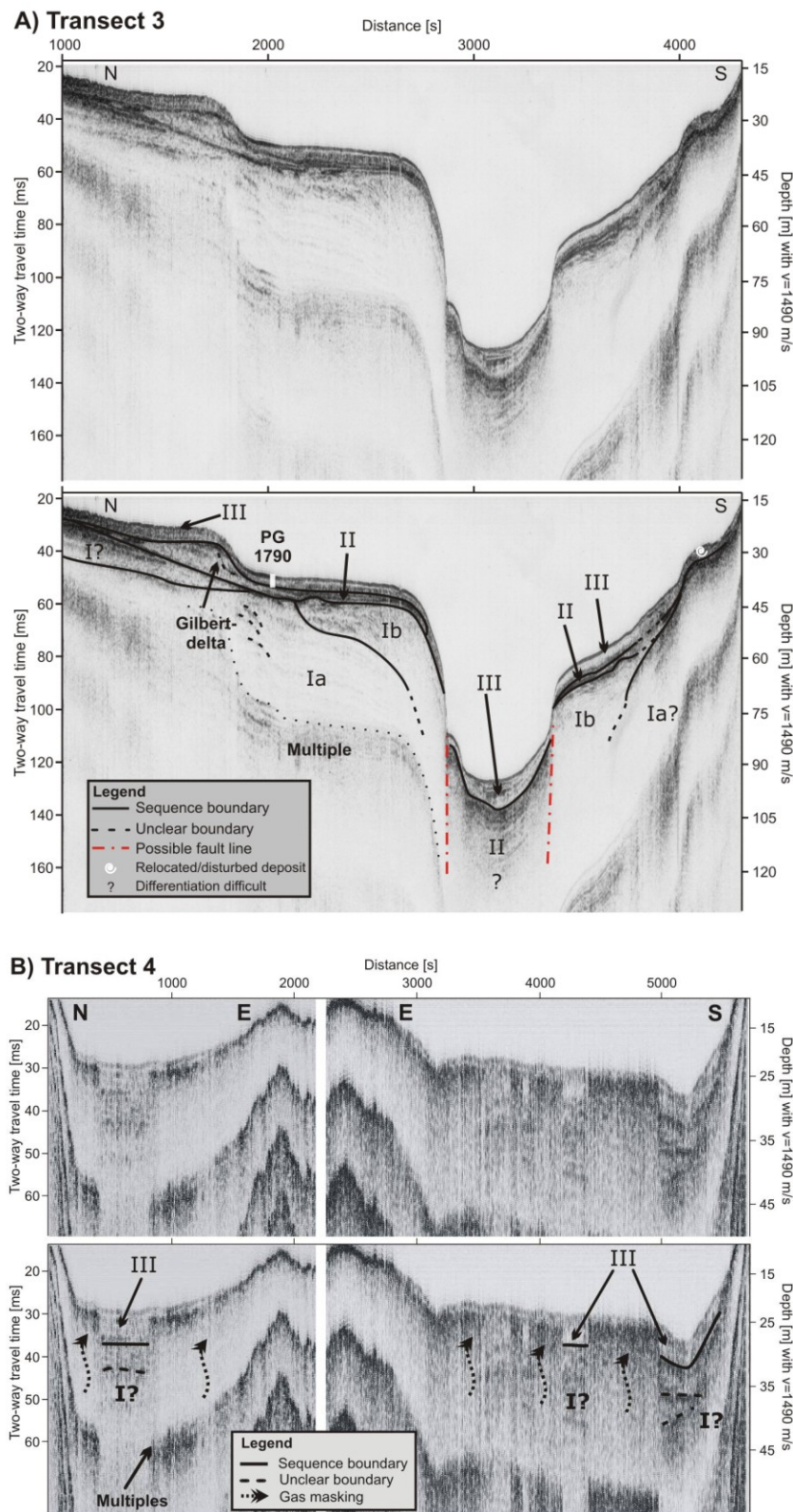


Figure 2.5: North-south seismic transects show several morphological levels and depositional units of varying thickness, as well as major fault lines. A) Transect 3 (western sub-basin) shows location of sediment core PG1790. B) Transect 4 is situated at the eastern part of the lake (see location in Figure 2.2).

At the eastern margin of the lake, where the large alluvial plain enters the lake, patches with higher penetration into partly distorted reflections showed only parts of the depositional stratigraphy (Figure 2.4B, 2.5B). There, some distorted reflections in lowermost Unit I may be attributed to the presence of coarser material or further secondary sequence boundaries. However, most of the stratigraphy is masked by gas, which creates acoustic diffraction and strong backscatter at or near the sediment surface.

2.5 BASIN AND LAKE DEVELOPMENT

2.5.1 TECTONIC BASIN STRUCTURES

Donggi Cona basin is an old, potentially Late Cenozoic pull-apart basin with inherited structures, which formed since strike-slip movement of the Kunlun Fault started. The graben structure in the western sub-basin is bounded by a major WNW to ESE striking fault. However, the continuation of the main branch of the Kunlun Fault remains undetected in the data presented here. In particular along the seismic transect 3 (Figure 2.5A), there is no clear evidence for the location of the main branch of the fault, because the steep WNW to ESE oriented flank separating the basin into a shallow northern and deep southern part is largely of sedimentary origin formed by prograding deltaic deposits. However, it seems reasonable to assume that this up to 52 m high flank was further oversteepened by synsedimentary strike slip movement and deepening of the graben. A secondary branch striking NW to SE bounds the southern steep shore and graben margin of the lake. Thus, a potential bifurcation of the Kunlun Fault at the lake's outflow opens the space for synsedimentary graben subsidence creating a partly stepped morphological height difference. Thus, subsidence alters relative base levels and together with sedimentation and hydrological changes, it is documented by the prominent morphological level at -39 m b.l.l. (Figure 2.4, 2.5A). A phase of high subsidence along the Kunlun fault might have triggered the formation of thick stacked prograding clinoform packages below this level (Unit I).

The two fault branches continue along the eastern part of the lake and clearly mark the northern and southern basin margins, as suggested by Van der Woerd et al. (2002) and Fu and Awata (2007). The southern branch also borders the southern margins of the southern limestone island. Off the island's northern shore the presence of a further fault suggests an island origin as a small-scale pressure ridge within the accommodation zone. The northern island seems to mark the continuation of the major graben fault towards the northern shore of the eastern part of the lake, though clear evidences for this could not be found in our study. As the island is composed of probably uplifted fluvial sediments, we suggest a former extension of the adjacent alluvial fan delta.

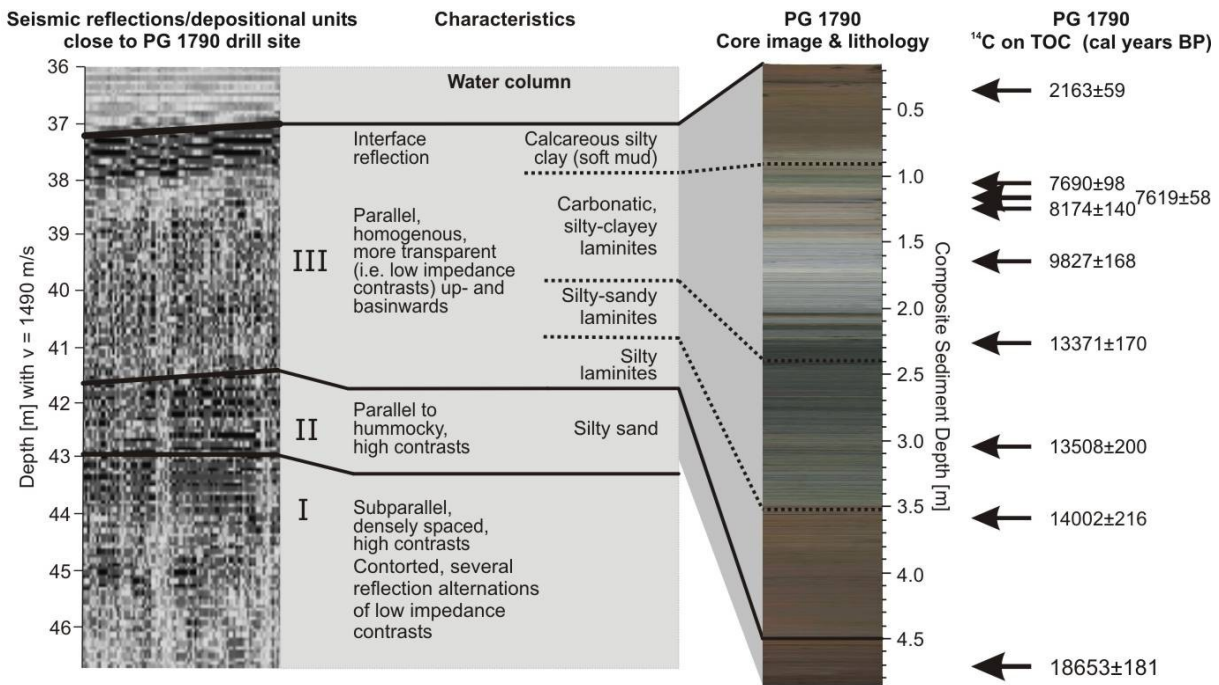


Figure 2.6: Characteristics of seismo-depositional units compared to PG1790 core lithology. Preliminary ages result from AMS-¹⁴C dating of TOC, corrected for a potential reservoir effect of 1983 years (unpublished data).

However, most tectonic structures, especially vertical faults like the step faults along the graben margins, as well as the tectonically altered depositional Unit I are covered now by a soft sedimentary drape, ranging in thickness between 6 m and more than 10 m. Thus, active neotectonic modification by ongoing lateral movement with its slight vertical offsets (Van der Woerd et al., 2002) is not detectable as a strong impact on present basin morphology within the resolvable sediment infill. If supporting evidences are present, they either cannot be detected by our seismic data, or might be even masked by the thick sediment fill of the basin. A minor neotectonic vertical displacement seems to occur along the accommodation zone, where we found a fault, which seems to affect also Unit II and III (Figure 2.4A, right). This structure, however, can also be interpreted as sediment compaction and accommodation along this tectonic hinge.

2.5.2 ORIGIN OF DEPOSITIONAL UNITS

In addition to tectonic processes, basin morphology has been principally shaped by sedimentary processes that were linked to lake level fluctuations and created distinct depositional features. This non-tectonic influence is well documented, e.g. by fossil delta wedges and shore-terraces, which form remarkable morphological steps, along the present shoreline and deeper in the lake at -24 m b.l.l. and -57 m b.l.l. (Figure 2.4).

The geometry of the recognized depositional units from shallow to deep water (Figure 2.5) allows a genetic interpretation on the basis of standard seismic sequence stratigraphy in sedimentary basins (Catuneanu et al., 2009). Additionally, three indicative sequence boundaries and stratigraphic surfaces could be distinguished at Donggi Cona basin: a more tentative downlap boundary within Unit I (Ia/Ib), a very distinct erosional surface (ES) truncating Unit I and a distinct MFS between Unit II and III. Thus in total, we derive a minimum of five process units of sediment accumulation and erosion. Therefore, we principally divided our seismo-depositional units and their respective upper sequence boundaries into high stand systems tracts (HST) and low stand systems tracts (LST) relative to the present lake level (Figure 2.7). Thus, geometrically more symmetric HST show the same thickness all over the lake basin, thinning out and onlapping at the present shores like Unit III. In contrast, during times of low lake stands and low sediment supply from the catchment, sediments of the shallow areas have been completely or partially eroded and/or sub-aerially exposed, leaving typical hummocky reflection surfaces in the shallow areas (sequence boundaries Unit I/II and I/III). However, correlative deposits in the graben could not be distinguished. Additionally, alluvial fan deltas and their correlative sediments prograded towards a lower base level (prograding low stand systems tracts; LST-P), when enough sediment was supplied in a slightly rising water body. They are recognised as sigmoidal to sigmoidal-oblique clinoforms with asymmetric geometry as visible in the depositional Units II and Ib. Former shoreline altitudes can be derived from the toplaps of the prograding clinoforms (Catuneanu et al., 2009) except for Unit Ia, which consisted of several stacked clinoforms missing clearly identifiable toplaps. Two different clinoform types could be traced at Donggi Cona. The sigmoidal-oblique clinoform reflects the steep, concave foreset beds of a Gilbert-type delta (Figure 2.5A), which has formed due to a density contrast between hyperpycnal inflow and the lake water, leading to an instantaneous separation of coarse and fine river load, either by a high suspension load or strong water temperature differences, both expected from melt water during glacial times. Another delta type with simple clinoforms as in Unit Ib (Figure 2.4A) represents a typical prograding alluvial fan delta system similar to those being formed at present, whose inflow channels have more graded fluvial profiles close to equilibrium, especially at the eastern inflow.

Additional information is provided by the internal structures of the seismo-depositional units and their characteristic acoustic impedance, which mainly depends on bulk density. From the lithological comparison with sediments of core PG1790 we propose acoustic impedance at Donggi Cona may be related to grain size distribution, with high impedance indicating sand rich sediments like in the thinner sections of Unit II. The increased sand content seems to be indicative of a lower than present lake stand. Thus, the close delta sys-

tem would bring coarser material to the PG1790 core location at the -39 m level causing the slightly higher impedance contrasts. Within the graben, along its walls and the steeper southern lake shores, higher impedance may also result from intense syn-sedimentary compaction and/or relocation of sediment (e.g. Unit II and upper parts of Unit Ib). The high impedance of the uppermost part of Unit III results from unconsolidated soft mud at the sediment-water interface.

In contrast, low acoustic impedance as in Unit III and the draping geometry of Unit III result from hemipelagic to pelagic environments during higher than present lake stands. In such settings mainly silty to clayey material settles down as is found in sediment core PG1790. However, lithological changes within the upper 4.5 m of the sediment core suggest several changes in the depositional environment during the Holocene, which are not detectable in the seismic profiles. The nature of these changes has to be evaluated by ongoing sediment-core analysis. Low impedance contrasts show also the probably finer grained melt water sediments within the Gilbert delta systems. Additionally, erosion and reworking along steep slopes towards the depocentre lead to thick accumulation of porous fine-grained sediments of low density.

At the eastern lake margin, a typical prodeltaic reflection pattern suggests the continuation of the large alluvial plain, though gas in sediments prevents a further characterization in places (Figure 2.5B). The biogenic gas production may be related to drowned peatland along the large alluvial plain, which developed during a time of lower lake levels. However, within the undisturbed parts an alternation between homogenous fine sediments (i.e. little impedance contrast), and darker, probably coarser material may also reflect submerged channelling or even subaerial erosion.

2.5.3 DEPOSITIONAL HISTORY AND LAKE LEVEL FLUCTUATIONS

Although the estimation of mean sedimentation rates and determination of the exact timing of environmental changes is hindered by poor age constraints, a synoptic view on seismic stratigraphy and lithological changes in sediment core PG1790 allows a tentative inference of lake history. In comparison with findings from nearby lakes, our interpretation provides a first trend of late Quaternary lake dynamics on the north-eastern Tibetan Plateau.

As the vertical neotectonic impact can be considered as relatively low, the morphological levels of the Lake Donggi Cona basin likely indicate substantial variations in lake level related to variations in water supply during at least the Late Quaternary. Based on the cir-

cumferences of sub-aqueous levels described above, estimated changes of the lake area and minimum volume through time are presented in Figure (2.7). A possible range of volumes was calculated without the volume of the uppermost 4 to 6 m thick drape of Unit III. A minimum volume is given for the oldest units, which carry more sedimentary drape than that of Unit III, excluding the temporal and spatial impact of tectonically induced subsidence, as this impact cannot be calculated yet.

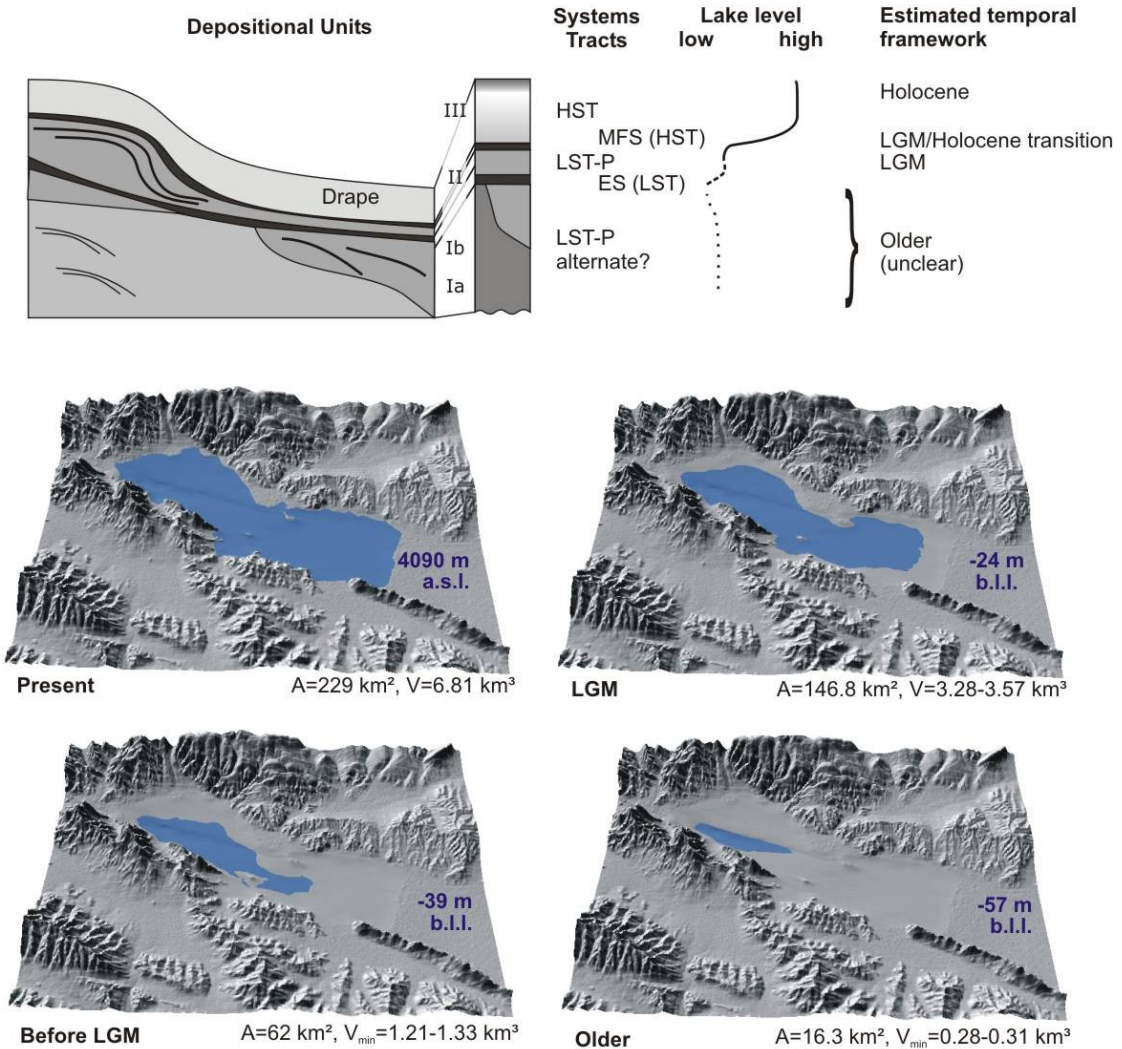


Figure 2.7: Interpretation of seismo-depositional units as high stand systems tracts (HST), low stand systems tracts (LST), and low stand systems tracts with prograding deltas (LST-P) as well as deduction of lake levels below present lake level (b.l.l.), and their respective volume (without Holocene high stand drape of 4 to 6 m). ES (erosional surface) and MFS (maximum flooding surface) are the main sequence boundaries.

During early basin development, Unit I has filled most of the basin with prograding delta sediments in a more or less continuously regressing, low lake level, probably associated with subsidence along the Kunlun fault. The toplaps depth of the delta and prograding low stand systems tracts filling up the space created by along the accommodation zone suggest

that Donggi Cona desiccated down to at least -68 m b.l.l. (i.e. -57 m morphological level, Unit Ib, Figure 2.4A). Due to missing sediment core data a time period cannot be estimated for this very low lake stand with a minimum lake volume of only 4 % of the present volume, thus, indicating a desiccated eastern part of the lake (Figure 2.7).

Later, Unit I has been truncated in a time of a pronounced lake level fall below the -39 m level, as its erosional upper boundary suggests. This truncation might have been of very high and/or long lasting intensity and due to either relative, i.e. subsidence induced, and/or absolute lake level changes (Figure 2.5A).

Afterwards, Unit II deposited during a time of stable, slow lake level rise to at least -29 m b.l.l., as toplap heights of its delta wedges suggest. High carrying capacities along the north-western and western shore of Donggi Cona may have promoted the progradation of the large Gilbert-type deltas. This kind of glacial influence or connection to intense hyperpycnal melt water fluxes could not be found along the eastern part of the lake basin. The inflows there drain generally lower mountain ranges without morphological evidence of near-shore past glaciation. Thus, only simple fluvial deltas without steep foreset beds prograded there towards the lower lake stand. A special case may be found in the large alluvial plain entering the lake from the east and draining the formerly glaciated A'nyêmaqên Shan with probably higher sedimentation rates. However, the respective deposits are masked by gas and could not be described in further detail. At this time, the lake may have reached around the half of its present area and volume (Figure 2.7).

From PG1790 we assume a preliminary age for this lake stand of ~19 cal ka BP, suggesting a time of delta formation during the Last Glacial Maximum (LGM), though still with lower than present lake level. This is in general accordance with low lake level stands at the Tibetan Plateau during this time, where generally cold and dry conditions between the global LGM (ca. 21 cal ka BP) and its termination at ca. 14 cal ka BP (e.g. Wünnemann et al., 1998, 2007b, Herzschuh, 2006) would have caused water to be bounded in a glacial environment causing relatively low run off and sedimentation (Herzschuh, 2006; Mischke et al., 2008). However, a striking explanation of the much lower lake stands and apparently no further higher lake stand before LGM is still missing.

After the LGM, we propose a rapid, continuous lake level rise leading to the formation of the MFS and Unit III. This assumption is in accordance with increasing lake levels in other regions of the Tibetan Plateau, though timing seemed to be asynchronous (e.g. Lehmkühl and Haselein, 2000; Mischke et al., 2008; Schütt et al., 2008). Thus, more moisture became available due to deglaciation and enhanced water supply as a response to a regional or

global warming and/or higher insolation on the Tibetan Plateau. This created a widely extended pelagic environment in the lake dominated by slow settling down of carbonate precipitates, aeolian dust, suspended detrital clay, and the biogenic remains of aquatic algae and plants, zooplankton and benthos, and allochthonous pollen in variable amounts. Changes in environmental conditions and potential short-term lake level fluctuations caused the sedimentation differences as reflected in the sediment core.

This lake level history is in general accordance with lake level reconstructions at various sites with lower than present Late Glacial and high Holocene lake levels (Lehmkuhl and Haselein, 2000; Mischke et al., 2008; Schütt et al., 2008), especially at the north-eastern Tibetan Plateau like at the nearby Lake Koucha (Mischke et al., 2008; Herzschuh et al., 2009). North of Donggi Cona, already Lister et al. (1991) found seismic evidences for rising lake levels and intensification of the East Asian Monsoon during early Holocene at Lake Qinghai. Furthermore, we find littoral terraces and on-shore palaeo-shorelines indicative of higher than present lake levels suggested to have been developed during Holocene.

However, the currently not further resolved and somehow contradictive lake level and sedimentation history of the deeper sediment sequences may be partly related to the chronology presented here. With radiocarbon measurements on bulk organic matter, an overestimation of the TOC ^{14}C -ages is likely due to contamination of aquatic carbon with older terrestrial organic matter washed into the lake. Thus, we can present only preliminary and maximum ages in Figure 2.6, which could be far too old, when considering erosion in the catchment at times of lower base levels. Thus, our data do not exclude a slightly other lake level history with very low lake levels (Unit I) during LGM (and older), while delta formation at slightly higher lake level (Unit II) might have been a response to deglaciation at the Pleistocene/Holocene transition followed by a high-stand phase during the Holocene (Unit III). Further investigation of longer sediment cores and better age control is needed.

2.6 CONCLUSIONS AND OUTLOOK

Basin morphology and the depositional stratigraphy of Donggi Cona lake basin provide useful and spatially connected information on basin development and sedimentation at a highly active Tibetan fault and in a region influenced by the East Asian Monsoon system. The morphological configuration is determined by old tectonical and depositional structures, though ongoing neotectonic activity could not be identified as main factor altering basin morphology at present. Principally, basin morphology is altered by the covering sediments of up to 20 m thickness at the lake margins and more than 30 m in the deeper parts on top of these inherited structures. Thereby, sediment architecture, in parts lithologically

characterised by sediment cores, is determined by sedimentation of terrestrial and lacustrine material, which is a function of basin morphology and lake level alternations. Thus, several morphological levels are created by high and low stand systems tracts, the latter including prograding delta wedges and erosional surfaces, suggesting strongly fluctuating lake levels during Late Quaternary over more than 57 m.

Further analysis of sediment core PG1790 and new core data from other representative sites of the lake identified to consist of well-stratified sediments will help to specify these general trends and enable a characterisation of deeper sediments and determination of the pre-LGM basin evolution. Further extension of the seismic sub-bottom profiling (i.e. deeper surveys) may allow a more detailed mapping of sediment architecture and fault pattern.

However, to resolve the Holocene lake level history quantitatively and in more detail, the on-shore palaeo-shorelines and littoral terraces around the lake resulting from higher lake levels need to be investigated. Additionally, palaeoenvironmental, i.e. glacial, fluvial, and aeolian archives will provide further evidence for the interrelated landscape and lake system dynamics on the north-eastern Tibetan Plateau during Late Quaternary.

ACKNOWLEDGEMENTS

Field work was supported by Ji Yanyun, Chen Jianhui, Yang Qili, Yin Shupeng, and Liu Xiaolong. We thank two anonymous reviewers for very valuable comments. The investigations were financially supported by the German Research Foundation (Deutsche Forschungsgemeinschaft; DFG) and Alfred Wegener Institute for Polar and Marine Research, Research Unit Potsdam.

3. AN END-MEMBER ALGORITHM FOR THE DECOMPOSITION OF GRAIN-SIZE DISTRIBUTIONS

This chapter appeared as an internationally peer-reviewed research article in the *Sedimentary Geology* in 2010 with the title “An end-member algorithm for deciphering modern detrital processes from lake sediments of Lake Donggi Cona, NE Tibetan Plateau, China”. (<http://www.sciencedirect.com/science/article/pii/S003707381100265X>).

ABSTRACT

Deciphering significant sedimentological processes from a set of sediment samples is an important step in reconstructing environmental changes. One approach going beyond classical methods is the unmixing of grain-size distributions. This paper presents a flexible end-member modelling algorithm that is based on eigenspace analysis and considers inherent uncertainties. It has been applied to the detrital grain-size components of lacustrine surface sediment samples of Lake Donggi Cona, Qinghai Province, China. It allows up to five grain-size end-members to be characterised and quantified in an optimal model. An end-member with a major mode in the clay domain accounts for 34 % of variance within the grain-size data set. It may represent sedimentation of suspension load from linear and laminar runoff during heavy precipitation events in summer. Three end-members in the fine sand to medium silt domains make up 60 % of lacustrine sedimentation. They may represent local to remote aeolian processes that peak in wintertime. A multimodal end-member explaining the remaining 6 % of variance may represent further fluvial and littoral dynamics or random fluctuations and measurement errors. Several model runs of different scaling and numbers of end-members provided a suitable way to determine uncertainties inherent to the model. A comparison of 12 different model runs and their respective uncertainties yielded a distinct model of robust end-members. The clay and medium silt end-members are robust features of detrital sedimentation within Lake Donggi Cona. They alone explain 54.4 % of total variance in the data. However, no spatial pattern or relation to water depth is found for any of the grain-size end-members. Thus, when past detrital sedimentation at Lake Donggi Cona is reconstructed, a special focus should be on the robust features attributed to aeolian and suspension-related sedimentation processes as well as on effective sediment mixing processes impeding a distinct correlation between grain size and spatial attributes. Further applications of the end-member modelling algorithm to other depositional environments are encouraged to demonstrate its universal applicability.

3.1 INTRODUCTION

Sediment archives are well suited to study past climatic change, tectonic processes and human impact, though in most cases sediment properties cannot be related to one of these external signal providers alone. An important precondition for extracting signals from sediments and for further reconstruction of signal-related process parameters back in time is to study the modern spatial variation of sediment parameters within a known setting of external signal providers (climate, tectonics, human impact) and to test methodological concepts for evaluating these patterns (Folk and Ward, 1957; Diekmann and Kuhn, 1999; Orpin and Woolfe, 1999; McLaren et al., 2007).

The observable archive properties are a result of multiple process interactions. Depending on the geomorphologic inventory, climatic signals (i.e. changes in temperature and precipitation) in sediments are buffered during and after deposition. Hence, physical and biological processes leave a complex fingerprint in sediments, resulting in correlations between observed sediment parameters. For example, downstream sediment transport is influenced by grain-size ranges in the source area, sediment supply and runoff, while coarser grain sizes within a lake may also be related to a drop in lake level. When sediments of different sources and transport processes are deposited in a sediment sink, they become mixed, e.g. by simultaneous deposition, (bio)turbation, or even by sampling of originally homogeneous layers. Evaluation of this mixture gives a first hint of the main driving forces and directions in sedimentation. Consequently, single archive properties alone are not sufficient to decipher process-related information, whereas correlated properties need to be “unmixed”. Hence, consideration of concept-, method- and scale-dependent uncertainties is crucial as they result in random fluctuations (Hartmann, 2007).

For describing sediment properties and underlying geomorphological, sedimentological or hydrological processes an almost infinite number of variables is possible. However, often only a limited number of properties – mostly physical (e.g. grain-size distribution), geochemical (e.g. mineral composition) and biological (e.g. pollen content) variables – can be measured. The aforementioned variables principally belong to the group of compositional data, i.e. they are nonnegative and sum to a constant (e.g. 100%; Aitchison, 1986; Kucera and Malmgren, 1998; Buccianti et al., 2006). They are mostly expressed as proportions, and a residual variable should be considered for incomplete representations. As a special property of compositional data, $(d-1)$ variables of the full d -dimensional data set are needed to completely describe the whole data (simplex) space. Aitchison (1986) provided first comprehensive approaches to deal with such data and proposed logratio-transformations to transfer the simplex into a Euclidian space.

From a mathematical point of view, many methods provide productive ways to identify different signal-related processes and pathways from compositional data (Arhonditsis et al., 2006; Dechert and O'Donnell, 2006; Christensen and Arora, 2007; Blanchet et al., 2008; Filzmoser et al., 2009). Multivariate statistics provide a popular ensemble of techniques based on concepts of eigenspace analysis for the extraction of palaeoclimatic and palaeohydrological proxies representative for geomorphological, sedimentological and other processes.

The most common representative is principal component analysis (PCA). PCA seeks the best way to describe the data in a low-dimensional linear subspace and, thus, provides a simple explorative-descriptive way to reduce dimensionality. The directions of pairwise orthogonal principal components (PCs) are given by the eigenvectors of the correlation matrix associated with the observed data; their variances derive from the associated eigenvalues. The sizes of the eigenvalues determine a hierarchical order of PCs regarding the amount of variance they capture. Hence, the first PC captures the direction of the highest amount of variance in a data set. Subsequently, all succeeding PCs capture the remaining variance and are orthogonal to (and hence independent of) each other (Reyment and Jöreskog, 1993). The orthogonal data transformation together with a suitable model of the errors allows discriminating PCs containing actual signal and statistical noise. However, a process-based explanation of the data structure is usually not possible.

By contrast, factor analysis (FA) aims to explain the observed data structure with a few linearly independent factors (the first eigenvectors), which are sometimes called "latent variables" (Reyment and Jöreskog, 1993). Not all variability is explained by the factors. FA can be used on a reduced data set (e.g. after a PCA) to consider only the supposed "signal" part of the data space. The factors are optimised, e.g. by a rotation of their low-dimensional orthogonal subspace. The optimisation avoids shortening of curved data clouds as known from PCA, facilitates interpretation of factors, and distributes variability more uniformly compared to the PCs.

Factors are often abstract and not directly comparable to the scales of the original data. That makes it difficult to interpret them in the context of underlying processes or sources. End-member analysis is based on principles of PCA and FA, but aims to provide a genetically meaningful data decomposition. Different scaling procedures ensure the compositional data constraints and characteristic features of the original data set to derive quantitative and geoscientifically meaningful end-members (i.e. unit and scale according to original data; see review in Weltje, 1997). After Weltje (1997), end-members "represent a series of fixed compositions, which can be regarded as distinct subpopulations within the dataset

being analyzed". Mathematically, an end-member may be defined as either a concrete or an idealised population of one or more variables showing a characteristic frequency distribution.

Eigenspace analysis can be combined with other multivariate statistical methods, e.g. with common analyses of the covariance structure such as the calculation of correlation coefficient r (or coefficient of determination r^2). They are popular for geoscientific questions (e.g. Papatheodorou et al., 2006) despite problems with compositional data, which may cause "spurious" results (Aitchison, 1986; Jackson and Somers, 1991; Filzmoser and Hron, 2009).

In this study, we present an algorithm of end-member modelling analysis (EMMA) based on PCA, factor rotation, variable data scaling and a nonnegative least-square estimation to derive previously unknown, geoscientifically meaningful end-members. Subsequently, our method is applied to measured grain-size distributions of lacustrine surface samples from a Tibetan lake as a representative sediment archive. Redundancy in a large set of measured grain-size classes is reduced, and the signal-to-noise ratio is quantified under consideration of the compositional data constraints. An optimal end-member model and the most robust signals within the grain-size distributions are derived from an ensemble of different end-member models. They allow a quantitative estimation of dominant detrital processes within the lake during modern times and an objective consideration of method-specific uncertainties. A flow chart and a MATLAB implementation of our algorithm are provided as an Online Supplement (Appendix 9.1).

3.2 BACKGROUND OF END-MEMBER MODELLING ANALYSIS

3.2.1 MATHEMATICAL CONCEPT OF EIGENSPACE ANALYSIS

In the following, we review the basic concepts of eigenspace analysis used in end-member modelling. A further compilation of the mathematical background of eigenspace analyses can be found in Reyment and Jöreskog (1993).

Let a matrix \mathbf{X}_{ij} contain original data of $i = 1, \dots, m$ observations (rows) concerning $j = 1, \dots, n$ measured variables (columns), e.g. sediment parameters. Observations can be samples from a record (in depth or time) or sites (in space). In multivariate statistics, an eigenspace is typically spanned by the eigenvectors \mathbf{v}_i of a similarity matrix \mathbf{A} with the associated eigenvalues λ_i as linear combinations with a similarity matrix \mathbf{A} :

$$\mathbf{A} * \mathbf{V} = \lambda * \mathbf{V} \quad (1).$$

The similarity matrix \mathbf{A} can be e.g. a correlation or covariance matrix of \mathbf{X} (Filzmoser et al., 2009), the minor product matrix $\mathbf{A} = \mathbf{X}^T * \mathbf{X}$ or the major product matrix $\mathbf{A} = \mathbf{X} * \mathbf{X}^T$ (Miesch, 1980; Weltje, 1997). Matrix \mathbf{V} contains the eigenvector (or PC) loadings, which represent the coefficients of an abstract, independent eigenvector from an input variable (i.e. the composition of the eigenvector). The smaller the angle between an eigenvector and a variable, the stronger the correlation between them. The contribution of each eigenvector \mathbf{v}_i to the variance of the total variable space can be determined from the eigenvalue λ_i . The dimension of the eigenspace equals the number of measured variables. There are different ways to calculate matrices \mathbf{V} from \mathbf{X} and to extract the eigenspace: a) from a similarity matrix \mathbf{A} (see above), b) by singular value decomposition (Renner et al., 1997 for geochemical data), and c) in a multiple way if different blocks of variables exist (Stanimirova et al., 2005).

In PCA and EMMA, the original data \mathbf{X} is predicted with a linear mixing model (Weltje, 1997):

$$\mathbf{X} = \mathbf{M} * \mathbf{V}^T \quad (2).$$

It describes a linear combination of the loading matrix \mathbf{V}_{ij} of j eigenvectors (or PCs) \mathbf{v}_j (for $j = 1, \dots, n$ variables) and the proportion matrix \mathbf{M}_{ij} of $i = 1, \dots, m$ observations concerning the $j = 1, \dots, n$ eigenvectors. Matrix \mathbf{M} contains the eigenvector scores, i.e. the proportions of the compositions of an eigenvector in sample space. It is determined from the inversion of equation (2):

$$\mathbf{M} = \mathbf{X} * \mathbf{V} \quad (3).$$

In most cases, not all variance within the original data set can be explained within the eigenspace (i.e. dimension reduction). Thus, only a few eigenvectors q (with $q < n$) explaining the highest proportion of variability in \mathbf{X} are used (i.e. the “signal portion”). Then, \mathbf{X} can no longer be predicted completely by the mixing model and is divided into a mixture matrix \mathbf{X}'_{ij} and an absolute error matrix \mathbf{E}_{ij} :

$$\mathbf{X}' = \mathbf{M} * \mathbf{V}^T \quad (4)$$

$$\mathbf{E} = \mathbf{X} - \mathbf{X}' \quad (5)$$

The error matrix \mathbf{E} remains an uncertainty representing the “noise portion” or “non-systematic contributions” (Weltje, 1997). There are difficulties to determine the statistical properties of \mathbf{E} , when dealing with compositional data – a problem that could not be solved until now. Hence, the relative error as determined from the correlation matrix of \mathbf{X} and \mathbf{X}' has received more attention than the error matrix \mathbf{E} (Weltje, 1997; Weltje and Prins, 2007).

Following the ideas of factor analysis, we suggest that a rotation of the axes of matrix \mathbf{V} can simplify the structure of the eigenvectors. Then, no order exists between the eigenvectors, and the loadings are distributed more evenly – a condition often used to decipher natural processes. This minimises the range of the mixing coefficients, which do not cover the entire mixing space compared to a standard PCA. However, the factors will be more extreme in general and deviate more from the original observations. Several criteria exist to decide how many factors should be used, though there is no satisfactory conclusive criterion yet. For instance, the criterion of Guttman (1954) takes all eigenvectors with eigenvalues $\lambda_i > 1$. Others use as many factors as needed to explain more than 95% of the cumulative variance (Reyment and Jöreskog, 1993).

3.2.2 APPLICATION OF EIGENSPACE ANALYSIS IN ENVIRONMENTAL RESEARCH

In a palaeoenvironmental and very ideal sense, an eigenspace is an attribute space of interrelated processes or sources recorded in a geo-archive. The axes (i.e. eigenvectors, \mathbf{v}_i) of this space are the underlying processes or sources as linear combinations of measured sediment properties. To “unmix” processes or sources from the properties of sediment archives, factor analysis (e.g. Hartmann and Wünnemann, 2009) and end-member analysis (e.g. Weltje and Prins, 2003; Weltje and Prins, 2007) can be used.

In mineralogy, petrology, geochemistry and provenance studies, factor analysis has been applied to a variety of fields since the 1960s (e.g. Klovan, 1966; Solohub and Klovan, 1970; Zimmerman and Owen, 1990; Reyment and Jöreskog, 1993; Reimann et al., 2002; Juliá and Luque, 2006; Filzmoser et al., 2009).

As stated above, end-members represent the sources involved and underlying processes more directly than factors. With regard to the geochemical components of pure rock, for instance, this rock can be regarded as an end-member described by its geochemical fingerprint. Unmixing the geochemical compositions of sediment samples allows the derivation of the original rock sources, a major topic of classical provenance and fingerprinting studies (Walling, 2005; Garzanti et al., 2009; Collins et al., 2010). Similarly, the grain-size distribution of recently transported sediment, which has been collected from sites obviously dominated by a single sedimentation process, is representative for the site and its typical process regime (Folk and Ward, 1957; McManus, 1988). This is a basic assumption in all types of grain-size analyses (e.g. in sediment trend analysis: McLaren et al., 2007).

To characterise depositional environments, the idea of end-members is statistically more robust than the conceptual, deterministic approach of descriptive moments of single sam-

ples in the sense of Krumbein (1936), Folk and Ward (1957) and McManus (1988) (see discussion in Flemming, 2007). Though Folk and Ward (1957) already identified the mixing processes and manually decomposed the grain-size distributions of sediment samples from the Brazos River bar into different populations, the method of moments meets with difficulties when confronted with multi-modal distributions, which are common in natural sediments (see review in Hartmann, 2007). Typical process-related sediments should rather be described by a grain-size distribution with a limited range of possible distribution shapes. Some approaches suggest that it can be approximated by fitting individual grain-size distributions with theoretical functions (Sun et al., 2002; Bartholdy et al., 2007). For this purpose, theoretical functions are selected with prior knowledge of natural end-members (Orpin and Woolfe, 1999; Flemming, 2007). However, an end-member is an idealised grain-size distribution, which is not necessarily of unimodal shape. As theoretical background for the statistical end-members, Weltje and Prins (2003) introduced the concept of dynamic grain size populations, which are subject to mixing during sediment production and dispersal. EMMA uses all available sediment samples from a mixture in space or within an archive to identify the respective, previously unknown end-members and their contributions to the final archive. This idea is considered to be one of the most promising ways of analysing multi-modal depositional processes from grain-size distributions (Flemming, 2007).

Technically, different types of EMMA are common in several fields of geosciences. In remote sensing, for example, EMMA is called spectral mixing analysis (SMA) and has been applied in the field of passive optical remote sensing associated with the mapping of all kinds of land cover changes (Song, 2005; Robichaud et al., 2007; Sonnentag et al., 2007). In hydrology, an end-member algorithm by Christophersen et al. (1990) helped to distinguish hydrological flow paths from soil water chemistry (Burns et al., 2001; Bernal et al., 2006).

In sedimentology, integrative FORTRAN algorithms for the interpretation of geochemical and grain-size data were designed by Renner et al. (1989, cited in Renner et al., 1997) and Weltje (1997), respectively. Evaluations of their algorithms have been provided by modelling of artificial and extreme compositions (Renner, 1995, 1996; Weltje and Prins, 2007). They unmixed source end-members from the geochemical composition of marine sediments (Renner et al., 1997; Renner et al., 1998; Szefer et al., 2009) or quantified mainly aeolian and fluvial components mixed in the oceans from grain-size distributions of marine sediments (Weltje and Prins, 2003; Holz et al., 2007; Prins et al., 2007; Wan et al., 2007; Hamann et al., 2008).

3.3 GEOGRAPHICAL SETTING

Lake Donggi Cona, also referred to as Dongxi Co or Tuosu Hu, is situated at the north-eastern margin of the Tibetan Plateau in Qinghai Province, China ($35^{\circ}18'N$, $98^{\circ}32'E$, 4090 m a.s.l., Figure 3.1), northwest of the A'nyêmaqên and east of the Kunlun mountain ranges. The summer climate is wet and warm, controlled by intense local convection, and comparable to other high mountain areas (Schmidt, 1999). It is dominated by the monsoon system as the lake basin is located close to the western limit of the East Asian Summer Monsoon trajectories (Domrös and Peng, 1988; An et al., 2001). During the cold and dry winters, extra-tropical westerlies prevail. The mean summer (May to October) and winter (November to April) precipitation is 278 mm and 26 mm, respectively. The mean January (July) air temperature is -16.8 (7.5) °C. Mean annual relative humidity, sunshine hours, total pan evaporation and wind velocity are 59%, 61 %, 1375 mm and 3.4 m/s, respectively (data from Madoi climate station 1958-2007, Chinese Central Meteorological Office, 2007).

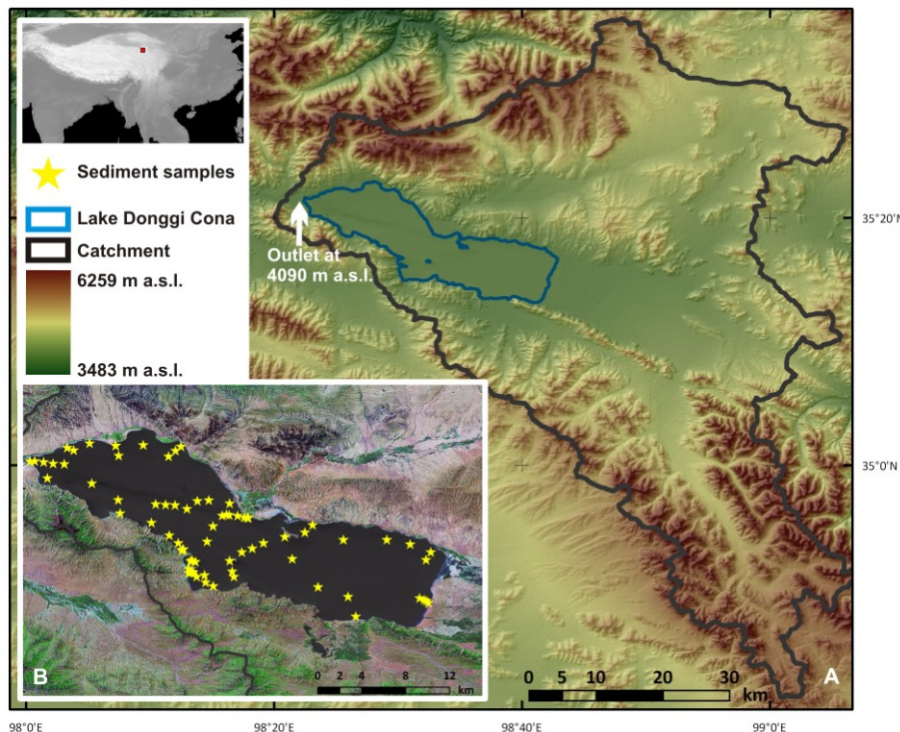


Figure 3.1: Map of (A) Lake Donggi Cona and its catchment, and (B) sampling sites of lacustrine surface sediment samples. Background: elevation (SRTM) and land cover (Landsat7 ETM+ MrSid image, NASA Landsat Program, 2003, USGS, Sioux Falls).

Lake Donggi Cona belongs to a series of pull-apart basins along the Kunlun Fault with a surface area of 229 km^2 and an asymmetric basin structure incised in heterogeneous Permian-Triassic and Neogene rocks (Dietze et al., 2010). Major perennial inflow along a large alluvial plain east of the lake drains the western A'nyêmaqên Shan with varying intra-

annual discharge. Outflow of the lake towards the endorheic Qaidam Basin is currently directed through an artificial channel at the western lake margin (Figure 3.1), which is controlled by a gauge station set up during the 1970s. However, morphological features such as palaeo-shorelines and ancient on-shore terraces occur in the vicinity of the lake and suggest former lake levels above present. Sedimentological and morphological indications for up to 57 m lower lake levels have been described by Dietze et al. (2010) for the Late Quaternary.

Currently the lake is an oligotrophic freshwater lake with oxygen supply down to the lake bottom and a maximum Secchi depth of 12 m (Mischke et al., 2010b). The lake is frozen from late November to early April. It shows no distinct stratification pattern during the unfrozen period owing to full circulation. Biological activity, i.e. ostracoda and aquatic macrophytes, shows a clear distribution with water depth (Mischke et al., 2010b).

At this high elevation site, climate influences the dominant modern geomorphological and depositional processes within the catchment. During summer, intense precipitation leads to fluvial erosion and alluvial accumulation, i.e. by laminar sheet floods along the gentle slopes, bringing the main suspension load towards the lake. The few perennial, some seasonal and numerous short episodic inflows lead to differently sized alluvial cones, which encircle the basin (Dietze et al., 2010; Figure 3.1). During winter time, aeolian displacement of sediment along the slopes and alluvial plain is forced by the dry winter monsoon and leads to several dune fields and loess-like sediments covering most of the slopes. Strong aeolian processes are supported by a sparse vegetation cover of alpine meadows and steppes (Kürschner et al., 2005), which are intensively grazed by yaks and sheep. In the past, glaciations in the northern catchment and at the outflow area supplied huge amounts of glacio-fluvial sediments to the lake during times of substantially lower lake levels (Dietze et al., 2010).

3.4 MATERIAL AND METHODS

3.4.1 FIELD AND LABORATORY ANALYSES

In August 2006, 77 surface sediment samples were collected from the upper 2 cm with a Hydro-Bios-Ekman grab from a boat (Mischke et al., 2010b). Parallel to sampling, water depth at each site was measured, and the position was determined with a handheld GPS. With a second boat, a bathymetric survey of 3977 points was conducted using a Dual-Beam Garmin fishfinder and acoustic sub-bottom profiling, and a bathymetric model of the lake basin was created (Dietze et al., 2010). All surface sediment samples covering a water depth range from 0.6 to 80 m were used to analyse the detrital components of their grain-size dis-

tributions. Therefore, they were pre-treated with 35 % H₂O₂ to remove organic matter and with 10 % HCl to remove the carbonate fractions before being placed on an overhead shaker for minimum eight hours together with 10 mg of a dispersion agent (Na₄O₇P₂*10 H₂O). Then, grain sizes less than 1 mm were finally measured with a laser diffraction particle size analyser (Coulter LS 200, Beckmann Coulter GmbH). Volume percentages of 85 grain-size classes ranging from 0 to 11.31 ϕ were measured and compiled in a data matrix.

3.4.2 END-MEMBER MODELLING ANALYSIS (EMMA) OF GRAIN-SIZE DISTRIBUTIONS

Internal correlation in the variable and sample space may affect the modelling process. Robust but complex procedures exist to resolve the problem of spurious correlation in compositional data (Filzmoser and Hron, 2009), but as the correlation analysis used here is just an additional tool to understand the data structure and modelling process, we calculated Kendall's τ measure of concordance to overcome at least the problems associated with Pearson's r (Aitchison, 1986; Jackson and Somers, 1991), which is very sensitive to outliers and spurious correlation.

The end-member algorithm used in this study is based on Imbrie (1963), Manson and Imbrie (1964), Klovan and Imbrie (1971) and Miesch (1976, 1980). The conceptual modifications of Weltje (1997) have only been partially implemented in our numerical algorithms (see below). Prior to end-member analysis, raw grain-size distributions have been transformed to sum to 100 %. Our algorithm allows two approaches:

- 1) is an iterative loop to find the best fit of the EM model in relation to the original data by testing different numbers of end-members q . The optimal, minimum and maximum numbers of end-members and best EMMA-internal transformations can be determined by overall goodness-of-fit tests.
- 2) defines q manually, i.e. optimal EM model, and allows detailed goodness-of-fit tests and estimation of model inherent uncertainty.

The principal steps of end-member calculation are (cf. Online Supplement):

Step 1. To minimise effects of scale, a transformation becomes necessary (Hartmann and Wünnemann, 2009), as large scale contrasts may result in weak or hidden correlations. Log-ratio transformations are quite popular for compositional data and suitable for geochemical data (Aitchison, 1986; Kucera and Malmgren, 1998). However, too many zero values exist within the grain-size distribution space resulting in numerical problems such as artificial extremes and divisions by zero. Thus, we apply a column-wise *weight transformation* as sug-

gested by Manson and Imbrie (1964) and Klovan and Imbrie (1971). It is based on percentiles P with various lower (l) and upper ($100-l$) boundaries as weights:

$$\mathbf{W} = (\mathbf{X} - \mathbf{h}) / (\mathbf{g} - \mathbf{h}) \quad (6)$$

In general terms, vectors \mathbf{h} and \mathbf{g} are defined by $\mathbf{h}_j = P_l(\mathbf{x}_j)$ and $\mathbf{g}_j = P_{100-l}(\mathbf{x}_j)$, deriving the weighted matrix \mathbf{W}_{ij} from the columns of the original matrix \mathbf{X}_{ij} . A value of $l = 0$ reflects the minimum and maximum of each column, i.e. the transformation after Miesch (1976), which has already been used in the end-member algorithm of Weltje (1997). Different percentiles between $P_{2.5} / P_{97.5}$ and P_{10} / P_{90} are tested to optimise the end-member model.

Step 2. The matrices of *eigenvectors* \mathbf{V} and *eigenvalues* Λ are extracted from the minor product matrix Γ calculated by $\Gamma = \mathbf{W}^T * \mathbf{W}$ as recommended by Weltje (1997). In our MATLAB implementation, we made use of the LAPACK package (Anderson et al., 1999; cf. equation (1)). It is most suitable for the grain-size data set. Normalisation of the eigenvalues gives the degree of variance explained by the eigenvectors.

Step 3. Analogous to factor analysis, rotation of the eigenspace of different numbers of end-members q optimises the unmixing process in our case (in contrast to Weltje, 1997). It is applied to simplify the structure of the end-members, which facilitates interpretation in terms of the original variables (Reimann et al., 2002; Filzmoser et al., 2009) and allows a clear unmixing. A standard orthogonal VARIMAX rotation according to Kaiser (1958) represents our data optimally in comparison to other rotation procedures (not shown).

Step 4. We normalise the *preliminary eigenvector loadings* (\mathbf{V}_{jq}) to ensure the nonnegativity of the rotated eigenvectors, which renders the resulting vectors slightly oblique (cf. similar approach: Clarke, 1978). The *eigenvector scores* (\mathbf{M}_{iq}) are estimated by a linear nonnegative least square algorithm after Lawson and Hanson (1974; cf. equation (3)).

Step 5. Following Weltje (1997), we *reverse* the initial *weight transformation* by using a scaling factor with the respective initial percentile values for \mathbf{h} and \mathbf{g} . This changes \mathbf{V}_{jq} and \mathbf{M}_{iq} to the original units of the initial data set. After a final normalisation to fulfil the initial 100%-sum constraint, we call them end-member loadings (\mathbf{V}_{jq}') and end-member scores (\mathbf{M}_{iq}'), respectively. The variance explained by each end-member is the proportion of total scores variance.

Step 6. Now we calculate the modelled data set \mathbf{X}' and the respective error matrix \mathbf{E} according to equations (4, 5). Goodness of fit is evaluated by calculating mean row- and column-wise linear coefficients of determinations ($r^2 \pm 2\sigma$) between \mathbf{X} and \mathbf{X}' as also suggested by Weltje (1997). This gives the explained proportion of variance of each sample and each

variable, respectively. Within the iterative loop, overall mean r^2 values are calculated. They are shown in the Q-R² mean plot.

The true number of final end-members q in the system is generally unknown. To consider the potential range of q , a minimum number of potential end-members can be estimated by testing whether the logratios of error matrix E are normally distributed (Renner, 1991). Hence, Weltje (1997) checked the multivariate normality of the centred logratio residuals of E by several normality tests, but declared it to be a “far from robust” method. Thus, we define the minimum number of potential end-members q_{min} here by taking at least as many eigenvectors into the VARIMAX rotation (step 3) as needed to explain more than 95 % of total variance in the original data.

As we encountered numerical instabilities with increasing q during the model setup we define the maximum number of end-members q_{max} at the maximum value of r^2 within the Q-R²_{mean} plot, when the model becomes instable. To derive the optimal q_{opt} using grain-size data we follow the general proposal (e.g. Reymert and Jöreskog, 1993; Prins and Weltje, 1999) to take q at the inflection point within the Q-R²_{mean} plot of the final goodness-of-fit test in the loop routine of the model.

Step 7. One single model result is just a scenario with a given likelihood. The likelihood of a model itself can only be reliably estimated by comparing large sets of other similarly likely model runs. Minimum and maximum end-member numbers of models with different weight transformations span the uncertainty range of our EMMA. Within this range different weight transformations are compared in the Q-R²_{mean} plot to derive the optimal percentile weight l_{opt} for step 1. It is defined by the highest r^2 -value at q_{max} . Thus, a certain weight transformation can result in a higher maximal number of end-members q_{max} , but must not necessarily have the highest r^2 of all models. The values l_{opt} and q_{opt} are the basis for the optimal end-member-model.

As an additional step, we test the robustness of the end-members within a narrower uncertainty range. Therefore, we use models with the most stable weight transformations from their respective q_{min} to q_{max} . From the loadings plot, we visually inspect whether there appear some robust end-members in all models. In our case, two end-members (EM1, EM2) are present in all models. Thus, we extract the preliminary eigenvector loadings \mathbf{V}_{jq} of these two end-members of all models under consideration and calculated their mean ($\mathbf{V}_{jq\text{ EMinvar1}}$, $\mathbf{V}_{jq\text{ EMinvar2}}$). Then we put it into the algorithm again, together with a third residual member $\mathbf{V}_{jq\text{ res}}$, and extract the final robust end-members. The residual member $\mathbf{V}_{jq\text{ res}}$ describes the remaining noise in our data, extending the two-dimensional space of our explainable end-

member set. Owing to the orthogonal geometry and the normalisation of the eigenvectors in $(d-1)$ dimensions $\mathbf{V}_{jq\text{res}}$ is given by

$$\mathbf{V}_{jq\text{res}}^2 = \mathbf{1} - \mathbf{V}_{jq\text{EMinvar1}}^2 - \mathbf{V}_{jq\text{EMinvar2}}^2 \quad (7)$$

In the case of random fluctuations and measurement errors, the loadings should be uniformly distributed over grain-size classes and we assume that there are no remaining processes of sediment sorting in our data.

For the reversal of the weight transformation (step 5), we applied the scaling factor with the optimal percentile weight l_{opt} . This type of end-member-model is called our robust end-member model. Confidence levels for the two robust end-members is given as 2σ of the extracted end-member loadings \mathbf{V}_{jq}' (cf. step 5) of each of the selected end-member model runs (i.e. independent of the robust model run).

3.5 RESULTS

3.5.1 GENERAL CHARACTERISATION OF LAKE SEDIMENTS AND EMMA

Grain sizes of surface sediment samples of Lake Donggi Cona showed multimodal distributions with local maxima at 4.2 , 5.4 and 7.5ϕ in the mean curve of all samples (Figure 3.2). However, samples were highly variable in space and did not show a distinct relation to water depth (not shown).

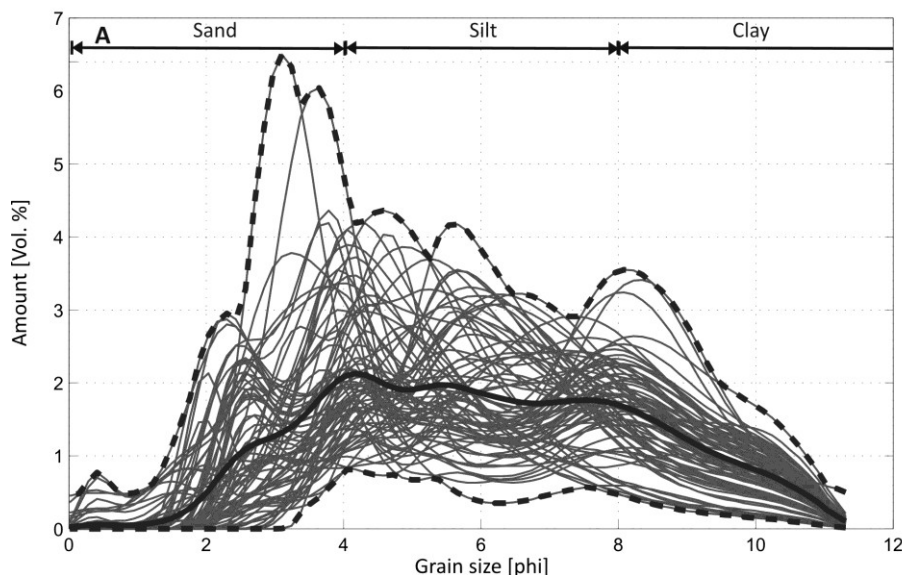


Figure 3.2: Individual grain-size distributions of lacustrine surface sediment samples from Lake Donggi Cona including their mean, absolute minimum and maximum for each grain-size class.

In the grain-size classes $< 1.4 \phi$, 62 % of the samples contained zero values. Kendall's τ coefficients revealed clear statistical associations between adjacent grain-size classes, which

are due partly to the compositional data constraints (i.e. spurious correlation) and partly to measurement-inherent problems (not shown).

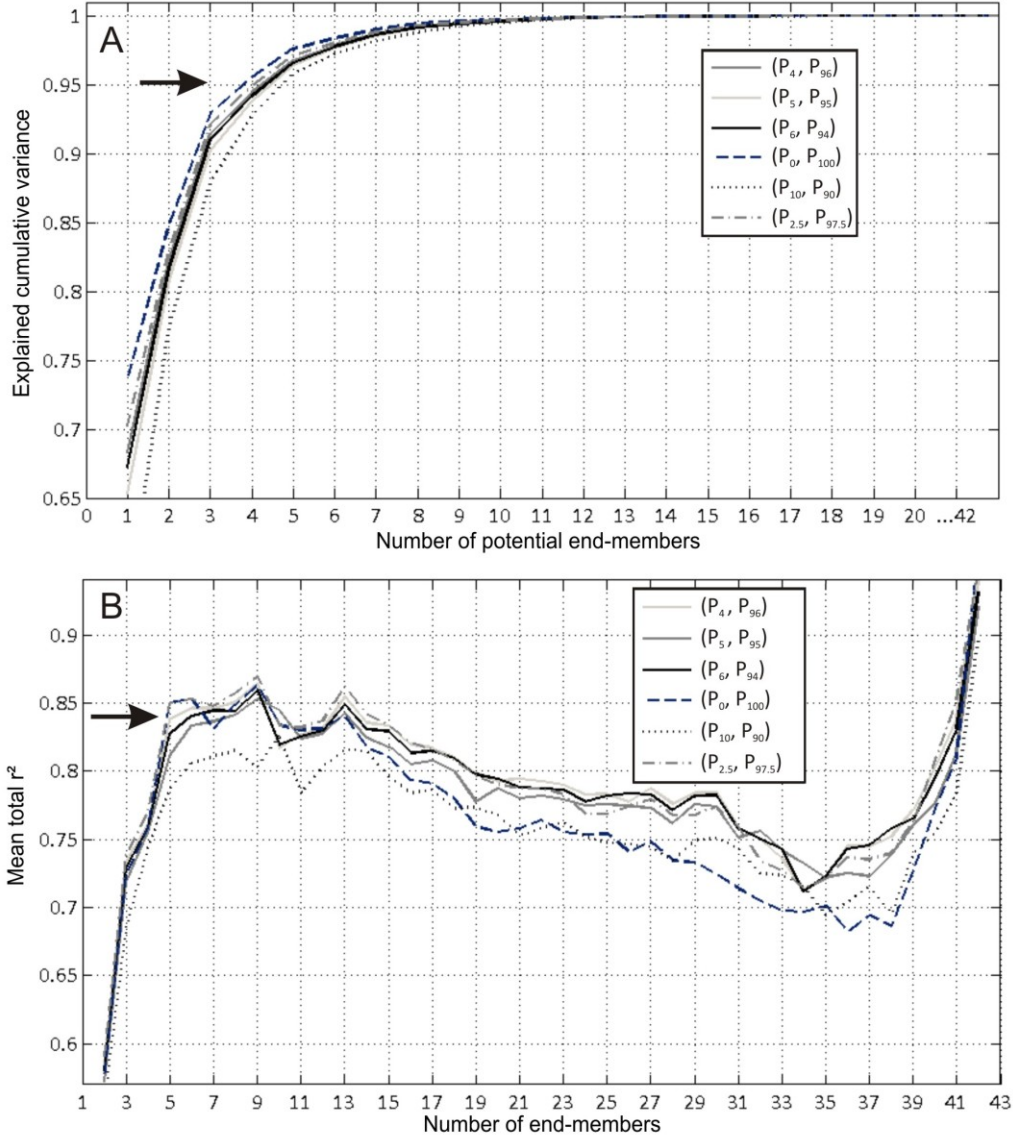


Figure 3.3: Different percentile weight transformations used within the end-member model, with (P_0, P_{100}) being the (min, max) transformation after Miesch (1976). (A) The explained cumulative variance (ECV) of initial eigenvalues is a function of numbers of normalised eigenvectors (i.e. potential end-members q). The minimum number of end-member q_{min} is reached at $ECV > 0.95$ (arrow). (B) The mean coefficient of determination r^2 as function of number of end-members q shows the stability of the model and defines the maximum number of end-members q_{max} at r^2_{max} . The optimal number of end-members q_{opt} can be determined from the inflection point of each curve (area around arrow).

These intense correlations together with an unbalanced variable-to-sample ratio of 85 to 77 lead to a high degree of numerical instabilities during the end-member model setup. As a result, mathematically unfavourable negative eigenvalues occurred and factor rotation broke down during the loop. Thus, we summed up every two adjacent and the coarsest three grain-size classes, which improved the variable-to-sample ratio to 42 to 77. This

avoided negative eigenvalues and led to a stable VARIMAX rotation during the loop. Then, the minimum number of end-members considering all weight transformations was $q_{min} = 4$ (with $l = 0$, Figure 3.3A). However, some numerical instability persisted because two third of the samples still had zero values in the coarsest grain-size classes. This instability became obvious when considering the final goodness-of-fit Q-R²mean plot (Figure 3.3B). The maximum number of end-members considering all weight transformations was $q_{max} = 9$ (with $l = 6$).

3.5.2 THE OPTIMAL END-MEMBER MODEL

The optimal, most stable end-member model showed the best performance when using the weight transformation with $l = 4$ (i.e. with the percentile range of P₄ to P₉₆) and an $r^2_{mean} = 0.85$ at q_{max} in the Q-R² mean plot, i.e. the signal-to-noise ratio in this optimal 5-EM model was 85 to 15. It was stable up to $q_{max} = 8$ end-members and yielded the highest coefficients of determination in the comparison of original with modelled data ($r^2_{max} = 0.86$). The inflection point for this optimum model was reached when using five end-members. Figure 3.4A shows the sedimentologically meaningful end-member loadings. A clear unmixing of the former multi-modal grain-size distributions has been achieved and resulted in end-members 1 to 5 with dominant modes at 8.4 ϕ (clay domain), 6 ϕ (medium silt), 3 ϕ (fine sand), 4.4 ϕ (coarse silt), and 1.7 ϕ (coarse to medium sand). Each of them has some additional minor modes of subordinate importance, whereas EM 5 showed two prominent minor modes in the coarse silt (4.7 ϕ) and clay domains (8.4 ϕ). EM 1 to 5 represent 33.6, 24.0, 19.7, 16.4, and 6.2 % of the total explained variance, respectively.

End-member scores represent the degree to which an end-member contributes to each sample. Therefore, they give quantitative information of end-members in sample space. As in the original data, there was no significant relation to water depth at the sampling site (Figure 3.4B). However, a dominance of the clay EM 1 appears visually in depth ranges around 24 m, which may correspond to a geomorphological level detected in bathymetry (Dietze et al., 2010).

Goodness of fit showed an overall representation of grain-size classes with $r^2 = 0.83 \pm 0.16$ and of samples with $r^2 = 0.85 \pm 0.16$. Figure 3.4C indicates an almost complete representation of some coarse grain-size classes (up to $r^2 = 0.96$ in the class of 0.9 ϕ), a slightly worse representation of ϕ classes around 2 ϕ and a very good representation of ϕ classes in the silt domain of $r^2 = 0.8$ to 0.9. Modelling of the smallest grain-size classes then degrades slightly to $r^2_{min} = 0.6$ at 11.1 ϕ , a class instrumentally difficult to measure. Sample composition was explained by the 5-EM optimal model to always more than 67 % (Figure 3.4D).

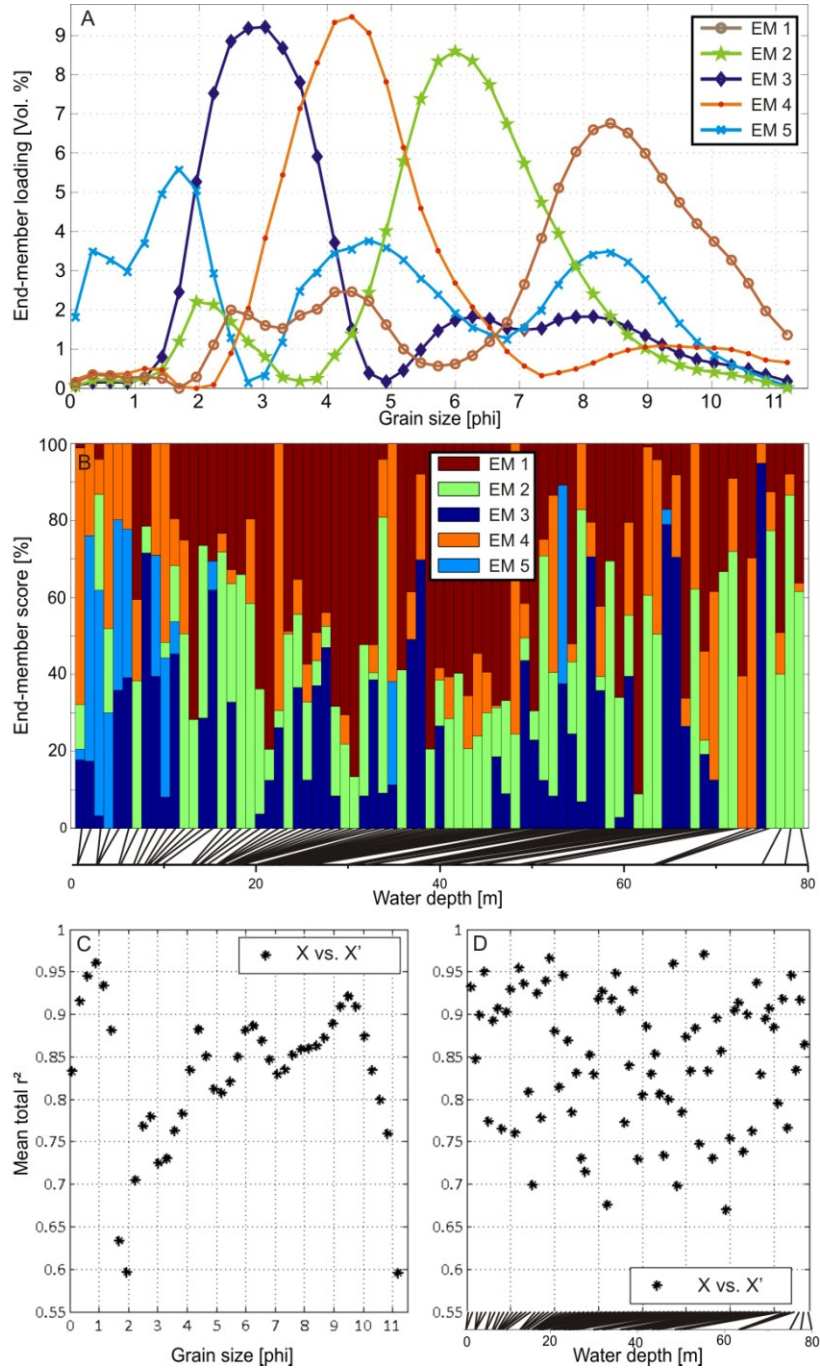


Figure 3.4: Results of the optimal end-member model. (A) End-member loadings represent sedimentologically interpretable unmixed grain-size distributions. (B) End-member scores [%] give the proportion of variance explained by the end-members for each surface sediment sample (sorted after water depth). (C) and (D) show mean variablewise and samplewise coefficients of determination (r^2) as quantitative error estimate.

3.5.3 THE ROBUST END-MEMBER MODEL

For the robust end-member model, we applied only the most stable weight transformations (in our case $l = 4, 5$, and 6 , i.e. the percentile ranges 4-96 %, 5-95 % and 6-94 %, respectively) with a constant minimum end-member number of 5, i.e. from more than 95 % of

initially explained variance, and maximum numbers of 7 to 9, i.e. from the initiation of instability in the Q-R²_{mean} plot (Figure 3.3). Thus, we calculated 12 different EM-models, which are assumed to be of similar probability.

Figure 3.5A (grey lines) shows a plot of all end-members between the minimum and maximum number of end-members possible within these scenarios. The representation of grain-size classes < 5.2 ϕ appears to be highly dependent on the model version and shows no consistent end-member. However, the clay and medium silt end-members (i.e. EM 1 and 2 of section 5.2 with major modes at 8.4 and 6 ϕ) are part of all these end-member models. They represent highly robust end-members. Their final end-member loadings $V_{jq'invar}$ are plotted in Figure 3.5A (coloured) together with their range of confidence as calculated from all 12 end-member models. The robust end-member loadings $V_{jq'invar}$ were clearly within the 2σ range, implying also a representative modelling of the residual member covering the coarser grain-size classes (< 5.2 ϕ). Thus, the clay EM and the medium silt EM explained 29.6 and 24.8 % of the variance, respectively, i.e. both robust end-members together represent 54.4 % of total variance within the original data set. In contrast, the residual member, i.e. the unexplained part of our model, accounted for 45.6 % of the data variance.

End-member scores again did not show a significant relation to water depth as seen also in the quite complex pattern when plotted in space (Figures 3.5B, 3.6). The residual member partly dominated samples of low water depths, especially close to the outlet of the lake and at the northern rim of the eastern sub-basin (Figure 3.6C). The medium silt end-member never constituted an entire sample ($mq'^{max} = 0.94$; Figure 3.6B).

Considering the goodness of variable and sample fit, we found a reasonably good modelling of variables with $r^2 = 0.54 \pm 0.40$ and of samples with $r^2 = 0.7 \pm 0.3$ in the robust end-member model (Figure 3.5C, D). As expected, grain-size classes < 5.2 ϕ were poorly represented (i.e. by the residual member) except for the classes where the two robust end-members had their secondary modes. The finer grain-size classes reached $r^2_{max} = 0.8$. Most of the samples could be explained to always more than 36 % (i.e. $mq'^{min} = 0.36$; Figure 3.5D).

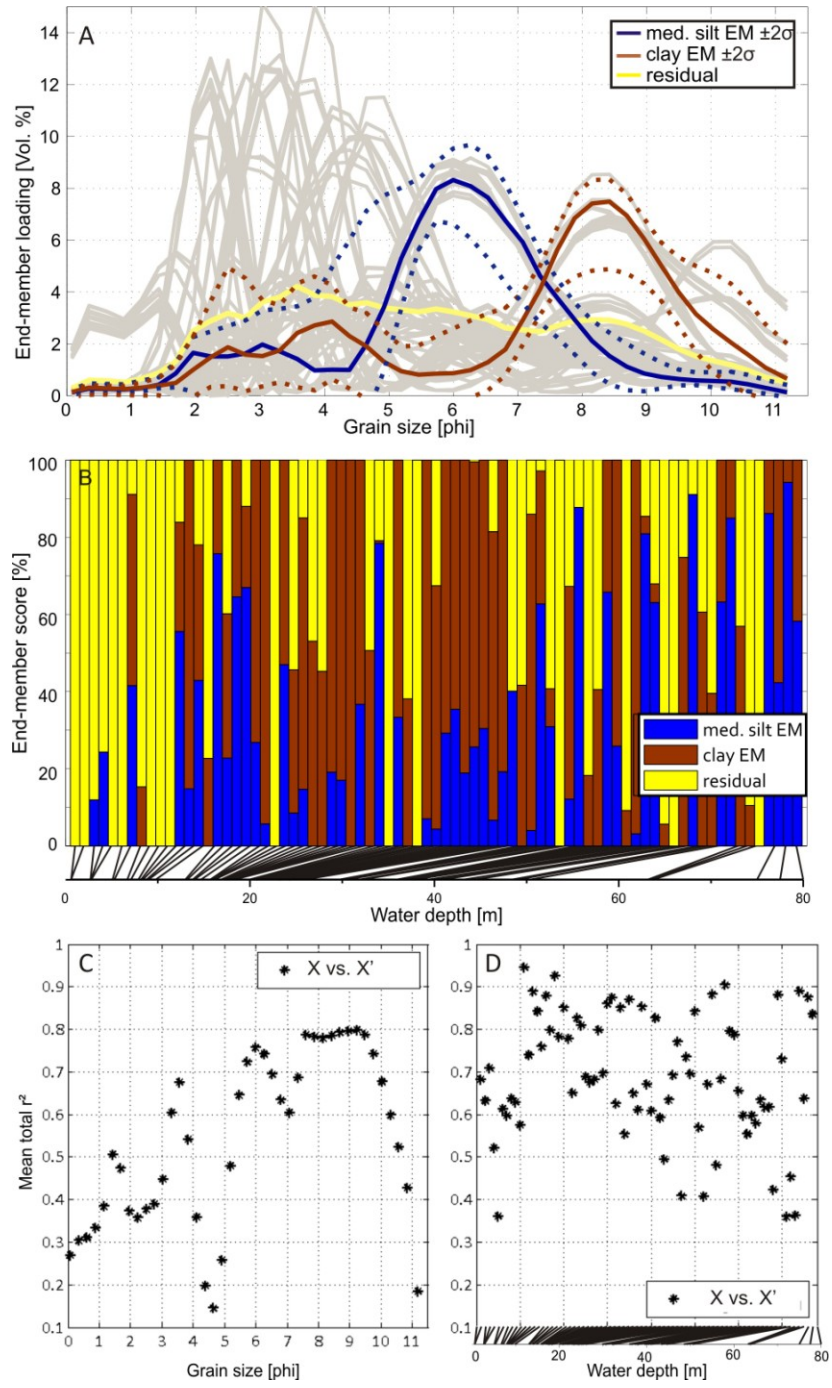


Figure 3.5: Results of the end-member model using only the most robust end-members. (A) End-member loadings represent sedimentologically interpretable unmixed grain-size distributions (gray solid lines: all end-members from the 12 most stable EM model versions; blue solid (dotted) line: mean ($\pm 2\sigma$) of the robust medium silt EM, brown solid (dotted) line: mean ($\pm 2\sigma$) of the robust clay EM, red solid line: residual). (B) End-member scores [%] give the proportion of variance explained by the robust end-members and the residual member for each surface sediment sample (sorted after water depth). (C) and (D) show mean variablewise and samplewise coefficient of determination (r^2) as quantitative error estimate.

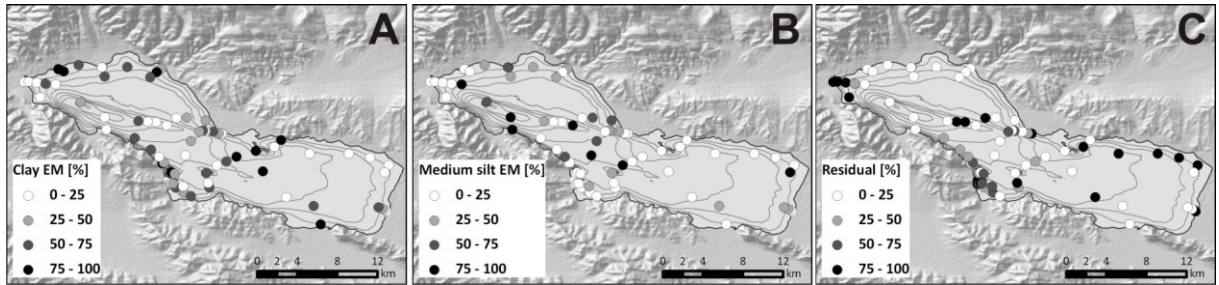


Figure 3.6: High (black) to low (white) end-member scores [%] of the robust (A) medium silt end-member, (B) clay end-member and (C) the residual member as the proportion of variance explained for each sample in space. Bathymetry indicates a water depth range from 0 to -92 m (after Dietze et al., 2010).

3.6 INTERPRETATION AND DISCUSSION

3.6.1 EVALUATION OF THE END-MEMBER MODELLING ALGORITHM

The overall gain of end-member modelling, i.e. the unmixing of geologically feasible, quantitative signals from a set of grain-size distributions, has already been comprehensively discussed by Weltje and Prins (2003, 2007) and users of their algorithm. It overcomes most of the problems in grain-size analyses associated with the methods of moments or fitting of theoretical functions to single distributions (Flemming, 2007; Hartmann, 2007).

Our EM-modelling algorithm provides an additional flexible tool to study mixing problems associated with grain-size distributions in sediment archives. It is partially based on concepts from factor analysis and overcomes problems of interpretability by keeping the scale, nonnegativity and constant-sum-constraint of the original data. It unmixes and derives meaningful end-members in a feasible way and has been implemented in the common programming environment of MATLAB (see Online Supplement). It is not restricted to the study of modern sediment compositions and contributes to a better operationalisation in grain-size analyses as demanded by Hartmann (2007).

Furthermore, the algorithm and its set-screws provide the opportunity to quantify the model's inherent setup uncertainty. Hence, models can be run considering different numbers of end-members and flexible weight transformations. They are assumed to have a similar likelihood, and a fixed single outcome is avoided. The overall gain of considering the uncertainties is the possibility to detect robust process components in any kind of sediment system, thus achieving a higher level of end-member modelling.

However, some limitations still remained unsolved in our algorithm. Thus, we had to deal with numerical instabilities, which could not be solved completely by the aggregation of grain-size classes. It seems to be a data-inherent problem and a result of the measuring

technique. First, the instabilities may result from the classical problem of redundancy, as compositional data are sufficiently described by $(d-1)$ variables. Thus, the transformation of the grain-size classes to the Euclidian data space could not be performed, as too many zero values hindered the classical use of logratio transformations, as e.g. suggested by Filzmoser et al. (2009) for the standard FA. Although we are aware of these limitations, we believe that applying the end-member analysis algorithm on grain-size distributions without a logratio transform is still possible (cf. Weltje, 1997).

Second, numerical instabilities may result from overspecification, when too many end-members have been chosen and noise is modelled. This may not only be a statistical problem alone, but depend on the natural conditions in the study area and the sampling strategy. Hence, we suggest a highly differentiated sediment production and dispersal results from the heterogeneous lithology in the subcatchments of Lake Donggi Cona, which cannot be resolved by the number of our samples. Additionally, the lacustrine sediment samples used in this study do not represent a purely random sampling strategy, as they were chosen according to ecological considerations (Mischke et al., 2010b). Thus, the deepest parts of the lake are poorly represented, and a clustering of samples occurs in a water depth around 24 m. Further, sedimentation rates cannot be assumed to be equal at all sites.

3.6.2 DETRITAL PROCESSES WITHIN LAKE DONGGI CONA

Within the limitations mentioned, detrital processes in Lake Donggi Cona can be interpreted from the end-members of the optimal 5-EM model. Typical distribution shapes may be linked with certain depositional processes following the classical understanding of grain-size sorting and distribution processes during sedimentation (in the tradition of, for example, Krumbein, 1936; Folk and Ward, 1957; McManus, 1988). Observations of sedimentological processes within the Donggi Cona catchment during field campaigns in the summers of 2006 and 2009 and the winters of 2007 and 2008 as well as reference surface samples from near-shore and catchment-wide characteristic depositional environments (IJmker et al., unpublished) allow further interpretation of the shapes of end-member grain-size distributions. Thus, we suggest that minor modes within the single end-members are more natural than an end-member from a fit with theoretical unimodal functions (Flemming, 2007).

Thus, the clay EM 1 represents suspended sediment from fluvial and alluvial processes. During field campaigns in summertime, a high load of suspension in linear and laminar runoff has always been observed during heavy precipitation events. Collected reference samples suggest multi-modal grain-size distributions within the runoff, though with an

obvious mode at the clay grain sizes, which has not been observed as such in reference samples of other depositional environments.

Further, we can specify EM 3 as sandy well-sorted, probably dune sediment and the well-sorted, silty EM 2 and 4 as local and remote dust, respectively. That implies that around 60 % of variance in modern Donggi Cona lacustrine sediment composition may be attributed to aeolian sedimentation, which is the most characteristic and effective transport process during wintertime.

Sand EM 5 is poorly sorted, has actually three prominent modes and explains only 6 % of total variance in the data. It represents sedimentation environments of more heterogeneity, as is typical of fluvial and on-shore depositional dynamics at the end of sediment cascades in subcatchments with heterogeneous sediment production and dispersal.

From the robust EM model runs, we learned that only the clay and medium silt end-members are robust features of surface sediment samples in Lake Donggi Cona. They are the most important detrital components of the lake sediments. As in the optimal end-member model, they are interpreted as representing sediment contributions from suspension load and remote dust. Within a range of uncertainty, they are signals which explain about 30 % and 25 % of the variance in the sediment's grain-size distributions, respectively. The residual variance represents different unspecific processes of higher energy during sedimentation, which may be linked with more random distribution of grain sizes at Lake Donggi Cona.

In contrast to biological activity (Mischke et al., 2010b), a clear relation of grain-size distributions to water depth and spatial pattern is missing (Figure 3.6). Apart from the sampling limitations mentioned above, two reasons for the rather random grain-size distribution of these sediments may be discussed. One is the freezing of the lake during half of the year at a time when aeolian processes peak. At that time, the wind carries most of the sediment to the lake, where it collects at ice cracks and on the partly snow-covered ice surface. It melts at random sites during spring and contributes randomly to the surface sediment composition. Also a contribution of poorly sorted ice rafted debris may superimpose a continuous sedimentation.

Further influence of lake-internal transport by currents has to be considered. During spring and summer, the lake is saturated by oxygen down to its bottom (Mischke et al., 2010b) suggesting an intense water circulation, which can bring coarser material to deeper sites. Suspension load seems to be mainly distributed along the prominent -24 m geomorphological level, whereas the remaining residual variation, as representative for unspecific

coarse grain sedimentation, could partly be associated with the near-shore areas and more turbulent water flow close to the outlet. However, the relation of the clay end- member and the residual to water depth was not significant at all and may also be an artefact from sampling strategy.

The effective mixing processes play a major role at Lake Donggi Cona and might not be as strong in other sediment systems. They pose special difficulties for determining process-related sediment properties, which we manage to deal with using the described EMMA algorithm. Within the given uncertainties we explained 55 % of the variance by only two robust end-members attributed to aeolian and suspension-related sedimentation. This is a fairly good result considering all sedimentological processes contributing to grain-size variation within a lake.

3.7 CONCLUSION AND OUTLOOK

We provide a flexible end-member algorithm based on eigenspace analysis with a combination of known scaling procedures and multivariate methods (see Online Supplement). It can be used to provide genetically meaningful, quantitative grain-size end-members. These are representative for sedimentological and geomorphological processes within a sediment sink of highly correlated variable structure. Our algorithm helped to decipher robust sediment components of the modern detrital system within a Tibetan lake by integrating several model runs of presumably similar likelihood. Hence, end-member loadings allow the respective end-members to be characterised, while end-member scores give the proportions of variance of each end-member within a sample.

Concerning the specific local environmental conditions at Lake Donggi Cona we gained two new insights: first, the missing association of the grain-size end-members to water depth suggests that effective sediment mixing processes take place within the lake. Second, only two components are robust features of our lake system, i.e. the clay and medium silt end-members attributed to suspension-related and aeolian sedimentation processes. Consequently, we should focus on them when decomposing grain-size data from sediments going back in time, as these are the main processes quantifiable in our lake system.

Our algorithm is not restricted to lacustrine depositional environments alone. It may be used in any grain-size analysis studying any kind of modern or past sediment system. When studying a variety of sediment archives along a topologically linked sediment cascade, alteration of end-member scores can be used to assign significant environmental changes to certain signal providers such as climate change, tectonics or human impact.

Insight into past variations of the robust sedimentological processes in the Donggi Cona area will be provided by end-member modelling using grain-size components from lake sediment cores and catchment-wide sediment archives as proxies for limnological and environmental changes. Their contribution to sediment composition can then be compared to modern times, allowing also a comparison of background sedimentation triggers. The interpretation of the end-members can further be specified by including geochemical data of certain grain-size fractions to better understand sediment provenance – a method already successfully applied by Weltje and Prins (2003).

Further alterations of the EMMA algorithm have to be considered: the problem of redundancy in the $(d-1)$ dimensional simplex has not yet been solved, and no rigorous model exists for the error matrix E . This may be partly related to the least-square estimation within EMMA, which may be inappropriate in the simplex space and might make EMMA still non-rigorous from a statistical point of view. Finding alternatives and solving these mathematical problems would be a big step forward. Further error estimation should include also Bayesian approaches like those performed by Palmer and Douglas (2008) on geochemical data. Background information can be derived from different model runs and the modern climatic, tectonic and human setting.

ACKNOWLEDGEMENTS

We would like to acknowledge the financial support within the frame of DFG priority programme 1372 “Tibetan Plateau: Formation - Climate - Ecosystems”, which enabled a PhD-workshop on EMMA. We warmly thank Gert Jan Weltje, three anonymous reviewers, Reik Donner and Michael Dietze for very constructive comments on the manuscript, and Anne Beck for language editing.

4. HIGHER THAN PRESENT LAKE STANDS AT LAKE DONGGI CONA

4.1 ONSHORE LAKE TERRACES

Onshore terraces that encircle Lake Donggi Cona were first mentioned by Van der Woerd et al. (2002). They represent higher than present lake stands, consisting in part of lacustrine and littoral sediments (Chapter 4.2). To assess and quantify the former lake extents, Lockot (2010) compiled data from geomorphological mapping, as well as tachymetric and differential topographical surveys. Four morphological levels with characteristic flat surfaces (treads) and scarplets (risers) were distinguished by applying statistical methods to the survey points. Hence, four higher lake stability phases are described at 3.5 ± 0.4 m, 6.1 ± 1.0 m, 10.1 ± 0.9 m, and 16.7 ± 1.2 m above the present lake level (a.p.l.l.; T1 to T4 including 1σ error, Figure 4.1). The lake reached areas (volumes) of 277 km^2 (7.85 km^3), 293 km^2 (8.58 km^3), 321 km^2 (9.88 km^3), and 358 km^2 (12.28 km^3) during the lake stages of T1 to T4, respectively (Lockot, 2010; cf. Figure 5.1).

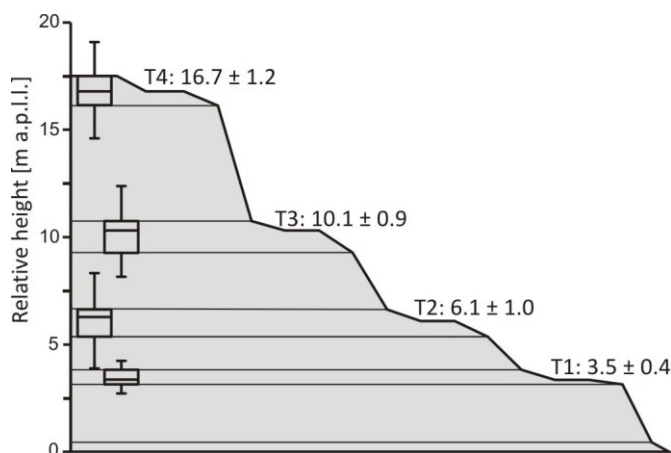


Figure 4.1: Onshore terrace heights above the present lake level of Lake Donggi Cona (after Lockot, 2010).

Lockot (personal communication, spring 2012) discusses several reasons for the varying ranges in terrace level elevation and the separation of terrace subgroups. Lockot concludes that mainly post-genetic, sub-catchment specific erosional and sedimentary processes contributed to the high variability of T3 and T4 terrace elevations, whereas short-term lake level fluctuations seem to be responsible for the site-independent subgroups of T2 terrace. Post-genetic alteration of the terrace heights by tectonic impact were excluded, because no association between height subgroups and the pattern of the Kunlun fault system was found. Terrace dating can be done indirectly using lake high-stand sediments, which provide a unique and highly resolved lake level archive.

4.2 LAKE HIGH-STAND SEDIMENTS

This chapter has been submitted to the international peer-reviewed journal Quaternary Research in August, 2012 as research article with the title “Early to mid-Holocene lake high-stand sediments at Lake Donggi Cona, north-eastern Tibetan Plateau” (<http://dx.doi.org/10.1016/j.yqres.2012.12.008>).

ABSTRACT

Lake high-stand sediments are found in three onshore terraces at Lake Donggi Cona, north-eastern Tibetan Plateau, and reveal characteristics of hydrological changes on lake shorelines triggered by climate change, geomorphological processes, and neo-tectonic movements. The terraces consist of fluvial, alluvial to littoral-lacustrine facies. End-member modeling of grain size distributions allowed quantification of sediment transport processes and relative lake levels during times of deposition. Radiocarbon dating revealed higher than modern lake levels during the early and mid-Holocene. Lake levels follow the trend of Asian monsoon dynamics, and are modified by local non-climatic drivers. Site-specific impacts explain fluctuations during the initial lake level rise ~11 cal ka BP. Maximum lake extension reached ~9.2 cal ka BP, at ~16.5 m above present lake level (a.p.l.l.). Littoral and lacustrine sediment deposition paused during a phase of fluvial activity and post-depositional cryoturbations at ~8.5 cal ka BP, when the lake level fell to ~8 m a.p.l.l. After a second maximum at ~7.5 cal ka BP, lake level declined slightly at ~6.8 cal ka BP, probably due to a non-climatic pulse that caused lake opening. The level remained high until a transition towards drier conditions of ~4.7 cal ka BP. Though discontinuous, high-stand sediments provide a unique, high-resolution archive.

Keywords: Lake level fluctuations; Lake high-stand sediment; End-member modeling (EMMA); Grain size distributions; Tibetan Plateau; Asian monsoon

4.2.1 INTRODUCTION

The Tibetan Plateau (TP) provides water to billions of people in Asia and heavily influences the global climate circulation (Qiu, 2008). Moisture availability on the TP is regulated by different circulation systems – wet summer monsoons from the Indian and Pacific Oceans interact with the westerlies and dry winter air masses from the Siberian anticyclone. However, the past interplay of these systems is still under discussion (Chen et al., 2008, Wang et al., 2010).

One way to better understand moisture variability is to study lake level changes. Ancient lake stands can record shifts in the precipitation-evaporation balance of a catchment (Cohen, 2003). Lake stands respond to water supply from glaciers and thawing permafrost, but can also reflect modifications of the basin and catchment configurations. Indications of lake high-stands have been observed on the TP for a long time (e.g., De Terra and Hutchinson, 1934). More recently, shorelines and beach ridges were dated with ^{14}C and OSL (Lee et al. 2009; Li et al., 2009). There are only a few studies from the western TP (Gasse et al., 1991), Ladakh (Wünnemann et al., 2010), and the northern foreland of the TP (Madsen et al. 2008, Long et al., 2010) that consider lake high-stand sediment sequences in detail, i.e., intercalations of lacustrine, littoral and terrestrial sediments deposited above present lake level (a.p.l.l.).

Using stratigraphy and granulometry, this study reconstructs sedimentological processes from intercalations of terrestrial and lacustrine sediment deposited during high-stands of Lake Donggi Cona. Because the Donggi Cona catchment is part of an active tectonic fault system, a major aim is to distinguish climatic from non-climatic triggers of lake level changes using environmental reconstructions of the lake and its vicinities.

4.2.2 STUDY AREA

Lake Donggi Cona fills a pull-apart basin at the Kunlun Fault ($35^{\circ}18'\text{N}$, $98^{\circ}32'\text{E}$; Figure 4.2), which has a mean annual slip rate of $\sim 10.3\text{ mm/a}$ along the Donggi Cona segment (Van der Woerd et al., 2002). Seismic studies (Dietze et al., 2010) and fluvial terraces (Van der Woerd et al., 2002) suggest that vertical motion has been of minor importance in the lake and its catchment during the Holocene.

Climatic conditions in the vicinity of Donggi Cona are characterised by a total pan evaporation of $\sim 1375\text{ mm/year}$, mean air temperatures in January (July) of -16.8 (7.5) $^{\circ}\text{C}$ and mean annual precipitation of $\sim 300\text{ mm}$ (Madoi station, 4272 m a.s.l., ~ 50 km southwest, Chinese Central Meteorological Office, 2008). Precipitation falls mainly in summer ($\sim 280\text{ mm}$ between May and October) as intense torrential rain from local convection of the Asian summer monsoon air masses, which reach their northern limit here (Domrös and Peng, 1988). Overland flows, reactivation of ephemeral channels, and rivers transport the main suspension load to the lake. The lake is normally frozen from late November until early April, when westerlies and the winter monsoon prevail, and bring dry winds that mobilize aeolian sediments from Pleistocene and Holocene dune fields, loess, and loess-like sediments (Lehmkuhl, 1997; IJmker et al., 2012a). In addition, dust can be captured discontinuously in the lake ice (Dietze et al., 2012). Several phases of aeolian activity and reworking of

aeolian sediment were reconstructed for the Holocene (Stauch et al., 2012). Yak and sheep grazing on alpine steppes and meadows also cause sediment mobilization (Schlütz and Lehmkühl, 2009). Wet hummocky land surfaces and small thermokarst depressions indicate that discontinuous permafrost affects saturated sediments close to the lake and in local depressions.

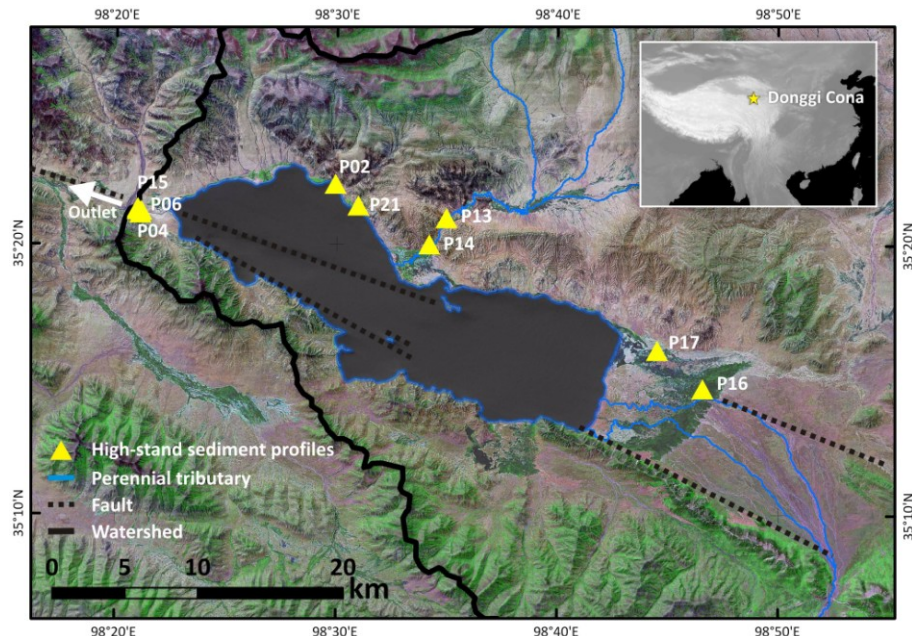


Figure 4.2: Donggi Cona lake basin and its catchment on the north-eastern TP [inset]. Main Kunlun fault after Van der Woerd et al. (2002) and assumed in-lake continuation after Dietze et al. (2010). Triangles indicate the locations of high-stand sediment sections (cf. Google Earth kmz-file).

The heterogeneous geological and geomorphological catchment configuration includes dissected series of carbonates, limestones and sandstones faulted against quartzites and shales, all partly overlain by conglomerates. In the upper catchment, lateral moraines and U-shaped valleys indicate past glaciations, while fluvial incision formed V-shaped valleys in the middle reaches. Major perennial inflow enters the lake from the east via a large alluvial plain. The only other perennial stream enters the lake from a flat basin north of Lake Donggi Cona via a transverse valley (Figure 4.2).

The current lake level is at 4090 m a.s.l. Palaeo-shorelines and ancient onshore terraces that contain lake sediments encircle the lake and indicate four higher lake stands at 3.5 ± 0.4 m, 6.1 ± 1.0 m, 10.1 ± 0.9 m and 16.7 ± 1.2 m a.p.l.l. (T1 to T4, Lockot, 2010). Three lower Pleistocene lake stands at 24, 39 and 57 m below the present lake level were reconstructed using bathymetry and seismic stratigraphy (Dietze et al., 2010). A deglaciation-related lake level rise with strong fluctuations between 17.5 and 14 cal ka BP, was followed by a drop at 14 cal ka BP that produced saline conditions (Mischke et al., 2010a, Opitz et al., 2012), while

higher levels prevailed between ~4.3 and 11.5 cal ka BP (Opitz et al., 2012). There is debate regarding when the lake switched to an open system: at ~6.8 cal ka BP when a change in ostracod assemblages from euryhaline (brackish) to fresh-water species occurred (Mischke et al., 2010a); or at ~4.3 cal ka BP as suggested by changes in the geochemical and mineralogical properties of lake sediments (Opitz et al., 2012).

Today, the lake drains through an artificial channel at the western margin, south of the active course of the Kunlun fault. It merges with a perennial stream that originates from the north and then drains towards the northwest (Figure 4.3A). A gauge station was set up during the 1970s to control the water supply towards the endorheic Qaidam Basin.

4.2.3 METHODS

4.2.3.1 FIELD METHODS

During May and September 2009, nine high-stand sediment sections at Lake Donggi Cona were described at modern fluvial channel exposures, permafrost decay fronts, anthropogenic gravel pits or were dug along terrace front slopes (Figures 4.2, and 4.3). The highest elevation of the lake sediments was determined using a differential GPS. Sedimentological structures and layering were described, including major macroscopic characteristics such as sediment colour, charcoal, and snail fragments. Burrows and distorted sediment layers indicate post-depositional alteration of the sections. Additionally, pedological description focused on features of redoximorphosis, clay and carbonate relocation, and root penetration.

4.2.3.2 LABORATORY METHODS

The complete sections of P06 and P14, and the lake sediment parts of sections P15, P02 (undisturbed parts) and P21 (including matrix material within gravel layers) were analysed. Prior to analysis, all samples (taken in 2cm slices at different intervals) were sieved to <1mm. Larger grain fractions were not considered, as only 26 samples had material >1mm. To account for the detrital components of the grain-size distributions, 262 samples were pre-treated with 10% acetic acid to remove the carbonate fraction, and 35% H₂O₂ for at least 72 h to remove organic matter, before being placed on an overhead shaker for at least 12 h, together with 10 mg of sodium pyrophosphate. Grain size distributions were measured with a laser diffraction particle size analyser (Beckmann Coulter LS 200, calculated with a Fraunhofer model). Volume percentages of 85 grain-size classes from 1000 to 0.38 µm were compiled in a data matrix.

4.2.3.3 STATISTICAL METHODS

Single grain size parameters such as sand, silt, and clay contents, or the associated methods of moments (e.g., mean, skewness, kurtosis), are biased when applied to multi-modal distributions (Dietze et al., 2012), which is why such results were omitted here. Instead, the original grain size distributions were unmixed using end-member modeling analysis (EMMA) – an eigenspace decomposition with different scaling procedures that extract genetically meaningful end-member grain size distributions (i.e., loadings) and their percentages in each sample (end-member composition, i.e., scores; Dietze et al., 2012). End-members (EMs) can be interpreted in terms of sediment transport processes, and thus, characterize typical depositional environments (following e.g., Folk and Ward, 1957).

The 10th quantile ($l = 0.1$) was applied in the weight transformation after Dietze et al. (2012), which yielded the best unmixing and modeling results compared to other model configurations. The robustness of the resulting end-members was tested by different weight transformation and single section EMMA runs (results not shown). A normalized difference between the finest and coarsest end-members (i.e., EM_{diff}) was calculated as a proxy for relative lake level change – assuming that the finest particles deposit in calm, deeper water, while fractions coarser than silt settle close to the shore, shortly after entering the lake.

4.2.3.4 RADIOCARBON DATING

AMS dating of eight sediment sections was done at Poznan radiocarbon laboratory. Because pollen dating failed due to poor preservation, 14 bulk lake sediment samples, two charcoal remains, and three non-recrystallized (aragonite) *Radix* shells were dated. The potential hard-water error for TOC was determined by dating the topmost samples of three lake cores, including their 2σ -errors (Opitz et al., 2012). The up-to-date absolute minimum and maximum hard-water errors for bulk sediment (i.e., 1920 and 2360 years, respectively) were subtracted from all bulk and snail ^{14}C ages. Then, all samples were calibrated with IntCal09 (Reimer et al., 2009) in Calib 6.1.0 (Stuiver and Reimer, 1993). The absolute minimum and maximum in the 2σ -ranges of the corrected and calibrated ages give a larger uncertainty than usual after calibration, but represent a more realistic consideration of the potential hard-water and reservoir effects. All mean ages mentioned in the text and figures refer to corrected, cal ka BP.

4.2.4 RESULTS AND INTERPRETATION

4.2.4.1 SEDIMENT SECTIONS AND RADIOCARBON DATING

High-stand sediment sections were grouped according to relative elevation and location. They are located at the outlet (P15, P04, P06), at the northern T3 shore (P02, P21, P14, P13) and at the eastern alluvial plain (P16, P17; Figure 4.2 and 4.3; Table 4.1).

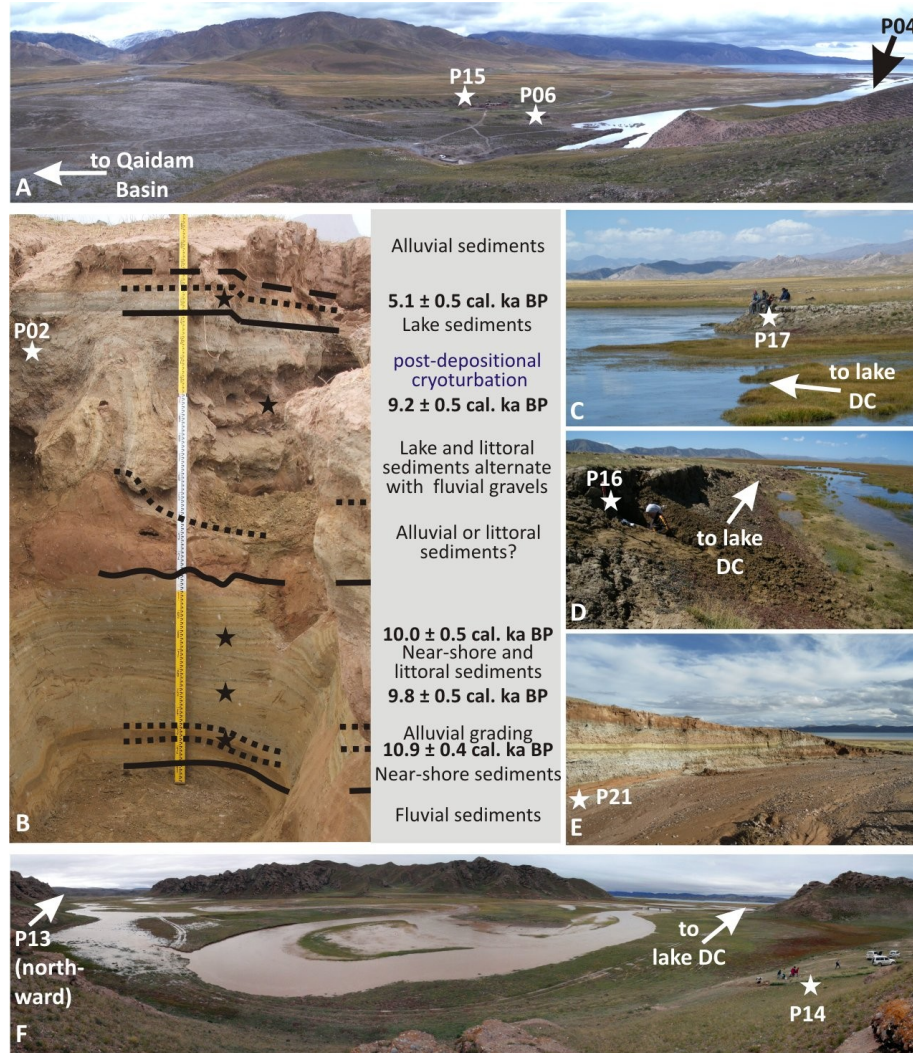


Figure 4.3: Sites of onshore lake high-stand sediment sections at the outlet (A, view to north), at the northern shore (B, E, F) and on the eastern alluvial plain (C, D). B shows the stratigraphy of section P02, exemplarily. For locations see Figure 4.2.

| High-stand sediment section | Latitude | Longitude | Elevation [m a.s.l.] | Relative height [m a.p.l.l.] | Terrace, where section is in* | Total profile length [cm] | Description | No. of dated samples | Analysed in lab |
|-----------------------------|----------|-----------|----------------------|------------------------------|-------------------------------|---------------------------|--------------------------------------|----------------------|-----------------|
| P02 | 35.3712 | 98.4989 | 4100.8 | 10.8 | T3 | 290 | Exposure in active gully system | 5 | yes** |
| P04 | 35.3529 | 98.3515 | 4099.5 | 9.5 | T3 | 242 | Stepped dig at lake sediment outcrop | 1 | no |
| P06 | 35.3550 | 98.3494 | 4094.8 | 4.8 | T2 | 340 | Old Tibetan cave entry | 3 | yes |
| P13 | 35.3503 | 98.5828 | 4101.2 | 11.2 | T3 | 70 | Dig at lake sediment outcrop | 0 | no |
| P14 | 35.3346 | 98.5705 | 4101.1 | 11.1 | T3 | 330 | Stepped dig at lake sediment outcrop | 3 | yes |
| P15 | 35.3561 | 98.3495 | 4106.4 | 16.4 | T4 | 132 | Exposure at sand pit | 1 | yes |
| P16 | 35.2451 | 98.7764 | 4100.5 | 10.5 | T3 | 260 | Exposure at edge of erosional hill | 2 | no |
| P17 | 35.2688 | 98.7420 | 4092.9 | 2.9 | T1 | 130 | Exposure at edge of thermokarst lake | 1 | no |
| P21 | 35.3579 | 98.5162 | 4099.7 | 9.7 | T3 | 278 | Exposure at river bank | 3 | yes |

Table 4.1: General characteristics of onshore high-stand sediment sections at Lake Donggi Cona.
*after Lockot (2010), **only for non-cryoturbated part

Table 4.2 contains all dating results with 2σ -errors. All high-stand sediments were deposited between ~11.4 and ~3.5 cal ka BP (Figure 4.4). There are two main age clusters in the early and mid-Holocene. High-stand lake sediments accumulated at >8 m a.p.l.l. until ~7 cal ka BP in T4 (P15) and T3-terraces (P04, P02, P21, P14, and P13), while mid-Holocene lake sediments dominate lower elevations and are exposed in T2 (P06) and T1 terraces (P17). The highest section, P15, has an age of ~6.9 corr.cal ka BP, which is ~1.5 ka younger than an OSL-age of the loess at its top (section P063 at the base: 8.5 ± 0.8 ka, Stauch et al., 2012). The OSL-age coincides with a hiatus in lake sedimentation between 8.2 and 8.7 cal ka BP (Figure 4.4). There are also stratigraphically inverted ages in P06 and P16.

| ID (Fig. 4.3) | Sediment section | Sample name | Depth below surface (cm) | Absolute height [m a.p.l.l.] | Sample material | Laboratory No. | Mean [^{14}C years] | 1 σ [^{14}C years] | Minimum [corr. years BP]* | Maximum [corr. years BP]* | Mean [corr. cal. years BP]** | 2 σ [corr. cal. years BP]** | Remark |
|---------------|------------------|-------------|--------------------------|------------------------------|---------------------------------|----------------|-------------------------------|-------------------------------------|---------------------------|---------------------------|------------------------------|------------------------------------|-----------|
| 1 | P15 | P15 222-224 | 69 | 15.722 | TOC (bulk sed. <0.3mm) | Poz-44734 | 8190 | 100 | 6270 | 5830 | 6905 | 400 | roots |
| 2 | P02 | P02_3 20-22 | 21 | 10.621 | TOC (bulk sed. <0.3mm) | Poz-44731 | 6620 | 80 | 4700 | 4260 | 5113 | 467 | roots |
| 3 | | P02_3 94-91 | 92.5 | 9.906 | TOC (bulk sediment) | Poz-44729 | 10490 | 140 | 8570 | 8130 | 9237.5 | 458.5 | |
| 4 | | P02_1 73-77 | 215 | 8.681 | TOC (bulk sediment) | Poz-32088 | 11100 | 160 | 9180 | 8740 | 10049 | 508 | |
| 5 | | P02_1 46-50 | 242 | 8.411 | TOC (bulk sediment) | Poz-32087 | 10920 | 180 | 9000 | 8560 | 9848.5 | 529.5 | |
| 6 | | P02_1 18-22 | 270 | 8.131 | TOC (bulk sediment) | Poz-32086 | 11710 | 160 | 9790 | 9350 | 10958 | 444 | |
| 7 | P04 | P04 10-12 | 151 | 7.961 | Charcoal pieces | Poz-44732 | 9000 | 100 | not necessary | 10085.5 | 160.5 | | |
| 8 | P14 | P14 274-276 | 55 | 10.583 | Radix snail | Poz-35904 | 8740 | 100 | 6820 | 6380 | 7464.5 | 286.5 | |
| 9 | | P14 53-55 | 276 | 8.373 | Radix snail | Poz-35903 | 11690 | 120 | 9770 | 9330 | 10801 | 503 | |
| 10 | | P14-131 | 296 | 8.173 | Charcoal (courtesy: S. Mischke) | Poz-45579 | 9190 | 120 | not necessary | 10371.5 | 135.5 | | |
| 11 | P16 | P16 210-212 | 49 | 10.01 | TOC (bulk sediment) | Poz-35943 | 6590 | 80 | 4670 | 4230 | 5101 | 474 | cryoturb. |
| 12 | | P16 30-32 | 229 | 8.21 | TOC (bulk sediment) | Poz-35942 | 5890 | 80 | 3970 | 3530 | 4110.5 | 416.5 | cryoturb. |
| 13 | P21 | P21 215-220 | 22.5 | 9.519 | TOC (bulk sediment) | Poz-35944 | 10460 | 120 | 8540 | 8100 | 9201 | 424 | |
| 14 | | P21 4-6 | 375 | 5.994 | TOC (bulk sed. 0.75mg C) | Poz-36025 | 10890 | 120 | 8970 | 8530 | 9833.5 | 402.5 | |
| 15a | P06 | P06 230-233 | 107 | 3.745 | Radix snail | Poz-32194 | 7330 | 100 | 5410 | 4970 | 5949 | 351 | |
| 15b | | P06 230-234 | 107 | 3.746 | TOC (bulk sediment) | Poz-32093 | 7640 | 120 | 5720 | 5280 | 6293 | 372 | |
| 16 | | P06 200-204 | 137 | 3.446 | TOC (bulk sediment) | Poz-32092 | 6660 | 80 | 4740 | 4300 | 5205.5 | 380.5 | |
| 17 | | P06 48-51 | 290 | 1.916 | TOC (bulk sediment) | Poz-44733 | 9140 | 120 | 7220 | 6780 | 7841 | 328 | |
| 18 | P17 | P17 42-44 | 43 | 2.505 | TOC (bulk sed. <0.3mm) | Poz-44735 | 5685 | 70 | 3765 | 3325 | 3852 | 388 | roots |

Table 4.2: Dating of high-stand sediments of Lake Donggi Cona. *Subtraction of absolute minimum and maximum ^{14}C -years (hard-water correction, corr.) of topmost samples of cores PG-1900, -1901, -1790 (i.e., 1920 and 2360 years; Opitz et al., 2012), **Calibration (cal.) using IntCal09 (Reimer et al., 2009)

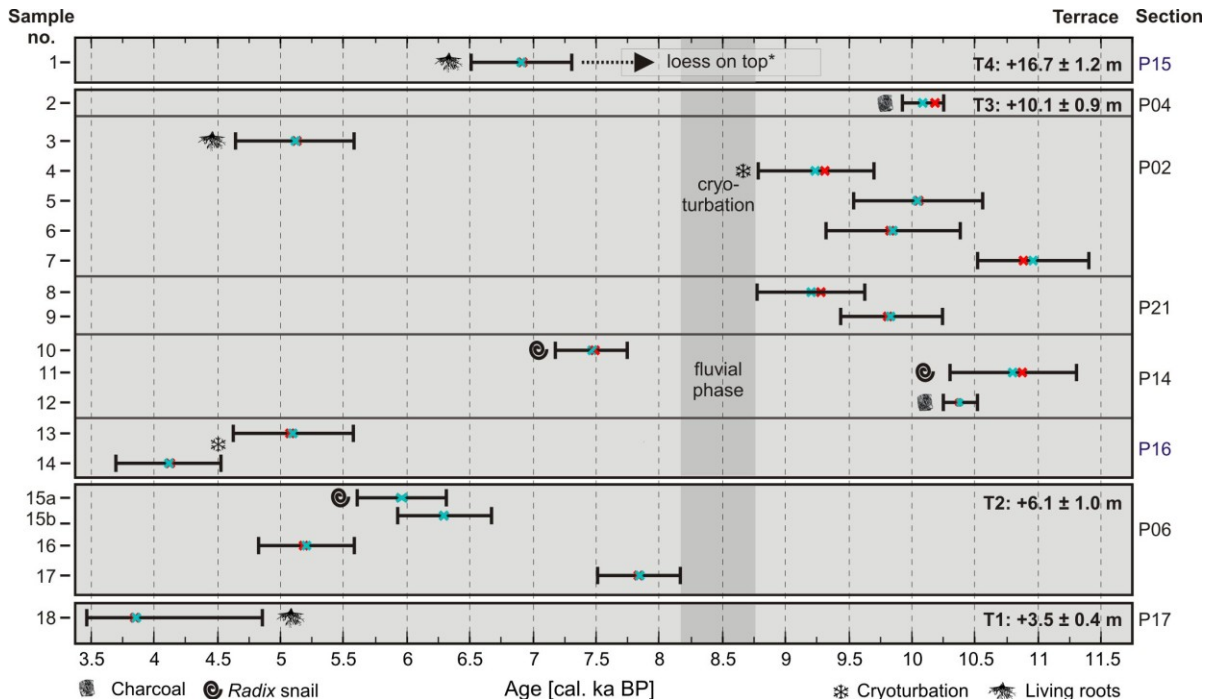


Figure 4.4: Corrected and calibrated ages of high-stand sediments including error bars. Sections are separated by bold lines. Dated sample numbers refer to Table 4.2 (left axis) and are sorted by depth in each section. Remarks are added, when distinct sediment properties may bias the reliability of the age. The grey blocks in the background show the associated onshore terrace (right axis, Lockot, 2010). Red and blue crosses mark the median and mean ages. *OSL-age P063 for comparison (Stauch et al., 2012)

4.2.4.2 CLASSIFICATION OF DEPOSITIONAL ENVIRONMENTS

All sections show several sedimentation unconformities (“U” in Figure 4.5), and have sub-catchment-specific sedimentation rates and grain sizes. Figure 4.5 shows generalized section sketches with depositional zones assigned to three sediment facies that represent different depositional environments along the littoral zone (Figure 4.6). Sites are too heterogeneous to integrate them in one “composite” section, but they can be preliminarily correlated using the elevation, ages, and characteristics of deposited sediments and their post-depositional overprint.

Sediments of Facies I bear a platy structure, high clay and carbonate contents, grayish-green or whitish-blue color with post-depositional oxidized spots. *Radix* and *Gyraulus* snails are common. Facies I can be found in all sections except for P13 and P15 (Figure 4.5). A large part of P06 contains mm-thick, clayey and silty laminae. In P14, high amounts of carbonate tubes were found above and below a unique thin, dark layer at ~67 cm depth. At sites P16 and P17 and at ~170 and ~210 cm depth of P04, Facies I sediments show a more

granular structure (Figures 4.5 and 4.6). Facies I is interpreted as lake sediment deposited in a deep water environment, below the wave-dominated zone (Figure 4.6). There, organic matter, carbonate precipitates, silt and clay can settle causing the typical platy structure, or even laminations. The black, organic-rich layer in P14 could represent short-term sapropel deposition.

Facies II sediments are generally loose, well-sorted, mainly sandy, coarser deposits that are found in most sections. In section P21, for example, the fine sands at the base and the shingle bedding of cobbles at ~165 cm depth are assigned to this Facies (Figure 4.5). Facies II is interpreted as littoral sediment (Figure 4.6); silts and clays are washed out and distributed by currents within the lake.

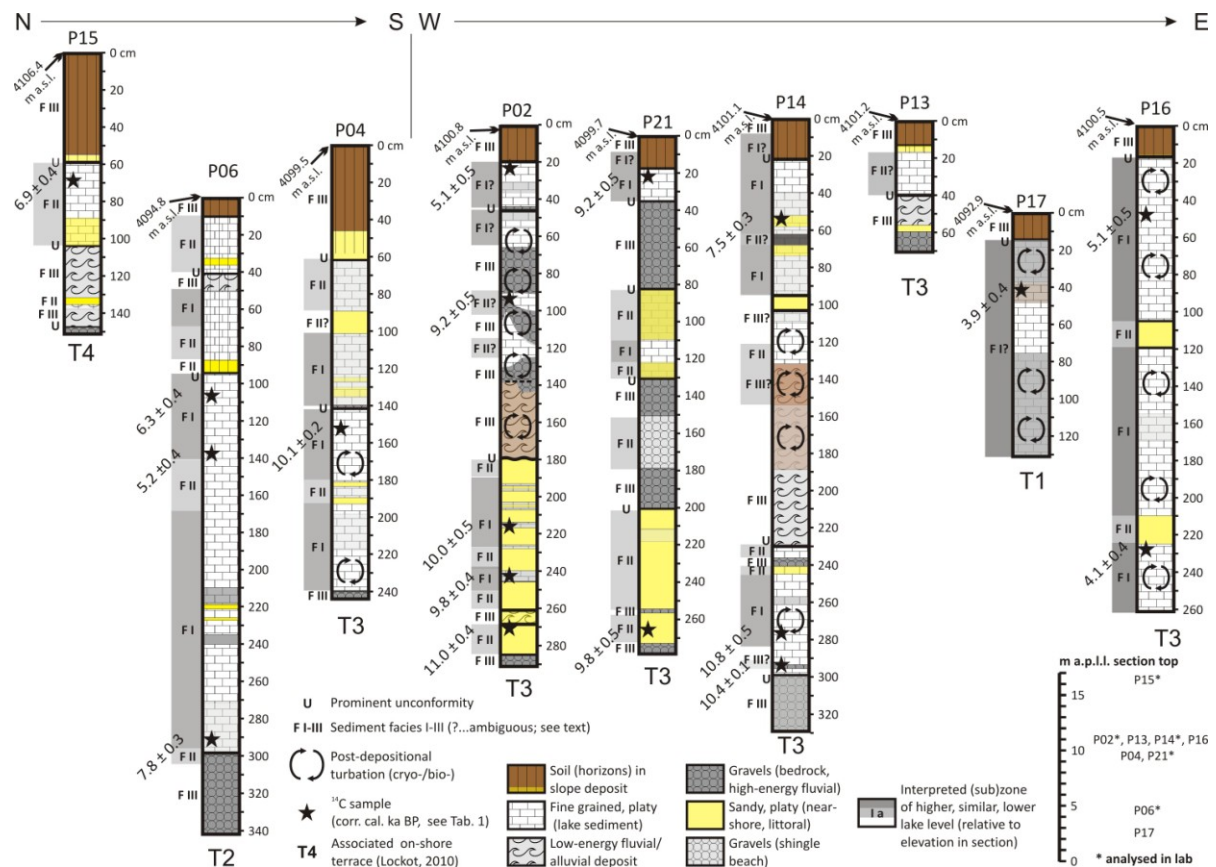


Figure 4.5: Generalized stratigraphic descriptions of the Donggi Cona high-stand sediment sections, including absolute position above sea level, Facies, interpreted lake level implications, and mean corrected, calibrated radiocarbon ages (BP, cf. Table 4.2, Figure 4.4). They are sorted by location and elevation of the section tops. Unspecified colors represent strata colors.

Depending on the site, sediments of Facies III show a more heterogeneous structure with either: a) cemented or loose, horizontally-bedded gravels (e.g., at the base of most sections, as well as at ~60, 140 and 190 cm depth in P21); b) unconsolidated sandy material with homogenous bedding or a coarsening upwards sequence at ~265 cm depth of P02; or

c) silty-sandy cross-laminations (e.g., 190-230 cm depth in P14, Figure 4.5). Facies III is interpreted as fluvial sediment, which is generally coarser than lake sediment, even in the littoral zone. The heterogeneity of this Facies results from diverse processes comprising confined (in-channel) and unconfined (out-of-channel, alluvial) sediment transport (North and Davidson, 2012). Loose layers of soft, silty aeolian sediment cover most of the sections. They were deposited on the slopes and reworked by unconfined overland flows during intense summer precipitation. As there was no in-situ loess in or on top of the sections, the dominant sedimentation process is assumed to be alluvial.

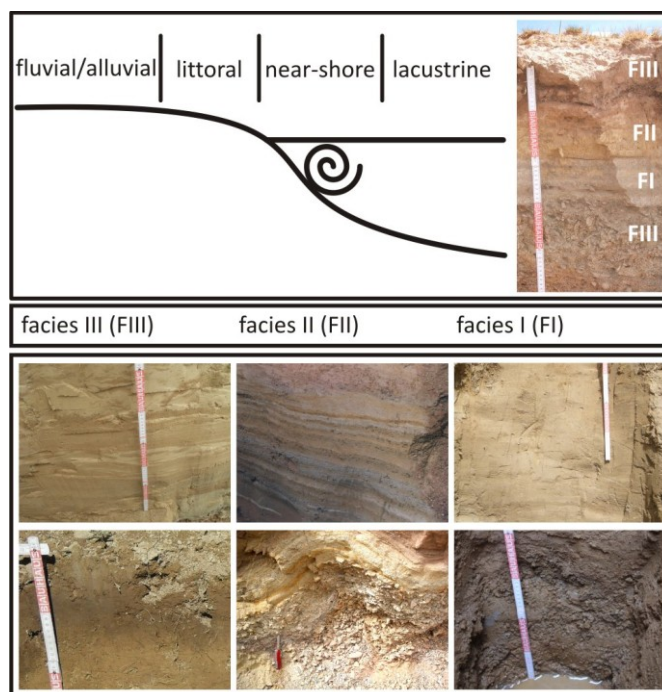


Figure 4.6: Examples for strata of different sediment Facies and their association with a terrestrial, littoral or lake depositional environment. The lower row shows strata that are overprinted by pedogenesis, cryoturbation, and ongoing active layer mixing (left to right).

Post-depositional overprint by pedogenesis, bio-, and cryoturbation varies slightly between sites. The topmost sequences always have a brownish or dark coloration, and sometimes translocated carbonate and clay. These are interpreted as the initial stages of Kastanozem- or Cambisol-like soils at dry, steppe sites (Miehe et al., 2008). Intense root penetration and animal burrows (e.g., *Ochotona spec.*) indicate sediment mixing, throughout section P14 and at section P15. Ongoing active layer mixing created a typical cryogenic granular structure in Facies I, especially at sites that are connected to groundwater (e.g., sections P04, P16, and P17 (grain sizes not analyzed)).

In section P02, intense post-depositional deformation and involution affect sediments of all Facies between 48 and 180 cm depth, including the gravel layers (Figure 4.3B). Although it is possible that these extensive involutions are seismites and their structures are related to

liquefaction in formerly near-shore, water-saturated sediments they are instead attributed to past periglacial mixing (cryoturbations).

An ambiguous zone in P14 between 100 and 190 cm depth contains involutions of fine sediment, burrows, and roots, with a distinct change from Facies III to II at 130 cm depth. Neither past cryoturbations, nor fluvial reworking (Figure 4.3F) can be excluded as deformation mechanisms for this zone.

4.2.4.3 DETRITAL GRAIN-SIZE END-MEMBERS

EM 1 has a broad mode in the coarse and medium sands with a maximum at 715 µm in its loadings (Figure 4.7A). It contributes to the sample compositions (i.e., scores) mainly at the base of the sections and in the coarse sediments of Facies III (e.g., 10% in the matrix material of P21 gravel layers, 80% of the P02 coarsening-upwards layer, Figure 4.8). EM 1 is interpreted to contain grain sizes that are deposited by high-energy fluvial transport, though it is also found in littoral sediments that are affected by high-energy wave activity.

EM 2 has a narrow peak in the very fine sand (mode at 76 µm). It has high scores in the fine sediments of Facies III (e.g., ~210 cm in P14, bases of P21, P06, and 20% of the coarsening-upward layer in P02). Hence, EM 2 represents sediment from low-energy unconfined alluvial flow, i.e., fine sand is deposited when flow velocity reduces, while finer particles are washed farther down into the lake. An aeolian origin for EM 2 is excluded, as it is too fine to represent dune sand, which would be similarly narrow-peaked but in a coarser range (Sun et al., 2002). Furthermore, dunes are unlikely to occur at the position of the included sections (IJmker et al., 2012a).

The coarse silt EM 3 has a narrow peak at 44 µm, while EM 4 shows a broad mode in the fine silt (maximum at 13 µm). Both are present in most of the samples with fractions of 30 ±24% and 31 ±19%, but it is found mainly at the top of the sections (Figure 4.8). EMs 3 and 4 are interpreted as aeolian deposits. EM 3 has the same mode as loess from the TP (Sun et al., 2007), which is transported in short-term suspension by near-surface, mainly winter monsoonal circulation (Sun et al., 2002; IJmker et al., 2012b). EM 4 represents background sedimentation of remote dust. EM 3 and EM 4 dust can be reworked along the slopes and reach the lake in fluvial suspension, but can also be trapped in ice off-shore (Dietze et al., 2012).

The finest grain size end-member, EM 5, has a broad mode in the clay fraction at 3.5 µm (Figure 4.7A). EM 5 is generally high in the strata of lacustrine sediments and low in fluvial/alluvial sediments. Hence, EM 5 is interpreted as the finest suspension that reaches deeper lake areas and accumulates very slowly under calm water conditions (off the wave-

dominated zone; Figure 4.6). EMs 4 and 5 are the robust end-members in modern lake surface sediments (Dietze et al., 2012).

EM_{diff} , the normalized difference of the low-energy fluvial EM 2 and the suspension EM 5, shows a similar but more pronounced pattern than EM 5, and can be readily interpreted as a proxy for lake depth.

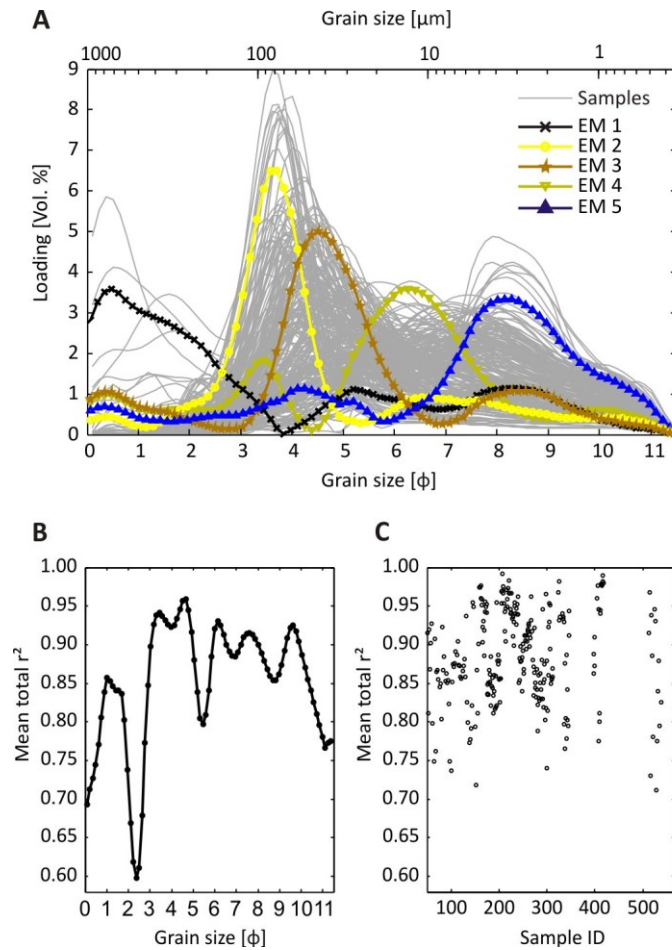


Figure 4.7: End-member loadings of all high-stand sediment grain size distributions (A). Mean total r^2 of data modelled with five end-members versus original data in variable (B) and sample space (C), after Dietze et al. (2012).

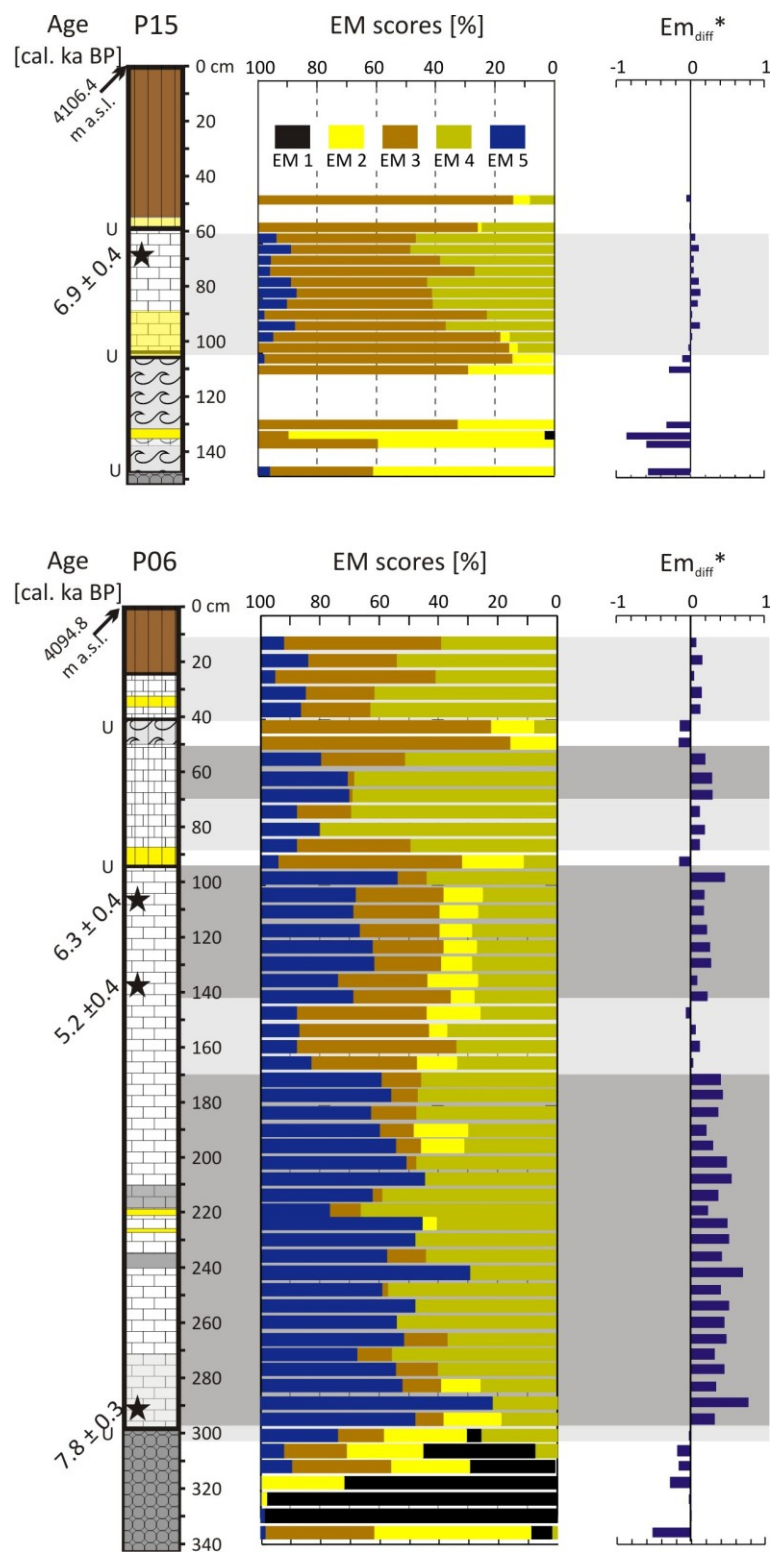


Figure 4.8: A) For description see page x.

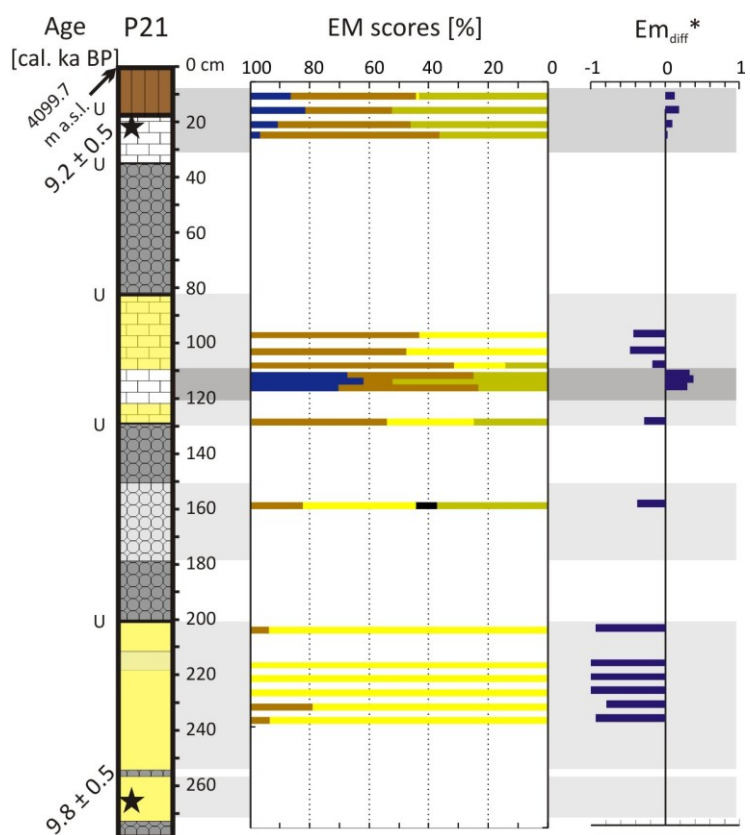
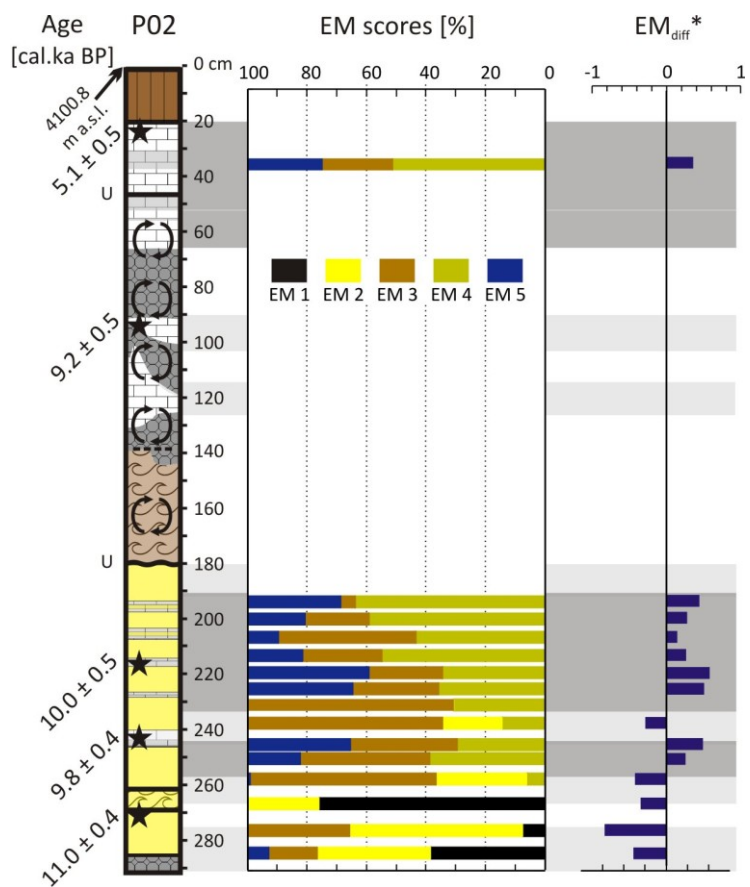


Figure 4.8: B) see page x.

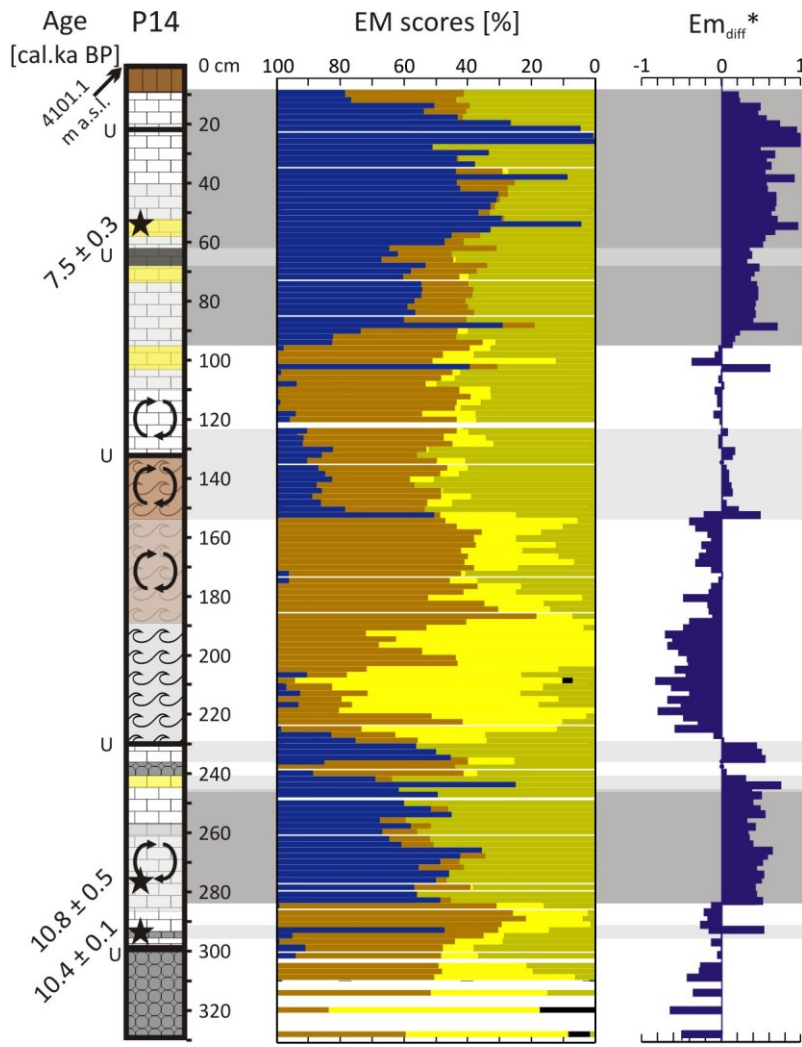


Figure 4.8: End-member scores, normalized difference of EM 2 and EM 5 ($EM_{diff} = (EM\ 2 - EM\ 5)/(EM\ 2 + EM\ 5)$), and their relation to field stratigraphy. Grey bars refer to sediment facies and relative lake level assumption (see Figure 4.5 for legend). P15 and P06 are sections at the outlet (A), and P02, P21 and P14 are sections at the northern shore (B).

4.2.4.4 LAKE LEVEL RECONSTRUCTION FROM SEDIMENT FACIES

When lacustrine, littoral/near-shore, or fluvial/alluvial sediments are identified using field observations and EMMA, phases of higher, similar, or lower lake levels are assigned relative to the present elevation of sediment in sections (Figure 4.5 and 4.8). Furthermore, post-depositional pedogenesis, bioturbation, and cryoturbation point to a lower lake level after deposition. For example, in section P02, cryoturbations distorted all sediments between 48 and 180 cm depth. Permafrost deforms sediments, when sufficient water is available, especially at sites with imperfect drainage (Van Vliet-Lanoë, 1998). Below 180 cm depth, sediments consist of a high percentage of sand (EMs 1 and 2), which would have allowed good drainage if the water level was much lower. Hence, it is assumed that a lake level elevation close to 8 m a.p.l.l. triggered cryoturbations between 48 and 180 cm.

4.2.5 DISCUSSION

Interpretation of Facies and depositional environments, as well as respective elevation is especially difficult for the ambiguous, fine-grained strata marked with “?” in Figure 4.5. Some strata contain sediments with platy structure, but high silt content and low amounts of suspension EM 5 (e.g., ~95 cm in P04, P14; Figure 4.8), as well as redoximorphic features (e.g., at ~80 and 110 cm depth of P02), and gastropods (e.g., P14 at 140 cm). An explanation is that littoral and near-shore environments can host fine-grained sediments of all Facies depending on the position along shore. Additionally, the presence of gastropods generally indicates near-shore conditions, but *Radix spec.* can also develop in small riverine and beach lagoons (Taft et al., 2012), independent of a large permanent lake. Alternatively, some strata contained high amounts of suspension EM 5 but lacked other Facies I features (e.g., P14 at 295 cm). However, wave action, fluvial deltas, and backshore configurations vary strongly between sites in this heterogeneous setting (Dietze et al., 2010), and a littoral deposit may lack typical, representative grain size end-members. Finally, other strata have been overprinted post-depositionally, convoluting their original depositional characteristics (e.g., P02, P14 and the top of P21). Hence, all of the ambiguous strata are tentatively assigned to the littoral zone or a deeper lake environment and, therefore, lake level reconstruction is also tentative.

Inverted ages may result from reworking of older material during lake level change or from varying hard-water contribution across time and space, which can only initially be considered here. High percentages of limestone in the catchment, and probably old CO₂ from groundwater, bring dead carbon into the system. The inverse ages in P06 – a section close to a limestone ridge at the outlet – may be related to hard-water effects, as there are no significant stratigraphic or granulometric differences in this depth range. Another likely explanation considers random mixing by tectonic shaking of saturated and unconsolidated sediments. However, no obvious signs for tectonic influence (e.g., vertical faults, or (micro)kinks in the sediments, Van Vliet-Lanoë, 1998) were found in any of the sediments.

An underestimation of bulk sediment ages may result from modern fine roots, bio- and/or cryoturbation that contribute younger atmospheric carbon to the sediments (symbols in Figure 4.4). Section P17 may suffer from all these effects. P16 has a similar intense cryogenic granular fabric and is much younger than sections at the same elevation. Neither is considered in the discussion. The ages of the root-rich, near-shore sediments in P15 and P02 might be ~2 ka older due to the age of the overlying loess (Stauch et al., 2012), and correlation with lake sediments was preserved at similar elevation and stratigraphic position

(top of P14, no. 10; Figure 4.4), respectively. Only unbiased ages and their large uncertainties were included in the following chronology (Figure 4.9).

4.2.5.1 CHRONOLOGY OF LAKE LEVEL CHANGES

The high-stand sediments are in agreement with the lake-core stratigraphy of Opitz et al. (2012). Their litho-unit 3 represents the time interval presented here, which can now be resolved in more detail.

Early Holocene (~11.4 to 6.8 cal. ka BP)

After the Younger Dryas, the lake level was fluctuating, but rising overall: at ~11 cal ka BP, littoral sediments intercalated with lacustrine and fluvial/alluvial sediments, forming the base of P14 and P02 at a minimum elevation of 7.1 m a.p.l.l. (Figure 4.4: age no. 7, 12). A discontinuous rise in lake level between ~10.5 and 9.8 cal ka BP is inferred from lacustrine and littoral sediments accumulated at the base of all northern shore sections and P04 at the outlet. Strong fluctuations in lake level and reworking of older sediment may be responsible for the inverted ages in P02. A prominent lake level drop around 10 cal ka BP is indicated by a clear erosional surface followed by a zone of reddish alluvial sediment at 180 cm depth of P02 (at 8.2 m a.p.l.l.). In P04 and P14 a thin gravel layer at 140 and 240 cm depth (8.1 and 8.7 m a.p.l.l.), respectively, and the first gravel/shingle phase in P21 (130-200 cm depth, ~8.5 m a.p.l.l) might coincide with this lower lake level.

Subsequently, lake level rose rapidly, with apparent fluctuations allowing deposition of near-shore sediments intercalating with fluvial Facies at 9 to 10 m a.p.l.l. (e.g., P02-sediments at 50-180 cm depth, up to 20 cm in P21). Starting at ~9.8 cal ka BP, this rise probably lasted a few centuries until ~8.7 cal ka BP, as the small base-top age differences in P02 and P21 suggest (Figure 4.4: age no. 4-7, 8-9). The highest lake levels (16.5 m a.p.l.l.) are tentatively assumed around 9.2 cal ka BP from associated lake sediments found in the cryoturbated strata of P02 (Figure 4.4: age no. 4) and from the OSL-age of the loess on top of the highest section P15. An upper erosional boundary is prominent in all northern shore sections (e.g., the thin pebble layer in P02 at 47 cm depth and a shift to cover sediments in P04 and P21). Hence, a significant lake level decline took place after this first lake maximum.

In P14, a distinct boundary between lacustrine and low-energy floodplain sediments (high scores of EM 2) occurs at 230 cm depth. The 1-m-thick floodplain sediments were deposited during a time of lower lake levels. They may contain a phase of lacustrine sedimentation, as end-members suggest (high EM_{diff} between 110 and 150 cm, Figure 4.8). However,

when the lake shifted to a lower level it is possible that dynamic fluvial activity, coupled with a much larger catchment than at P02 and P21 (Figure 4.2), intensively eroded sediments of the previous high stand, leaving behind only the thin lacustrine layer at ~235 cm below the floodplain sediments (i.e., at ~8.75 m a.p.l.l.).

A prominent lake level drop likely occurred at ~8.7 cal ka BP. So far no lacustrine sediments have been dated that were deposited between ~8.7 and 8.2 cal ka BP (Figure 4.4). Instead, P02-sediments are intensively cryoturbated, supported by saturated sediments below, which provided the water for frost action. Therefore, the lake level was probably at an elevation close to ~8 m a.p.l.l. Slightly cooler conditions are suggested by a short-term reduction in offshore TOC and biological activity (Aichner et al., 2012). At the same time, the floodplain sediments in P14 may have accumulated (above 8.8 m a.p.l.l.), supporting the idea that the local river bed was slightly above 8 m a.p.l.l. However, as discussed above, these sediments might be much older, and the distortions seen in the ambiguous zone could be dominantly of cryogenic origin, similar to P02. Regardless, all explanations suggest a lower lake level after the lake maximum.

After ~8.2 cal ka BP, another significant lake extension led to the accumulation of lake sediments that overlie the distorted strata in P02 and comprise the topmost lake sediment in P14. This lake stand at ~7.5 cal ka BP (Figure 4.4: age no. 10) reached far into the transverse valley, to a minimum of 10.6 m a.p.l.l. in section P14. However, because there are no higher lake sediments at other sites with unbiased ages or similarly clayey sediments, as found in P14, a secondary lake maximum likely occurred at this time (Figure 4.9). The sapropel layer in P14 has probably formed during a slight lake reduction (see EM_{diff} , Figure 4.8) during times of high biological productivity at ~8 cal ka BP (offshore TOC maximum, Aichner et al., 2012). Lacustrine sedimentation also commenced at the outlet at ~7.8 cal ka BP (P06 base, Figure 4.5).

Mid-Holocene (6.8 – 4.3 cal. ka BP)

A further lake level decline to below 10 m a.p.l.l. caused the topmost transition from lake to alluvial sediment in P02, P13 and P14. Compared to the lake decline at ~8.5 cal ka BP, this sequence has not been overprinted post-depositionally by cryoturbation, suggesting either different climatic conditions, or a decoupling of the topmost sediments from ascending water. To date, there are no further recognized lake sediments in T3 or T4 terraces with unbiased ages younger than 7 cal ka BP. Hence, this lake decline might coincide with the abrupt lake opening at ~6.8 cal ka BP, when ostracods in offshore lake sediments changed from euryhaline to freshwater assemblages (Mischke et al., 2010).

However, massive, finely laminated lake sediment accumulated at P06 in the T2 terrace (Figure 4.8), even after this transition. The only sedimentological indication for a lake opening at this site might be the reduction of EM_{diff} and an increase in aeolian activity (dust EMs) between 143 and 170 cm depths.

Afterwards, EM_{diff} suggests a lake rise to a level slightly lower than before. The inverted ages in P06 after this transition may suggest either a change in the hard-water nature of the lake, or a reworking of some older organic material. After ~5 cal ka BP the lake gradually reduced with some fluctuations (unconformity overlain by a sandy layer at 100 cm depth, and silty alluvial sediment at 45 cm depth; Figure 4.8). P06 top sediments still contain some detrital clay associated either with soil formation, or near-shore conditions, but consist mainly of (reworked) dust marking the end of high-stand sedimentation at a minimum elevation of 4.3 m a.p.l.l. This transition might coincide with the suggested change in lake chemistry and stratification recorded at ~4.3 cal ka BP in offshore lake sediments (Opitz et al., 2012).

4.2.5.2 SYNTHESIS

Although a truly quantitative lake level reconstruction is restricted by the high spatial variability in the accumulation, erosion, and post-depositional overprint of the different sites, and the importance of water contributions from local sources (i.e., melt and ground water) is difficult to assess, the mechanisms involved in Lake Donggi Cona hydrological variations can now be discussed in a larger context. The basin-wide correlation of facies and lake level assumptions (Figure 4.10) can be compared to known patterns in Asian monsoon precipitation. Both the Indian and East Asian monsoons may have dominated the site. However, in a comparison with several monsoon reconstructions (not shown) the pattern of an Indian monsoon proxy record, i.e., the $\delta^{18}\text{O}$ of Oman speleothems from Fleitmann et al. (2003) (Figure 4.9) showed trends similar to this study. Additionally, Wang et al. (2010) found that the Indian monsoon was the dominant influence at the TP during the early Holocene.

The trend of rapidly rising lake level correlates well with the trend of increasingly warmer and wetter conditions during the early Holocene. These resulted from stronger Asian monsoons and are related to the Northern Hemisphere insolation maximum (e.g., Fleitmann et al., 2003; Dykoski et al., 2005). As a result, lakes extended all over the TP during the early Holocene, fed also by melting glaciers, permafrost (Mischke and Zhang, 2010), and increased fluvial activity (Schlütz and Lehmkühl, 2009). The ~16.5 m a.p.l.l. maximum of Lake Donggi Cona at ~9.2 cal ka BP correlates with this pattern. However, the onset and

timing of the ‘Holocene Optimum’ and maximum lake levels varied between sites across Tibet (Mischke et al., 2009; Wang et al., 2010). Lake high-stands during the early Holocene are reported, e.g., from Lake Qinghai (~200 km north-east of Donggi Cona, +8-12 m prior to 8.4 cal ka BP, Madsen et al., 2008), Selin Co (+48 m at ~9.2 ka, Li et al., 2009), and others (Lehmkuhl and Haselein, 2000).

Lake Donggi Cona may have responded to the prominent centennial cooling and drying at ~8.5 cal ka BP described at various sites around the world (e.g., Rohling and Pälike, 2005; Wanner et al., 2011). Between ~8.2 and 8.7 cal ka BP, intense cryoturbations at site P02, probable floodplain deposition at the second largest inflow (P14), and incision at many sites took place (e.g., probably formation of T4-lake terrace). However, the cooling’s impact and timing on the TP are debated (Morrill et al., 2003; Jin et al., 2007) and it is only recognized at some sites in Tibet between 8.7 and 8.2 cal ka BP (e.g., W-Tibet: Gasse et al., 1991; central Tibet: Herzschuh et al., 2006; Lake Qinghai: Colman et al., 2007; E-Tibet: Mischke et al., 2008), suggesting site-specific response times.

The trend of rapidly rising lake level correlates well with the trend of increasingly warmer and wetter conditions during the early Holocene. These resulted from stronger Asian monsoons and are related to the Northern Hemisphere insolation maximum (e.g., Fleitmann et al., 2003; Dykoski et al., 2005). As a result, lakes extended all over the TP during the early Holocene, fed also by melting glaciers, permafrost (Mischke and Zhang, 2010), and increased fluvial activity (Schlütz and Lehmkuhl, 2009). The ~16.5 m a.p.l.l. maximum of Lake Donggi Cona at ~9.1 cal. ka BP correlates with this pattern. However, the onset and timing of the ‘Holocene Optimum’ and maximum lake levels varied between sites across Tibet (Mischke et al., 2009; Wang et al., 2010). Lake high-stands during the early Holocene are reported, e.g., from Lake Qinghai (~200 km north-east of Donggi Cona, +8-12 m prior to 8.4 cal. ka BP, Madsen et al., 2008), Selin Co (+48 m at ~9.2 ka, Li et al., 2009), and others (Lehmkuhl and Haselein, 2000).

Donggi Cona again reached a level of ~11.5 m a.p.l.l. at ~7.5 cal ka BP, correlating with a maximum in monsoon intensity (e.g., Fleitmann et al., 2003; Figure 4.9). Lake Kuhai, around 40 km to the east of Lake Donggi Cona, reached its highest levels between 12.8 and 7.1 cal ka BP (Mischke et al., 2009). Several other lakes reached their maximum extent during the Mid-Holocene (e.g., Lake Koucha ~230 km SW of Lake Donggi Cona, Mischke et al., 2008) in accordance with the dominance of the East Asian monsoon on the TP (Wang et al., 2010), though this maximum is often attributed to local non-climatic dynamics (Wünneman et al., 2010).

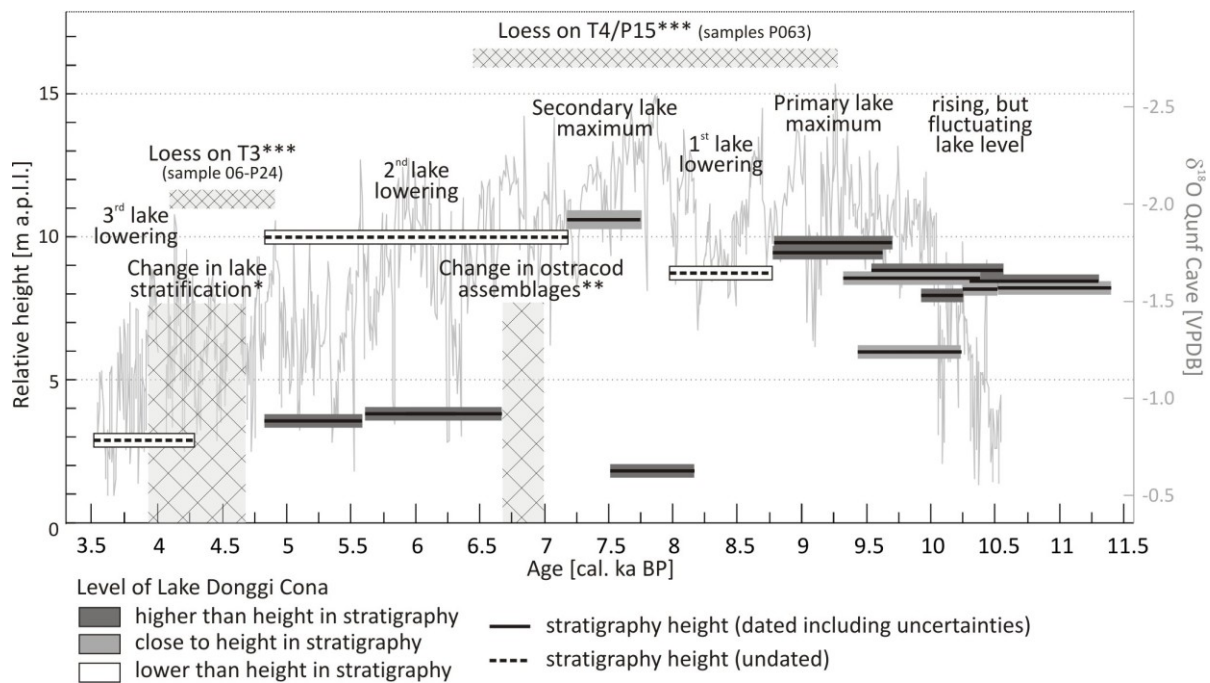


Figure 4.9: Higher than present lake-level phases at Lake Donggi Cona compared with the lake-core proxies, ages of loess on top of onshore terraces, and Indian monsoon-dominated $\delta^{18}\text{O}$ of Oman speleothems in the background (Fleitmann et al., 2003). *Opitz et al. (2012); **Mischke et al. (2010); ***OSL ages of loess sections on lake terraces, Stauch et al. (2012).

After 7 cal ka BP Asian monsoon intensities gradually decreased (Fleitmann et al., 2003). This led to a transition towards a cooler and drier late Holocene at around 4.5 cal ka BP that can be observed globally (so-called “Neoglacial”, e.g., Wanner et al., 2011) and across the TP (e.g., Colman et al., 2007; Mischke and Zhang, 2010, Wünnemann et al., 2010). Similarly, this transition might be reflected by a basin-wide change that is prominent in most offshore lake sediment proxies between 3.9 and 4.7 cal ka BP (Opitz et al., 2012) and is associated with the gradual lake decline seen in section P06. Donggi Cona lake level fell permanently below 4.3 m a.p.l.l. after ~4.7 cal ka BP. This climatic transition towards drier conditions could have allowed a deeper incision of the outflow, probably associated with a reduction of alluvial aggradation there and the initiation of T2-terrace formation. Incision probably stopped at the level of T1, which was formed prior to the artificial extension of the outlet in the 1970s (Lockot, 2010).

However, as in other Tibetan lake catchments, the Donggi Cona area is affected by active tectonic and geomorphological dynamics that can randomly intensify or weaken the sedimentological response to climatic change significantly, possibly invalidating hydrological reconstructions. Two main stratigraphic features may dominantly reflect these local pro-

cesses. One is the fluctuation during the early Holocene lake level rise. It can hardly be correlated between different high-stand sections, and may instead be associated with varying melt-water contributions and distinct adaptations of the sub-catchments to the changing climatic conditions (e.g., sediment mobilisation, interaction with changing vegetation, and permafrost thawing). The site most sensitive to such variations is the outlet spillway that could have randomly been eroded or blocked by the large alluvial fan from the north (Figure 4.3A).

Another feature is the abrupt opening of Lake Donggi Cona as reflected by ostracod assemblages at ~6.8 cal ka BP (Mischke et al., 2010). A tectonic and/or geomorphological event is more likely responsible for the change than hydrological and climatic drivers. On- and offshore lake sediment cores show short-term excursions in sedimentological, mineralogical, and geochemical parameters at this time that may be linked to a short-term decline of lake level, probably incising T3 terrace. However, no consistent shift in stratification and geochemical processes took place (Opitz et al., 2012). The lake remained at a high level afterwards (5 to 7 m a.p.l.l., i.e., T2-level after Lockot, 2010). Furthermore, to date no significant lake level decline or moisture reduction has been reconstructed for the north-eastern TP (Wang et al., 2010). A significant global cooling phase at ~6.3 ka rather occurred after the opening (Wanner et al., 2011, Figure 4.9).

4.2.6 CONCLUSIONS

Complex geomorphological and sedimentological processes interact in the littoral zone that can be recorded in onshore high-stand sediments. At Lake Donggi Cona, these sediments, while more discontinuous, provide a unique, multi-process archive of past lake level variations and associated sedimentological dynamics that are more diverse and detailed than profundal lake sediments. Stratigraphy, end-member modeling of grain size distributions, and radiocarbon dating considering hard-water uncertainty ranges, allowed quantification of sediment transport processes and relative lake levels during times of deposition.

Lake levels generally follow the trend of Asian monsoon dynamics, and are modified by local non-climatic drivers. During a warmer, wetter climate, Donggi Cona rose from its glacial low-stands to above its present level (starting ~11 cal ka BP), reaching separate maximums during the early and mid-Holocene. A major cold and dry phase at ~8.5 cal ka BP caused a reduction in lake size and significantly overprinted the high-stand sediments by cryoturbation. The end of high-stand sedimentation correlates with the decline of monsoon dynamics at the transition to the Neoglacial.

However, Lake Donggi Cona is one of many lakes in an active tectonic setting. Its spill-way can be affected by small-scale tectonic and geomorphologic processes that could cause the lake to outflow, incise, and erase information that is otherwise recorded. Such non-climatic dynamics may explain the lake opening at ~6.8 cal ka BP, while sub-catchment specific processes may explain the spatial variations between sites during lake level fluctuations at the beginning of the high-stand period.

ACKNOWLEDGEMENTS

We thank all Chinese and German colleagues for the support and discussions during the field campaigns. M. Runge and M. Paprotzki helped with lab analysis. DFG-priority program 1372 provided financial support. Hucai Zhang and an anonymous reviewer made some useful suggestions.

5. SYNTHESIS

This dissertation had two main foci. The first focus was to assess the sensitivity of the Lake Donggi Cona basin and its sediment cascade to climatic changes and to distinguish important driving factors of environmental change that play a role in the catchment. The second focus was the quantification of lake level changes and their relation to the responsible driving mechanisms in a larger context.

5.1 LANDSCAPE SENSITIVITY AND THE LOCAL DRIVING FORCES

For hydrological reconstructions, the sensitivity of the Donggi Cona lake basin morphology and catchment-wide sediment cascade can be evaluated by considering the influence of different sediment components that affect the sedimentary record of the lake and its littoral zone. Human activity has apparently affected the landscape and hydrological processes in only a minor way. It must be taken into account for the reconstruction of the aeolian cycle in the catchment and aeolian sedimentation in the lake during the last 2000 to 3500 years (Schlütz and Lehmkuhl, 2009; Stauch et al., 2012) – a sediment mobilisation that was probably independent of water level changes. However, for the late Quaternary prior to this period only geomorphological, tectonic, and climatic impacts on hydrological changes are discussed from here forward.

5.1.1 BASIN MORPHOLOGY AND THE LITTORAL ZONE

Analysing the basin morphology and sediment architecture of a lake is a powerful tool to assess the evolution of a lake basin, though it was studied only at a few sites on the Tibetan Plateau (e.g., Schütt et al., 2008; Daut et al., 2010). The Donggi Cona *lake basin* and its *littoral sedimentary environment* are very heterogeneous in structure, which complicates interpretation of the sedimentological inventory, especially the grain size patterns of the lake sediments. Because the lake resides in a pull-apart-basin at the Kunlun fault, the deepest part of the lake is not at its centre, as would be optimal from a palaeolimnological point of view, but instead is located in the western sub-basin, close to the steep limestone mountain ridge at the southern shore (Chapter 2.4.1, Dietze et al., 2010). Sediment structures at this position could be disturbed by slumping from the steep southern rim of the graben and, therefore, studying cores from this position was not advised.

Undisturbed stratified lake sediments are not distributed evenly within the lake basin. They cover the flat morphological levels restricted to certain water depths (Chapter 2.4.2, Dietze et al., 2010). Hence, studied sediment cores cluster at 30 to 35 m water depth (Opitz et al., 2012). The lake basin morphology may further influence the pattern of water currents

that could remobilise and redistribute unconsolidated sediment that was previously deposited in shallower areas (Chapter 3.6.2, Dietze et al., 2012). From measurements of oxygen availability in the water column, it was inferred that the lake is fully ventilated during summers (Mischke et al., 2010a), though ventilation probably started 4.5 ka ago, when also sediment distribution by water currents changed (Opitz et al., 2012; Opitz et al., in review).

Furthermore, the depositional environments along the Donggi Cona shore vary strongly in relation to sub-catchment morphology and lithology, including many different shore types – from direct contacts of lake with bedrock with narrow bars of gravelly material, to fine-grained and even clay-rich lagoons along flat backshores. Large onshore areas are also prone to permafrost activity, which can buffer the climatic response of the hydrological and sediment cycle, whereas pedogenesis, despite providing valuable post-depositional environmental proxies, may overprint the sedimentary records onshore as well, complicating the reconstructions of lake levels. Both buffers within the Donggi Cona sediment cascade were discussed in Chapter 4.2 (Dietze et al., 2013).

Age control of sediment deposition along the shore and in the lake is also complicated by the catchment configuration. High percentages of ^{14}C -dead limestone, the ^{14}C -depleted wetland on the eastern alluvial plain, varying inflows from heterogeneous sub-catchments, and ^{14}C -dead CO_2 rising from faults and groundwater have to be considered as sources of error in radiocarbon dating of bulk sediments (cf. Hou et al., 2012). Hard-water errors of the shore sediments may be more heterogeneous than those of sediments from the mixed deeper lake. To account for these uncertainties, as well as for potential changes of the reservoir effect in the past, larger than usual error ranges of similar probability were calculated for dating the onshore high-stand sediments using a modern calibration approach (Chapter 4.2.3.4, Dietze et al., 2013).

Despite these ambiguities, some wide, flat reaches, mainly along the northern shore, preserved valuable onshore terraces and high-stand sediments that recorded past hydrological variations. Such a littoral archive is rare at other sites; hence, the littoral zone of Lake Donggi Cona can still be seen as a highly sensitive and comprehensive record of even slight changes in the driving forces of environmental change (climate, tectonic, man). Therefore, it was a key region to study hydrological variations in the Donggi Cona catchment.

5.1.2 IMPACTS FROM THE CATCHMENT

Together with direct precipitation and runoff, glacial *meltwater* is seen as the most important water contributor to a lake basin (Zhang and Mischke, 2009). In the Donggi Cona

catchment, glaciers are absent under modern climatic conditions. However, glacial landforms (i.e., cirques, kame terraces, and moraines) can be found in the northern catchment, at the outlet and close to the north-western Donggi Cona shore, including a moraine that seems to be associated with a Gilbert-type delta within the lake (Chapter 2.5.2, Dietze et al., 2010).

The reflector of the sandy Gilbert-type delta topsets found below the -24 m level could have resulted from meltwater input from the end of the last glacial stage (Chapter 2.5.3, Dietze et al., 2010), based on a comparison with the ~18.5 cal. ka BP old base of sediment core PG1790 (Opitz et al., 2012). However, results of ^{10}Be exposure dating of the onshore moraines yielded ages of 90 to 100 ka (H. Rother, personal communication, July 2012). Then, the at least 40 m thick sediment sequences and multiple stacked delta sediments below the -39 m bathymetric level (Chapter 2.4.3, Dietze et al., 2010) may be associated with large amount of meltwater and sediment produced during deglaciation following the MIS 5 glacial advance. In this case, the Gilbert-type delta on top could be related to a second glacial advance dated to MIS 3 and the final deglaciation 35 to 40 ka ago (exposure ages of cirques and moraines, H. Rother, personal communication, July 2012) – in close accordance with deglaciation in the Bayan Har mountains (Heyman et al., 2011). Evidence of a minor glacial advance during the dry MIS 2 is only found in the much higher, and still glaciated A'nyêmaqên Shan, where a small early Holocene advance has also been documented (Owen et al., 2003).

Hence, glacial meltwater input in the Donggi Cona catchment could have been much less important over the last 20 ka than previously thought. As a result, if the correlation of the seismic reflections with the sediment core base is correct, the Gilbert-type delta should actually consist of sandy periglacially weathered sediment transported after intense precipitation events in hyperpycnal flows during the Pleistocene-Holocene transition. However, no analyses of past glaciations have been performed from the steep and much higher (up to 5400 m a.s.l.) south-eastern part of the catchment, but morphological indications of past glaciations can be mapped from satellite data (G. Stauch, personal communication, July 2012). Hence, meltwater input, via the large alluvial fan east of the lake, cannot be completely excluded for the Late Quaternary.

The *aeolian cycle* does not affect the water level of Lake Donggi Cona directly, but has considerable influence on total detrital sedimentation in the lake and the reconstruction of hydrological changes. EMMA revealed that approximately 60 % of the modern lake surface sediment is composed of local and remote dust – similar to the amounts found in fossil high-stand sediments (Chapters 3.6.2, 4.2.4.3, Dietze et al., 2012, submitted). Aeolian sedi-

ment could be washed into the lake by overland flow along the slopes or trapped in ice cracks on the lake, as observed in winter 2007, leaving a rather random fingerprint of silty material in the lake (i.e., no significant relation with water depth). Sandy material can be transported onto the lake ice by intense winds during the winter as well, and sink into the lake following melt in the spring, overprinting the common association of sand with near-shore or littoral conditions (Chapter 3.6.2, Dietze et al., 2013).

The heterogeneous detrital sediment input and effective in-lake sediment mixing complicate the interpretation of sediment proxy records, especially grain size distributions in the classical sense (i.e., fines would dominate in the centre and coarse material at the shore). With these constraints in mind, the interpretation of grain size distribution using the newly developed EMMA focuses on the differentiation of grain size end-members that can be explained by distinct sediment transport processes. Transport processes can only tentatively be related to a certain water depth (Chapter 3.6.2, Dietze et al., 2012). However, two particular grain size end-members, with main modes in the clay and medium silt fractions, are a robust feature of the Donggi Cona lake sediments – not only at the modern lake bottom (Chapters 3.5.3, 3.6.2, Dietze et al., 2012), but also in fossil onshore lake sediments (Chapter 4.2.4.3). Sedimentation of these two end-members can only result from suspension within a calm water column. The normalized difference between a fluvial-transported end-member and the robust lacustrine clay end-member from onshore high-stand sediments can then be interpreted as a proxy for water level change (Chapter 4.2, Dietze et al., 2013).

However, the settling of very fine particles can also occur in backshore or floodplain ponds and lagoons. Hence, reconstruction of water depth and lake level changes using granulometric methods is limited. Other methods or proxies are needed to clearly distinguish between a large water body (i.e., Lake Donggi Cona) and small littoral or fluvial lagoons (e.g., ostracod assemblages, Mischke et al., 2010b).

At Lake Donggi Cona, *fluvial and alluvial processes* have not been studied in detail yet, although they do play a major role in the composition of onshore high-stand sediments (Chapter 4.2, Dietze et al., 2013). Van der Woerd et al. (2002) discuss fluvial and alluvial terrace formation and incision along the Kunlun fault, based on early and mid-Holocene CRN and ^{14}C ages (i.e., between 5 and 13 ka). At the Dongxi Co segment east of Donggi Cona, terraces had ages of 6.7 cal. ka BP, ~8.5 cal. ka BP, 11 cal. ka BP and ~37 ^{14}C ka BP (Van der Woerd et al., 2002). Even though the age of 6.7 cal. ka BP supports the theory that Lake Donggi Cona opened as a result of a seismic event (Chapter 4.2.5, Dietze et al., 2013), Van der Woerd et al. (2002) suggest a regional, mainly climatically driven response of ter-

race formation coeval with times of fluctuating precipitation (incision in wet phases) and exclude a major response to vertical tectonic movements for the last 40 ka.

Preliminary mapping of fluvial terraces on the large alluvial plain in the east of the lake shows that the elevation and number of fluvial terrace levels can be correlated with onshore lake terraces (G. Stauch, personal communication, December 2011). The correlation suggests lake water changes are the main control of local base level.

5.1.3 TECTONIC IMPACT

Nevertheless, terrace incision and base level changes related to tectonic movements are very likely along an active major fault system. The high fluvial terraces, up to several tens of m above the modern river bed, downstream of Lake Donggi Cona, are an impressive example that may indicate strong backward erosion of the Qaidam basin tributary in response to the uplift of the northern Tibetan Plateau (Wang et al., 2009).

Two types of tectonic impact have to be distinguished: a direct impact via subsidence and vertical displacement along the Kunlun fault, and an indirect impact via shaking and horizontal displacement. The direct impact of subsidence from the ongoing extension of the lake basin may explain the thickness of stacked delta sediments at the northern rim of the deep graben in the western sub-basin (Chapter 2.5.3, Dietze et al., 2010), and may lead to an exaggeration of the onshore terrace elevations. Lockot (personal communication, spring 2012) compared onshore terrace section elevations in relation to the assumed fault pattern and found vertical displacement north and south of the major course of the Kunlun Fault that differed between terrace generations. He concluded that post-genetic sedimentation processes, rather than vertical tectonic activity, were responsible for this displacement.

Van der Woerd et al. (2002) reconstructed a horizontal slip rate of 11.5 mm/year for the Kunlun fault and estimated the apparent vertical throw along the fault to be 0.085 % of the sinistral displacement from fluvial terrace offsets. Hence, a mean vertical displacement of 0.88 m within 9000 years should be considered (9 cal. ka BP was the assumed lake level maximum; Chapter 4.2.5, Dietze et al., 2013) or 1.96 m for the time recorded in the lake sediment cores (i.e., last 20 ka; Opitz et al., 2012). This is within the uncertainty range of terrace surveys (Lockot, 2010) and relatively low considering onshore terrace elevations of up to 16.7 m, and a mean step height of at least 40 m between graben base and the most prominent morphological level at the 39 m water depth. Though ~1 cm/ka seems to be a minimum estimate for the lake basin, considering the weight of overlying sediments and further

potential extensional forces, vertical tectonic displacement apparently plays only a minor role within the timescales considered here.

The indirect tectonic influence seems to be of greater importance. Tectonic shocks could efficiently mix unconsolidated lake sediments and alter the sediment structure by slumping and reworking of sediment (Chapters 2.4.2, 4.2.5.2, Dietze et al., 2010, submitted) that is difficult to identify in the sedimentary records. It is most likely the influence of tectonic movements, interacting with geomorphological dynamics that altered the lake spillway and modern outlet. The 1937-earthquake is recorded in the mole tracks north of the outlet, whereas the steep, inactive alluvial fans south of the outlet show a reversed bedding of gravels that suggest an old tectonic displacement. Hence, it is likely that the major fault line changed course from south to north, and could have ruptured the outlet on the way.

Furthermore, earthquakes may have induced blocking of the outlet with alluvial fan material from the north and/or the south. Lockot (2010) calculated a minimum volume of 870000 m³ of sediment necessary to dam the lake to a level of +10.1 m at the current outlet – a small size compared to Pleistocene valley fills in northern Tibet (Wang et al., 2009).

In addition, random feeding of the lake with water and sediment from the large alluvial fan north of the outlet may have contributed to the lake water and sediment budget as well, although glacial meltwater may be excluded from the time of the Pleistocene-Holocene transition (H. Rother, personal communication, July 2012). In times of high precipitation and sufficient sediment availability (i.e., after the last glacial stage), the fan was aggradating and a blockage of the outlet was very likely (probably until at least 5.5 ka ago; G. Stauch, personal communication, April 2012). However, the aggradation and incision of this alluvial fan needs further investigation considering the backward and lateral erosion, as well as erosion that is tectonically induced.

5.2 HYDROLOGICAL VARIATIONS AT LAKE DONGGI CONA

The Donggi Cona lake basin and littoral zone provide many morphological and sedimentological features related to past lake level changes. Delta sediments and morphological levels at 24, 39 and 57 m water depth indicate past lake low-stands, though only the uppermost level could be preliminarily dated to the last glacial stage (~20 ka) using the correlation with a sediment core (Figure 2.6, Dietze et al., 2010). Sediment cores did not reach deeper into the seismo-depositional units, so the lower lake stages can only be assumed to be of older age and distinct delta sediments may be associated with past meltwater input. Four lacustrine terraces were found onshore at 3.5, 6.1, 10.1 and 16.7 m above the present lake level (Chapter 4.1). They contain fossil lake sediments that allowed the characterisation

of depositional changes during early and mid-Holocene lake high-stands (Chapter 4.2, Dietze et al., 2013). As a result, the variation in lake area and water volume for Lake Donggi Cona can be reconstructed quantitatively (Figure 5.1).

It can be assumed that a lake has filled the Donggi Cona basin throughout the late, and possibly earlier stages of the Quaternary. During phases of dry and cold conditions, this lake probably survived with a drastically reduced lake volume (minimum of ~0.3 km³, Figure 2.7), in contrast to other lakes on the north-eastern Tibetan Plateau (e.g., Mischke et al., 2008, 2009, 2010a), but similar to other large lakes, such as Lakes Qinghai or Nam Co (Lister et al., 1991; Colman et al., 2007). Lake Donggi Cona may have been fed by meltwater until as late as ~35 ka, but there is no direct evidence for the existence of glaciers in the catchment after this time.

From comparison of the seismic and bathymetric studies with sediment cores (Opitz et al., 2012), it can be assumed that the lake filled the basin up to the -24 m bathymetric level at ~19 cal. ka BP – the deposition time of the oldest recovered sediments. The lake had an area and volume of ~150 km² and 3.5 km³ during this stage (Figures 2.7, 5.1, Dietze et al., 2010). The first post-glacial lake level rise and sedimentation rates of around 65 cm/ka seem to be related to the warming at the end of the glacial period, after 17.5 cal. ka BP (clayey-silty laminites, Opitz et al., 2012). Some potential meltwater inflow from the southern catchment could have contributed to this lake level rise (cf. Chapter 5.1.2). The onset of the Asian monsoons and initial post-glacial warming, however, are generally assumed to have occurred later at ~14.5 ka ago, corresponding with the Northern Hemisphere Bølling/ Allerød (B/A) warm period (Dykoski et al., 2005; Colman et al., 2007; Wang et al., 2010), which is recorded in all studied north-eastern Tibetan lakes (e.g., Lakes Koucha, Kuhai, Qinghai, and Ximenco; Shen et al., 2005; Herzschuh et al., 2009; Zhang and Mischke, 2009; Wischnewski et al., 2011), but seems to be missing in Lake Donggi Cona (Opitz et al., 2012).

Opitz et al. (2012) found the highest sedimentation rates of the last 20 ka (i.e., 177 cm/ka) between 13.8 and 11.5 cal. ka BP, which they attribute to a lake level decline and the Younger Dryas (YD) cooling phase. End-member modelling of grain size distributions of the sediment cores indicates intensively fluctuating lake levels with short-term peaks centred at 12.8, 12.2 and 11.8 cal. ka BP (PG1901 age model, own calculation). Further evidence for a cooling/drying period during the Younger Dryas phase remains scarce from adjacent lakes (Zhang and Mischke et al., 2009).

A marked decline in detrital input and sedimentation rates was found in lake sediment cores after ~11.5 cal. ka BP (Opitz et al., 2012). At this time, lake high-stand sediments start-

ed deposition onshore (Chapter 4.2.5, Dietze et al., 2013) corresponding to the onset of the Holocene monsoon activity, in accordance with other sites in the region (e.g., Lister et al., 1991; Morrill et al., 2003; Dykoski et al., 2005). Increased precipitation led to a rapid lake level rise during the early Holocene with minor, probably sub-catchment specific fluctuations, culminating in the highest levels at ~9.1 cal. ka BP (Chapter 4.2.5, Dietze et al., 2013) in accordance with records from other Tibetan lakes (e.g., Lehmkuhl and Haselein, 2000; Madsen et al., 2008; Li et al., 2009). The lake reached a volume of ~12.3 km³. No glaciers were present in the Donggi Cona catchment at that time and meltwater did not play any role in this lake level rise.

In the Donggi Cona catchment enhanced sand and loess deposition was associated with rather wet conditions, when vegetation could act as efficient sediment trap, i.e., beginning ~14 ka ago and culminating during the early Holocene (Stauch et al., 2012). After 9 ka, and during the mid-Holocene, runoff along the slopes caused reworking of aeolian sediments and transported silty material in suspension to the lake from mainly local sources (IJmker et al., 2012a). Therefore, aeolian deposits can be related to moister conditions, supporting the inference of higher precipitation rates from onshore lake high-stand sediments. This is, however, in contrast to the inferred relation between cold and dry periods and enhanced aeolian activity at the Chinese Loess Plateau, ~600 km north-east of Lake Donggi Cona, for example (Stauch et al., 2012).

A short-term climatic reversal to cold and dry conditions at ~8.5 cal. ka BP is suggested from a lake level reduction, inferred from erosional unconformities, cryogenic sediment distortion, and a potential fluvial phase in the onshore high-stand sediments (Chapter 4.2.5, Dietze et al., 2013). Loess was deposited on the highest onshore terrace T4 (Stauch et al., 2012), which could have been incised during that time. Though it is not discussed for the Lake Donggi Cona sediment cores, this onshore evidence for a cool/dry phase correlates with the global centennial cooling at ~8.2 ka (Rohling and Pälike, 2005). This event was also interpreted, e.g., from peat in the Nianbaoyeze mountains, and Lakes Qinghai and Koucha on the north-eastern Tibetan Plateau (Shen et al., 2005, Schlütz and Lehmkuhl, 2009, Mischke et al., 2008). Hence, a climatic explanation for this lake level decline, down to around 8 m a.p.l.l. (Figure 5.1, Chapter 4.2.5, Dietze et al., 2013), is very likely, but did not leave behind a recognizable onshore landform.

A further secondary lake level maximum between ~7 to 7.5 ka may correspond to the formation of the tread of terrace T3 at ~10.1 m a.p.l.l. (Figure 5.1). Many lake records across the Tibetan Plateau suggest the maximum of the Holocene climatic optimum during this time (Zhang and Mischke, 2009). However, at ~6.8 cal. ka BP Lake Donggi Cona opened and

turned into a freshwater system, which is documented by a change in ostracod assemblages (Mischke et al., 2010a). The opening could have been caused either by a strong seismic event, or a geomorphologically-driven capture by lateral erosion from the large alluvial fan, allowing the spillway to be eroded prior to a deterioration of climatic conditions.

After the outlet incision, the lake level probably stabilized at 6.1 m a.p.l.l. and the T3-terrace was incised. At the same time the large alluvial fan at the outlet kept aggradating, as an OSL age of $\sim 5.5 \pm 0.5$ ka from a sand lens in 188 cm depth suggests (G. Stauch, personal communication, April 2012).

Around 4.5 cal. ka BP, a change in carbonate precipitation and lake stratification was documented in the lake sediment cores (Opitz et al., 2012) and no high-stand sediments were deposited thereafter. This change to a lower lake level probably stabilized at the T1-terrace level at 3.5 m a.p.l.l. and corresponds to a further abrupt global transition (similar to the event at ~ 11.5 cal. ka BP, Morrill et al., 2003) towards drier and/or cooler conditions reflected at many sites in central Asia (e.g., reviews in Morrill et al., 2003; Wanner et al., 2011) that affected also Chinese society (Wu and Liu, 2004).

The formation by incision of the lowermost onshore terrace generation (T1) probably occurred after the outlet was artificially altered by man in the 1970s (Lockot, 2010) – at the time when water demand in the Qaidam basin rose after the extension of agricultural areas, and when population grew in the Donggi Cona area. Except for this young human impact, lake level changes were mainly driven by climate and altered by indirect tectonic and/or geomorphological dynamics.

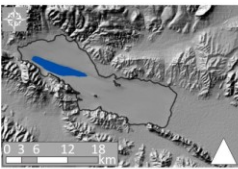
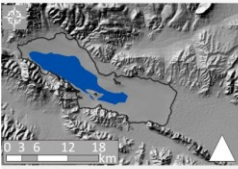
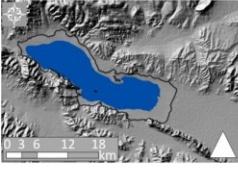
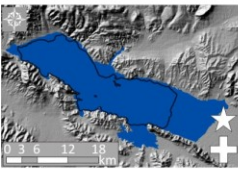
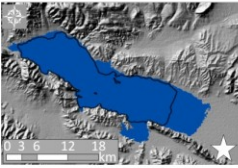
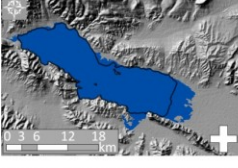
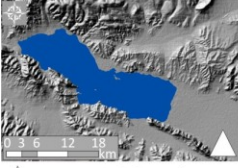
| Water levels of Lake Donggi Cona relative to p.l.l. | Lake extents (mean elevation, area, volume) | Age (cal. ka BP) | Assumed sedimentary and environmental processes |
|---|--|------------------|--|
|  | - 57 m, 16 km ² min. 0.3 km ³ | older than 20 | <ul style="list-style-type: none"> Delta sediment deposition (Unit Ib) in eastern sub-basin Coldest, driest conditions |
|  | - 39 m, 62 km ² min. 1.3 km ³ | older than 20 | <ul style="list-style-type: none"> Several stacked deltas on northern graben rim (Unit Ia,b) Probably deglaciation |
|  | - 24 m, 147 km ² 3.4 km ³ | ~20 | <ul style="list-style-type: none"> Gilbert-type delta at northern rim (Unit II), topsets correlate with PG 1970 silty sand base (Opitz et al., 2012) LGM stand |
|  | + 16.5 m, max. 360 km ² max. 12.3 km ³ | ~9.0-9.2 | <ul style="list-style-type: none"> Littoral sediments in onshore section P15 (T4 terrace) Highest lake stand from maximum monsoon precipitation |
|  | + 8 m, 308 km ² 9.3 km ³ | ~8.5 | <ul style="list-style-type: none"> Cryoturbation, erosion phase, no littoral/lacustrine, but fluvial onshore sediments Incision of T4 terrace Short-term cooler, drier |
|  | + 10 m, 320 km ² 9.9 km ³ | ~7.0-7.5 | <ul style="list-style-type: none"> Highest lake sediments in T3 terrace (e.g., section P14) Secondary lake maximum, mid-Holocene optimum |
|  | + 6 m, 295 km ² 8.6 km ³ | ~4.5-6.7 | <ul style="list-style-type: none"> Lake sediment deposition on T2 level, incision of T3 terrace Lake stand after non-climatic, locally-induced lake opening Discontinuous lake level decline |
|  | + 3 m, 280 km ² 7.9 km ³ | younger than 4.3 | <ul style="list-style-type: none"> End of high-stand sedimentation Incision of T2 terrace, T1 lake stand Stratification/geochemical change in offshore lake sediments Transition to cooler, drier conditions |
|  | 0 m, 229 km ² 6.8 km ³ | modern | <ul style="list-style-type: none"> Artificial outflow regulation since 1970s Incision of T1 terrace (Lockot, 2010) |

Figure 5.1: Extents of Lake Donggi Cona and associated sedimentary and environmental processes. Evidence for lake high-stands after Dietze et al. (2010, submitted) and calculation of lake extents after Dietze et al. (2010) and Lockot (2010).

6. CONCLUSIONS

The dissertation presented here considered the sensitivity of the Donggi Cona lake basin and its sediment cascade to climatic changes by investigating the lake basin morphology, sedimentary processes in the littoral zone and the lake, as well as past water level changes. In general, to quantitatively reconstruct past hydrological conditions in a lake catchment it is essential to consider the lake basin and littoral morphology, as well as related sedimentary processes, and a robust analysis of proxy data.

Aeolian, fluvial/alluvial, littoral, and lacustrine sedimentation dominate the local sediment cascade. A meaningful analysis of grain size distributions helped to assess sediment transport processes from modern lacustrine and fossil high-stand sediments. Robust grain size end-members that represent the deep lake environment can be used to infer past lake level changes, assuming that the finest particles settle only in a calm water column. These are implications that can be transferred easily to other lake catchments and their sedimentary environments.

However, the heterogeneous geological and geomorphological catchment, shore, and basin configurations of Lake Donggi Cona complicated the interpretation of past lake level changes using granulometric data, and probably affected the uncertainty in radiocarbon dating, as well. Hence, further approaches and proxy data (e.g., geochemical data, ostracod assemblages) are needed to include and interpret ambiguous sediment strata in the lake level history, especially the complex section, P14. A better age control using different carbon fractions for ^{14}C -dating or dating approaches independent of hard-water and reservoir effects (e.g., OSL dating of high-stand sediments) could help reduce the current large hard-water uncertainties.

Despite these ambiguities, Lake Donggi Cona seems to have been highly sensitive to past hydrological variations, although it is currently an open, freshwater system. Water level changes left a distinct fingerprint in the basin and littoral morphology, as well as the sediment architecture. Extensive lake level changes during the late Quaternary were recorded, displaying previous lake stands ranging from 57 m below to 16.5 m above the present lake level, corresponding to a change in lake area and volume of \sim 16 to 360 km 2 and \sim 0.3 to 12.3 km 3 , respectively, or a range from \sim 4 to 180 % compared to the present volume (i.e., 229 km 2 , 6.8 km 3 ; Figure 5.1).

Direct displacement of lake terraces below and above the present lake level caused by vertical tectonic movements seems to be negligible for the time scales considered here. Instead, tectonic impacts must be considered in an indirect way; as earthquakes that shake

unconsolidated sediments, or in the effects that tectonics have on the configuration and geomorphological processes at the lake's spillway.

Climatic impact seems to be the main driver of lake changes. Water supply to the lake is derived mainly from Asian summer monsoon precipitation and runoff. The lake was drastically reduced during cold and dry periods of the Pleistocene, but did not desiccate. Deeper delta sediments may be related tentatively to past, mid Pleistocene meltwater input. However, meltwater input seems to have played only a minor role in the lake level rise after the -24 m lake stand during MIS 2, starting at ~11.5 cal. ka BP. Lake Donggi Cona reached its highest levels during the early and mid-Holocene. Onshore high-stand sediments further indicate a short-term lake level decline at ~8.5 cal. ka BP and a general shift towards lower lake levels at ~4.5 cal. ka BP, in accordance with major global climate shifts. Local geomorphological and tectonic impacts on lake level changes further modified the initial lake level rise, and may be responsible for the opening of the lake system at ~6.8 cal. ka BP.

Human impact played a minor role during the last 3500 years, when grazing could have started to affect aeolian sediment mobilisation (Stauch et al., 2012). Since the 1970s, lake level is controlled at an artificial outlet to provide water for the cultivated land of the Qaidam Basin. This human intervention not only led to the incision of the lowest onshore terrace (Lockot, 2010) but now alters the association of the present lake level to modern climatic conditions, because discharge measurements at the outlet are not available.

If further studies utilize quantitative reconstructions of past lake volumes to establish a local water balance model (e.g., as Morrill, 2004 did), then the lake stand prior to 1970 should be used (i.e., the T1 level). However, hydrological and climatic data are sparse from that time period and a preliminary study using the downscaled, grid-based regional WRF climate model suggests some deviations of the Donggi Cona area compared to the nearest climate station Madoi, especially in the total amount and seasonality of precipitation (F. Maussion, personal communication, July 2012). Furthermore, several lines of error in estimating past lake volumes need to be studied in more detail (e.g., DEM internal deviations, interpolation errors from calculating lake bathymetry, and ranges in reconstructed lake stands, including assumed post-genetic sedimentation).

7. ACKNOWLEDGEMENTS

All the work would not have been possible without the support of several people:

First of all I thank Prof. Dr. Bernd Wünnemann for giving me the chance to participate in a unique project in fascinating China and the Tibetan Plateau. Kai Hartmann opened my eyes for the importance of uncertainties and the world of mathematics and geostatistics. He was always there to discuss and share his enthusiasm, ideas and motivation with me, which contributed significantly to all of my scientific work and personal development. I thank Bernhard Diekmann, Georg Stauch, and Frank Lehmkuhl for fruitful discussions on the separate issues of this thesis and the entire Northern Transect group (including Janneke, Stephan, Gregori, Maggi, Miri, Steffen P., Henrik) for supporting me in many ways during different stages during the last years. Our joint field trips to China will be in my mind forever – don't forget that we meet at Donggi in the year 2025.

I warmly thank all the colleagues and friends that discussed and motivated my work, e.g., Linda, Reik, Andreas, Hans, Roland, Hanna, Steffen M., Robert W. and H., Boris, Christian, Jens, the Young Geomorphologists "family", and the Dresden Geography people, who gave me a home, a lab and motivation in the last nine months, especially Beate, Christopher, Daniel, Dominik, Fritz, Martina, Sascha.

I thank Jin Ming for help with sample mailing and internet access in Lanzhou and for translation of the thesis title. Ian Johnson improved my English (reverseenglishfaults.com).

Alfred joined most of my PhD-time and is the best that happened in the last two years. The time with him on the playground inspired my work most directly and made it more effective. However, most important of all is Micha, who plays sooo many incomparable roles in my life, including work, that it would be too long to mention them all. *Sabes que eres para mi – el segundo ala.*

8. OVERALL REFERENCES

- Abu-Ghazleh S, Kempe S. 2009. Geomorphology of Lake Lisan terraces along the eastern coast of the Dead Sea, Jordan. *Geomorphology* 108: 246-263.
- Aichner B, Herzschuh U, Wilkes H, Schulz H-M, Wang Y, Plessen B, Mischke S, Diekmann B, Zhang C. 2012. Ecological development of Lake Donggi Cona, north-eastern Tibetan Plateau, since the late glacial on basis of organic geochemical proxies and non-pollen palynomorphs. *Palaeogeography, Palaeoclimatology, Palaeoecology* 313-314: 140-149.
- Aitchison J. 1986. The statistical analysis of compositional data. Monographs on statistics and applied probability, Chapman and Hall, London.
- An Z. 2000. The history and variability of the East Asian paleomonsoon climate. *Quaternary Science Reviews* 19: 171-187.
- An Z, Kutzbach JE, Prell WL, Porter SC. 2001. Evolution of Asian monsoons and phased uplift of the Himalaya-Tibetan plateau since Late Miocene times. *Nature* 411: 62-66.
- An Z, Clemens SC, Shen J, Qiang X, Jin Z, Sun Y, Prell WL, Luo J, Wang S, Xu H, Cai Y, Zhou W, Liu X, Liu W, Shi Z, Yan L, Xiao X, Chang H, Wu F, Ai L, Lu F. 2011. Glacial-Interglacial Indian Summer Monsoon Dynamics. *Science* 333: 719-723.
- Anderson E, Bai Z, Bischof C, Blackford S, Demmel J, Dongarra J, Du Croz J, Greenbaum A, Hammarling S, McKenney A, Sorensen D. 1999. LAPACK User's Guide, third edition, SIAM, Philadelphia.
- Anselmetti FS, Ariztegui D, Hodell DA, Hillesheim MB, Brenner M, Gilli A, McKenzie JA, Mueller AD. 2006. Late Quaternary climate-induced lake level variations in Lake Petén Itzá, Guatemala, inferred from seismic stratigraphic analysis, *Palaeogeography, Palaeoclimatology, Palaeoecology* 230: 52–69.
- Arhonditsis GB, Stow CA, Steinberg LJ, Kenney MA, Lathrop RC, McBride SJ, Reckhow KH. 2006. Exploring ecological patterns with structural equation modeling and Bayesian analysis. *Ecological Modelling* 192: 385-409.
- Bartholdy J, Christiansen C, Pedersen JBT. 2007. Comparing spatial grain-size trends inferred from textural parameters using percentile statistical parameters and those based on the log-hyperbolic method. *Sedimentary Geology* 202: 436-452.
- Beres M, Gilli A, Ariztegui D, Anselmetti FS. 2008. The Lago Cardiel Basin, Argentina (49°S), Origin and evolution revealed by high-resolution multichannel seismic reflection studies. *Journal of South American Earth Sciences* 25: 74-85.
- Bernal S, Butturini A, Sabater F. 2006. Inferring nitrate sources through end member mixing analysis in an intermittent Mediterranean stream. *Biogeochemistry* 81: 269-289.
- Blais JM, Kalff J. 1995. The influence of lake morphometry on sediment focussing. *Limnology and Oceanography* 40: 582-588.
- Blanchet FG, Legendre P, Borcard D. 2008. Modelling directional spatial processes in ecological data. *Ecological Modelling* 215: 325-336.
- Böhner J. 2006. General climatic controls and topoclimatic variations in Central and High Asia. *Boreas* 35: 279-295.

- Bolch T, Kulkarni A, Käab A, Huggel C, Paul F, Cogley JG, Frey H, Kargel JS, Fujita K, Scheel M, Bajracharya S, Stoffel M. 2012. The State and Fate of Himalayan Glaciers. *Science* 336: 310-314.
- Bräuning A, Mantwill B. 2004. Summer temperature and summer monsoon history on the Tibetan Plateau during the last 400 years recorded by tree rings. *Geophysical Research Letters* 31: L24205.
- Brooks K, Scholz CA, King JW, Peck J, Overpeck JT, Russell JM, Amoako PYO. 2005. Late-Quaternary lowstands of lake Bosumtwi, Ghana, evidence from high-resolution seismic-reflection and sediment-core data. *Palaeogeography, Palaeoclimatology, Palaeoecology* 216: 235-249.
- Brown ET, Bendick R, Bourlas DL, Gaur V, Molnar P, Raisbeck GM, Yiou F. 2003. Early Holocene climate recorded in geomorphological features in Western Tibet. *Palaeogeography, Palaeoclimatology, Palaeoecology* 199: 141-151.
- Buccianti A, Mateu-Figueras G, Pawlowsky-Glahn V. (Eds.), 2006. Compositional Data Analysis in the Geosciences: From Theory to Practice. Special Publication 264, Geological Society, London.
- Burns DA, McDonnell JJ, Hooper RP, Peters NE, Freer LE, Kendall C, Beven K. 2001. Quantifying contributions to storm runoff through end-member mixing analysis and hydrologic measurements at the Panola Mountain Research Watershed (Georgia, USA). *Hydrological Processes* 15: 1903-1924.
- Catuneanu O, Abreu V, Bhattacharya JP, Blum MD, Dalrymple RW, Eriksson PG, Fielding CR, Fisher WL, Galoway WE, Gibling MR, Giles KA, Holbrook JM, Jordan R, Kendall CGSC, Macurda B, Martinsen OJ, Miall AD, Neal JE, Nummedal D, Pomar L, Posamentier HW, Pratt BR, Sarg JF, Shanley KW, Steel RJ, Strasser A, Tucker ME, Winkler C. 2009. Towards the standardization of sequence stratigraphy. *Earth-Science Reviews* 92: 1-33.
- Charlet F, Fagel N, De Batist M, Hauregard F, Minnebo B, Meischner D. 2005. Sedimentary dynamics on isolated highs in Lake Baikal: evidence from detailed high-resolution geophysical data and sediment cores. *Global and Planetary Change* 46: 125-144.
- Chen CTA, Lan HC, Lou JY, Chen YC. 2003. The dry Holocene Megathermal in Inner Mongolia. *Palaeogeography, Palaeoclimatology, Palaeoecology* 193: 181-200.
- Chen F, Zhu Y, Li JJ, Shi Q, Jin LY, Wünnemann B. 2001. Abrupt Holocene changes of the Asian monsoon at millennial-and centennial-scales, evidence from lake sediment document in Minqin Basin, NW China. *Chinese Science Bulletin* 46: 1942-1947.
- Chen F-H, Chen J-H, Holmes J, Boomer I, Austin P, Gates JB, Wang N-L, Brooks SJ, Zhang JW. 2010. Moisture changes over the last millennium in arid central Asia: a review, synthesis and comparison with monsoon region. *Quaternary Science Reviews* 29: 1055-1068.
- Chen F, Cheng B, Zhao Y, Zhu Y, Madsen D 2006. Holocene environmental change inferred from a high-resolution pollen record, Lake Zhuyeze, arid China. *The Holocene* 16: 675-684.
- Chen F, Yu Z, Yang M, Ito E, Wang S, Madsen DB, Huang X, Zhao Y, Sato T, John B, Birks H, Boomer I, Chen J, An C, Wünnemann B. 2008. Holocene moisture evolution in arid central Asia and its out-of-phase relationship with Asian monsoon history. *Quaternary Science Reviews* 27: 351-364.
- Chen Q, Freymueller JT, Wang Q, Yang Z, Xu C. 2004. A deforming block model for the present-day tectonics of Tibet. *Journal Geophysical Research* 109: B01403.
- Chen Y, Li Y, Zhang Y, Zhang M, Zhang J, Yi C, Liu G. 2011. Late Quaternary deposition and incision sequences of the Golmud River and their environmental implications. *Quaternary International* 236: 48-56.

- Chinese Central Meteorological Office. 2008. Average climatology for 841 meteorological stations throughout China, 1951-2007 (Meteorological Data of China). Meteorology Press, Beijing.
- Christensen ER, Arora S. 2007. Source apportionment of PAHs in sediments using factor analysis by time records: Application to Lake Michigan, USA. *Water Research* 41: 168-176.
- Christophersen N, Neal C, Hooper RP, Vogt RD, Andersen S. 1990. Modelling streamwater chemistry as a mixture of soilwater end-members – A step towards second-generation acidification models. *Journal of Hydrology* 116: 307-320.
- Clarke T. 1978. An oblique factor analysis solution for the analysis of mixtures. *Mathematical Geology* 10: 225-241.
- Cohen AS. 2003. Paleolimnology: the history and evolution of lake systems. Oxford University Press, New York.
- Collins AL, Walling DE, Webb L, King P. 2010. Apportioning catchment scale sediment sources using a modified composite fingerprinting technique incorporating property weightings and prior information. *Geoderma* 155: 249-261.
- Colman SM. 2006. Acoustic stratigraphy of Bear Lake, Utah-Idaho, Late Quaternary sedimentation patterns in a simple half-graben. *Sedimentary Geology* 185: 113-125
- Colman SM, Kelts KR, Dinter DA. 2002. Depositional history and neotectonics in Great Salt Lake, Utah, from high-resolution seismic stratigraphy. *Sedimentary Geology* 148: 61-78.
- Colman SM, Yu S-Y, An Z, Shen J, Henderson ACG. 2007. Late Cenozoic climate changes in China's western interior: a review of research on Lake Qinghai and comparison with other records. *Quaternary Science Reviews* 26: 2281-2300.
- D'Agostino K, Seltzer G, Baker P, Fritz S, Dunbar R. 2002. Late-Quaternary lowstands of Lake Titicaca, evidence from high-resolution seismic data. *Palaeogeography, Palaeoclimatology, Palaeoecology* 179: 97-111.
- Daut G, Mäusbacher R, Baade J, Gleixner G, Kroemer E, Mügler I, Wallner J, Wang J, Zhu L. 2010. Late Quaternary hydrological changes inferred from lake level fluctuations of Nam Co (Tibetan Plateau, China). *Quaternary International* 218: 86-93.
- De Terra H, Hutchinson GE. 1934. Evidence of recent climate change shown by Tibetan highland lakes. *Geographical Journal* 84: 311-320.
- Dechert WD, O'Donnell SI. 2006. The stochastic lake game: A numerical solution. *Journal of Economic Dynamics and Control* 30: 1569-1587.
- Diekmann B, Kuhn G. 1999. Provenance and dispersal of glacial-marine surface sediments in the Weddell Sea and adjoining areas, Antarctica: ice-rafting versus current transport. *Marine Geology* 158: 209-231.
- Dietze E, Wünnemann B, Diekmann B, Aichner B, Hartmann K, Herzschuh U, Ijmker J, Jin H, Kopsch C, Lehmkuhl F, Li S, Mischke S, Niessen F, Opitz S, Stauch G, Yang S. 2010. Basin morphology and seismic stratigraphy of Lake Donggi Cona, north-eastern Tibetan Plateau, China. *Quaternary International* 218: 131-142.
- Dietze E, Hartmann K, Diekmann B, Ijmker J, Lehmkuhl F, Opitz S, Stauch G, Wünnemann B, Borchers A. 2012. An end-member algorithm for deciphering modern detrital processes from lake sediments of Lake Donggi Cona, NE Tibetan Plateau, China. *Sedimentary Geology* 243-244: 169-180.

- Ding L, Kapp P, Wan X. 2005. Paleocene-Eocene record of ophiolite obduction and initial India-Asia collision, south central Tibet. *Tectonics* 24, TC3001, doi:10.1029/2004TC001729, 18p.
- Domrös M, Peng G. 1988. The climate of China. Springer, Berlin, Heidelberg, New York.
- Dykoski CA, Edwards RL, Cheng H, Yuan D, Cai Y, Zhang M, Lin Y, Qing J, An Z, Revenaugh J. 2005. A high-resolution, absolute-dated Holocene and deglacial Asian monsoon record from Dongge Cave, China. *Earth and Planetary Science Letters* 233: 71-86.
- Filzmoser P, Hron K. 2009. Correlation Analysis for Compositional Data. *Mathematical Geosciences* 41: 905-919.
- Filzmoser P, Hron K, Reimann C, Garrett R. 2009. Robust factor analysis for compositional data. *Computers & Geosciences*, 35: 1854-1861.
- Fleitmann D, Burns SJ, Mudelsee M, Neff U, Kramers J, Mangini A, Matter A. 2003. Holocene Forcing of the Indian Monsoon Recorded in a Stalagmite from Southern Oman. *Science* 300: 1737-1739.
- Flemming BW. 2007. The influence of grain-size analysis methods and sediment mixing on curve shapes and textural parameters: Implications for sediment trend analysis. *Sedimentary Geology* 202: 425-435.
- Folk RL, Ward WC. 1957. Brazos river bar: a study in the significance of grain size parameters. *Journal of Sedimentary Petrology* 27: 3-26.
- Fu B, Awata Y. 2007. Displacement and timing of left-lateral faulting in the Kunlun Fault Zone, northern Tibet, inferred from geologic and geomorphic features. *Journal of Asian Earth Sciences* 29: 253-265.
- Fu B, Awata Y, Du J, He W. 2005. Late Quaternary systematic stream offsets caused by repeated large seismic events along the Kunlun fault, northern Tibet. *Geomorphology* 71: 278-292.
- Garzanti E, Andò S, Vezzosi G. 2009. Grain-size dependence of sediment composition and environmental bias in provenance studies. *Earth and Planetary Science Letters* 277: 422-432.
- Gasse F, Arnold M, Fontes JC, Fort M, Gibert E, Huc A, Bingyan L, Yuanfang L, Qing L, Melieres F, van Campo E, Fubao W, Qingsong Z. 1991. A 13.000-year climate record from western Tibet. *Nature* 353: 742-745.
- GLCF. 2008. Global Landcover Facility. <http://glcf.umiacs.umd.edu/index.shtml> [10.12.2008]
- Guttman L. 1954. Some necessary conditions for common-factor analysis. *Psychometrika* 19: 149-161.
- Hamann Y, Ehrmann W, Schmiedl G, Krüger S, Stuut J-B, Kuhn T. 2008. Sedimentation processes in the Eastern Mediterranean Sea during the Late Glacial and Holocene revealed by end-member modelling of the terrigenous fraction in marine sediments. *Marine Geology* 248: 97-114.
- Harris N. 2006. The elevation history of the Tibetan Plateau and its implications for the Asian monsoon. *Palaeogeography, Palaeoclimatology, Palaeoecology* 241: 4-15.
- Harrison SP, Digerfeldt G. 1993. European lakes as palaeohydrological and palaeoclimatic indicators. *Quaternary Science Reviews* 12: 233-248.
- Hartmann D. 2007. From reality to model: Operationalism and the value chain of particle-size analysis of natural sediments. *Sedimentary Geology* 202: 383-401.
- Hartmann K, Wünnemann B. 2009. Hydrological changes and Holocene climate variations in NW China, inferred from lake sediments of Juyanze palaeolake by factor analyses. *Quaternary International* 194: 28-44.

- Henderson ACG, Holmes JA, Zhang J, Leng MJ, Carvalho LR. 2003. A carbon- and oxygen-isotope record of recent environmental change from Qinghai Lake, NE Tibetan Plateau. *Chinese Science Bulletin* 48: 1463-1468.
- Herzschuh U. 2006. Palaeo-moisture evolution in monsoonal Central Asia during the last 50,000 years. *Quaternary Science Reviews* 25: 163-178.
- Herzschuh U, Tarasov P, Wünnemann B, Hartmann K. 2004. Holocene vegetation and climate of the Alashan Plateau, NW China, reconstructed from pollen data. *Palaeogeography, Palaeoclimatology, Palaeoecology* 211: 1-17.
- Herzschuh U, Winter K, Wünnemann B, Li S. 2006. A general cooling trend on the central Tibetan Plateau throughout the Holocene recorded by the Lake Zigelang pollen spectra. *Quaternary International* 154-155: 113-121.
- Herzschuh U, Kramer A, Mischke S, Zhang C. 2009. Quantitative climate and vegetation trends since the late glacial on the northeastern Tibetan Plateau deduced from Koucha Lake pollen spectra. *Quaternary Research* 71: 162-171.
- Heyman J, Stroeven AP, Caffee MW, Hättestrand C, Harbor JM, Li Y, Alexanderson H, Zhou L, Hubbard A. 2011. Palaeoglaciology of Bayan Har Shan, NE Tibetan Plateau: exposure ages reveal a missing LGM expansion. *Quaternary Science Reviews* 30: 1988-2001.
- Hofmann MH, Hendrix MS, Moore JN, Sperazza M. 2006. Late Pleistocene and Holocene depositional history of sediments in Flathead Lake, Montana, Evidence from high-resolution seismic reflection interpretation. *Sedimentary Geology* 184: 111-131.
- Holmes JA, Zhang J, Chen F, Qiang M. 2007. Paleoclimatic implications of an 850-year oxygen-isotope record from the northern Tibetan Plateau. *Geophysical Research Letters* 34: doi:10.1029/2007GL032228.
- Holz C, Stuut J-B, Henrich R, Meggers H. 2007. Variability in terrigenous sedimentation processes off northwest Africa and its relation to climate changes: Inferences from grain-size distributions of a Holocene marine sediment record. *Sedimentary Geology* 202: 499-508.
- Hou J, D'Andrea WJ, Liu Z. 2012. The influence of ^{14}C reservoir age on interpretation of paleolimnological records from the Tibetan Plateau. *Quaternary Science Reviews* 48: 67-79.
- Huang X, Sillanpää M, Duo B, Gjessing ET. 2008. Water quality in the Tibetan Plateau: metal contents of four selected rivers. *Environmental Pollution* 156: 270-277.
- IJmker J, Stauch G, Pötsch S, Diekmann B, Wünnemann B, Lehmkühl F. 2012a. Dry periods on the NE Tibetan Plateau during the late Quaternary. *Palaeogeography, Palaeoclimatology, Palaeoecology* 346-347: 108-119.
- IJmker J, Stauch G, Hartmann K, Diekmann B, Dietze E, Opitz S, Wünnemann B, Lehmkühl F. 2012b. Environmental conditions in the Donggi Cona lake catchment, NE Tibetan Plateau, based on factor analysis of geochemical data. *Journal of Asian Earth Sciences* 44: 176-188.
- Imbrie J. 1963. Factor and vector analysis programs for analyzing geologic data. Technical Report 6, ONR Task No. 389-135, Office of Naval Research, Geography Branch.
- Jackson DA, Somers KM. 1991. The spectre of 'spurious' correlations. *Oecologia*: 86, 147-151.
- Ji S, Liu X, Wang S, Ryo M. 2005. Palaeoclimatic changes in the Qinghai Lake area during the last 18,000 years. *Quaternary International* 136: 131-140.

- Jin Z, Yu J, Chen H, Wu Y, Wang S, Chen S. 2007. The influence and chronological uncertainties of the 8.2 ka cooling event on continental climate records in China. *The Holocene* 17: 1041-1050.
- Jones RT, Jordan JT. 2007. Lake level studies - Overview. In: Scott A, Elias A, (Eds.). *Encyclopedia of Quaternary Science*, Elsevier, Oxford, 1319-1336.
- Julià R, Luque JA. 2006. Climatic changes vs. catastrophic events in lacustrine systems: A geochemical approach. *Quaternary International* 158: 162-171.
- Kaiser HF. 1958. The VARIMAX criterion for analytic rotation in factor analysis. *Psychometrika* 23: 187-200.
- Kaiser K, Schoch WH, Miehe G. 2007. Holocene paleosols and colluvial sediments in Northeast Tibet (Qinghai Province, China): Properties, dating and paleoenvironmental implications. *Catena* 69: 91-102.
- Kirby E, Harkins N, Wang E, Shi X, Fan C, Burbank D. 2007. Slip rate gradients along the eastern Kunlun fault. *Tectonics* 26: 1-16.
- Kirkbride MP, Winkler S. 2012. Correlation of Late Quaternary moraines: impact of climate variability, glacier response, and chronological resolution. *Quaternary Science Reviews* 46: 1-29.
- Klovan JE. 1966. The use of factor analysis in determining depositional environments from grain-size distributions. *Journal of Sedimentary Petrology* 36: 115-126.
- Klovan JE, Imbrie J. 1971. An Algorithm and FORTRAN-IV Program for Large-Scale Q-Mode Factor Analysis and Calculation of Factor Scores. *Mathematical Geology* 3: 61-77.
- Kong P, Na C, Brown R, Fabel D, Freeman S, Xiao W, Wang Y. 2011. Cosmogenic ^{10}Be and ^{26}Al dating of paleolake shorelines in Tibet. *Journal of Asian Earth Sciences* 41: 263-273.
- Korup O, Montgomery DR. 2008. Tibetan Plateau river incision inhibited by glacial stabilization of the Tsangpo gorge. *Nature* 455: 786-790.
- Krumbein WC. 1936. Application of logarithmic moments to size frequency distribution of sediments. *Journal of Sedimentary Petrology* 6: 35-47.
- Kucera M, Malmgren BA. 1998. Logratio transformation of compositional data- a resolution of the constant sum constraint. *Marine Micropalaeontology* 34: 117-120.
- Kuhle M. 2003. New geomorphological indicators of a former Tibetan ice sheet in the central and northeastern part of the high plateau. *Zeitschrift für Geomorphologie N.F. Supplement* 130: 75-97.
- Kuhle M. 2011. The High Glacial (Last Ice Age and Last Glacial Maximum) Ice Cover of High and Central Asia, with a Critical Review of Some Recent OSL and TCN Dates. In: Ehlers J, Gibbard PL, Hughes PD, (Eds.). *Developments in Quaternary Sciences*, Elsevier, Oxford, 943-965.
- Kürschner H, Herzschuh U, Wagner D. 2005. Phytosociological studies in the north-eastern Qinghai-Xizang Plateau (NW China) – A first contribution to the subalpine scrub and alpine meadow vegetation. *Botanische Jahrbücher der Systematik* 126: 273-315.
- Lawson CL, Hanson RJ. 1974. *Solving Least Squares Problems*. Prentice Hall, New Jersey.
- Lee J, Li S-H, Aitchison JC. 2009. OSL dating of paleoshorelines at Lagkor Tso, western Tibet. *Quaternary Geochronology* 4: 335-343.

- Lehmkuhl F. 1997. The spatial distribution of loess and loess-like sediments in the mountain areas of Central and High Asia. *Zeitschrift f. Geomorphologie*, N.F., Suppl.-Bd. 111: 97-116.
- Lehmkuhl F, Haselein F. 2000. Quaternary paleoenvironmental change on the Tibetan Plateau and adjacent areas (Western China and Western Mongolia). *Quaternary International* 65/66: 121-145.
- Li CF, He QL, Zhao GG. 2005. Paleo-earthquake studies on the eastern section of the Kunlun fault. *Acta Seismologica Sinica* 18: 64-71.
- Li D, Li Y, Ma B, Dong G, Wang L, Zhao J. 2009. Lake-level fluctuations since the Last Glaciation in Selin Co (lake), Central Tibet, investigated using optically stimulated luminescence dating of beach ridges. *Environmental Research Letters* 4: doi:10.1088/1748-9326/4/4/045204.
- Lister GS, Kelts K, Zao CK, Yu J-Q, Niessen F. 1991. Lake Qinghai, China, closed-basin lake levels and the oxygen isotope record for ostracoda since the latest Pleistocene. *Palaeogeography, Palaeoclimatology, Palaeoecology* 84: 141-162.
- Liu J, Wang S, Yu S, Yang D, Zhang L. 2009. Climate warming and growth of high-elevation inland lakes on the Tibetan Plateau. *Global and Planetary Change* 67: 209-217.
- Liu X, Lai Z, Fan Q, Long H, Sun Y. 2010. Timing for high lake levels of Qinghai Lake in the Qinghai-Tibetan Plateau since the Last Interglaciation based on quartz OSL dating. *Quaternary Geochronology* 5: 218-222.
- Lockot G. 2010. Geomorphologisch-fernerkundliche Untersuchungen zur litoralen Entwicklung des Donggi Cona, Tibet Plateau (China). Diplom thesis, Institute of Geographical Sciences, Free University Berlin.
- Long H, Lai Z, Wang N, Li Y. 2010. Holocene climate variations from Zhuyeze terminal lake records in East Asian monsoon margin in arid northern China. *Quaternary Research* 74: 46-56.
- Madsen DB, Haizhou M, Rhode D, Brantingham PJ, Forman SL. 2008. Age constraints on the late Quaternary evolution of Qinghai Lake, Tibetan Plateau. *Quaternary Research* 69: 316-325.
- Manson V, Imbrie J. 1964. FORTRAN program for factor and vector analysis of geological data using an IBM 7090 or 7094/1401 computer system. *Kansas Geological Survey Special Distribution Publications* 13.
- McManus J. 1988. Grain size determination and interpretation. In: Tucker M, (Ed.). *Techniques in sedimentology*, Blackwell, Oxford, 63-85.
- McLaren P, Hill SH, Bowles D. 2007. Deriving transport pathways in a sediment trend analysis (STA). *Sedimentary Geology* 202: 489-498.
- Miall AD. 1984. *Principles of sedimentary basin analysis*. Springer, New York.
- Miehe G, Kaiser K, Sonam Co, Zhao XQ, Liu JQ. 2008. Geo-ecological transect Studies in Northeast Tibet (Qinghai, China) reveal human-made mid-Holocene environmental changes in the upper Yellow River catchment changing forest to grassland. *Erdkunde* 62: 187-199.
- Miehe G, Miehe S, Kaiser K, Reudenbach C, Behrendes L, La D, Schlütz F. 2009. How old is pastoralism in Tibet? An ecological approach to the making of a Tibetan landscape. *Palaeogeography, Palaeoclimatology, Palaeoecology* 276: 130-147.
- Miesch AT. 1976. Q-Mode factor analysis of geochemical and petrologic data matrices with constant row sums. *U.S. Geological Survey Professional Papers* 574.

- Miesch AT. 1980. Scaling variables and interpretation of eigenvalues in principal component analysis of geologic data. *Mathematical Geology* 12: 523-538.
- Mischke S, Zhang C. 2010. Holocene cold events on the Tibetan Plateau. *Global and Planetary Change* 72: 155-163.
- Mischke S, Kramer M, Zhang C, Shang H, Herzschuh U, Erzinger J. 2008. Reduced early Holocene moisture availability in the Bayan Har Mountains, northeastern Tibetan Plateau, inferred from a multi-proxy lake record. *Palaeogeography, Palaeoclimatology, Palaeoecology* 267: 59-76.
- Mischke S, Zhang C, Börner A, Herzschuh U. 2009. Lateglacial and Holocene variation in aeolian sediment flux over the northeastern Tibetan Plateau recorded by laminated sediments of a saline meromictic lake. *Journal of Quaternary Science* 25: 162-177.
- Mischke S, Aichner B, Diekmann B, Herzschuh U, Plessen B, Wünnemann B, Zhang C. 2010a. Ostracods and stable isotopes of a late glacial and Holocene lake record from the NE Tibetan Plateau. *Chemical Geology* 276: 95-103.
- Mischke S, Bößneck U, Diekmann B, Herzschuh U, Jin H, Kramer A, Wünnemann B, Zhang C. 2010b. Quantitative relationship between water-depth and sub-fossil ostracod assemblages in Lake Donggi Cona, Qinghai Province, China. *Journal of Paleolimnology* 43: 589-609.
- Morrill C. 2004. The influence of Asian summer monsoon variability on the water balance of a Tibetan lake. *Journal of Paleolimnology* 32: 273-286.
- Morrill C, Overpeck JT, Cole JE. 2003. A synthesis of abrupt changes in the Asian summer monsoon since the last deglaciation. *The Holocene* 13: 465-476.
- Muhs DR. 2007. Loess deposits, origins and properties. In: Scott A, Elias A, (Eds.). *Encyclopedia of Quaternary Science*, Elsevier, Oxford, 1405-1418.
- Nelson KD, Zhao W, Brown LD, Kuo J, Che J, Liu X, Klemperer SL, Makovsky Y, Meissner R, Mechie J, Kind R, Wenzel F, Ni J, Nabelek J, Leshou C, Tan H, Wei W, Jones AG, Booker J, Unsworth M, Kidd WSF, Hauck M, Alsdorf D, Ross A, Cogan M, Wu C, Sandvol E, Edwards M. 1996. Partially molten middle crust beneath southern Tibet: synthesis of project INDEPTH results. *Science* 274: 1684-1688.
- Niessen F, Ebel T, Kopsch C, Fedorov GB. 1999. High-resolution seismic stratigraphy of lake sediments on the Taymyr Peninsula, Central Siberia. In: Kassens H, Bauch A, Dmitrenko I, Eicken H, Hubberten HW, Melles M, Thiede J, Timokhov L, (Eds.). *Land-ocean systems in the Siberian Arctic, dynamics and history*, Springer, Berlin, 437-456.
- North CP, Davidson SK. 2012. Unconfined alluvial flow processes: Recognition and interpretation of their deposits, and the significance for palaeogeographic reconstruction. *Earth-Science Reviews* 111: 199-223.
- Opitz S, Wünnemann B, Aichner B, Dietze E, Hartmann K, Herzschuh U, Ijmker J, Lehmkuhl F, Li S, Mischke S, Plotzki A, Stauch G, Diekmann B. 2012. Late Glacial and Holocene development of Lake Donggi Cona, northeastern Tibetan Plateau, inferred from sedimentological analysis. *Palaeogeography, Palaeoclimatology, Palaeoecology* 337-338: 159-176.
- Opitz S, Ramisch A, Ijmker J, Lehmkuhl F, Mischke S, Stauch G, Wünnemann B, Zhang Y, Diekmann B, in review. Spatio-temporal pattern of detrital clay-mineral supply to a lake system on the north-eastern Tibetan Plateau, and its relationship to late Quaternary paleoenvironmental changes. *Journal of Asian Earth Sciences*.

- Orpin AR, Woolfe KJ. 1999. Unmixing relationships as a method of deriving a semi-quantitative terrigenous sediment budget, central Great Barrier Reef lagoon, Australia. *Sedimentary Geology* 129: 25-35.
- Owen LA. 2009. Latest Pleistocene and Holocene glacier fluctuations in the Himalaya and Tibet. *Quaternary Science Reviews* 28: 2150-2164.
- Owen LA, Finkel RC, Haizhou M, Spencer JQ, Derbyshire E, Barnard PL, Caffee MW. 2003. Timing and style of Late Quaternary glaciation in northeastern Tibet. *Geological Society of America Bulletin* 115: 1356-1364.
- Owen LA, Caffee MW, Finkel RC, Seong YB. 2008. Quaternary glaciation of the Himalayan-Tibetan orogen. *Journal of Quaternary Science* 23: 513-531.
- Palmer MJ, Douglas GB. 2008. A Bayesian statistical model for end member analysis of sediment geochemistry, incorporating spatial dependences. *Journal of the Royal Statistical Society Series C-Applied Statistics* 57: 313-327.
- Pan B, Su H, Hu Z, Hu X, Gao H, Li J, Kirby E. 2009. Evaluating the role of climate and tectonics during non-steady incision of the Yellow River: evidence from a 1.24 Ma terrace record near Lanzhou, China. *Quaternary Science Reviews* 28: 3281-3290.
- Pan G, Wang L, Li R, Yuan S, Ji W, Yin F, Zhang W, Wang B. 2012. Tectonic evolution of the Qinghai-Tibet Plateau. *Journal of Asian Earth Sciences* 53: 3-14.
- Papatheodorou G, Demopoulou G, Lambrakis N. 2006. A long-term study of temporal hydrochemical data in a shallow lake using multivariate statistical techniques. *Ecological Modelling* 193: 759-776.
- Peng Y, Xiao J, Nakamura T, Liu B, Inouchi Y. 2005. Holocene East Asian monsoonal precipitation pattern revealed by grain-size distribution of core sediments of Daihai lake, Inner Mongolia of north-central China. *Earth and Planetary Science Letters* 233: 467-479.
- Prins, MA, Weltje GJ. 1999. End-member modelling of grain-size distributions of sediment mixtures. In: Prins MA, (PhD thesis). Pelagic, hemipelagic and turbidite deposition in the Arabian Sea during the late Quaternary: Unravelling the signals of aeolian and fluvial sediment supply as functions of tectonics, sea-level and climate change by means of end-member modelling of siliciclastic grain-size distributions. *Geologica Ultrajectina* 168: Utrecht University, 47-68.
- Prins MA Vriend M, Nugteren G, Vandenberghe J, Lu H, Zheng H, Weltje GJ. 2007. Late Quaternary aeolian dust input variability on the Chinese Loess Plateau: inferences from unmixing of loess grain-size records. *Quaternary Science Reviews* 26: 230-242.
- Pye K. 1995. The nature, origin and accumulation of loess. *Quaternary Science Reviews* 14: 653-667
- Qiang XK, Li ZX, Powell C, Zheng H. 2001. Magnetostratigraphic record of the Late Miocene onset of the East Asian monsoon, and Pliocene uplift of northern Tibet. *Earth Planetary Science Letters* 187: 83-93.
- Qiu J. 2008. The third pole. *Nature* 454: 393-396.
- Reimann C, Filzmoser P, Garrett RG. 2002. Factor analysis applied to regional geochemical data: problems and possibilities. *Applied Geochemistry* 17: 185-206.
- Reimer PJ, Baillie MGL, Bard E, Bayliss A, Beck JW, Bertrand CHJ, Blackwell PG, Buck CE, Burr GS, Cutler KB, Damon PE, Edwards RL, Fairbanks RG, Friedrich M, Guilderson TP, Hogg AG, Hughen KA, Kromer B, McCormac G, Manning SW, Bronk Ramsey C, Reimer RW, Plicht JVD, Weyhenmeyer CE. 2004. IntCal04 terrestrial radiocarbon age calibration, 0–26 cal kyr BP. *Radiocarbon* 46: 1029-1058.

- Reimer PJ, Baillie MGL, Bard E, Bayliss A, Beck JW, Blackwell PG, Bronk Ramsey C, Buck CE, Burr GS, Edwards RL, Friedrich M, Guilderson TP, Hajdas I, Heaton TJ, Hogg AG, Hughen KA, Kaiser KF, Kromer B, McCormac G, Manning SW, Reimer RW, Richards DA, Southon JR, Talamo S, Turney CSM, van der Plicht J, Weyhenmeyer CE. 2009. IntCal09 and Marine09 radiocarbon age calibration curves, 0–50,000 years cal BP. *Radio-carbon* 51: 1111-1150.
- Renner RM. 1991. An examination of the use of the logratio transformation for the testing of endmember hypotheses. *Mathematical Geology* 23: 549-563.
- Renner RM. 1995. The construction of extreme compositions. *Mathematical Geology* 27: 485-497.
- Renner RM. 1996. An algorithm for constructing extreme composition. *Camp. Geosciences* 21: 15-25.
- Renner RM, Glasby GP, Walter P. 1997. Endmember analysis of metalliferous sediments from the Galapagos Rift and East Pacific Rise between 2°N and 42°S. *Applied Geochemistry* 12: 383-395.
- Renner RM, Glasby GP, Szefer P. 1998. Endmember analysis of heavy-metal pollution in surficial sediments from the Gulf of Gdańsk and the southern Baltic Sea off Poland. *Applied Geochemistry* 13: 313-318.
- Reyment RA, Jöreskog KG. 1993. Applied factor analysis in the natural sciences. Cambridge University Press, Cambridge.
- Robichaud PR, Lewis SA, Laes DYM, Hudak AT, Kokaly RF, Zamudio JA. 2007. Postfire soil burn severity mapping with hyperspectral image unmixing. *Remote Sensing of Environment* 108: 467-480.
- Rohling EJ, Palike H. 2005. Centennial-scale climate cooling with a sudden cold event around 8,200 years ago. *Nature* 434: 975-979.
- Royden LH, Burchfiel BC, van der Hilst RD. 2008. The Geological Evolution of the Tibetan Plateau. *Science* 321: 1054-1058.
- Schlüter F, Lehmkühl F. 2009. Holocene climatic change and the nomadic Anthropocene in Eastern Tibet: palynological and geomorphological results from the Nianbaoyeze Mountains. *Quaternary Science Reviews* 28: 1449-1471.
- Schmidt D. 1999. Das Extremklima der nordchilenischen Hochatacama unter besonderer Berücksichtigung der Höhengradienten. *Dresdener Geographische Beiträge* 4, pp 122.
- Schütt B, Berking J, Frechen M, Yi C. 2008. Late Pleistocene lake level fluctuations of the Nam Co, Tibetan Plateau, China. *Zeitschrift für Geomorphologie* 52: 57-74.
- Shen J, Liu X, Wang S, Matsumoto R. 2005. Palaeoclimatic changes in the Qinghai Lake area during the last 18,000 years. *Quaternary International* 136: 131-140.
- Shi Z, Liu X, Cheng X. 2012. Anti-phased response of northern and southern East Asian summer precipitation to ENSO modulation of orbital forcing. *Quaternary Science Reviews* 40: 30-38.
- Slaymaker O, Spencer T, Dadson S. 2009. Landscape and landscape-scale processes as the unfilled niche in the global environmental changes debate: an introduction. In: Slaymaker O, Spencer T, Embleton-Hamann C, (Eds.). *Geomorphology and global environmental change*, Cambridge University Press, Cambridge, 1-36.
- Solohub JT, Klovan JE. 1970. Evaluation of grain-size parameters in lacustrine environments. *Journal of Sedimentary Petrology* 40: 81-101.

- Song C. 2005. Spectral mixture analysis for subpixel vegetation fractions in the urban environment: How to incorporate endmember variability? *Remote Sensing of Environment* 95: 248-263.
- Sonnentag O, Chen JM, Roberts DA, Talbot J, Halligan KQ, Govind A. 2007. Mapping tree and shrub leaf area indices in an ombrotrophic peatland through multiple endmember spectral unmixing. *Remote Sensing of Environment* 109: 342-360.
- Stanimirova I, Walczak B, Massart DL. 2005. Multiple factor analysis in environmental chemistry. *Analytica Chimica Acta* 545: 1-12.
- Stauch G, Ijmker J, Pötsch S, Zhao H, Hilgers A, Diekmann B, Dietze E, Hartmann K, Opitz S, Wünnemann B, Lehmkühl F, in review. Aeolian sediments on the north-eastern Tibetan Plateau. *Quaternary Science Reviews*.
- Stokes M, Cunha PP, Martins AA. 2012. Techniques for analysing Late Cenozoic river terrace sequences. *Geomorphology* 165-166: 1-6.
- Street-Perrott FA, Harrison SP. 1985. Lake levels and climate reconstruction. In: Hect AD, (Ed.). *Paleoclimate Analysis and Modeling*, Wiley, New York, 291-340.
- Stroeven AP, Hättestrand C, Heyman J, Harbor J, Li YK, Zhou LP, Caffee MW, Alexanderson H, Kleman J, Ma HZ, Liu GN. 2009. Landscape analysis of the Huang He headwaters, NE Tibetan Plateau - Patterns of glacial and fluvial erosion. *Geomorphology* 103: 212-226.
- Stuiver M, Reimer PJ 1993. Radiocarbon 35: 215-230.
- Sun D, Bloemendal J, Rea DK, Vandenberghe J, Jiang F, An Z, Su R. 2002. Grain-size distribution function of polymodal sediments in hydraulic and aeolian environments, and numerical partitioning of the sedimentary components. *Sedimentary Geology* 152: 263-277.
- Sun J, Li S-H, Muhs DR, Li B. 2007. Loess sedimentation in Tibet: provenance, processes, and link with Quaternary glaciations. *Quaternary Science Reviews* 26: 2265-2280.
- Szefer P, Glasby GP, Geldon J, Renner RM, Bjorn E, Snell J, Frech W, Warzocha J. 2009. Heavy-metal pollution of sediments from the Polish exclusive zone, southern Baltic Sea. *Environmental Geology* 57: 847-862.
- Taft L, Wiechert U, Riedel F, Weynell M, Zhang H. 2012. Sub-seasonal oxygen and carbon isotope variations in shells of modern *Radix* sp. (Gastropoda) from the Tibetan Plateau: potential of a new archive for palaeoclimatic studies. *Quaternary Science Reviews* 34: 44-56.
- Tapponnier P, Xu Z, Roger F, Meyer B, Arnaud N, Wittlinger G, Yang J. 2001. Oblique stepwise rise and growth of the Tibet Plateau. *Science* 294: 1671-1677.
- Thompson LG, Mosley-Thompson E, Davis M, Lin PN, Yao T, Dyurgerov M, Dai J. 1993. "Recent warming": ice core evidence from tropical ice cores with emphasis on Central Asia. *Global and Planetary Change* 7: 145-156.
- USGS/NEIC. 2012. Seismicity and seismic hazard map of China and rectangular area earthquake search. <http://earthquake.usgs.gov/earthquakes/> [06. August 2012].
- Van der Woerd J, Ryerson FJ, Tapponnier P, Meriaux A-S, Gaudemer Y, Meyer B, Finkel RC, Caffee MW, Guoguang Z, Zhiqing X. 2000. Uniform slip-rate Along the Kunlun Fault, implications for seismic behaviour and large-scale tectonics. *Geophysical Research Letters* 27: 2353-2356.
- Van der Woerd J, Tapponnier P, Ryerson FJ, Meriaux A-S, Meyer B, Gaudemer Y, Finkel RC, Caffee MW, Guoguang Z, Zhiqing X. 2002. Uniform postglacial slip-rate along the central 600 km of the Kunlun Fault (Ti-

- bet), from ^{26}Al , ^{10}Be , and ^{14}C dating of riser offsets, and climatic origin of the regional morphology. *Geophysical Journal International* 148: 356-388.
- Van Vliet-Lanoë B. 1998. Frost and soils: implications for paleosols, paleoclimates and stratigraphy. *Catena* 34: 157-183.
- Van Wagoner JC, Mitchum RM, Campion KM, Rahmanian VD. 1990. Siliciclastic sequence stratigraphy in well logs, cores, and outcrops, concepts for high-resolution correlation of time and facies. *The American Association of Petroleum Geologists, Tulsa*.
- Vandenberghhe J, Wang X, Lu H. 2011. Differential impact of small-scaled tectonic movements on fluvial morphology and sedimentology (the Huang Shui catchment, NE Tibet Plateau). *Geomorphology* 134: 171-185.
- Wagner B, Reicherter K, Daut G, Wessels M, Matzinger A, Schwab A, Spirkovski Z, Sanxhaku M. 2008. The potential of Lake Ohrid for long-term palaeoenvironmental reconstructions. *Palaeogeography, Palaeoclimatology, Palaeoecology* 259: 341-356.
- Walling DE. 2005. Tracing suspended sediment sources in catchments and river systems. *Science of the Total Environment* 344: 159-184.
- Wan S, Li A, Clift PD, Stuut J-B. 2007. Development of the East Asian monsoon: Mineralogical and sedimentologic records in the northern South China Sea since 20 Ma. *Palaeogeography, Palaeoclimatology, Palaeoecology* 254: 561-582.
- Wang A, Smith JA, Wang G, Zhang K, Xiang S, Liu D. 2009. Late Quaternary river terrace sequences in the eastern Kunlun Range, northern Tibet: A combined record of climatic change and surface uplift. *Journal of Asian Earth Sciences* 34: 532-543.
- Wang B, Ding Q. 2006. Changes in global monsoon precipitation over the past 56 years. *Geophys. Res. Letters*, 33: L06711, doi: 10.1029/2005GL025347.
- Wang Y, Yang H. 2004. Middle Permian palaeobiogeography study in East Kunlun, A'nyêmaqên and Bayan Har. *Science in China* 47: 1120-1126.
- Wang Y, Xu G, Lin Q, Gong S. 2001. Depositional model of Early Permian reef-island ocean in Eastern Kunlun. *Science in China* 44: 808-815.
- Wang Y, Liu X, Herzschuh U. 2010. Asynchronous evolution of the Indian and East Asian Summer Monsoon indicated by Holocene moisture patterns in monsoonal central Asia. *Earth-Science Reviews* 103: 135-153.
- Wanner H, Solomina O, Grosjean M, Ritz SP, Jetel MT. 2011. Structure and origin of Holocene cold events. *Quaternary Science Reviews* 30: 3109-3123.
- Weltje J. 1997. End-Member Modeling of Compositional Data: Numerical-Statistical Algorithms for Solving the Explicit Mixing Problem. *Mathematical Geology* 29: 503-549.
- Weltje GJ, Prins MA. 2003. Muddled or mixed? Inferring palaeoclimate from size distributions of deep-sea clastics. *Sedimentary Geology* 162: 39-62.
- Weltje J, Prins MA. 2007. Genetically meaningful decomposition of grain-size distributions. *Sedimentary Geology* 202: 409-424.
- Whipple KX. 2009. The influence of climate on the tectonic evolution of mountain belts. *Nature Geoscience* 2: 97-104.

- Wischnewski J, Mischke S, Wang Y, Herzschuh U. 2011. Reconstructing climate variability on the northeastern Tibetan Plateau since the last Lateglacial - a multi-proxy, dual-site approach comparing terrestrial and aquatic signals. *Quaternary Science Reviews* 30: 82-97.
- Wobus C, Whipple KX, Kirby E, Snyder N, Johnson J, Spyropolou K, Crosby B, Sheehan D. 2006. Tectonics from topography: Procedures, promise, and pitfalls. *Geological Society of America Special Papers* 398: 55-74.
- Wu S, Yin Y, Zheng D, Yang Q. 2006. Moisture conditions and climate trends in China during the period 1971-2000. *International Journal of Climatology* 26: 193-206.
- Wu W, Liu T. 2004. Possible role of the "Holocene Event 3" on the collapse of Neolithic cultures around the central plain of China. *Quaternary International* 117: 153-166.
- Wu Y, Cui Z, Liu G, Ge D, Yin J, Xu Q, Pang Q. 2001. Quaternary geomorphological evolution of the Kunlun Pass area and uplift of the Qinghai-Xizang (Tibet) Plateau. *Geomorphology* 36: 203-216.
- Wu Y, Lücke A, Zhangdong J, Sumin W, Schleser GH, Battarbee RW, Weilan X. 2006. Holocene climate development on the central Tibetan Plateau, A sedimentary record from Cuoe Lake. *Palaeogeography, Palaeoclimatology, Palaeoecology* 234: 328-340.
- Wünnemann B, Pachur H-J, Zhang H. 1998. Climatic and environmental changes in the deserts of Inner Mongolia, China, since the Late Pleistocene. In: Alsharhan A, Glennie KW, Whittle GL, Kendall CG, (Eds.). *Quaternary Deserts and Climatic Change*. Balkema Publishing House, Rotterdam, 381-394.
- Wünnemann B, Mischke S, Chen F. 2006. A Holocene sedimentary record from Bosten Lake, China. *Palaeogeography, Palaeoclimatology, Palaeoecology* 234: 223-238.
- Wünnemann B, Hartmann K, Altmann N, Hambach U, Pachur H-J, Zhang H. 2007a. Interglacial and glacial fingerprints from lake deposits in the Gobi Desert, NW China. In: Sirocko F, María Fernanda Sánchez Goñi MC, Litt T, (Eds.). *The Climate of Past Interglacials*, Elsevier, Oxford, 323-347.
- Wünnemann B, Hartmann K, Janssen M, Zhang H. 2007b. Responses of Chinese desert lakes to climate instability during the past 45,000 years. In: Madsen DB, (Ed.). *Late Quaternary Climate Change and Human Adaptation in Arid China*, Elsevier, Oxford, 11-24.
- Wünnemann B, Reinhardt C, Kotlia BS, Riedel F. 2009. Observations on the relationship between lake formation, permafrost activity and lithalsa development during the last 20,000 years in the Tso Kar basin, Ladakh, India. *Permafrost and Periglacial Processes* 19: 341-358.
- Wünnemann B, Demske D, Tarasov P, Kotlia BS, Reinhardt C, Bloemendal J, Diekmann B, Hartmann K, Krois J, Riedel F, Arya N. 2010. Hydrological evolution during the last 15 kyr in the Tso Kar lake basin (Ladakh, India), derived from geomorphological, sedimentological and palynological records. *Quaternary Science Reviews* 29: 1138-1155.
- Xin H. 2008. A Green Fervor Sweeps the Qinghai-Tibetan Plateau. *Science* 321: 633-635.
- Xu H, Hou ZH, Ai L, Tan LC. 2007. Precipitation at Lake Qinghai, NE Qinghai-Tibet Plateau, and its relation to Asian summer monsoons on decadal/interdecadal scales during the past 500 years. *Palaeogeography, Palaeoclimatology, Palaeoecology* 254: 541-549.
- Yin A, Harrison TM. 2000. Geological evolution of the Himalayan-Tibetan Orogen. *Annual Review of Earth and Planetary Sciences* 28: 211-280.

- Yu G, Harrison SP, Xue B. 2001. Lake status records from China: Data Base Documentation. Technical Reports - Max-Planck-Institute für Biogeochemie 4, pp 243.
- Zhang C, Mischke S. 2009. A Lateglacial and Holocene lake record from the Nianbaoyeze Mountains and inferences of lake, glacier and climate evolution on the eastern Tibetan Plateau. Quaternary Science Reviews 28: 1970-1983.
- Zhang HC, Ma YZ, Wünnemann B, Pachur H-J. 2000. A Holocene climatic record from arid northwestern China. Palaeogeography, Palaeoclimatology, Palaeoecology 162: 389-401.
- Zhang H, Wünnemann B, Ma Y, Peng J, Pachur H-J, Li J, Qi Y, Chen G, Fang H, Feng Z. 2002. Lake Level and Climate Changes between 42,000 and 18,000 14C yr B.P. in the Tengger Desert, Northwestern China. Quaternary Research 58: 62-72.
- Zhao Y, Yu Z. 2012. Vegetation response to Holocene climate change in East Asian monsoon-margin region. Earth-Science Reviews 113: 1-10.
- Zheng H, McAulay Powell C, An Z, Zhou J, Dong G. 2000. Pliocene uplift of the northern Tibetan Plateau. Geology 28: 715-718.
- Zimmerman ARB, Owen RM. 1990. A Quantitative Model of the Dispersal of Detrital Inputs and Minor Compositional Components in Lake Michigan Sediments. Journal of Great Lakes Research 16: 444-456.

9. APPENDIX

9.1 END-MEMBER MODELING SCRIPT FOR MATLAB

```
% % End-member modelling script published in Dietze et al., 2012
% % by E. Dietze, A. Borchers & K. Hartmann (2009/2010)
%
% % Preconditions of input data:
% % grain size classes as variables in columns with header row in 1st row, samples in rows
% with header column % as 1st column, optional water depth (or e.g. depth in core) in 2nd
% column
%
% % Locations of necessary parameters
% % 1. Constant sum value: c, line 35
% % 2. Percentile weight for scaling and transformation: l, line 44
% % 3. Loop (9A) to find optimal EM model: start line 91, end line 202
% % Alternative: number of end-members for manual choice (9B): q, line 95. If 9A is active,
% put loop lines 91 % and 202 in comment (%) (also lines 204 to 232) and remove comment signs
% from line 235 on
% % 4. Visualisation steps (no. 20 and 21 to 22) only reasonable for loop
% % routine (9A) and manually chosen end-member number (9B), respectively

%% 1. Import dataset
clear all
data = load('GSD.txt'); % data import including labels
X = data(2:end, 3:end);
[m,n] = size(X); % size of the matrix
% X: (mxn) matrix with original data
% m rows: observations (e.g. sample ID/ sites/ depths)
% n columns: variables (e.g. phi classes of grain sizes)

% for labelling
phi = data(1,3:end)'; % variables
dcs = data(2:end,1); % observations
depth = data(2:end,2); % additional information from sampling

% Scaling of data to constant sum
c = 100;
% c: scalar, value of constant sum

for j = 1:m
    X(j,:) = X(j,:) / sum(X(j,:)) * c;
end
% X: matrix with data scaled to constant sum

%% 2. Weight transformation
l = 4;
% l: percentile weight after Manson & Imbrie (1964), Klovan & Imbrie (1971)
% special case: l = 0 (Miesch, 1976)
for i = 1:m
    for j = 1:n
        h = prctile(X(:,j), l);
        g = prctile(X(:,j), 100-l);
        w(i,j) = (X(i,j) - h) / (g - h);
    end
end
% w: (mxn) matrix with weight transformed data

%% 3. Definition of the similarity matrix
A = w' * w;
% A: (mxm) matrix Gamma, i.e. minor product matrix after Weltje (1997)

%% 4. Extraction of the eigenspace (Reyment & Jöreskog, 1993)
[V,D] = eig(A);
% V: (nxn) matrix with eigenvectors
% D: (nxn) matrix with eigenvalues in the diagonal

%% 5. Eigenvalues in column vector
L = diag(D);
% L: vector Lambda of size n which contains all eigenvalues from D

%% 6. Calculation of eigenvalue proportions
Ln = L / sum(L);
% Ln: vector Lambda normalised, which gives the fraction of variance of the principal components

%% 7. Proportion of variance for decision on minimum number of eigenvectors
Lv = cumsum(flipud(Ln));
% Lv: vector Lambda cumulative, with cumulative fractions of the
% eigenvector's variance concerning the absolute variance of w

%% 8. A plot for visualisation of Lv
% serves for evaluating the proportions and how many factors are necessary
figure(1)
tickstep = 1:1:n;
plot(tickstep, Lv), xlabel('Number of eigenvectors'),
ylabel('Explained cumulative variance'), grid
```

```

set(gca, 'xTick', tickstep)

%% 9A. Loop for decision on maximum or optimal number of end-members
for q = 2:n
% start of loop depending on number of eigenvectors, if the loop is instable change to a
number < n

%% 9B. Definition of number of end-members (i.e. alternative to 9A)
% q = 5;
% q: number of end-members, manually defined from figure 1 (change q if goodness of fit is
poor)

%% 10. Creation of the rotation matrix (only the signal space is rotated)
clear vq % clear variables, necessary for alternative 9B
vq = rotatefactors(v(:,(n - q + 1):n), 'Normalize', 'off'); % default = varimax
% Vq: (nxq) matrix with rotated loadings
% Alternative: e.g. oblique rotation
% Vqobl = rotatefactors(v(:,(n - q + 1):n), 'Method', 'promax');
% Vq = Vqobl;

%% 11. Normalisation of factor loadings to interval (0,1)
for k = 1:q
    vq(:,k) = vq(:,k) / sum(vq(:,k)) * c;
    vqn(:,k) = (vq(:,k) - min(vq(:,k))) / (max(vq(:,k)) - min(vq(:,k)));
end
% Vqn: (nxq) matrix with rotated, normalised, nonnegative loadings

%% 12. Estimation of M (eigenvector scores) with nonnegative least squares
clear Mq
for i = 1:m
    Mq(i,:) = lsqnonneg(Vqn, (w(i,:))');
end
% Mq: (nxq) matrix with nonnegative eigenvector scores

%% 13. Linear modelling of w
clear Wq
Wm = Mq * Vqn';
% Wm: (nxp) matrix with modelled, weighted dataset after Weltje (1997)

%% 14. Inverse transformation Vq to initial units by S (after Miesch, 1976)
for k = 1:q
    for j = 1:n
        h = prctile(x(:,j), 1);
        g = prctile(x(:,j), 100-1);
        s(k) = (c - sum(h)) / (sum(vqn(:,k)) * (g - h));
    end
end
% S: scaling factor of size q to invert the initial weight transformation

for k = 1:q
    for j = 1:n
        h = prctile(x(:,j), 1);
        g = prctile(x(:,j), 100-1);
        Vqs(j,k) = s(k) * vqn(j,k) * (g - h) + h;
    end
end
% Vqs: (nxq) matrix with inversely scaled loadings

%% 15. Scale data to constant sum
for k = 1:q
    for j = 1:n
        Vqsn(j,k) = Vqs(j,k) / sum(Vqs(:,k)) * c;
    end
end
% Vqsn: (nxq) matrix with scaled, inversely scaled end-member loadings

%% 16. Re-transformation of factor scores Mq by S
for i = 1:m
    for k = 1:q
        Mqs(i,k) = (Mq(i,k) / s(k)) / sum(Mq(i,:)) / s(k);
    end
end
% Mqs: (mxq) matrix with normalised, inversely scaled end-member scores

% Calculation of relative variance, explained by each end-member
Mqsvar = var(Mqs) / sum(var(Mqs)) * 100;
% Mqsvar: vector of relative explained variance by each end-member

%% 17. Linear modelling of X'
clear Xm
Xm = Mqs * Vqs';
% Xm: (mxn) matrix with modelled data set X'

%% 18. Evaluation of model deviation from original dataset
% Absolute difference between re-transformed, modelled dataset and
% original dataset
Ex = X - Xm;
% Ex: (mxn) matrix with absolute errors, i.e. residuals

mean_sax(q,:) = mean(Ex');
mean_gsx(q,:) = mean(Ex);
mean_ex(q,q) = mean(mean_gsx(q,:));

```

```

% mean_sax: vector with mean deviations of all observations
% mean_gsx: vector with mean deviations of all variables
% mean_ex: mean deviation of all data

% Relative measure of relationship between modelled and original data
% (squared Pearson's correlation coefficient)
for i = 1:m
    pearsx = corrcoef(x(i,:), xm(i,:)); % correlation of observations
    corr_xm(q,i) = pearsx(1,2).^2;
end
mean_r2_xm(q,q) = mean(corr_xm(q,:));
% mean_r2_xm: vector with mean r2 for modelled and original observations

for j = 1:n
    pearsx = corrcoef(x(:,j), xm(:,j)); % correlation of variables
    corr_xn(q,j) = pearsx(1,2).^2;
end
mean_r2_xn(q,q) = mean(corr_xn(q,:));
% mean_r2_xn: vector with mean r2 for modelled and original variables

% 19. End of q-loop and goodness of fit evaluation, if 9A is activated
end

mean_ex1 = diag(mean_ex);
mean_r2_xm1 = diag(mean_r2_xm);
mean_r2_xn1 = diag(mean_r2_xn);
mean_xr2 = mean([mean_r2_xm1, mean_r2_xn1]');?>
% mean_ex1: vector with mean absolute error of  $x - x'$ 
% mean_r2_xm1: vector with mean r2 for modelled and original observations
% mean_r2_xn1: vector with mean r2 for modelled and original variables
% mean_xr2: vector with mean r2 for all data

%% 20. Visualisation of loop-gained goodness of fit parameters
% plot of mean absolute error of  $x - x'$ 
figure(2),
plot(2:n, mean_ex1(2:n), 'k'), grid, hold on
xlabel('Number of end-member'), ylabel('Mean absolute error [vol. %]'),
legend('X vs. Xm')

% plot of mean r2 (observations, variables, all data) for visual decision
% on maximum number of end-members qmax
figure(3),
plot(2:n, mean_xr2(2:n), 'k'), grid, hold on,
xlabel('Number of end-member'), ylabel('Mean total r2'),
legend('X vs. X_m')

% alternative to the figure above: only mean r2 for all data
figure(3),
plot(2:n, mean_r2_xm1(2:n), 'b', 2:n, mean_r2_xn1(2:n), 'r'), grid,
hold on, xlabel('Number of end-member'), ylabel('r2 of X to X_m'),
legend('Observations', 'Grain size classes')

%% 21. Visualisation of goodness of fit for manual q (alternative 9B)
% figure(4),
% subplot(1,2,1); plot(phi, mean_gsx(q,:), 'k*')
% xlabel('GSD [phi]'), ylabel('Mean absolute difference [vol. %]'), grid,
% legend('X vs. X_m')
% subplot(1,2,2); plot(dcs, mean_sax(q,:), 'k*')
% xlabel('DCS sample ID'), ylabel('Mean absolute difference [vol. %]'), grid,
% legend('X vs. X_m')
%
% figure(5),
% subplot(1,2,1); plot(phi, corr_xn(q,:), 'k*')
% xlabel('Grain size [phi]'), ylabel('Mean total r2'), grid,
% legend('X vs. X_m')
% subplot(1,2,2); plot(dcs, corr_xn(q,:), 'k*')
% xlabel('Sample ID'), ylabel('Mean total r2'), grid,
% legend('X vs. X_m')

%% 22. Visualisation of end-members for manual q (alternative 9B)
% % Plot of the factor loadings
% figure(6)
% plot(phi, vqsn), xlabel('Grain size [phi]'),
% ylabel('End-member loading [vol. %]'), grid, hold on
% legend('EM1', 'EM2', 'EM3', 'EM4', 'EM5')
% % save('Phi2B_96er5EM_Vqsn.txt', 'vqsn', '-ascii');
%
% % Plot of the factor scores
% figure(7)
% bar(dcs, Mqs), xlabel('Sample ID'), ylabel('End-member score [%]'), grid,
% legend('EM1', 'EM2', 'EM3', 'EM4', 'EM5', 'EM6')
% % save('Phi2B_Mqs_96er5EM.txt', 'Mqs', '-ascii');
% % Fin

```

9.2 LIST OF PUBLICATIONS AND PRESENTATIONS

All own and co-authored publications since July 2008 are presented.

PUBLICATIONS IN PEER-REVIEWED JOURNALS

Biskaborn BK, Herzschuh U, Bolshiyanov DY, **Dietze E**, Schwamborn G, Diekmann B. **in review**. Physico-chemical processes and cyclic depositional events in thermokarst lakes of the NE Siberian tundra. *Permafrost and Periglacial Processes*.

Borchers A, **Dietze E**, Kuhn G, Esper O, Voigt I, Hartmann K, Diekmann B., **in review**. Ice dynamics and bottom-water formation due to Cape Darnley polynya activity in the Burton Basin, East Antarctica, since the last glacial. *Palaeogeography, Palaeoclimatology, Palaeoecology*.

Dietze E, Diekmann B, Wünnemann B, Aichner B, Hartmann K, Herzschuh U, Ijmker J, Kopsch C, Lehmkuhl F, Li S, Mischke S, Niessen F, Opitz S, Stauch G. **2010**. Basin morphology and seismic stratigraphy of Lake Donggi Cona, north-eastern Tibetan Plateau, China. *Quaternary International* 218, 131-142.

Dietze E, Hartmann K, Diekmann B, Ijmker J, Lehmkuhl F, Opitz S, Stauch G, Wünnemann B, Borchers A. **2012**. An end-member algorithm for deciphering modern detrital processes from lake sediments of Lake Donggi Cona, NE Tibetan Plateau, China. *Sedimentary Geology* 243-244, 149-180.

Dietze E, Wünnemann B, Hartmann K, Diekmann B, Jin H, Yang S, Stauch G, Lehmkuhl F., 2013. Early to mid-Holocene lake high-stand sediments at Lake Donggi Cona, north-eastern Tibetan Plateau, China. *Quaternary Research*, <http://dx.doi.org/10.1016/j.yqres.2012.12.008>.

Dietze M, Muhs S, **Dietze E**. **2011**. Ambiguities of relative age indicators on abandoned surfaces of arid environments. *Zeitschrift für Geomorphologie, Supplementbände* 55-3, 49 - 75.

Dietze M, Kleber A, **Dietze E. in review**. Environmental history recorded in stone pavement-covered soil-sediment complexes, Cima volcanic field, USA. *Journal of Quaternary Science*.

Ijmker J, Stauch G, Hartmann K, Diekmann B, **Dietze E**, Opitz S, Wünnemann B, Lehmkuhl F. **2012**. Environmental conditions in the Donggi Cona lake catchment, NE Tibetan Plateau, based on factor analysis of geochemical data. *Journal of Asian Earth Sciences* 44, 176-188.

Ijmker J, Stauch G, Hartmann K, Diekmann B, **Dietze E**, Opitz S, Wünnemann B, Lehmkuhl F. **in review**. Definition of transport processes and sedimentary deposits based on end-member mixing analysis of terrestrial sediments in the Donggi Cona lake catchment, NE Tibetan Plateau, *Sedimentary Geology*.

Opitz S, Wünnemann B, Aichner B, **Dietze E**, Hartmann K, Herzschuh U, Ijmker J, Lehmkuhl F, Li S, Mischke S, Plotzki A, Stauch G, Diekmann B. **2012**. Late glacial and Holocene development of Lake Donggi Cona, north-eastern Tibetan Plateau, inferred from sedimentological analysis. *Palaeogeography, Palaeoclimatology, Palaeoecology* 337-338, 159-176.

Stauch G, Ijmker J, Pötsch S, Zhao H, Hilgers A, Diekmann B, **Dietze E**, Hartmann K, Opitz S, Wünnemann B, Lehmkuhl F. **in review**. Aeolian sediments on the north-eastern Tibetan Plateau. *Quaternary Science Reviews*.

ORAL PRESENTATIONS

Dietze E. 2012. Eigenspace analysis of multiple proxies. DFG-TiP Proxy Workshop Berlin, 3. April 2012.

Dietze E. 2012. Spätquartäre Seespiegelschwankungen am Donggi Cona See, nordöstliches Tibet Plateau. Invited talk, Geographisches Kolloquium Freie Universität Berlin, 17. April, 2012.

Dietze E. 2012. Spätquartäre Seespiegelschwankungen des Donggi Cona Sees im nordöstlichen Hochland von Tibet. Invited talk, Physisch-geographisches Forschungskolloquium Universität Leipzig, 11. January, 2012.

Dietze E, Lockot G. 2012. Landscape and Lake-System Response to Late Quaternary Monsoon Dynamics on the Tibetan Plateau. TiP-BMBF PhD Workshop Oberjoch, 20.-26. January 2012.

Dietze E, Wünnemann B, Hartmann K, Diekmann B, Opitz S, Paprotzki M, Runge M, Yang S, Lockot G. 2012. Windows into the past: On-shore high-stand sediments from lake Donggi Cona, NE Tibetan Plateau. EGU General Assembly 2012, Vienna, 23.-27. April 2012.

Dietze E, Maussion F, Seeber E. 2011. The TiP Young Scientist and Early Career Programme - Pictures tell more than words: impressions from TiP YSc courses. 7th workshop for Tibetan Plateau Research, Hamburg, 3.-5. March 2011.

Dietze E, Hartmann K, Wünnemann B, Borchers A, Diekmann B, IJmker J, Lehmkuhl F, Stauch G, Opitz S. 2010. Quantifying geomorphological response to climate change by "unmixing" of lake sediments. EGU General Assembly 2010, Vienna, 2.-7. May 2010.

Dietze E. 2010. Lake level changes of Lake Donggi Cona, north-eastern Tibetan Plateau. AK Wüstenrandforschung, Rauschholzhausen, 5.-6. February 2010.

Dietze E. 2009. Basin morphology and seismic stratigraphy of lake Donggi Cona, north-eastern Tibetan Plateau, China. 6th workshop for Tibetan Plateau Research, Qingdao, 8-12 October 2009.

Dietze E. 2008. Lake level changes at Donggi Cona and Lake Ayakhum, north(east)ern Tibetan Plateau. Invited talk, TU Bergakademie Freiberg, 5. December, 2008.

POSTER PRESENTATIONS

Dietze E, Hartmann K. 2011. End-member modelling analysis (EMMA) - deciphering modern detrital processes from lake sediments of Lake Donggi Cona, NE Tibetan Plateau, China. AK Wüstenrandforschung, Rauschholzhausen, 4.-5. February 2011.

Dietze E, Hartmann K, Diekmann B, Opitz S, Lehmkuhl F, IJmker J, Stauch G, Wünnemann B. 2011. Modern detrital processes in Lake Donggi Cona from end-member modelling analysis (EMMA). 7th workshop for Tibetan Plateau Research, Hamburg, 3.-5. March 2011.

Dietze E, Wünnemann B, Hartmann K, Paprotzki M, Runge M, Lockot G. 2011. Höhere Seespiegelstände am Donggi Cona, NE Tibet Plateau, aus geomorphologischen und sedimentologischen Ansätzen. AK Geomorphologie, Leipzig, 28.September-01.October 2011.

Dietze E, Wünnemann B, Hartmann K, Paprotzki M, Runge M, Lockot G. 2011. Higher lake stands at Lake Donggi Cona, northeastern Tibetan Plateau – combining geomorphological and sedimentological approaches. INQUA, Bern, 21.-27. June 2011. *NATURE GEOSCIENCE POSTER AWARD*

Dietze E, Diekmann B, Kopsch C, Hartmann K, Wünnemann B. 2009. Basin morphology of Lake Donggi Cona, north-eastern Tibetan Plateau, as a combined result of tectonic and climatic forcing. EGU General Assembly 2009, Vienna, 19.-24. April 2009.

Dietze E, Wünnemann B, Hartmann K, Diekmann B, Opitz S, Lehmkuhl F, IJmker J, Stauch G, Rother H. 2009. Higher lake levels at the north-eastern Tibetan Plateau – Geomorphological and sedimentological indications at

Lake Donggi Cona, China. 6th workshop for Tibetan Plateau Research, Qingdao (China), 8.-12. October 2009.

Dietze E, Diekmann B, Opitz S, Mischke S, Hartmann K, Lockot G, Stauch G, Lehmkühl F, Ijmker J, Wünnemann B. 2008. Basin morphology of Donggi Cona from echo soundings and seismic profiling. 4th Sino-German Workshop on Environmental Changes Central Asia in Nanjing, 6.-11. October 2008.

9.3 LIST OF ORIGINAL GRAIN SIZE DATA SETS

| Section | Height (cm) original | | Depth (cm) | | Grain size distributions (Laser Coulter Counter, AWI Potsdam) in ϕ | | | | | | | | | | | | | | | | | | | | |
|------------|----------------------|----------|------------|---------------|---|--------|--------|--------|--------|--------|--------|--------|--------|--------|--------|--------|-------|-------|-------|-------|-------|-------|-------|-------|-------|
| | & ID | (base=0) | mean | depth (top=0) | mean | 11.381 | 11.245 | 11.111 | 10.977 | 10.841 | 10.708 | 10.572 | 10.438 | 10.304 | 10.168 | 10.035 | 9.900 | 9.765 | 9.631 | 9.496 | 9.362 | 9.227 | 9.092 | 8.959 | |
| P02 | | | | | | | | | | | | | | | | | | | | | | | | | |
| 512 | 5 | 9 | 7.0 | 285 | 281 | 283 | 0.036 | 0.064 | 0.095 | 0.140 | 0.170 | 0.210 | 0.240 | 0.280 | 0.320 | 0.360 | 0.410 | 0.460 | 0.520 | 0.590 | 0.660 | 0.740 | 0.820 | 0.910 | 1.000 |
| 514 | 13 | 18 | 15.5 | 277 | 272 | 274.5 | 0.038 | 0.067 | 0.099 | 0.140 | 0.180 | 0.210 | 0.240 | 0.260 | 0.290 | 0.300 | 0.320 | 0.330 | 0.340 | 0.350 | 0.360 | 0.360 | 0.370 | 0.370 | 0.370 |
| 516 | 22 | 29 | 25.5 | 268 | 261 | 264.5 | 0.020 | 0.035 | 0.052 | 0.075 | 0.094 | 0.110 | 0.130 | 0.150 | 0.160 | 0.180 | 0.190 | 0.200 | 0.210 | 0.220 | 0.230 | 0.240 | 0.250 | 0.250 | 0.260 |
| 518 | 33 | 37 | 35.0 | 257 | 253 | 255 | 0.062 | 0.110 | 0.160 | 0.230 | 0.290 | 0.340 | 0.380 | 0.430 | 0.460 | 0.490 | 0.520 | 0.540 | 0.560 | 0.570 | 0.580 | 0.600 | 0.610 | 0.630 | 0.650 |
| 520 | 41 | 44 | 42.5 | 249 | 246 | 247.5 | 0.110 | 0.190 | 0.280 | 0.390 | 0.490 | 0.570 | 0.640 | 0.710 | 0.770 | 0.810 | 0.850 | 0.880 | 0.900 | 0.920 | 0.940 | 0.950 | 0.980 | 1.010 | 1.040 |
| 522 | 46 | 50 | 48.0 | 244 | 240 | 242 | 0.070 | 0.120 | 0.180 | 0.260 | 0.330 | 0.390 | 0.460 | 0.530 | 0.600 | 0.670 | 0.750 | 0.850 | 0.950 | 1.080 | 1.210 | 1.360 | 1.520 | 1.690 | 1.870 |
| 524 | 54 | 58 | 56.5 | 236 | 232 | 233.5 | 0.058 | 0.100 | 0.150 | 0.220 | 0.270 | 0.320 | 0.360 | 0.400 | 0.430 | 0.460 | 0.480 | 0.490 | 0.510 | 0.520 | 0.530 | 0.540 | 0.550 | 0.560 | 0.570 |
| 526 | 62 | 64 | 63.5 | 228 | 226 | 226.5 | 0.067 | 0.120 | 0.180 | 0.250 | 0.310 | 0.370 | 0.420 | 0.460 | 0.500 | 0.540 | 0.560 | 0.580 | 0.590 | 0.610 | 0.610 | 0.620 | 0.630 | 0.640 | 0.650 |
| 528 | 68 | 70 | 69.5 | 222 | 220 | 220.5 | 0.068 | 0.120 | 0.180 | 0.250 | 0.320 | 0.390 | 0.450 | 0.520 | 0.600 | 0.680 | 0.770 | 0.870 | 0.990 | 1.130 | 1.290 | 1.470 | 1.660 | 1.860 | 2.060 |
| 530 | 73 | 77 | 75.5 | 217 | 213 | 214.5 | 0.091 | 0.160 | 0.240 | 0.340 | 0.430 | 0.510 | 0.590 | 0.670 | 0.760 | 0.840 | 0.930 | 1.040 | 1.150 | 1.280 | 1.420 | 1.580 | 1.750 | 1.930 | 2.110 |
| 532 | 80 | 83 | 81.5 | 210 | 207 | 208.5 | 0.100 | 0.180 | 0.270 | 0.380 | 0.480 | 0.560 | 0.630 | 0.700 | 0.760 | 0.810 | 0.850 | 0.890 | 0.920 | 0.950 | 0.990 | 1.020 | 1.060 | 1.110 | 1.170 |
| 534 | 87 | 90 | 88.5 | 203 | 200 | 201.5 | 0.089 | 0.160 | 0.230 | 0.330 | 0.410 | 0.480 | 0.540 | 0.600 | 0.650 | 0.690 | 0.720 | 0.750 | 0.770 | 0.790 | 0.810 | 0.830 | 0.860 | 0.890 | 0.930 |
| 536 | 94 | 97 | 95.5 | 196 | 193 | 194.5 | 0.110 | 0.190 | 0.290 | 0.410 | 0.510 | 0.590 | 0.670 | 0.750 | 0.820 | 0.880 | 0.920 | 0.960 | 1.000 | 1.040 | 1.080 | 1.120 | 1.170 | 1.220 | 1.280 |
| 538 | 100 | 104 | 102.0 | 190 | 186 | 188 | 0.120 | 0.220 | 0.320 | 0.460 | 0.570 | 0.670 | 0.750 | 0.840 | 0.910 | 0.960 | 1.010 | 1.050 | 1.090 | 1.140 | 1.180 | 1.230 | 1.290 | 1.360 | 1.440 |
| 567 | 265 | 270 | 267.5 | 25 | 20 | 22.5 | 0.120 | 0.210 | 0.310 | 0.450 | 0.550 | 0.650 | 0.730 | 0.820 | 0.890 | 0.950 | 0.990 | 1.030 | 1.070 | 1.110 | 1.150 | 1.180 | 1.230 | 1.280 | 1.340 |
| P06 | | | | | | | | | | | | | | | | | | | | | | | | | |
| 49 | 4 | 7 | 5.5 | 336.0 | 333.0 | 334.5 | 0.035 | 0.062 | 0.092 | 0.130 | 0.170 | 0.210 | 0.240 | 0.280 | 0.330 | 0.370 | 0.420 | 0.480 | 0.540 | 0.600 | 0.670 | 0.740 | 0.810 | 0.880 | 0.950 |
| 51 | 10 | 13 | 11.5 | 330.0 | 327.0 | 328.5 | 0.033 | 0.059 | 0.088 | 0.130 | 0.170 | 0.200 | 0.240 | 0.290 | 0.330 | 0.380 | 0.430 | 0.470 | 0.530 | 0.580 | 0.630 | 0.670 | 0.720 | 0.760 | 0.800 |
| 53 | 16 | 19 | 17.5 | 324.0 | 321.0 | 322.5 | 0.026 | 0.047 | 0.070 | 0.100 | 0.130 | 0.170 | 0.200 | 0.240 | 0.280 | 0.330 | 0.380 | 0.430 | 0.480 | 0.540 | 0.590 | 0.650 | 0.700 | 0.750 | 0.800 |
| 55 | 22 | 25 | 23.5 | 318.0 | 315.0 | 316.5 | 0.024 | 0.043 | 0.065 | 0.094 | 0.120 | 0.150 | 0.180 | 0.210 | 0.250 | 0.290 | 0.330 | 0.370 | 0.410 | 0.460 | 0.510 | 0.560 | 0.610 | 0.650 | 0.700 |
| 57 | 28 | 31 | 29.5 | 312.0 | 309.0 | 310.5 | 0.052 | 0.092 | 0.140 | 0.190 | 0.240 | 0.280 | 0.330 | 0.370 | 0.410 | 0.450 | 0.530 | 0.590 | 0.650 | 0.710 | 0.790 | 0.870 | 0.950 | 1.040 | |
| 59 | 34 | 36 | 35.0 | 306.0 | 304.0 | 305.0 | 0.052 | 0.093 | 0.140 | 0.200 | 0.250 | 0.300 | 0.340 | 0.390 | 0.440 | 0.480 | 0.520 | 0.570 | 0.610 | 0.660 | 0.700 | 0.750 | 0.790 | 0.840 | 0.890 |
| 61 | 39 | 42 | 40.5 | 301.0 | 298.0 | 299.5 | 0.089 | 0.160 | 0.230 | 0.330 | 0.410 | 0.480 | 0.540 | 0.600 | 0.660 | 0.710 | 0.750 | 0.790 | 0.840 | 0.890 | 0.950 | 1.010 | 1.080 | 1.150 | 1.230 |
| 63 | 45 | 48 | 46.5 | 295.0 | 292.0 | 293.5 | 0.160 | 0.280 | 0.410 | 0.590 | 0.720 | 0.840 | 0.940 | 1.040 | 1.120 | 1.180 | 1.230 | 1.280 | 1.330 | 1.380 | 1.430 | 1.490 | 1.560 | 1.630 | 1.710 |
| 65 | 51 | 54 | 52.5 | 289.0 | 286.0 | 287.5 | 0.210 | 0.360 | 0.530 | 0.760 | 0.940 | 1.090 | 1.230 | 1.370 | 1.480 | 1.580 | 1.660 | 1.730 | 1.810 | 1.900 | 1.990 | 2.080 | 2.190 | 2.300 | 2.420 |
| 67 | 57 | 60 | 58.5 | 283.0 | 280.0 | 281.5 | 0.140 | 0.260 | 0.380 | 0.530 | 0.660 | 0.770 | 0.860 | 0.960 | 1.040 | 1.100 | 1.160 | 1.210 | 1.260 | 1.320 | 1.380 | 1.450 | 1.530 | 1.610 | 1.700 |
| 69 | 63 | 66 | 64.5 | 277.0 | 274.0 | 275.5 | 0.150 | 0.260 | 0.380 | 0.540 | 0.670 | 0.790 | 0.890 | 0.990 | 1.080 | 1.150 | 1.220 | 1.280 | 1.340 | 1.400 | 1.470 | 1.540 | 1.610 | 1.700 | 1.780 |
| 71 | 69 | 71 | 70.0 | 271.0 | 269.0 | 270.0 | 0.110 | 0.200 | 0.300 | 0.430 | 0.530 | 0.630 | 0.720 | 0.810 | 0.890 | 0.960 | 1.020 | 1.080 | 1.150 | 1.210 | 1.260 | 1.320 | 1.390 | 1.460 | 1.530 |
| 73 | 74 | 77 | 75.5 | 266.0 | 263.0 | 264.5 | 0.140 | 0.250 | 0.360 | 0.520 | 0.650 | 0.760 | 0.870 | 0.970 | 1.070 | 1.150 | 1.220 | 1.290 | 1.370 | 1.440 | 1.520 | 1.590 | 1.680 | 1.760 | 1.850 |
| 75 | 80 | 83 | 81.5 | 260.0 | 257.0 | 258.5 | 0.150 | 0.260 | 0.380 | 0.540 | 0.670 | 0.790 | 0.900 | 1.000 | 1.090 | 1.160 | 1.220 | 1.280 | 1.340 | 1.390 | 1.450 | 1.510 | 1.580 | 1.660 | 1.740 |
| 77 | 86 | 89 | 87.5 | 254.0 | 251.0 | 252.5 | 0.160 | 0.280 | 0.410 | 0.580 | 0.720 | 0.840 | 0.960 | 1.070 | 1.160 | 1.240 | 1.310 | 1.380 | 1.440 | 1.510 | 1.580 | 1.660 | 1.750 | 1.850 | 1.950 |
| 79 | 92 | 95 | 93.5 | 248.0 | 245.0 | 246.5 | 0.150 | 0.270 | 0.390 | 0.560 | 0.690 | 0.810 | 0.920 | 1.020 | 1.110 | 1.190 | 1.250 | 1.300 | 1.360 | 1.410 | 1.470 | 1.530 | 1.590 | 1.670 | 1.750 |
| 81 | 98 | 101 | 99.5 | 242.0 | 239.0 | 240.5 | 0.200 | 0.350 | 0.510 | 0.720 | 0.900 | 1.050 | 1.180 | 1.320 | 1.430 | 1.530 | 1.620 | 1.710 | 1.800 | 1.890 | 2.000 | 2.110 | 2.240 | 2.380 | 2.530 |
| 83 | 104 | 107 | 105.5 | 236.0 | 233.0 | 234.5 | 0.120 | 0.220 | 0.320 | 0.450 | 0.570 | 0.660 | 0.750 | 0.840 | 0.920 | 0.990 | 1.060 | 1.120 | 1.180 | 1.250 | 1.320 | 1.400 | 1.480 | 1.580 | 1.670 |
| 85 | 110 | 113 | 111.5 | 230.0 | 227.0 | 228.5 | 0.150 | 0.270 | 0.400 | 0.570 | 0.710 | 0.830 | 0.940 | 1.050 | 1.150 | 1.220 | 1.290 | 1.360 | 1.420 | 1.490 | 1.560 | 1.630 | 1.710 | 1.800 | 1.900 |
| 87 | 116 | 119 | 117.5 | 224.0 | 221.0 | 222.5 | 0.140 | 0.250 | 0.360 | 0.510 | 0.640 | 0.750 | 0.840 | 0.940 | 1.030 | 1.100 | 1.170 | 1.230 | 1.310 | 1.380 | 1.460 | 1.550 | 1.660 | 1.770 | 1.890 |
| 89 | 121 | 123 | 122.0 | 219.0 | 217.0 | 218.0 | 0.097 | 0.170 | 0.250 | 0.360 | 0.450 | 0.530 | 0.610 | 0.680 | 0.750 | 0.810 | 0.860 | 0.910 | 0.960 | 1.010 | 1.060 | 1.110 | 1.170 | 1.230 | 1.300 |
| 91 | 126 | 129 | 127.5 | 214.0 | 211.0 | 212.5 | 0.130 | 0.220 | 0.330 | 0.470 | 0.580 | 0.690 | 0.780 | 0.870 | 0.950 | 1.020 | 1.080 | 1.140 | 1.200 | 1.260 | 1.320 | 1.380 | 1.460 | 1.540 | 1.620 |
| 93 | 132 | 135 | 133.5 | 208.0 | 205.0 | 206.5 | 0.170 | 0.300 | 0.440 | 0.630 | 0.780 | 0.910 | 1.030 | 1.150 | 1.250 | 1.340 | 1.410 | 1.480 | 1.560 | 1.630 | 1.710 | 1.800 | 1.910 | 2.030 | 2.150 |
| 95 | 138 | 141 | 139.5 | 202.0 | 199.0 | 200.5 | 0.140 | 0.25 | | | | | | | | | | | | | | | | | |

| | Height (cm) original | | Depth (cm) | | Grain size distributions (Laser Coulter Counter, AWI Potsdam) in ϕ | | | | | | | | | | | | | | | | | | | | | |
|------------|-------------------------|------|---------------|-------|---|--------|--------|--------|--------|--------|--------|--------|--------|--------|--------|-------|-------|-------|-------|-------|-------|-------|-------|-------|-------|--|
| ID | (base=0) | mean | depth (top=0) | mean | 11.381 | 11.245 | 11.111 | 10.977 | 10.841 | 10.708 | 10.572 | 10.438 | 10.304 | 10.168 | 10.035 | 9.900 | 9.765 | 9.631 | 9.496 | 9.362 | 9.227 | 9.092 | 8.959 | | | |
| 103 | 162 | 166 | 163.5 | 178.0 | 174.0 | 176.5 | 0.140 | 0.240 | 0.360 | 0.510 | 0.630 | 0.740 | 0.840 | 0.930 | 1.010 | 1.080 | 1.140 | 1.200 | 1.260 | 1.320 | 1.380 | 1.450 | 1.530 | 1.610 | 1.700 | |
| 105 | 168 | 171 | 169.5 | 172.0 | 169.0 | 170.5 | 0.130 | 0.230 | 0.340 | 0.480 | 0.600 | 0.700 | 0.800 | 0.890 | 0.970 | 1.040 | 1.100 | 1.160 | 1.220 | 1.280 | 1.330 | 1.400 | 1.460 | 1.540 | 1.620 | |
| 107 | 174 | 177 | 175.5 | 166.0 | 163.0 | 164.5 | 0.085 | 0.150 | 0.220 | 0.320 | 0.400 | 0.470 | 0.540 | 0.610 | 0.670 | 0.720 | 0.770 | 0.820 | 0.870 | 0.920 | 0.960 | 1.010 | 1.060 | 1.110 | 1.160 | |
| 109 | 180 | 183 | 181.5 | 160.0 | 157.0 | 158.5 | 0.077 | 0.140 | 0.200 | 0.290 | 0.360 | 0.430 | 0.490 | 0.550 | 0.610 | 0.670 | 0.720 | 0.770 | 0.820 | 0.870 | 0.920 | 0.970 | 1.020 | 1.080 | 1.140 | |
| 111 | 186 | 189 | 187.5 | 154.0 | 151.0 | 152.5 | 0.082 | 0.150 | 0.210 | 0.310 | 0.380 | 0.450 | 0.510 | 0.570 | 0.630 | 0.670 | 0.710 | 0.750 | 0.790 | 0.830 | 0.860 | 0.900 | 0.940 | 0.990 | 1.030 | |
| 113 | 192 | 195 | 193.5 | 148.0 | 145.0 | 146.5 | 0.073 | 0.130 | 0.190 | 0.270 | 0.340 | 0.400 | 0.460 | 0.520 | 0.570 | 0.620 | 0.660 | 0.710 | 0.750 | 0.790 | 0.840 | 0.890 | 0.940 | 0.990 | 1.040 | |
| 115 | 198 | 201 | 199.5 | 142.0 | 139.0 | 140.5 | 0.100 | 0.180 | 0.270 | 0.380 | 0.470 | 0.560 | 0.640 | 0.720 | 0.790 | 0.850 | 0.910 | 0.970 | 1.040 | 1.100 | 1.170 | 1.240 | 1.310 | 1.390 | 1.470 | |
| 117 | 204 | 207 | 205.5 | 136.0 | 133.0 | 134.5 | 0.094 | 0.170 | 0.240 | 0.350 | 0.430 | 0.510 | 0.580 | 0.650 | 0.710 | 0.760 | 0.810 | 0.860 | 0.920 | 0.970 | 1.030 | 1.090 | 1.160 | 1.230 | 1.310 | |
| 119 | 210 | 213 | 211.5 | 130.0 | 127.0 | 128.5 | 0.110 | 0.200 | 0.290 | 0.410 | 0.520 | 0.600 | 0.680 | 0.760 | 0.830 | 0.900 | 0.960 | 1.010 | 1.080 | 1.150 | 1.220 | 1.300 | 1.390 | 1.490 | 1.590 | |
| 121 | 216 | 219 | 217.5 | 124.0 | 121.0 | 122.5 | 0.110 | 0.200 | 0.290 | 0.410 | 0.520 | 0.600 | 0.690 | 0.760 | 0.840 | 0.900 | 0.950 | 1.010 | 1.070 | 1.140 | 1.210 | 1.280 | 1.370 | 1.460 | 1.550 | |
| 123 | 222 | 225 | 223.5 | 118.0 | 115.0 | 116.5 | 0.110 | 0.190 | 0.280 | 0.390 | 0.490 | 0.580 | 0.650 | 0.730 | 0.800 | 0.860 | 0.920 | 0.970 | 1.030 | 1.090 | 1.160 | 1.230 | 1.310 | 1.400 | 1.490 | |
| 125 | 229 | 232 | 230.5 | 111.0 | 108.0 | 109.5 | 0.110 | 0.190 | 0.270 | 0.390 | 0.490 | 0.570 | 0.650 | 0.720 | 0.790 | 0.850 | 0.900 | 0.950 | 1.000 | 1.060 | 1.120 | 1.190 | 1.260 | 1.330 | 1.410 | |
| 127 | 235 | 238 | 236.5 | 105.0 | 102.0 | 103.5 | 0.110 | 0.190 | 0.280 | 0.400 | 0.500 | 0.590 | 0.660 | 0.740 | 0.810 | 0.860 | 0.910 | 0.960 | 1.010 | 1.070 | 1.120 | 1.190 | 1.260 | 1.330 | 1.410 | |
| 129 | 241 | 244 | 242.5 | 99.0 | 96.0 | 97.5 | 0.140 | 0.240 | 0.360 | 0.500 | 0.630 | 0.730 | 0.830 | 0.920 | 1.010 | 1.080 | 1.140 | 1.190 | 1.250 | 1.320 | 1.380 | 1.450 | 1.530 | 1.620 | 1.710 | |
| 131 | 247 | 250 | 248.5 | 93.0 | 90.0 | 91.5 | 0.057 | 0.100 | 0.150 | 0.210 | 0.270 | 0.320 | 0.370 | 0.420 | 0.470 | 0.520 | 0.560 | 0.610 | 0.660 | 0.700 | 0.750 | 0.800 | 0.850 | 0.900 | 0.950 | |
| 133 | 253 | 256 | 254.5 | 87.0 | 84.0 | 85.5 | 0.089 | 0.160 | 0.230 | 0.330 | 0.420 | 0.490 | 0.560 | 0.630 | 0.700 | 0.750 | 0.810 | 0.850 | 0.900 | 0.950 | 0.990 | 1.040 | 1.080 | 1.130 | 1.190 | |
| 135 | 258 | 262 | 260.5 | 82.0 | 78.0 | 79.5 | 0.110 | 0.190 | 0.280 | 0.390 | 0.490 | 0.580 | 0.660 | 0.740 | 0.810 | 0.870 | 0.920 | 0.970 | 1.010 | 1.050 | 1.090 | 1.130 | 1.180 | 1.230 | 1.280 | |
| 137 | 265 | 268 | 266.5 | 75.0 | 72.0 | 73.5 | 0.095 | 0.170 | 0.250 | 0.360 | 0.450 | 0.530 | 0.610 | 0.690 | 0.760 | 0.820 | 0.880 | 0.930 | 0.980 | 1.030 | 1.080 | 1.120 | 1.160 | 1.210 | 1.260 | |
| 139 | 271 | 274 | 272.5 | 69.0 | 66.0 | 67.5 | 0.120 | 0.210 | 0.310 | 0.440 | 0.550 | 0.650 | 0.740 | 0.830 | 0.910 | 0.980 | 1.050 | 1.100 | 1.170 | 1.220 | 1.280 | 1.340 | 1.410 | 1.490 | 1.570 | |
| 141 | 277 | 280 | 278.5 | 63.0 | 60.0 | 61.5 | 0.120 | 0.210 | 0.300 | 0.430 | 0.540 | 0.630 | 0.720 | 0.810 | 0.890 | 0.960 | 1.020 | 1.070 | 1.130 | 1.190 | 1.250 | 1.310 | 1.380 | 1.450 | 1.530 | |
| 143 | 284 | 287 | 285.5 | 56.0 | 53.0 | 54.5 | 0.100 | 0.180 | 0.270 | 0.380 | 0.480 | 0.560 | 0.640 | 0.720 | 0.800 | 0.860 | 0.910 | 0.970 | 1.020 | 1.070 | 1.120 | 1.180 | 1.230 | 1.290 | 1.350 | |
| 145 | 290 | 293 | 291.5 | 50.0 | 47.0 | 48.5 | 0.040 | 0.070 | 0.100 | 0.150 | 0.190 | 0.230 | 0.270 | 0.310 | 0.340 | 0.380 | 0.420 | 0.450 | 0.490 | 0.520 | 0.560 | 0.590 | 0.630 | 0.660 | 0.690 | |
| 147 | 296 | 299 | 297.5 | 44.0 | 41.0 | 42.5 | 0.046 | 0.082 | 0.120 | 0.180 | 0.220 | 0.260 | 0.310 | 0.350 | 0.390 | 0.430 | 0.460 | 0.500 | 0.530 | 0.560 | 0.590 | 0.620 | 0.650 | 0.680 | 0.700 | |
| 149 | 302 | 305 | 303.5 | 38.0 | 35.0 | 36.5 | 0.092 | 0.160 | 0.240 | 0.350 | 0.430 | 0.510 | 0.590 | 0.660 | 0.730 | 0.790 | 0.840 | 0.890 | 0.940 | 0.990 | 1.030 | 1.080 | 1.130 | 1.180 | 1.230 | |
| 151 | 308 | 311 | 309.5 | 32.0 | 29.0 | 30.5 | 0.096 | 0.170 | 0.250 | 0.360 | 0.450 | 0.530 | 0.610 | 0.690 | 0.760 | 0.820 | 0.870 | 0.920 | 0.970 | 1.020 | 1.060 | 1.110 | 1.160 | 1.220 | 1.270 | |
| 153 | 314 | 317 | 315.5 | 26.0 | 23.0 | 24.5 | 0.074 | 0.130 | 0.190 | 0.280 | 0.350 | 0.410 | 0.470 | 0.530 | 0.590 | 0.630 | 0.680 | 0.720 | 0.760 | 0.790 | 0.830 | 0.860 | 0.900 | 0.940 | 0.970 | |
| 155 | 320 | 323 | 321.5 | 20.0 | 17.0 | 18.5 | 0.090 | 0.160 | 0.240 | 0.340 | 0.420 | 0.500 | 0.570 | 0.650 | 0.710 | 0.770 | 0.830 | 0.880 | 0.940 | 0.990 | 1.040 | 1.100 | 1.160 | 1.220 | 1.280 | |
| 157 | 326 | 329 | 327.5 | 14.0 | 11.0 | 12.5 | 0.074 | 0.130 | 0.190 | 0.280 | 0.350 | 0.410 | 0.470 | 0.530 | 0.590 | 0.630 | 0.680 | 0.720 | 0.760 | 0.790 | 0.830 | 0.860 | 0.900 | 0.940 | 0.970 | |
| P14 | | | | | | | | | | | | | | | | | | | | | | | | | | |
| 159 | 318 | 320 | 319.0 | 12.0 | 10.0 | 11.0 | 0.046 | 0.081 | 0.120 | 0.170 | 0.210 | 0.250 | 0.280 | 0.310 | 0.340 | 0.360 | 0.370 | 0.380 | 0.390 | 0.390 | 0.400 | 0.400 | 0.410 | 0.410 | | |
| 160 | 316 | 318 | 317.0 | 14.0 | 12.0 | 13.0 | 0.048 | 0.085 | 0.120 | 0.180 | 0.220 | 0.250 | 0.290 | 0.310 | 0.340 | 0.350 | 0.360 | 0.360 | 0.360 | 0.350 | 0.340 | 0.330 | 0.330 | 0.320 | 0.310 | |
| 161 | 314 | 316 | 315.0 | 16.0 | 14.0 | 15.0 | 0.062 | 0.110 | 0.160 | 0.230 | 0.280 | 0.330 | 0.370 | 0.410 | 0.450 | 0.470 | 0.490 | 0.500 | 0.510 | 0.520 | 0.520 | 0.530 | 0.540 | 0.550 | 0.560 | |
| 162 | 312 | 314 | 313.0 | 18.0 | 16.0 | 17.0 | 0.058 | 0.100 | 0.150 | 0.220 | 0.270 | 0.310 | 0.350 | 0.390 | 0.420 | 0.440 | 0.450 | 0.460 | 0.470 | 0.470 | 0.470 | 0.470 | 0.470 | 0.480 | 0.490 | |
| 163 | 310 | 312 | 311.0 | 20.0 | 18.0 | 19.0 | 0.064 | 0.110 | 0.170 | 0.240 | 0.300 | 0.350 | 0.390 | 0.430 | 0.470 | 0.500 | 0.520 | 0.530 | 0.550 | 0.560 | 0.570 | 0.580 | 0.590 | 0.610 | | |
| 164 | 308 | 310 | 309.0 | 22.0 | 20.0 | 21.0 | 0.065 | 0.120 | 0.170 | 0.240 | 0.300 | 0.350 | 0.400 | 0.440 | 0.480 | 0.510 | 0.530 | 0.540 | 0.560 | 0.570 | 0.580 | 0.590 | 0.610 | 0.630 | | |
| 165 | 306 | 308 | 307.0 | 24.0 | 22.0 | 23.0 | 0.076 | 0.140 | 0.200 | 0.280 | 0.350 | 0.410 | 0.460 | 0.520 | 0.560 | 0.590 | 0.610 | 0.630 | 0.650 | 0.670 | 0.680 | 0.690 | 0.710 | 0.730 | 0.760 | |
| 166 | 304 | 306 | 305.0 | 26.0 | 24.0 | 25.0 | 0.091 | 0.160 | 0.240 | 0.340 | 0.420 | 0.490 | 0.540 | 0.600 | 0.650 | 0.680 | 0.700 | 0.710 | 0.720 | 0.730 | 0.730 | 0.740 | 0.750 | 0.760 | 0.780 | |
| 167 | 302 | 304 | 303.0 | 28.0 | 26.0 | 27.0 | 0.067 | 0.120 | 0.180 | 0.250 | 0.310 | 0.370 | 0.420 | 0.460 | 0.500 | 0.530 | 0.560 | 0.570 | 0.590 | 0.600 | 0.610 | 0.620 | 0.630 | 0.650 | 0.670 | |
| 168 | 300 | 302 | 301.0 | 30.0 | 28.0 | 29.0 | 0.077 | 0.140 | 0.200 | 0.290 | 0.360 | 0.420 | 0.470 | 0.530 | 0.570 | 0.610 | 0.640 | 0.660 | 0.680 | 0.690 | 0.710 | 0.720 | 0.740 | 0.760 | 0.780 | |
| 169 | 298 | 300 | 299.0 | 32.0 | 30.0 | 31.0 | 0.110 | 0.190 | 0.280 | 0.410 | 0.510 | 0.610 | 0.700 | 0.810 | 0.900 | 1.000 | 1.100 | 1.210 | 1.330 | 1.460 | 1.600 | 1.750 | | | | |

| ID | Height (cm) original | | Depth (cm) | | Grain size distributions (Laser Coulter Counter, AWI Potsdam) in ϕ | | | | | | | | | | | | | | | | | | | | |
|---------|-------------------------|------|---------------|-------|---|--------|--------|--------|--------|--------|--------|--------|--------|--------|--------|-------|-------|-------|-------|-------|-------|-------|-------|-------|-------|
| | (base=0) | mean | depth (top=0) | mean | 11.381 | 11.245 | 11.111 | 10.977 | 10.841 | 10.708 | 10.572 | 10.438 | 10.304 | 10.168 | 10.035 | 9.900 | 9.765 | 9.631 | 9.496 | 9.362 | 9.227 | 9.092 | 8.959 | | |
| 174 | 288 | 290 | 289.0 | 42.0 | 40.0 | 41.0 | 0.065 | 0.120 | 0.170 | 0.240 | 0.300 | 0.360 | 0.410 | 0.450 | 0.490 | 0.530 | 0.550 | 0.570 | 0.590 | 0.610 | 0.620 | 0.630 | 0.650 | 0.670 | 0.680 |
| 175 (1) | 286 | 288 | 287.0 | 44.0 | 42.0 | 43.0 | 0.160 | 0.280 | 0.420 | 0.590 | 0.730 | 0.850 | 0.960 | 1.070 | 1.150 | 1.220 | 1.280 | 1.330 | 1.380 | 1.430 | 1.480 | 1.540 | 1.610 | 1.690 | 1.780 |
| 175 (2) | 286 | 288 | 287.0 | 44.0 | 42.0 | 43.0 | 0.180 | 0.310 | 0.460 | 0.650 | 0.810 | 0.940 | 1.050 | 1.150 | 1.230 | 1.290 | 1.330 | 1.360 | 1.380 | 1.410 | 1.430 | 1.460 | 1.510 | 1.580 | 1.660 |
| 176 | 284 | 286 | 285.0 | 46.0 | 44.0 | 45.0 | 0.170 | 0.290 | 0.430 | 0.610 | 0.760 | 0.880 | 0.990 | 1.090 | 1.180 | 1.240 | 1.290 | 1.330 | 1.370 | 1.410 | 1.440 | 1.480 | 1.540 | 1.610 | 1.690 |
| 177 | 282 | 284 | 283.0 | 48.0 | 46.0 | 47.0 | 0.150 | 0.270 | 0.400 | 0.560 | 0.690 | 0.810 | 0.900 | 0.990 | 1.060 | 1.110 | 1.150 | 1.180 | 1.200 | 1.230 | 1.260 | 1.290 | 1.340 | 1.400 | 1.470 |
| 178 | 280 | 282 | 281.0 | 50.0 | 48.0 | 49.0 | 0.190 | 0.330 | 0.490 | 0.690 | 0.840 | 0.970 | 1.090 | 1.180 | 1.260 | 1.310 | 1.340 | 1.350 | 1.360 | 1.370 | 1.380 | 1.400 | 1.430 | 1.480 | 1.550 |
| 179 | 278 | 280 | 279.0 | 52.0 | 50.0 | 51.0 | 0.160 | 0.290 | 0.420 | 0.590 | 0.740 | 0.870 | 0.980 | 1.090 | 1.190 | 1.270 | 1.340 | 1.400 | 1.470 | 1.540 | 1.610 | 1.690 | 1.790 | 1.890 | 2.010 |
| 180 | 276 | 278 | 277.0 | 54.0 | 52.0 | 53.0 | 0.160 | 0.280 | 0.410 | 0.580 | 0.710 | 0.830 | 0.930 | 1.020 | 1.090 | 1.150 | 1.190 | 1.220 | 1.250 | 1.280 | 1.310 | 1.350 | 1.400 | 1.460 | 1.540 |
| 181 | 274 | 276 | 275.0 | 56.0 | 54.0 | 55.0 | 0.170 | 0.300 | 0.430 | 0.610 | 0.760 | 0.890 | 1.000 | 1.110 | 1.200 | 1.270 | 1.330 | 1.370 | 1.420 | 1.460 | 1.510 | 1.560 | 1.610 | 1.680 | 1.760 |
| 182 | 272 | 274 | 273.0 | 58.0 | 56.0 | 57.0 | 0.210 | 0.370 | 0.540 | 0.760 | 0.930 | 1.080 | 1.200 | 1.310 | 1.390 | 1.440 | 1.470 | 1.480 | 1.500 | 1.510 | 1.530 | 1.550 | 1.590 | 1.640 | 1.710 |
| 183 | 270 | 272 | 271.0 | 60.0 | 58.0 | 59.0 | 0.200 | 0.350 | 0.510 | 0.730 | 0.900 | 1.050 | 1.190 | 1.320 | 1.430 | 1.520 | 1.600 | 1.670 | 1.740 | 1.820 | 1.900 | 1.980 | 2.080 | 2.200 | 2.320 |
| 184 | 268 | 270 | 269.0 | 62.0 | 60.0 | 61.0 | 0.140 | 0.240 | 0.360 | 0.510 | 0.630 | 0.730 | 0.820 | 0.910 | 0.990 | 1.040 | 1.090 | 1.120 | 1.160 | 1.200 | 1.240 | 1.280 | 1.330 | 1.400 | 1.470 |
| 185 | 266 | 268 | 267.0 | 64.0 | 62.0 | 63.0 | 0.150 | 0.260 | 0.380 | 0.540 | 0.670 | 0.770 | 0.870 | 0.950 | 1.020 | 1.060 | 1.090 | 1.120 | 1.140 | 1.150 | 1.170 | 1.190 | 1.230 | 1.270 | 1.330 |
| 186 | 264 | 266 | 265.0 | 66.0 | 64.0 | 65.0 | 0.130 | 0.230 | 0.340 | 0.490 | 0.610 | 0.710 | 0.800 | 0.880 | 0.950 | 1.000 | 1.040 | 1.080 | 1.110 | 1.140 | 1.160 | 1.200 | 1.240 | 1.290 | 1.350 |
| 187 | 262 | 264 | 263.0 | 68.0 | 66.0 | 67.0 | 0.160 | 0.280 | 0.410 | 0.580 | 0.720 | 0.840 | 0.940 | 1.040 | 1.120 | 1.180 | 1.230 | 1.260 | 1.300 | 1.340 | 1.370 | 1.410 | 1.460 | 1.520 | 1.590 |
| 188 | 260 | 262 | 261.0 | 70.0 | 68.0 | 69.0 | 0.140 | 0.240 | 0.360 | 0.510 | 0.630 | 0.740 | 0.830 | 0.920 | 0.990 | 1.040 | 1.090 | 1.120 | 1.150 | 1.180 | 1.210 | 1.240 | 1.280 | 1.330 | 1.390 |
| 189 | 258 | 260 | 259.0 | 72.0 | 70.0 | 71.0 | 0.200 | 0.350 | 0.520 | 0.730 | 0.900 | 1.040 | 1.170 | 1.280 | 1.370 | 1.430 | 1.470 | 1.500 | 1.530 | 1.560 | 1.590 | 1.620 | 1.670 | 1.730 | 1.800 |
| 190 | 256 | 258 | 257.0 | 74.0 | 72.0 | 73.0 | 0.180 | 0.330 | 0.480 | 0.670 | 0.830 | 0.960 | 1.070 | 1.170 | 1.250 | 1.300 | 1.340 | 1.360 | 1.380 | 1.400 | 1.410 | 1.440 | 1.480 | 1.530 | 1.600 |
| 191 | 254 | 256 | 255.0 | 76.0 | 74.0 | 75.0 | 0.150 | 0.270 | 0.400 | 0.560 | 0.700 | 0.810 | 0.910 | 1.010 | 1.080 | 1.140 | 1.190 | 1.230 | 1.260 | 1.300 | 1.340 | 1.390 | 1.450 | 1.530 | 1.620 |
| 192 | 252 | 254 | 253.0 | 78.0 | 76.0 | 77.0 | 0.180 | 0.330 | 0.480 | 0.680 | 0.840 | 0.970 | 1.090 | 1.190 | 1.280 | 1.330 | 1.370 | 1.410 | 1.430 | 1.460 | 1.490 | 1.520 | 1.570 | 1.640 | 1.720 |
| 193 | 250 | 252 | 251.0 | 80.0 | 78.0 | 79.0 | 0.150 | 0.270 | 0.390 | 0.560 | 0.690 | 0.800 | 0.900 | 1.000 | 1.080 | 1.130 | 1.180 | 1.210 | 1.250 | 1.280 | 1.310 | 1.350 | 1.410 | 1.470 | 1.550 |
| 194 | 248 | 250 | 249.0 | 82.0 | 80.0 | 81.0 | 0.110 | 0.190 | 0.280 | 0.400 | 0.510 | 0.610 | 0.710 | 0.830 | 0.950 | 1.070 | 1.200 | 1.360 | 1.530 | 1.720 | 1.940 | 2.160 | 2.410 | 2.660 | 2.910 |
| 195 | 246 | 248 | 247.0 | 84.0 | 82.0 | 83.0 | 0.120 | 0.210 | 0.300 | 0.430 | 0.540 | 0.630 | 0.710 | 0.790 | 0.860 | 0.920 | 0.960 | 1.010 | 1.050 | 1.090 | 1.130 | 1.180 | 1.240 | 1.310 | 1.390 |
| 196 | 244 | 246 | 245.0 | 86.0 | 84.0 | 85.0 | 0.095 | 0.170 | 0.250 | 0.350 | 0.440 | 0.510 | 0.570 | 0.630 | 0.680 | 0.720 | 0.740 | 0.760 | 0.770 | 0.780 | 0.790 | 0.800 | 0.820 | 0.840 | 0.870 |
| 197 | 242 | 244 | 243.0 | 88.0 | 86.0 | 87.0 | 0.075 | 0.130 | 0.200 | 0.280 | 0.350 | 0.400 | 0.460 | 0.510 | 0.550 | 0.580 | 0.600 | 0.620 | 0.630 | 0.640 | 0.650 | 0.660 | 0.670 | 0.680 | |
| 198 | 240 | 242 | 241.0 | 90.0 | 88.0 | 89.0 | 0.092 | 0.160 | 0.240 | 0.340 | 0.420 | 0.490 | 0.550 | 0.610 | 0.660 | 0.700 | 0.730 | 0.750 | 0.770 | 0.790 | 0.800 | 0.820 | 0.840 | 0.870 | 0.900 |
| 199 | 238 | 240 | 239.0 | 92.0 | 90.0 | 91.0 | 0.190 | 0.330 | 0.480 | 0.680 | 0.840 | 0.980 | 1.100 | 1.220 | 1.320 | 1.390 | 1.450 | 1.500 | 1.550 | 1.600 | 1.650 | 1.710 | 1.790 | 1.880 | 1.980 |
| 200 | 236 | 238 | 237.0 | 94.0 | 92.0 | 93.0 | 0.160 | 0.280 | 0.410 | 0.580 | 0.730 | 0.850 | 0.960 | 1.070 | 1.160 | 1.230 | 1.290 | 1.350 | 1.410 | 1.470 | 1.530 | 1.600 | 1.690 | 1.780 | 1.890 |
| 201 | 234 | 236 | 235.0 | 96.0 | 94.0 | 95.0 | 0.150 | 0.260 | 0.380 | 0.550 | 0.680 | 0.790 | 0.890 | 0.980 | 1.060 | 1.130 | 1.180 | 1.220 | 1.270 | 1.320 | 1.370 | 1.430 | 1.500 | 1.590 | 1.700 |
| 202 | 232 | 234 | 233.0 | 98.0 | 96.0 | 97.0 | 0.110 | 0.200 | 0.300 | 0.420 | 0.520 | 0.600 | 0.680 | 0.740 | 0.790 | 0.830 | 0.860 | 0.870 | 0.890 | 0.910 | 0.920 | 0.940 | 0.970 | 1.010 | 1.060 |
| 203 | 230 | 232 | 231.0 | 100.0 | 98.0 | 99.0 | 0.098 | 0.170 | 0.260 | 0.360 | 0.450 | 0.520 | 0.590 | 0.650 | 0.700 | 0.730 | 0.760 | 0.780 | 0.800 | 0.810 | 0.830 | 0.850 | 0.880 | 0.910 | 0.950 |
| 204 | 228 | 230 | 229.0 | 102.0 | 100.0 | 101.0 | 0.065 | 0.120 | 0.170 | 0.240 | 0.300 | 0.350 | 0.390 | 0.430 | 0.460 | 0.480 | 0.500 | 0.510 | 0.520 | 0.530 | 0.540 | 0.550 | 0.560 | 0.580 | 0.600 |
| 205 | 226 | 228 | 227.0 | 104.0 | 102.0 | 103.0 | 0.052 | 0.093 | 0.140 | 0.200 | 0.240 | 0.290 | 0.320 | 0.360 | 0.390 | 0.410 | 0.430 | 0.440 | 0.460 | 0.470 | 0.470 | 0.470 | 0.480 | 0.490 | 0.490 |
| 206 | 224 | 226 | 225.0 | 106.0 | 104.0 | 105.0 | 0.053 | 0.095 | 0.140 | 0.200 | 0.250 | 0.290 | 0.330 | 0.360 | 0.390 | 0.410 | 0.430 | 0.440 | 0.450 | 0.460 | 0.470 | 0.470 | 0.480 | 0.490 | 0.500 |
| 207 | 222 | 224 | 223.0 | 108.0 | 106.0 | 107.0 | 0.030 | 0.054 | 0.080 | 0.110 | 0.140 | 0.170 | 0.190 | 0.210 | 0.230 | 0.250 | 0.260 | 0.270 | 0.280 | 0.290 | 0.290 | 0.290 | 0.300 | 0.300 | 0.300 |
| 208 | 220 | 222 | 221.0 | 110.0 | 108.0 | 109.0 | 0.079 | 0.140 | 0.210 | 0.290 | 0.360 | 0.420 | 0.470 | 0.510 | 0.550 | 0.570 | 0.590 | 0.600 | 0.610 | 0.620 | 0.620 | 0.640 | 0.650 | 0.680 | |
| 209 | 218 | 220 | 219.0 | 112.0 | 110.0 | 111.0 | 0.063 | 0.110 | 0.160 | 0.230 | 0.290 | 0.340 | 0.380 | 0.420 | 0.450 | 0.470 | 0.490 | 0.500 | 0.510 | 0.520 | 0.530 | 0.540 | 0.560 | 0.580 | |
| 210 | 216 | 218 | 217.0 | 114.0 | 112.0 | 113.0 | 0.079 | 0.140 | 0.210 | 0.290 | 0.360 | 0.420 | 0.470 | 0.520 | 0.560 | 0.590 | 0.610 | 0.620 | 0.640 | 0.650 | 0.660 | 0.680 | 0.700 | 0.730 | |
| 211 | 214 | 216 | 215.0 | 116.0 | 114.0 | 115.0 | 0.070 | 0.125 | 0.185 | 0.255 | 0.320 | 0.370 | 0.415 | 0.455 | 0.490 | 0.515 | 0.535 | 0.545 | 0.555 | 0.565 | 0.565 | 0.575 | 0.590 | 0.610 | 0.630 |
| 212 | 212 | 214 | 213.0 | 118.0 | 116.0 | 117.0 | 0.060 | 0.110 | 0.160 | 0.220 | 0.280 | 0.320 | 0.360 | 0.390 | 0.420 | 0.440 | 0.460 | 0.470 | 0.470 | 0.480 | 0.480 | | | | |

| ID | Height (cm) original | | Depth (cm) | | Grain size distributions (Laser Coulter Counter, AWI Potsdam) in ϕ | | | | | | | | | | | | | | | | | | | |
|-----|-------------------------|------|---------------|-------|---|--------|--------|--------|--------|--------|--------|--------|--------|--------|--------|-------|-------|-------|-------|-------|-------|-------|-------|-------|
| | (base=0) | mean | depth (top=0) | mean | 11.381 | 11.245 | 11.111 | 10.977 | 10.841 | 10.708 | 10.572 | 10.438 | 10.304 | 10.168 | 10.035 | 9.900 | 9.765 | 9.631 | 9.496 | 9.362 | 9.227 | 9.092 | 8.959 | |
| 218 | 200 | 202 | 201.0 | 130.0 | 128.0 | 129.0 | 0.040 | 0.072 | 0.110 | 0.150 | 0.190 | 0.220 | 0.250 | 0.280 | 0.300 | 0.320 | 0.330 | 0.340 | 0.350 | 0.350 | 0.360 | 0.360 | 0.360 | 0.370 |
| 219 | 198 | 200 | 199.0 | 132.0 | 130.0 | 131.0 | 0.039 | 0.070 | 0.100 | 0.150 | 0.180 | 0.210 | 0.240 | 0.270 | 0.290 | 0.310 | 0.320 | 0.330 | 0.340 | 0.340 | 0.340 | 0.340 | 0.350 | 0.350 |
| 220 | 196 | 198 | 197.0 | 134.0 | 132.0 | 133.0 | 0.030 | 0.054 | 0.080 | 0.110 | 0.140 | 0.170 | 0.190 | 0.210 | 0.230 | 0.250 | 0.260 | 0.270 | 0.280 | 0.280 | 0.280 | 0.280 | 0.280 | 0.290 |
| 221 | 194 | 196 | 195.0 | 136.0 | 134.0 | 135.0 | 0.055 | 0.098 | 0.140 | 0.200 | 0.250 | 0.300 | 0.330 | 0.370 | 0.400 | 0.420 | 0.440 | 0.450 | 0.460 | 0.470 | 0.470 | 0.480 | 0.490 | 0.500 |
| 222 | 192 | 194 | 193.0 | 138.0 | 136.0 | 137.0 | 0.044 | 0.079 | 0.120 | 0.170 | 0.210 | 0.240 | 0.270 | 0.300 | 0.330 | 0.350 | 0.360 | 0.380 | 0.390 | 0.390 | 0.390 | 0.400 | 0.400 | 0.410 |
| 223 | 190 | 192 | 191.0 | 140.0 | 138.0 | 139.0 | 0.051 | 0.091 | 0.130 | 0.190 | 0.240 | 0.280 | 0.320 | 0.360 | 0.390 | 0.410 | 0.430 | 0.450 | 0.460 | 0.470 | 0.480 | 0.480 | 0.490 | 0.500 |
| 224 | 188 | 190 | 189.0 | 142.0 | 140.0 | 141.0 | 0.053 | 0.095 | 0.140 | 0.200 | 0.250 | 0.290 | 0.330 | 0.370 | 0.400 | 0.430 | 0.440 | 0.460 | 0.470 | 0.480 | 0.480 | 0.490 | 0.490 | 0.500 |
| 225 | 186 | 188 | 187.0 | 144.0 | 142.0 | 143.0 | 0.056 | 0.099 | 0.150 | 0.210 | 0.260 | 0.300 | 0.340 | 0.380 | 0.410 | 0.430 | 0.450 | 0.460 | 0.480 | 0.480 | 0.490 | 0.490 | 0.500 | 0.500 |
| 226 | 184 | 186 | 185.0 | 146.0 | 144.0 | 145.0 | 0.049 | 0.087 | 0.130 | 0.180 | 0.230 | 0.270 | 0.300 | 0.330 | 0.360 | 0.380 | 0.400 | 0.410 | 0.420 | 0.430 | 0.430 | 0.430 | 0.440 | 0.450 |
| 227 | 182 | 184 | 183.0 | 148.0 | 146.0 | 147.0 | 0.063 | 0.110 | 0.170 | 0.240 | 0.290 | 0.340 | 0.390 | 0.430 | 0.470 | 0.490 | 0.510 | 0.530 | 0.540 | 0.550 | 0.560 | 0.560 | 0.570 | 0.580 |
| 228 | 180 | 182 | 181.0 | 150.0 | 148.0 | 149.0 | 0.062 | 0.110 | 0.160 | 0.230 | 0.290 | 0.340 | 0.380 | 0.420 | 0.460 | 0.490 | 0.510 | 0.520 | 0.540 | 0.550 | 0.550 | 0.560 | 0.570 | 0.580 |
| 229 | 178 | 180 | 179.0 | 152.0 | 150.0 | 151.0 | 0.076 | 0.140 | 0.200 | 0.280 | 0.350 | 0.410 | 0.460 | 0.510 | 0.560 | 0.590 | 0.610 | 0.630 | 0.640 | 0.650 | 0.660 | 0.670 | 0.680 | 0.700 |
| 230 | 176 | 178 | 177.0 | 154.0 | 152.0 | 153.0 | 0.078 | 0.140 | 0.200 | 0.290 | 0.360 | 0.420 | 0.480 | 0.530 | 0.570 | 0.600 | 0.630 | 0.640 | 0.660 | 0.670 | 0.680 | 0.690 | 0.710 | 0.720 |
| 231 | 176 | 178 | 177.0 | 154.0 | 152.0 | 153.0 | 0.064 | 0.110 | 0.170 | 0.240 | 0.300 | 0.350 | 0.390 | 0.440 | 0.470 | 0.500 | 0.520 | 0.530 | 0.540 | 0.550 | 0.560 | 0.570 | 0.570 | 0.590 |
| 232 | 174 | 176 | 175.0 | 156.0 | 154.0 | 155.0 | 0.047 | 0.084 | 0.120 | 0.180 | 0.220 | 0.260 | 0.290 | 0.320 | 0.350 | 0.370 | 0.380 | 0.390 | 0.400 | 0.400 | 0.400 | 0.400 | 0.400 | 0.400 |
| 233 | 172 | 174 | 173.0 | 158.0 | 156.0 | 157.0 | 0.052 | 0.093 | 0.140 | 0.200 | 0.240 | 0.280 | 0.320 | 0.360 | 0.390 | 0.410 | 0.430 | 0.440 | 0.450 | 0.460 | 0.460 | 0.470 | 0.470 | 0.480 |
| 234 | 170 | 172 | 171.0 | 160.0 | 158.0 | 159.0 | 0.064 | 0.110 | 0.170 | 0.240 | 0.300 | 0.350 | 0.390 | 0.430 | 0.470 | 0.490 | 0.510 | 0.520 | 0.530 | 0.540 | 0.540 | 0.550 | 0.560 | 0.570 |
| 235 | 168 | 170 | 169.0 | 162.0 | 160.0 | 161.0 | 0.053 | 0.094 | 0.140 | 0.200 | 0.250 | 0.290 | 0.330 | 0.360 | 0.390 | 0.420 | 0.430 | 0.450 | 0.460 | 0.460 | 0.470 | 0.470 | 0.480 | 0.490 |
| 236 | 166 | 168 | 167.0 | 164.0 | 162.0 | 163.0 | 0.064 | 0.110 | 0.170 | 0.240 | 0.300 | 0.350 | 0.400 | 0.440 | 0.480 | 0.500 | 0.530 | 0.540 | 0.560 | 0.570 | 0.570 | 0.580 | 0.590 | 0.600 |
| 237 | 164 | 166 | 165.0 | 166.0 | 164.0 | 165.0 | 0.054 | 0.097 | 0.140 | 0.200 | 0.250 | 0.300 | 0.340 | 0.370 | 0.400 | 0.430 | 0.450 | 0.460 | 0.470 | 0.480 | 0.480 | 0.490 | 0.500 | 0.510 |
| 238 | 162 | 164 | 163.0 | 168.0 | 166.0 | 167.0 | 0.055 | 0.098 | 0.140 | 0.210 | 0.260 | 0.300 | 0.340 | 0.380 | 0.410 | 0.430 | 0.440 | 0.460 | 0.470 | 0.470 | 0.470 | 0.480 | 0.480 | 0.490 |
| 239 | 160 | 162 | 161.0 | 170.0 | 168.0 | 169.0 | 0.051 | 0.090 | 0.130 | 0.190 | 0.230 | 0.270 | 0.310 | 0.350 | 0.370 | 0.400 | 0.410 | 0.420 | 0.430 | 0.440 | 0.440 | 0.450 | 0.450 | 0.460 |
| 240 | 158 | 160 | 159.0 | 172.0 | 170.0 | 171.0 | 0.069 | 0.120 | 0.180 | 0.260 | 0.320 | 0.370 | 0.420 | 0.460 | 0.500 | 0.530 | 0.550 | 0.560 | 0.570 | 0.580 | 0.580 | 0.590 | 0.600 | 0.630 |
| 241 | 156 | 158 | 157.0 | 174.0 | 172.0 | 173.0 | 0.190 | 0.340 | 0.500 | 0.700 | 0.870 | 1.010 | 1.130 | 1.240 | 1.330 | 1.400 | 1.440 | 1.480 | 1.510 | 1.530 | 1.560 | 1.590 | 1.630 | 1.680 |
| 242 | 154 | 156 | 155.0 | 176.0 | 174.0 | 175.0 | 0.110 | 0.190 | 0.280 | 0.400 | 0.500 | 0.580 | 0.660 | 0.730 | 0.790 | 0.840 | 0.880 | 0.910 | 0.950 | 0.970 | 1.000 | 1.030 | 1.070 | 1.120 |
| 243 | 152 | 154 | 153.0 | 178.0 | 176.0 | 177.0 | 0.097 | 0.170 | 0.250 | 0.360 | 0.450 | 0.520 | 0.580 | 0.640 | 0.690 | 0.720 | 0.750 | 0.760 | 0.780 | 0.790 | 0.800 | 0.820 | 0.840 | 0.900 |
| 244 | 150 | 152 | 151.0 | 180.0 | 178.0 | 179.0 | 0.084 | 0.150 | 0.220 | 0.310 | 0.390 | 0.450 | 0.510 | 0.570 | 0.610 | 0.650 | 0.680 | 0.700 | 0.720 | 0.740 | 0.760 | 0.780 | 0.810 | 0.840 |
| 245 | 148 | 150 | 149.0 | 182.0 | 180.0 | 181.0 | 0.092 | 0.160 | 0.240 | 0.340 | 0.430 | 0.500 | 0.560 | 0.620 | 0.670 | 0.710 | 0.740 | 0.760 | 0.790 | 0.810 | 0.820 | 0.850 | 0.870 | 0.940 |
| 246 | 146 | 148 | 147.0 | 184.0 | 182.0 | 183.0 | 0.083 | 0.150 | 0.220 | 0.310 | 0.380 | 0.450 | 0.510 | 0.570 | 0.620 | 0.660 | 0.700 | 0.730 | 0.760 | 0.790 | 0.820 | 0.860 | 0.900 | 0.950 |
| 247 | 144 | 146 | 145.0 | 186.0 | 184.0 | 185.0 | 0.097 | 0.170 | 0.250 | 0.360 | 0.450 | 0.520 | 0.590 | 0.650 | 0.700 | 0.740 | 0.770 | 0.800 | 0.820 | 0.840 | 0.870 | 0.890 | 0.920 | 0.960 |
| 248 | 142 | 144 | 143.0 | 188.0 | 186.0 | 187.0 | 0.096 | 0.170 | 0.250 | 0.350 | 0.440 | 0.510 | 0.570 | 0.640 | 0.680 | 0.720 | 0.750 | 0.770 | 0.790 | 0.810 | 0.820 | 0.840 | 0.860 | 0.900 |
| 249 | 140 | 142 | 141.0 | 190.0 | 188.0 | 189.0 | 0.091 | 0.160 | 0.240 | 0.340 | 0.420 | 0.490 | 0.550 | 0.610 | 0.660 | 0.700 | 0.730 | 0.750 | 0.770 | 0.790 | 0.800 | 0.820 | 0.840 | 0.870 |
| 250 | 138 | 140 | 139.0 | 192.0 | 190.0 | 191.0 | 0.085 | 0.150 | 0.220 | 0.320 | 0.390 | 0.460 | 0.520 | 0.570 | 0.620 | 0.650 | 0.670 | 0.690 | 0.710 | 0.720 | 0.740 | 0.750 | 0.770 | 0.790 |
| 251 | 136 | 138 | 137.0 | 194.0 | 192.0 | 193.0 | 0.093 | 0.170 | 0.240 | 0.350 | 0.430 | 0.500 | 0.560 | 0.630 | 0.680 | 0.710 | 0.740 | 0.770 | 0.790 | 0.810 | 0.830 | 0.850 | 0.880 | 0.910 |
| 252 | 134 | 136 | 135.0 | 196.0 | 194.0 | 195.0 | 0.096 | 0.170 | 0.250 | 0.360 | 0.440 | 0.520 | 0.580 | 0.640 | 0.700 | 0.740 | 0.770 | 0.800 | 0.820 | 0.850 | 0.870 | 0.900 | 0.930 | 0.970 |
| 253 | 132 | 134 | 133.0 | 198.0 | 196.0 | 197.0 | 0.081 | 0.140 | 0.210 | 0.300 | 0.380 | 0.440 | 0.490 | 0.550 | 0.590 | 0.620 | 0.650 | 0.670 | 0.680 | 0.700 | 0.710 | 0.720 | 0.740 | 0.760 |
| 254 | 130 | 132 | 131.0 | 200.0 | 198.0 | 199.0 | 0.083 | 0.150 | 0.220 | 0.310 | 0.380 | 0.440 | 0.500 | 0.550 | 0.600 | 0.630 | 0.660 | 0.670 | 0.690 | 0.700 | 0.720 | 0.730 | 0.750 | 0.770 |
| 255 | 128 | 130 | 129.0 | 202.0 | 200.0 | 201.0 | 0.078 | 0.140 | 0.200 | 0.290 | 0.360 | 0.420 | 0.480 | 0.530 | 0.570 | 0.610 | 0.630 | 0.650 | 0.670 | 0.680 | 0.700 | 0.710 | 0.730 | 0.750 |
| 256 | 126 | 128 | 127.0 | 204.0 | 202.0 | 203.0 | 0.082 | 0.150 | 0.220 | 0.310 | 0.380 | 0.450 | 0.500 | 0.560 | 0.610 | 0.650 | 0.680 | 0.700 | 0.720 | 0.740 | 0.760 | 0.780 | 0.810 | 0.830 |
| 257 | 124 | 126 | 125.0 | 206.0 | 204.0 | 205.0 | 0.075 | 0.130 | 0.200 | 0.280 | 0.350 | 0.410 | 0.460 | 0.510 | 0.550 | 0.580 | 0.610 | 0.630 | 0.650 | 0.660 | 0.670 | 0.680 | 0.700 | 0.720 |
| 258 | 122 | 124 | 123.0 | 208.0 | 206.0 | 207.0 | 0.077 | 0.140 | 0.200 | 0.290 | 0.360 | 0.420 | 0.470 | 0.520 | 0.560 | 0.590 | 0.620 | 0.640 | 0.650 | 0.660 | 0.680 | 0.690 | 0.700 | |

| ID | Height (cm) original | | Depth (cm) | | Grain size distributions (Laser Coulter Counter, AWI Potsdam) in ϕ | | | | | | | | | | | | | | | | | | | | |
|-----|-------------------------|------|---------------|-------|---|--------|--------|--------|--------|--------|--------|--------|--------|--------|--------|-------|-------|-------|-------|-------|-------|-------|-------|-------|-------|
| | (base=0) | mean | depth (top=0) | mean | 11.381 | 11.245 | 11.111 | 10.977 | 10.841 | 10.708 | 10.572 | 10.438 | 10.304 | 10.168 | 10.035 | 9.900 | 9.765 | 9.631 | 9.496 | 9.362 | 9.227 | 9.092 | 8.959 | | |
| 263 | 112 | 114 | 113.0 | 218.0 | 216.0 | 217.0 | 0.084 | 0.150 | 0.220 | 0.310 | 0.390 | 0.450 | 0.510 | 0.560 | 0.600 | 0.630 | 0.660 | 0.670 | 0.690 | 0.690 | 0.700 | 0.710 | 0.720 | 0.730 | 0.760 |
| 264 | 110 | 112 | 111.0 | 220.0 | 218.0 | 219.0 | 0.066 | 0.120 | 0.170 | 0.250 | 0.310 | 0.360 | 0.400 | 0.450 | 0.490 | 0.510 | 0.540 | 0.550 | 0.570 | 0.580 | 0.580 | 0.590 | 0.600 | 0.620 | 0.640 |
| 265 | 108 | 110 | 109.0 | 222.0 | 220.0 | 221.0 | 0.070 | 0.130 | 0.180 | 0.260 | 0.330 | 0.380 | 0.430 | 0.480 | 0.520 | 0.550 | 0.580 | 0.600 | 0.610 | 0.630 | 0.640 | 0.650 | 0.660 | 0.680 | 0.700 |
| 266 | 106 | 108 | 107.0 | 224.0 | 222.0 | 223.0 | 0.110 | 0.200 | 0.290 | 0.420 | 0.540 | 0.640 | 0.750 | 0.860 | 0.980 | 1.090 | 1.210 | 1.340 | 1.490 | 1.640 | 1.810 | 1.980 | 2.160 | 2.340 | 2.510 |
| 267 | 104 | 106 | 105.0 | 226.0 | 224.0 | 225.0 | 0.060 | 0.110 | 0.160 | 0.220 | 0.280 | 0.320 | 0.360 | 0.400 | 0.430 | 0.460 | 0.470 | 0.480 | 0.490 | 0.500 | 0.500 | 0.500 | 0.500 | 0.510 | 0.520 |
| 268 | 102 | 104 | 103.0 | 228.0 | 226.0 | 227.0 | 0.068 | 0.120 | 0.180 | 0.250 | 0.320 | 0.370 | 0.420 | 0.470 | 0.510 | 0.540 | 0.560 | 0.580 | 0.590 | 0.600 | 0.610 | 0.620 | 0.630 | 0.650 | 0.660 |
| 269 | 100 | 102 | 101.0 | 230.0 | 228.0 | 229.0 | 0.074 | 0.130 | 0.190 | 0.270 | 0.340 | 0.400 | 0.450 | 0.510 | 0.550 | 0.580 | 0.610 | 0.630 | 0.650 | 0.660 | 0.670 | 0.680 | 0.690 | 0.700 | 0.720 |
| 270 | 98 | 100 | 99.0 | 232.0 | 230.0 | 231.0 | 0.098 | 0.170 | 0.260 | 0.360 | 0.460 | 0.530 | 0.610 | 0.680 | 0.740 | 0.790 | 0.840 | 0.880 | 0.920 | 0.950 | 0.990 | 1.020 | 1.060 | 1.100 | 1.130 |
| 271 | 96 | 98 | 97.0 | 234.0 | 232.0 | 233.0 | 0.100 | 0.180 | 0.260 | 0.370 | 0.460 | 0.540 | 0.610 | 0.680 | 0.740 | 0.790 | 0.830 | 0.860 | 0.900 | 0.930 | 0.960 | 0.990 | 1.030 | 1.070 | 1.120 |
| 272 | 94 | 94 | 94.0 | 236.0 | 230.0 | 236.0 | 0.120 | 0.210 | 0.310 | 0.440 | 0.550 | 0.640 | 0.720 | 0.790 | 0.860 | 0.900 | 0.940 | 0.970 | 1.000 | 1.030 | 1.050 | 1.080 | 1.120 | 1.170 | 1.220 |
| 273 | 94 | 96 | 95.0 | 236.0 | 234.0 | 235.0 | 0.130 | 0.230 | 0.330 | 0.480 | 0.610 | 0.720 | 0.840 | 0.960 | 1.090 | 1.210 | 1.340 | 1.480 | 1.640 | 1.810 | 1.990 | 2.180 | 2.370 | 2.570 | 2.760 |
| 274 | 91 | 94 | 92.5 | 239.0 | 236.0 | 237.5 | 0.150 | 0.260 | 0.390 | 0.550 | 0.680 | 0.790 | 0.890 | 0.980 | 1.050 | 1.110 | 1.150 | 1.190 | 1.230 | 1.260 | 1.300 | 1.340 | 1.390 | 1.450 | 1.520 |
| 275 | 89 | 91 | 90.0 | 241.0 | 239.0 | 240.0 | 0.160 | 0.280 | 0.400 | 0.570 | 0.710 | 0.830 | 0.930 | 1.030 | 1.100 | 1.160 | 1.210 | 1.250 | 1.290 | 1.320 | 1.360 | 1.400 | 1.450 | 1.510 | 1.580 |
| 276 | 87 | 89 | 88.0 | 243.0 | 241.0 | 242.0 | 0.150 | 0.270 | 0.400 | 0.560 | 0.700 | 0.810 | 0.910 | 1.000 | 1.070 | 1.130 | 1.160 | 1.190 | 1.230 | 1.250 | 1.280 | 1.320 | 1.360 | 1.420 | 1.490 |
| 277 | 85 | 87 | 86.0 | 245.0 | 243.0 | 244.0 | 0.160 | 0.280 | 0.400 | 0.570 | 0.710 | 0.820 | 0.920 | 1.020 | 1.090 | 1.150 | 1.190 | 1.230 | 1.260 | 1.290 | 1.320 | 1.360 | 1.410 | 1.460 | 1.530 |
| 278 | 83 | 85 | 84.0 | 247.0 | 245.0 | 246.0 | 0.160 | 0.290 | 0.420 | 0.600 | 0.740 | 0.860 | 0.970 | 1.070 | 1.150 | 1.200 | 1.250 | 1.280 | 1.320 | 1.350 | 1.380 | 1.420 | 1.480 | 1.540 | 1.610 |
| 279 | 81 | 83 | 82.5 | 249.0 | 247.0 | 247.5 | 0.170 | 0.300 | 0.430 | 0.610 | 0.760 | 0.880 | 0.980 | 1.080 | 1.160 | 1.210 | 1.260 | 1.290 | 1.320 | 1.360 | 1.390 | 1.430 | 1.490 | 1.560 | 1.630 |
| 280 | 79 | 81 | 80.0 | 251.0 | 249.0 | 250.0 | 0.160 | 0.280 | 0.410 | 0.580 | 0.720 | 0.840 | 0.940 | 1.040 | 1.110 | 1.170 | 1.210 | 1.250 | 1.280 | 1.310 | 1.340 | 1.380 | 1.430 | 1.490 | 1.560 |
| 281 | 77 | 79 | 78.0 | 253.0 | 251.0 | 252.0 | 0.150 | 0.270 | 0.390 | 0.550 | 0.680 | 0.790 | 0.880 | 0.970 | 1.040 | 1.090 | 1.130 | 1.160 | 1.190 | 1.220 | 1.240 | 1.280 | 1.320 | 1.380 | 1.440 |
| 282 | 75 | 77 | 76.0 | 255.0 | 253.0 | 254.0 | 0.160 | 0.290 | 0.420 | 0.600 | 0.740 | 0.850 | 0.950 | 1.040 | 1.120 | 1.170 | 1.200 | 1.220 | 1.250 | 1.270 | 1.290 | 1.320 | 1.370 | 1.420 | 1.490 |
| 283 | 73 | 75 | 74.0 | 257.0 | 255.0 | 256.0 | 0.160 | 0.290 | 0.430 | 0.600 | 0.740 | 0.860 | 0.970 | 1.060 | 1.140 | 1.200 | 1.240 | 1.280 | 1.320 | 1.360 | 1.400 | 1.450 | 1.510 | 1.580 | 1.660 |
| 284 | 71 | 73 | 72.0 | 259.0 | 257.0 | 258.0 | 0.130 | 0.230 | 0.340 | 0.480 | 0.600 | 0.700 | 0.790 | 0.870 | 0.940 | 0.990 | 1.030 | 1.060 | 1.090 | 1.120 | 1.150 | 1.180 | 1.220 | 1.270 | 1.330 |
| 285 | 69 | 71 | 70.0 | 261.0 | 259.0 | 260.0 | 0.140 | 0.260 | 0.380 | 0.530 | 0.660 | 0.770 | 0.870 | 0.960 | 1.040 | 1.100 | 1.140 | 1.180 | 1.220 | 1.260 | 1.290 | 1.340 | 1.390 | 1.450 | 1.520 |
| 286 | 67 | 69 | 68.0 | 263.0 | 261.0 | 262.0 | 0.160 | 0.280 | 0.410 | 0.580 | 0.720 | 0.830 | 0.930 | 1.020 | 1.090 | 1.130 | 1.160 | 1.170 | 1.180 | 1.190 | 1.200 | 1.210 | 1.230 | 1.270 | 1.310 |
| 287 | 65 | 67 | 66.0 | 265.0 | 263.0 | 264.0 | 0.200 | 0.350 | 0.520 | 0.730 | 0.900 | 1.040 | 1.160 | 1.260 | 1.350 | 1.400 | 1.430 | 1.450 | 1.460 | 1.480 | 1.490 | 1.510 | 1.550 | 1.600 | 1.670 |
| 288 | 63 | 65 | 64.0 | 267.0 | 265.0 | 266.0 | 0.180 | 0.320 | 0.470 | 0.660 | 0.820 | 0.950 | 1.070 | 1.180 | 1.270 | 1.340 | 1.390 | 1.440 | 1.490 | 1.530 | 1.580 | 1.630 | 1.700 | 1.770 | 1.860 |
| 289 | 61 | 63 | 62.0 | 269.0 | 267.0 | 268.0 | 0.210 | 0.370 | 0.550 | 0.770 | 0.960 | 1.110 | 1.240 | 1.370 | 1.470 | 1.540 | 1.600 | 1.650 | 1.700 | 1.750 | 1.810 | 1.870 | 1.950 | 2.050 | 2.150 |
| 290 | 59 | 61 | 60.0 | 271.0 | 269.0 | 270.0 | 0.180 | 0.320 | 0.470 | 0.670 | 0.840 | 0.990 | 1.140 | 1.290 | 1.440 | 1.580 | 1.720 | 1.880 | 2.060 | 2.260 | 2.470 | 2.700 | 2.940 | 3.190 | 3.430 |
| 291 | 57 | 59 | 58.0 | 273.0 | 271.0 | 272.0 | 0.250 | 0.440 | 0.640 | 0.900 | 1.100 | 1.270 | 1.410 | 1.540 | 1.630 | 1.690 | 1.730 | 1.760 | 1.780 | 1.800 | 1.830 | 1.870 | 1.930 | 2.010 | 2.090 |
| 292 | 55 | 57 | 56.0 | 275.0 | 273.0 | 274.0 | 0.200 | 0.360 | 0.520 | 0.740 | 0.910 | 1.050 | 1.180 | 1.290 | 1.390 | 1.450 | 1.500 | 1.540 | 1.580 | 1.620 | 1.670 | 1.720 | 1.790 | 1.870 | 1.960 |
| 293 | 53 | 55 | 54.0 | 277.0 | 275.0 | 276.0 | 0.210 | 0.370 | 0.540 | 0.760 | 0.930 | 1.080 | 1.200 | 1.320 | 1.410 | 1.470 | 1.520 | 1.560 | 1.590 | 1.630 | 1.680 | 1.740 | 1.810 | 1.900 | 1.990 |
| 294 | 50 | 53 | 51.5 | 280.0 | 277.0 | 278.5 | 0.230 | 0.400 | 0.590 | 0.830 | 1.020 | 1.170 | 1.300 | 1.420 | 1.510 | 1.570 | 1.610 | 1.640 | 1.670 | 1.700 | 1.740 | 1.780 | 1.850 | 1.930 | 2.030 |
| 295 | 48 | 50 | 49.0 | 282.0 | 280.0 | 281.0 | 0.220 | 0.380 | 0.560 | 0.790 | 0.980 | 1.130 | 1.270 | 1.390 | 1.490 | 1.560 | 1.620 | 1.660 | 1.710 | 1.760 | 1.810 | 1.870 | 1.950 | 2.050 | 2.150 |
| 296 | 46 | 48 | 47.0 | 284.0 | 282.0 | 283.0 | 0.220 | 0.380 | 0.560 | 0.790 | 0.970 | 1.120 | 1.240 | 1.350 | 1.440 | 1.490 | 1.520 | 1.540 | 1.560 | 1.570 | 1.590 | 1.620 | 1.670 | 1.730 | 1.800 |
| 297 | 44 | 46 | 45.0 | 286.0 | 284.0 | 285.0 | 0.200 | 0.350 | 0.520 | 0.730 | 0.900 | 1.040 | 1.170 | 1.280 | 1.370 | 1.430 | 1.480 | 1.510 | 1.550 | 1.580 | 1.610 | 1.650 | 1.710 | 1.770 | 1.840 |
| 298 | 42 | 44 | 43.0 | 288.0 | 286.0 | 287.0 | 0.130 | 0.240 | 0.350 | 0.500 | 0.630 | 0.740 | 0.860 | 0.980 | 1.110 | 1.230 | 1.360 | 1.520 | 1.690 | 1.880 | 2.100 | 2.330 | 2.580 | 2.840 | 3.100 |
| 299 | 40 | 42 | 41.0 | 290.0 | 288.0 | 289.0 | 0.200 | 0.350 | 0.520 | 0.730 | 0.900 | 1.040 | 1.150 | 1.260 | 1.350 | 1.400 | 1.440 | 1.470 | 1.500 | 1.520 | 1.550 | 1.590 | 1.640 | 1.710 | 1.780 |
| 300 | 38 | 40 | 39.0 | 292.0 | 290.0 | 291.0 | 0.210 | 0.370 | 0.540 | 0.760 | 0.930 | 1.070 | 1.200 | 1.300 | 1.390 | 1.440 | 1.480 | 1.500 | 1.530 | 1.560 | 1.590 | 1.630 | 1.700 | 1.790 | 1.890 |
| 301 | 36 | 38 | 37.0 | 294.0 | 292.0 | 293.0 | 0.190 | 0.330 | 0.490 | 0.690 | 0.850 | 0.990 | 1.110 | 1.220 | 1.310 | 1.370 | 1.420 | 1.450 | 1.490 | 1.520 | 1.550 | 1.590 | 1.640 | 1.710 | 1.790 |
| 302 | 36 | 38 | 37.0 | 294.0 | 292.0 | 293.0 | 0.110 | 0.190 | 0.280 | 0.400 | 0.510 | 0.600 | 0.700 | 0.800 | 0.910 | 1.010 | 1.130 | 1.260 | | | | | | | |

| ID | Height (cm) | | Depth (cm) | | Grain size distributions (Laser Coulter Counter, AWI Potsdam) in ϕ | | | | | | | | | | | | | | | | | | | | |
|--------------|-------------|------|---------------|-------|---|--------|--------|--------|--------|--------|--------|--------|--------|--------|--------|-------|-------|-------|-------|-------|-------|-------|-------|-------|-------|
| | original | mean | depth (top=0) | mean | 11.381 | 11.245 | 11.111 | 10.977 | 10.841 | 10.708 | 10.572 | 10.438 | 10.304 | 10.168 | 10.035 | 9.900 | 9.765 | 9.631 | 9.496 | 9.362 | 9.227 | 9.092 | 8.959 | | |
| 308 | 22 | 24 | 23.0 | 308.0 | 306.0 | 307.0 | 0.190 | 0.330 | 0.490 | 0.690 | 0.850 | 0.990 | 1.100 | 1.210 | 1.300 | 1.360 | 1.400 | 1.440 | 1.470 | 1.500 | 1.540 | 1.590 | 1.650 | 1.720 | 1.810 |
| 309 | 20 | 22 | 21.0 | 310.0 | 308.0 | 309.0 | 0.160 | 0.290 | 0.420 | 0.590 | 0.730 | 0.850 | 0.950 | 1.050 | 1.120 | 1.180 | 1.220 | 1.250 | 1.280 | 1.310 | 1.340 | 1.380 | 1.430 | 1.490 | 1.570 |
| 310 | 15 | 17 | 16.0 | 315.0 | 313.0 | 314.0 | 0.170 | 0.300 | 0.440 | 0.620 | 0.770 | 0.890 | 1.000 | 1.100 | 1.180 | 1.240 | 1.280 | 1.320 | 1.350 | 1.390 | 1.420 | 1.460 | 1.520 | 1.590 | 1.670 |
| 311 | 9 | 11 | 10.0 | 321.0 | 319.0 | 320.0 | 0.120 | 0.210 | 0.310 | 0.430 | 0.540 | 0.620 | 0.700 | 0.770 | 0.830 | 0.870 | 0.900 | 0.930 | 0.950 | 0.970 | 0.980 | 1.000 | 1.030 | 1.070 | 1.120 |
| 312 | 0 | 4 | 2.0 | 330.0 | 326.0 | 328.0 | 0.120 | 0.200 | 0.300 | 0.430 | 0.530 | 0.610 | 0.690 | 0.760 | 0.820 | 0.860 | 0.890 | 0.910 | 0.940 | 0.950 | 0.970 | 0.990 | 1.020 | 1.050 | 1.090 |
| P15 | | | | | | | | | | | | | | | | | | | | | | | | | |
| 324 | 161 | 163 | 162.0 | 148.0 | 146.0 | 147.0 | 0.040 | 0.070 | 0.100 | 0.150 | 0.190 | 0.220 | 0.260 | 0.300 | 0.340 | 0.370 | 0.410 | 0.460 | 0.510 | 0.570 | 0.630 | 0.690 | 0.770 | 0.840 | 0.920 |
| 325 | 171 | 173 | 172.0 | 138.0 | 136.0 | 137.0 | 0.037 | 0.066 | 0.097 | 0.140 | 0.180 | 0.220 | 0.250 | 0.300 | 0.340 | 0.380 | 0.420 | 0.460 | 0.500 | 0.550 | 0.600 | 0.640 | 0.690 | 0.730 | 0.770 |
| 326 | 174 | 176 | 175.0 | 135.0 | 133.0 | 134.0 | 0.021 | 0.037 | 0.055 | 0.080 | 0.100 | 0.120 | 0.150 | 0.170 | 0.200 | 0.230 | 0.250 | 0.280 | 0.320 | 0.350 | 0.380 | 0.410 | 0.450 | 0.480 | 0.510 |
| 327 | 178 | 180 | 179.0 | 131.0 | 129.0 | 130.0 | 0.027 | 0.048 | 0.071 | 0.100 | 0.130 | 0.160 | 0.190 | 0.230 | 0.260 | 0.300 | 0.340 | 0.380 | 0.430 | 0.480 | 0.540 | 0.590 | 0.650 | 0.710 | 0.770 |
| 332 | 198 | 200 | 199.0 | 111.0 | 109.0 | 110.0 | 0.034 | 0.061 | 0.090 | 0.130 | 0.170 | 0.200 | 0.230 | 0.270 | 0.310 | 0.340 | 0.380 | 0.420 | 0.460 | 0.500 | 0.550 | 0.590 | 0.640 | 0.690 | 0.730 |
| 333 | 202 | 204 | 203.0 | 107.0 | 105.0 | 106.0 | 0.043 | 0.077 | 0.110 | 0.160 | 0.210 | 0.250 | 0.290 | 0.330 | 0.380 | 0.420 | 0.470 | 0.510 | 0.560 | 0.610 | 0.670 | 0.720 | 0.780 | 0.830 | 0.890 |
| 334 | 206 | 208 | 207.0 | 103.0 | 101.0 | 102.0 | 0.046 | 0.082 | 0.120 | 0.170 | 0.220 | 0.260 | 0.310 | 0.350 | 0.390 | 0.430 | 0.470 | 0.510 | 0.550 | 0.590 | 0.620 | 0.660 | 0.700 | 0.730 | 0.760 |
| 335 | 210 | 212 | 211.0 | 99.0 | 97.0 | 98.0 | 0.053 | 0.094 | 0.140 | 0.200 | 0.250 | 0.300 | 0.350 | 0.400 | 0.450 | 0.500 | 0.550 | 0.600 | 0.650 | 0.700 | 0.760 | 0.810 | 0.870 | 0.930 | 0.990 |
| 336 | 214 | 216 | 215.0 | 95.0 | 93.0 | 94.0 | 0.080 | 0.140 | 0.210 | 0.300 | 0.380 | 0.450 | 0.520 | 0.580 | 0.650 | 0.700 | 0.760 | 0.820 | 0.870 | 0.930 | 0.990 | 1.050 | 1.120 | 1.190 | 1.250 |
| 337 | 218 | 220 | 219.0 | 91.0 | 89.0 | 90.0 | 0.055 | 0.098 | 0.150 | 0.210 | 0.260 | 0.320 | 0.370 | 0.420 | 0.470 | 0.520 | 0.570 | 0.620 | 0.680 | 0.730 | 0.780 | 0.840 | 0.890 | 0.950 | 1.000 |
| 338 | 222 | 224 | 223.0 | 87.0 | 85.0 | 86.0 | 0.078 | 0.140 | 0.200 | 0.290 | 0.370 | 0.440 | 0.500 | 0.570 | 0.630 | 0.690 | 0.740 | 0.800 | 0.850 | 0.910 | 0.960 | 1.020 | 1.080 | 1.150 | 1.210 |
| 339 | 226 | 228 | 227.0 | 83.0 | 81.0 | 82.0 | 0.089 | 0.160 | 0.230 | 0.330 | 0.420 | 0.490 | 0.560 | 0.630 | 0.700 | 0.750 | 0.800 | 0.850 | 0.900 | 0.950 | 0.990 | 1.040 | 1.090 | 1.150 | 1.200 |
| 340 | 230 | 232 | 231.0 | 79.0 | 77.0 | 78.0 | 0.082 | 0.150 | 0.210 | 0.310 | 0.390 | 0.460 | 0.520 | 0.590 | 0.660 | 0.710 | 0.770 | 0.820 | 0.870 | 0.920 | 0.970 | 1.030 | 1.080 | 1.140 | 1.200 |
| 341 | 234 | 236 | 235.0 | 75.0 | 73.0 | 74.0 | 0.064 | 0.110 | 0.170 | 0.240 | 0.300 | 0.360 | 0.420 | 0.470 | 0.530 | 0.580 | 0.620 | 0.670 | 0.720 | 0.770 | 0.820 | 0.860 | 0.910 | 0.960 | 1.010 |
| 342 | 238 | 240 | 239.0 | 71.0 | 69.0 | 70.0 | 0.070 | 0.120 | 0.180 | 0.260 | 0.330 | 0.390 | 0.450 | 0.510 | 0.570 | 0.620 | 0.670 | 0.710 | 0.760 | 0.800 | 0.850 | 0.890 | 0.940 | 0.980 | 1.030 |
| 343 | 242 | 244 | 241.0 | 67.0 | 65.0 | 68.0 | 0.100 | 0.180 | 0.270 | 0.380 | 0.470 | 0.560 | 0.630 | 0.710 | 0.770 | 0.820 | 0.860 | 0.900 | 0.930 | 0.960 | 0.980 | 1.000 | 1.020 | 1.050 | 1.080 |
| 344 | 246 | 248 | 247.0 | 63.0 | 61.0 | 62.0 | 0.079 | 0.140 | 0.210 | 0.300 | 0.370 | 0.440 | 0.510 | 0.570 | 0.630 | 0.690 | 0.730 | 0.780 | 0.830 | 0.870 | 0.920 | 0.960 | 1.010 | 1.050 | 1.100 |
| 345 | 250 | 252 | 251.0 | 59.0 | 57.0 | 58.0 | 0.050 | 0.088 | 0.130 | 0.190 | 0.240 | 0.280 | 0.330 | 0.380 | 0.420 | 0.460 | 0.500 | 0.540 | 0.590 | 0.630 | 0.670 | 0.710 | 0.750 | 0.790 | 0.830 |
| 346 | 260 | 262 | 261.0 | 49.0 | 47.0 | 48.0 | 0.045 | 0.080 | 0.120 | 0.170 | 0.220 | 0.260 | 0.300 | 0.350 | 0.390 | 0.430 | 0.480 | 0.520 | 0.570 | 0.610 | 0.660 | 0.710 | 0.760 | 0.810 | 0.850 |
| P21-H | | | | | | | | | | | | | | | | | | | | | | | | | |
| 397 | 225 | 230 | 227.5 | 15.0 | 10.0 | 12.5 | 0.110 | 0.190 | 0.270 | 0.390 | 0.480 | 0.560 | 0.620 | 0.680 | 0.730 | 0.760 | 0.780 | 0.790 | 0.800 | 0.800 | 0.800 | 0.820 | 0.840 | 0.860 | |
| 398 | 220 | 225 | 222.5 | 20.0 | 15.0 | 17.5 | 0.120 | 0.210 | 0.310 | 0.440 | 0.550 | 0.640 | 0.710 | 0.780 | 0.830 | 0.860 | 0.880 | 0.890 | 0.900 | 0.910 | 0.910 | 0.920 | 0.940 | 0.960 | 1.000 |
| 399 | 215 | 220 | 217.5 | 25.0 | 20.0 | 22.5 | 0.097 | 0.170 | 0.250 | 0.360 | 0.440 | 0.520 | 0.580 | 0.640 | 0.690 | 0.720 | 0.750 | 0.770 | 0.780 | 0.790 | 0.800 | 0.810 | 0.830 | 0.850 | 0.880 |
| 400 | 212 | 215 | 213.5 | 28.0 | 25.0 | 26.5 | 0.078 | 0.140 | 0.200 | 0.290 | 0.360 | 0.420 | 0.480 | 0.530 | 0.570 | 0.610 | 0.630 | 0.650 | 0.670 | 0.680 | 0.690 | 0.700 | 0.720 | 0.740 | 0.760 |
| 405 | 138 | 145 | 141.5 | 102.0 | 95.0 | 98.5 | 0.043 | 0.076 | 0.110 | 0.160 | 0.200 | 0.230 | 0.260 | 0.290 | 0.320 | 0.340 | 0.350 | 0.360 | 0.370 | 0.380 | 0.380 | 0.390 | 0.400 | 0.400 | |
| 406 | 133 | 138 | 135.5 | 107.0 | 102.0 | 104.5 | 0.037 | 0.066 | 0.098 | 0.140 | 0.170 | 0.200 | 0.230 | 0.260 | 0.280 | 0.300 | 0.310 | 0.320 | 0.320 | 0.330 | 0.330 | 0.330 | 0.330 | 0.330 | |
| 407 | 128 | 133 | 130.5 | 112.0 | 107.0 | 109.5 | 0.062 | 0.110 | 0.160 | 0.230 | 0.290 | 0.330 | 0.380 | 0.420 | 0.450 | 0.480 | 0.500 | 0.520 | 0.530 | 0.540 | 0.540 | 0.550 | 0.560 | 0.570 | 0.580 |
| 408 | 126 | 128 | 127.0 | 114.0 | 112.0 | 113.0 | 0.073 | 0.130 | 0.190 | 0.270 | 0.350 | 0.420 | 0.490 | 0.570 | 0.650 | 0.740 | 0.830 | 0.930 | 1.040 | 1.170 | 1.300 | 1.440 | 1.590 | 1.740 | 1.890 |
| 409 | 124 | 126 | 125.0 | 116.0 | 114.0 | 115.0 | 0.081 | 0.140 | 0.210 | 0.300 | 0.380 | 0.460 | 0.530 | 0.610 | 0.690 | 0.760 | 0.850 | 0.940 | 1.050 | 1.160 | 1.290 | 1.420 | 1.570 | 1.730 | 1.890 |
| 410 | 121 | 124 | 122.5 | 119.0 | 116.0 | 117.5 | 0.068 | 0.120 | 0.180 | 0.250 | 0.320 | 0.390 | 0.460 | 0.530 | 0.600 | 0.680 | 0.770 | 0.860 | 0.960 | 1.080 | 1.200 | 1.330 | 1.470 | 1.610 | 1.740 |
| 411 | 100 | 120 | 110.0 | 140.0 | 120.0 | 130.0 | 0.066 | 0.120 | 0.170 | 0.240 | 0.300 | 0.350 | 0.400 | 0.440 | 0.480 | 0.500 | 0.520 | 0.540 | 0.550 | 0.560 | 0.570 | 0.580 | 0.600 | 0.620 | 0.640 |
| 412 | 70 | 90 | 80.0 | 170.0 | 150.0 | 160.0 | 0.052 | 0.093 | 0.140 | 0.190 | 0.240 | 0.280 | 0.310 | 0.350 | 0.370 | 0.390 | 0.410 | 0.420 | 0.440 | 0.460 | 0.470 | 0.500 | 0.520 | 0.560 | 0.600 |
| 413 | 30 | 40 | 35.0 | 210.0 | 200.0 | 205.0 | 0.021 | 0.037 | 0.055 | 0.079 | 0.099 | 0.120 | 0.140 | 0.150 | 0.170 | 0.180 | 0.200 | 0.210 | 0.220 | 0.230 | 0.240 | 0.250 | 0.260 | 0.260 | |
| 414 | 20 | 25 | 22.5 | 220.0 | 215.0 | 217.5 | 0.017 | 0.032 | 0.054 | 0.075 | 0.094 | 0.110 | 0.130 | 0.140 | 0.150 | 0.160 | 0.170 | 0.170 | 0.170 | 0.170 | 0.170 | 0.170 | 0.170 | 0.170 | |
| 415 | 15 | 20 | 17.5 | 225.0 | 220.0 | 22 | | | | | | | | | | | | | | | | | | | |

| ID | 8.824 | 8.689 | 8.554 | 8.420 | 8.285 | 8.151 | 8.016 | 7.881 | 7.747 | 7.612 | 7.478 | 7.343 | 7.209 | 7.074 | 6.940 | 6.805 | 6.670 | 6.535 | 6.401 | 6.266 | 6.132 | 5.998 | 5.863 | 5.729 | 5.594 | 5.459 | |
|------------|-------|-------|-------|-------|-------|-------|-------|-------|-------|-------|-------|-------|-------|-------|-------|-------|-------|-------|-------|-------|-------|-------|-------|---------|-------|-------|-------|
| P02 | | | | | | | | | | | | | | | | | | | | | | | | | | | |
| 512 | 1.090 | 1.170 | 1.250 | 1.310 | 1.350 | 1.370 | 1.370 | 1.350 | 1.300 | 1.230 | 1.150 | 1.050 | 0.940 | 0.830 | 0.720 | 0.630 | 0.560 | 0.510 | 0.490 | 0.480 | 0.500 | 0.540 | 0.600 | 0.670 | 0.750 | 0.830 | |
| 514 | 0.380 | 0.390 | 0.400 | 0.410 | 0.430 | 0.440 | 0.460 | 0.470 | 0.490 | 0.510 | 0.520 | 0.530 | 0.550 | 0.560 | 0.570 | 0.590 | 0.610 | 0.630 | 0.660 | 0.690 | 0.730 | 0.790 | 0.860 | 0.960 | 1.080 | 1.210 | |
| 516 | 0.260 | 0.270 | 0.280 | 0.280 | 0.290 | 0.300 | 0.310 | 0.310 | 0.320 | 0.330 | 0.330 | 0.340 | 0.340 | 0.350 | 0.350 | 0.360 | 0.360 | 0.370 | 0.380 | 0.390 | 0.400 | 0.420 | 0.450 | 0.480 | 0.520 | 0.570 | |
| 518 | 0.670 | 0.690 | 0.720 | 0.750 | 0.780 | 0.810 | 0.840 | 0.870 | 0.900 | 0.920 | 0.940 | 0.960 | 0.980 | 0.990 | 1.000 | 1.010 | 1.020 | 1.030 | 1.050 | 1.080 | 1.120 | 1.170 | 1.250 | 1.370 | 1.520 | 1.690 | |
| 520 | 1.070 | 1.110 | 1.150 | 1.200 | 1.250 | 1.300 | 1.350 | 1.390 | 1.440 | 1.480 | 1.520 | 1.560 | 1.600 | 1.630 | 1.670 | 1.720 | 1.770 | 1.820 | 1.880 | 1.950 | 2.020 | 2.090 | 2.180 | 2.270 | 2.370 | 2.480 | |
| 522 | 2.040 | 2.210 | 2.350 | 2.480 | 2.570 | 2.630 | 2.650 | 2.630 | 2.570 | 2.480 | 2.350 | 2.210 | 2.050 | 1.890 | 1.740 | 1.600 | 1.500 | 1.440 | 1.420 | 1.440 | 1.490 | 1.590 | 1.710 | 1.850 | 1.980 | 2.090 | |
| 524 | 0.590 | 0.610 | 0.640 | 0.670 | 0.700 | 0.730 | 0.760 | 0.800 | 0.830 | 0.860 | 0.900 | 0.930 | 0.960 | 0.990 | 1.020 | 1.060 | 1.100 | 1.150 | 1.210 | 1.280 | 1.370 | 1.480 | 1.630 | 1.810 | 2.030 | 2.260 | |
| 526 | 0.660 | 0.680 | 0.700 | 0.730 | 0.750 | 0.780 | 0.820 | 0.860 | 0.900 | 0.950 | 1.000 | 1.050 | 1.110 | 1.180 | 1.260 | 1.350 | 1.460 | 1.590 | 1.740 | 1.900 | 2.080 | 2.280 | 2.500 | 2.720 | 2.940 | 3.160 | |
| 528 | 2.270 | 2.470 | 2.640 | 2.790 | 2.910 | 2.990 | 3.020 | 3.000 | 2.940 | 2.840 | 2.700 | 2.530 | 2.350 | 2.160 | 1.990 | 1.830 | 1.720 | 1.650 | 1.640 | 1.680 | 1.770 | 1.910 | 2.060 | 2.200 | 2.320 | 2.390 | |
| 530 | 2.280 | 2.450 | 2.590 | 2.720 | 2.810 | 2.860 | 2.870 | 2.840 | 2.770 | 2.670 | 2.530 | 2.380 | 2.210 | 2.050 | 1.890 | 1.770 | 1.680 | 1.640 | 1.640 | 1.680 | 1.760 | 1.870 | 1.990 | 2.120 | 2.220 | 2.280 | |
| 532 | 1.230 | 1.300 | 1.380 | 1.460 | 1.560 | 1.650 | 1.740 | 1.840 | 1.930 | 2.010 | 2.090 | 2.160 | 2.230 | 2.280 | 2.340 | 2.380 | 2.430 | 2.470 | 2.500 | 2.530 | 2.560 | 2.600 | 2.640 | 2.690 | 2.730 | 2.760 | |
| 534 | 0.970 | 1.020 | 1.070 | 1.130 | 1.200 | 1.260 | 1.330 | 1.400 | 1.460 | 1.530 | 1.580 | 1.640 | 1.690 | 1.750 | 1.800 | 1.850 | 1.900 | 1.960 | 2.020 | 2.100 | 2.180 | 2.290 | 2.420 | 2.570 | 2.730 | 2.890 | |
| 536 | 1.350 | 1.430 | 1.510 | 1.600 | 1.690 | 1.790 | 1.890 | 1.990 | 2.080 | 2.170 | 2.250 | 2.330 | 2.410 | 2.480 | 2.550 | 2.610 | 2.680 | 2.740 | 2.800 | 2.860 | 2.910 | 2.960 | 3.010 | 3.040 | 3.050 | 3.020 | |
| 538 | 1.520 | 1.620 | 1.730 | 1.850 | 1.970 | 2.090 | 2.210 | 2.330 | 2.430 | 2.530 | 2.610 | 2.680 | 2.730 | 2.780 | 2.810 | 2.840 | 2.840 | 2.820 | 2.780 | 2.730 | 2.670 | 2.600 | 2.520 | 2.420 | 2.290 | | |
| 567 | 1.410 | 1.480 | 1.560 | 1.650 | 1.740 | 1.820 | 1.910 | 1.990 | 2.060 | 2.130 | 2.190 | 2.230 | 2.280 | 2.310 | 2.340 | 2.370 | 2.390 | 2.410 | 2.430 | 2.450 | 2.470 | 2.510 | 2.550 | 2.610 | 2.670 | 2.720 | |
| P06 | | | | | | | | | | | | | | | | | | | | | | | | | | | |
| 49 | 1.010 | 1.060 | 1.090 | 1.110 | 1.120 | 1.110 | 1.090 | 1.050 | 1.010 | 0.950 | 0.890 | 0.840 | 0.780 | 0.730 | 0.700 | 0.680 | 0.670 | 0.690 | 0.730 | 0.780 | 0.850 | 0.940 | 1.050 | 1.180 | 1.330 | 1.470 | |
| 51 | 0.830 | 0.850 | 0.860 | 0.860 | 0.860 | 0.840 | 0.810 | 0.770 | 0.720 | 0.650 | 0.580 | 0.510 | 0.440 | 0.380 | 0.330 | 0.290 | 0.280 | 0.270 | 0.270 | 0.270 | 0.260 | 0.250 | 0.250 | 0.260 | 0.270 | 0.290 | |
| 53 | 0.840 | 0.870 | 0.890 | 0.900 | 0.900 | 0.880 | 0.860 | 0.820 | 0.770 | 0.710 | 0.640 | 0.560 | 0.490 | 0.420 | 0.370 | 0.320 | 0.290 | 0.280 | 0.270 | 0.270 | 0.270 | 0.270 | 0.270 | 0.280 | 0.280 | 0.290 | |
| 55 | 0.740 | 0.770 | 0.800 | 0.820 | 0.830 | 0.830 | 0.820 | 0.790 | 0.760 | 0.720 | 0.670 | 0.610 | 0.560 | 0.500 | 0.450 | 0.410 | 0.380 | 0.370 | 0.370 | 0.380 | 0.400 | 0.430 | 0.470 | 0.520 | 0.580 | 0.640 | |
| 57 | 1.120 | 1.200 | 1.260 | 1.320 | 1.350 | 1.370 | 1.360 | 1.330 | 1.280 | 1.220 | 1.130 | 1.040 | 0.950 | 0.860 | 0.780 | 0.710 | 0.670 | 0.650 | 0.660 | 0.690 | 0.740 | 0.820 | 0.920 | 1.030 | 1.160 | 1.300 | |
| 59 | 0.940 | 0.980 | 1.020 | 1.050 | 1.080 | 1.100 | 1.110 | 1.110 | 1.100 | 1.080 | 1.050 | 1.020 | 0.980 | 0.940 | 0.910 | 0.880 | 0.860 | 0.850 | 0.850 | 0.880 | 0.920 | 0.980 | 1.060 | 1.160 | 1.250 | | |
| 61 | 1.310 | 1.390 | 1.470 | 1.540 | 1.600 | 1.640 | 1.670 | 1.690 | 1.700 | 1.680 | 1.660 | 1.620 | 1.580 | 1.540 | 1.490 | 1.450 | 1.420 | 1.390 | 1.370 | 1.350 | 1.320 | 1.290 | 1.260 | 1.250 | 1.260 | 1.260 | |
| 63 | 1.780 | 1.850 | 1.910 | 1.950 | 1.980 | 1.990 | 1.940 | 1.890 | 1.820 | 1.730 | 1.640 | 1.540 | 1.440 | 1.360 | 1.290 | 1.240 | 1.210 | 1.170 | 1.130 | 1.090 | 1.060 | 1.060 | 1.090 | 1.140 | 1.180 | | |
| 65 | 2.540 | 2.640 | 2.730 | 2.790 | 2.840 | 2.850 | 2.830 | 2.780 | 2.700 | 2.590 | 2.460 | 2.300 | 2.140 | 1.970 | 1.820 | 1.680 | 1.570 | 1.470 | 1.380 | 1.290 | 1.220 | 1.160 | 1.120 | 1.090 | 1.050 | 0.980 | |
| 67 | 1.780 | 1.860 | 1.920 | 1.980 | 2.010 | 2.030 | 2.020 | 2.000 | 1.950 | 1.890 | 1.800 | 1.720 | 1.620 | 1.530 | 1.460 | 1.400 | 1.370 | 1.360 | 1.370 | 1.380 | 1.380 | 1.380 | 1.370 | 1.370 | 1.370 | | |
| 69 | 1.860 | 1.940 | 2.010 | 2.070 | 2.120 | 2.150 | 2.170 | 2.150 | 2.120 | 2.070 | 2.020 | 1.970 | 1.920 | 1.890 | 1.870 | 1.870 | 1.880 | 1.900 | 1.920 | 1.940 | 1.950 | 1.960 | 1.960 | 1.940 | 1.910 | | |
| 71 | 1.600 | 1.670 | 1.740 | 1.800 | 1.870 | 1.930 | 1.980 | 2.030 | 2.080 | 2.120 | 2.150 | 2.190 | 2.220 | 2.250 | 2.290 | 2.320 | 2.370 | 2.410 | 2.440 | 2.460 | 2.460 | 2.440 | 2.410 | 2.370 | 2.300 | 2.200 | |
| 73 | 1.930 | 2.000 | 2.060 | 2.110 | 2.150 | 2.160 | 2.170 | 2.150 | 2.120 | 2.070 | 2.020 | 1.950 | 1.890 | 1.830 | 1.780 | 1.750 | 1.730 | 1.740 | 1.750 | 1.760 | 1.770 | 1.780 | 1.790 | 1.800 | 1.800 | | |
| 75 | 1.830 | 1.920 | 2.020 | 2.120 | 2.220 | 2.310 | 2.400 | 2.480 | 2.540 | 2.600 | 2.630 | 2.660 | 2.660 | 2.660 | 2.640 | 2.610 | 2.570 | 2.520 | 2.450 | 2.370 | 2.270 | 2.170 | 2.070 | 1.990 | 1.920 | 1.840 | |
| 77 | 2.060 | 2.170 | 2.280 | 2.390 | 2.490 | 2.570 | 2.650 | 2.700 | 2.740 | 2.760 | 2.760 | 2.740 | 2.710 | 2.670 | 2.620 | 2.560 | 2.500 | 2.430 | 2.340 | 2.240 | 2.130 | 2.010 | 1.900 | 1.810 | 1.720 | 1.630 | |
| 79 | 1.840 | 1.930 | 2.030 | 2.130 | 2.220 | 2.310 | 2.400 | 2.470 | 2.540 | 2.590 | 2.630 | 2.660 | 2.680 | 2.700 | 2.700 | 2.710 | 2.710 | 2.710 | 2.710 | 2.690 | 2.670 | 2.630 | 2.580 | 2.530 | 2.470 | 2.390 | 2.280 |
| 81 | 2.670 | 2.820 | 2.950 | 3.070 | 3.160 | 3.230 | 3.270 | 3.240 | 3.170 | 3.060 | 2.920 | 2.770 | 2.600 | 2.430 | 2.260 | 2.110 | 1.970 | 1.830 | 1.700 | 1.570 | 1.450 | 1.350 | 1.250 | 1.170 | 1.080 | | |
| 83 | 1.770 | 1.870 | 1.960 | 2.050 | 2.130 | 2.190 | 2.240 | 2.270 | 2.290 | 2.290 | 2.280 | 2.250 | 2.210 | 2.170 | 2.120 | 2.080 | 2.040 | 2.000 | 1.960 | 1.920 | 1.870 | 1.830 | 1.800 | 1.770 | 1.760 | 1.730 | |
| 85 | 2.010 | 2.110 | 2.220 | 2.320 | 2.420 | 2.500 | 2.580 | 2.640 | 2.680 | 2.700 | 2.710 | 2.700 | 2.670 | 2.630 | 2.580 | 2.520 | 2.460 | 2.390 | 2.300 | 2.200 | 2.080 | 1.950 | 1.820 | 1.700 | 1.580 | 1.460 | |
| 87 | 2.010 | 2.130 | 2.250 | 2.360 | 2.450 | 2.530 | 2.590 | 2.630 | 2.640 | 2.590 | 2.530 | 2.460 | 2.370 | 2.270 | 2.170 | 2.070 | 1.960 | 1.850 | 1.740 | 1.610 | 1.490 | 1.380 | 1.280 | 1.180 | 1.080 | | |
| 89 | 1.370 | 1.440 | 1.520 | 1.600 | 1.680 | 1.770 | 1.850 | 1.940 | 2.020 | 2.110 | 2.190 | 2.270 | 2.360 | 2.450 | 2.530 | 2.620 | 2.710 | 2.780 | 2.840 | 2.870 | 2.870 | 2.830 | 2.750 | 2.630 | 2.460 | 2.260 | |
| 91 | 1.710 | 1.800 | 1.890 | 1.980 | 2.070 | 2.150 | 2.230 | 2.300 | 2.360 | 2.410 | 2.460 | 2.500 | 2.530 | 2.550 | 2.580 | 2.600 | 2.610 | 2.620 | 2.610 | 2.590 | 2.530 | 2.460 | 2.380 | 2.270</ | | | |

| ID | 8.824 | 8.689 | 8.554 | 8.420 | 8.285 | 8.151 | 8.016 | 7.881 | 7.747 | 7.612 | 7.478 | 7.343 | 7.209 | 7.074 | 6.940 | 6.805 | 6.670 | 6.535 | 6.401 | 6.266 | 6.132 | 5.998 | 5.863 | 5.729 | 5.594 | 5.459 | |
|-----|-------|-------|-------|-------|-------|-------|-------|-------|-------|-------|-------|-------|-------|-------|-------|-------|-------|-------|-------|-------|-------|-------|-------|-------|-------|-------|-------|
| 103 | 1.790 | 1.880 | 1.970 | 2.050 | 2.130 | 2.190 | 2.240 | 2.280 | 2.300 | 2.310 | 2.310 | 2.290 | 2.270 | 2.240 | 2.210 | 2.180 | 2.150 | 2.130 | 2.100 | 2.080 | 2.040 | 2.010 | 1.970 | 1.940 | 1.890 | 1.830 | |
| 105 | 1.700 | 1.780 | 1.850 | 1.930 | 2.000 | 2.050 | 2.100 | 2.140 | 2.160 | 2.170 | 2.170 | 2.160 | 2.140 | 2.120 | 2.100 | 2.080 | 2.070 | 2.060 | 2.050 | 2.040 | 2.020 | 1.990 | 1.970 | 1.950 | 1.930 | 1.890 | |
| 107 | 1.200 | 1.240 | 1.280 | 1.310 | 1.340 | 1.360 | 1.380 | 1.390 | 1.400 | 1.400 | 1.410 | 1.410 | 1.420 | 1.430 | 1.450 | 1.480 | 1.520 | 1.580 | 1.650 | 1.720 | 1.800 | 1.890 | 1.980 | 2.070 | 2.170 | 2.250 | |
| 109 | 1.190 | 1.240 | 1.290 | 1.330 | 1.370 | 1.400 | 1.420 | 1.430 | 1.440 | 1.450 | 1.450 | 1.450 | 1.450 | 1.470 | 1.490 | 1.520 | 1.570 | 1.650 | 1.740 | 1.850 | 1.980 | 2.130 | 2.290 | 2.450 | 2.630 | 2.800 | |
| 111 | 1.080 | 1.130 | 1.180 | 1.220 | 1.270 | 1.310 | 1.340 | 1.380 | 1.400 | 1.430 | 1.450 | 1.470 | 1.500 | 1.520 | 1.550 | 1.590 | 1.650 | 1.710 | 1.780 | 1.860 | 1.940 | 2.040 | 2.140 | 2.250 | 2.360 | 2.460 | |
| 113 | 1.090 | 1.140 | 1.190 | 1.230 | 1.260 | 1.290 | 1.310 | 1.330 | 1.330 | 1.330 | 1.330 | 1.330 | 1.320 | 1.320 | 1.320 | 1.330 | 1.340 | 1.370 | 1.410 | 1.460 | 1.520 | 1.590 | 1.670 | 1.760 | 1.870 | 1.990 | 2.100 |
| 115 | 1.540 | 1.600 | 1.660 | 1.710 | 1.750 | 1.770 | 1.780 | 1.780 | 1.760 | 1.740 | 1.700 | 1.660 | 1.620 | 1.580 | 1.540 | 1.520 | 1.500 | 1.510 | 1.530 | 1.550 | 1.580 | 1.630 | 1.680 | 1.740 | 1.800 | | |
| 117 | 1.390 | 1.460 | 1.530 | 1.590 | 1.640 | 1.670 | 1.690 | 1.700 | 1.700 | 1.680 | 1.650 | 1.610 | 1.570 | 1.520 | 1.490 | 1.460 | 1.440 | 1.440 | 1.450 | 1.470 | 1.500 | 1.550 | 1.600 | 1.670 | 1.730 | | |
| 119 | 1.690 | 1.790 | 1.880 | 1.950 | 2.010 | 2.040 | 2.060 | 2.060 | 2.030 | 1.980 | 1.920 | 1.850 | 1.770 | 1.690 | 1.620 | 1.560 | 1.520 | 1.490 | 1.470 | 1.460 | 1.450 | 1.460 | 1.470 | 1.500 | 1.530 | 1.560 | |
| 121 | 1.650 | 1.730 | 1.810 | 1.880 | 1.930 | 1.970 | 1.980 | 1.980 | 1.950 | 1.910 | 1.850 | 1.780 | 1.710 | 1.630 | 1.570 | 1.510 | 1.480 | 1.460 | 1.450 | 1.450 | 1.440 | 1.430 | 1.430 | 1.450 | 1.500 | | |
| 123 | 1.570 | 1.650 | 1.730 | 1.790 | 1.840 | 1.870 | 1.890 | 1.890 | 1.870 | 1.840 | 1.790 | 1.730 | 1.670 | 1.620 | 1.570 | 1.530 | 1.510 | 1.500 | 1.510 | 1.530 | 1.550 | 1.570 | 1.600 | 1.640 | 1.680 | | |
| 125 | 1.490 | 1.570 | 1.630 | 1.690 | 1.740 | 1.770 | 1.790 | 1.790 | 1.780 | 1.750 | 1.710 | 1.670 | 1.610 | 1.560 | 1.520 | 1.480 | 1.460 | 1.450 | 1.450 | 1.470 | 1.490 | 1.530 | 1.570 | 1.630 | 1.680 | | |
| 127 | 1.490 | 1.560 | 1.630 | 1.690 | 1.740 | 1.770 | 1.780 | 1.780 | 1.770 | 1.740 | 1.700 | 1.650 | 1.590 | 1.540 | 1.490 | 1.450 | 1.430 | 1.420 | 1.430 | 1.460 | 1.490 | 1.540 | 1.600 | 1.660 | | | |
| 129 | 1.810 | 1.900 | 1.990 | 2.070 | 2.150 | 2.210 | 2.250 | 2.280 | 2.300 | 2.290 | 2.280 | 2.240 | 2.210 | 2.160 | 2.120 | 2.080 | 2.050 | 2.020 | 1.990 | 1.950 | 1.910 | 1.850 | 1.800 | 1.750 | 1.690 | 1.630 | |
| 131 | 0.990 | 1.030 | 1.070 | 1.090 | 1.110 | 1.120 | 1.120 | 1.120 | 1.100 | 1.080 | 1.060 | 1.030 | 1.010 | 0.990 | 0.970 | 0.970 | 0.980 | 1.010 | 1.060 | 1.130 | 1.220 | 1.350 | 1.510 | 1.690 | 1.900 | 2.100 | |
| 133 | 1.240 | 1.290 | 1.340 | 1.390 | 1.440 | 1.490 | 1.540 | 1.580 | 1.630 | 1.670 | 1.720 | 1.770 | 1.830 | 1.890 | 1.970 | 2.060 | 2.160 | 2.280 | 2.410 | 2.550 | 2.700 | 2.840 | 2.990 | 3.110 | 3.200 | 3.230 | |
| 135 | 1.340 | 1.410 | 1.490 | 1.580 | 1.680 | 1.800 | 1.920 | 2.060 | 2.200 | 2.360 | 2.520 | 2.690 | 2.860 | 3.040 | 3.210 | 3.380 | 3.530 | 3.660 | 3.750 | 3.780 | 3.740 | 3.630 | 3.460 | 3.230 | 2.950 | 2.630 | |
| 137 | 1.310 | 1.360 | 1.410 | 1.470 | 1.530 | 1.590 | 1.660 | 1.740 | 1.830 | 1.920 | 2.030 | 2.140 | 2.270 | 2.410 | 2.560 | 2.730 | 2.900 | 3.090 | 3.280 | 3.450 | 3.590 | 3.670 | 3.730 | 3.760 | 3.760 | 3.700 | |
| 139 | 1.660 | 1.750 | 1.840 | 1.940 | 2.050 | 2.150 | 2.250 | 2.360 | 2.460 | 2.560 | 2.660 | 2.750 | 2.840 | 2.920 | 3.010 | 3.080 | 3.150 | 3.200 | 3.230 | 3.220 | 3.180 | 3.110 | 3.010 | 2.870 | 2.700 | 2.480 | |
| 141 | 1.610 | 1.700 | 1.800 | 1.900 | 2.000 | 2.110 | 2.210 | 2.320 | 2.420 | 2.520 | 2.620 | 2.710 | 2.800 | 2.890 | 2.970 | 3.050 | 3.110 | 3.160 | 3.180 | 3.170 | 3.130 | 3.050 | 2.940 | 2.800 | 2.620 | 2.400 | |
| 143 | 1.420 | 1.480 | 1.540 | 1.610 | 1.670 | 1.720 | 1.780 | 1.830 | 1.880 | 1.920 | 1.970 | 2.010 | 2.060 | 2.110 | 2.160 | 2.230 | 2.310 | 2.390 | 2.480 | 2.570 | 2.650 | 2.730 | 2.800 | 2.860 | 2.890 | 2.880 | |
| 145 | 0.720 | 0.740 | 0.760 | 0.780 | 0.780 | 0.790 | 0.780 | 0.780 | 0.760 | 0.740 | 0.720 | 0.700 | 0.690 | 0.670 | 0.660 | 0.660 | 0.670 | 0.710 | 0.760 | 0.850 | 0.970 | 1.140 | 1.360 | 1.640 | 1.970 | 2.350 | |
| 147 | 0.720 | 0.740 | 0.760 | 0.770 | 0.780 | 0.780 | 0.780 | 0.780 | 0.770 | 0.770 | 0.770 | 0.780 | 0.780 | 0.800 | 0.830 | 0.870 | 0.930 | 1.020 | 1.130 | 1.270 | 1.440 | 1.650 | 1.900 | 2.180 | 2.490 | | |
| 149 | 1.290 | 1.350 | 1.410 | 1.480 | 1.540 | 1.610 | 1.690 | 1.770 | 1.850 | 1.930 | 2.020 | 2.120 | 2.220 | 2.330 | 2.450 | 2.570 | 2.710 | 2.840 | 2.980 | 3.100 | 3.210 | 3.290 | 3.360 | 3.380 | 3.370 | 3.290 | |
| 151 | 1.330 | 1.400 | 1.470 | 1.550 | 1.630 | 1.710 | 1.800 | 1.900 | 2.000 | 2.110 | 2.220 | 2.330 | 2.450 | 2.570 | 2.680 | 2.810 | 2.930 | 3.040 | 3.130 | 3.200 | 3.250 | 3.280 | 3.300 | 3.270 | 3.170 | 3.000 | |
| 153 | 1.010 | 1.050 | 1.080 | 1.120 | 1.160 | 1.190 | 1.230 | 1.270 | 1.300 | 1.340 | 1.380 | 1.430 | 1.480 | 1.540 | 1.620 | 1.700 | 1.800 | 1.920 | 2.050 | 2.200 | 2.370 | 2.550 | 2.750 | 2.950 | 3.150 | 3.340 | |
| 155 | 1.340 | 1.410 | 1.470 | 1.530 | 1.590 | 1.650 | 1.710 | 1.760 | 1.810 | 1.860 | 1.910 | 1.970 | 2.030 | 2.090 | 2.160 | 2.240 | 2.330 | 2.430 | 2.530 | 2.630 | 2.730 | 2.820 | 2.910 | 2.980 | 3.030 | 3.040 | |
| 157 | 1.010 | 1.050 | 1.090 | 1.120 | 1.160 | 1.190 | 1.230 | 1.260 | 1.300 | 1.340 | 1.370 | 1.420 | 1.470 | 1.520 | 1.590 | 1.660 | 1.750 | 1.840 | 1.950 | 2.060 | 2.180 | 2.310 | 2.440 | 2.570 | 2.700 | 2.830 | |

P14

| | | | | | | | | | | | | | | | | | | | | | | | | | | |
|-----|-------|-------|-------|-------|-------|-------|-------|-------|-------|-------|-------|-------|-------|-------|-------|-------|-------|-------|-------|-------|-------|-------|-------|-------|-------|-------|
| 159 | 0.420 | 0.430 | 0.450 | 0.470 | 0.490 | 0.510 | 0.530 | 0.560 | 0.580 | 0.610 | 0.630 | 0.650 | 0.680 | 0.700 | 0.730 | 0.750 | 0.780 | 0.810 | 0.850 | 0.890 | 0.940 | 1.000 | 1.080 | 1.180 | 1.300 | 1.430 |
| 160 | 0.310 | 0.310 | 0.320 | 0.320 | 0.340 | 0.350 | 0.360 | 0.370 | 0.390 | 0.400 | 0.410 | 0.420 | 0.430 | 0.430 | 0.440 | 0.440 | 0.440 | 0.450 | 0.460 | 0.470 | 0.490 | 0.510 | 0.550 | 0.600 | 0.670 | 0.740 |
| 161 | 0.580 | 0.600 | 0.630 | 0.660 | 0.700 | 0.730 | 0.770 | 0.810 | 0.850 | 0.890 | 0.920 | 0.960 | 0.990 | 1.020 | 1.050 | 1.090 | 1.120 | 1.160 | 1.200 | 1.250 | 1.300 | 1.380 | 1.470 | 1.580 | 1.710 | 1.860 |
| 162 | 0.500 | 0.510 | 0.530 | 0.550 | 0.580 | 0.610 | 0.640 | 0.670 | 0.700 | 0.730 | 0.770 | 0.800 | 0.830 | 0.860 | 0.880 | 0.910 | 0.950 | 0.980 | 1.020 | 1.070 | 1.120 | 1.190 | 1.280 | 1.380 | 1.510 | 1.640 |
| 163 | 0.620 | 0.650 | 0.670 | 0.710 | 0.740 | 0.780 | 0.820 | 0.860 | 0.910 | 0.950 | 0.990 | 1.030 | 1.080 | 1.120 | 1.160 | 1.200 | 1.240 | 1.290 | 1.340 | 1.390 | 1.450 | 1.530 | 1.630 | 1.750 | 1.890 | 2.030 |
| 164 | 0.650 | 0.670 | 0.700 | 0.730 | 0.770 | 0.810 | 0.850 | 0.890 | 0.930 | 0.970 | 1.010 | 1.050 | 1.090 | 1.120 | 1.160 | 1.200 | 1.240 | 1.290 | 1.340 | 1.400 | 1.470 | 1.560 | 1.660 | 1.780 | 1.920 | 2.070 |
| 165 | 0.790 | 0.830 | 0.870 | 0.920 | 0.980 | 1.040 | 1.100 | 1.160 | 1.220 | 1.290 | 1.350 | 1.410 | 1.470 | 1.530 | 1.580 | 1.640 | 1.700 | 1.750 | 1.810 | 1.870 | 1.920 | 1.990 | 2.060 | 2.150 | 2.250 | 2.350 |
| 166 | 0.810 | 0.840 | 0.880 | 0.930 | 0.990 | 1.040 | 1.110 | 1.170 | 1.240 | 1.300 | 1.370 | 1.430 | 1.490 | 1.550 | 1.610 | 1.670 | 1.730 | 1.790 | 1.860 | 1.920 | 1.990 | 2.070 | 2.170 | 2.270 | 2.370 | 2.460 |
| 167 | 0.690 | 0.710 | 0.740 | 0.780 | 0.820 | 0.860 | 0.910 | 0.950 | 1.010 | 1.060 | 1.110 | | | | | | | | | | | | | | | |

| ID | 8.824 | 8.689 | 8.554 | 8.420 | 8.285 | 8.151 | 8.016 | 7.881 | 7.747 | 7.612 | 7.478 | 7.343 | 7.209 | 7.074 | 6.940 | 6.805 | 6.670 | 6.535 | 6.401 | 6.266 | 6.132 | 5.998 | 5.863 | 5.729 | 5.594 | 5.459 |
|---------|-------|-------|-------|-------|-------|-------|-------|-------|-------|-------|-------|-------|-------|-------|-------|-------|-------|-------|-------|-------|-------|-------|-------|-------|-------|-------|
| 174 | 0.700 | 0.730 | 0.750 | 0.780 | 0.810 | 0.840 | 0.870 | 0.900 | 0.920 | 0.950 | 0.970 | 0.990 | 1.020 | 1.040 | 1.060 | 1.080 | 1.110 | 1.150 | 1.210 | 1.280 | 1.380 | 1.500 | 1.670 | 1.890 | 2.140 | 2.420 |
| 175 (1) | 1.870 | 1.980 | 2.080 | 2.180 | 2.280 | 2.370 | 2.440 | 2.500 | 2.540 | 2.560 | 2.560 | 2.530 | 2.490 | 2.430 | 2.370 | 2.290 | 2.220 | 2.140 | 2.060 | 1.970 | 1.880 | 1.800 | 1.740 | 1.710 | 1.690 | 1.670 |
| 175 (2) | 1.760 | 1.870 | 2.010 | 2.150 | 2.300 | 2.460 | 2.620 | 2.770 | 2.900 | 3.020 | 3.120 | 3.190 | 3.240 | 3.260 | 3.260 | 3.220 | 3.160 | 3.060 | 2.930 | 2.770 | 2.590 | 2.390 | 2.200 | 2.030 | 1.870 | 1.700 |
| 176 | 1.780 | 1.880 | 2.000 | 2.120 | 2.260 | 2.390 | 2.520 | 2.650 | 2.760 | 2.860 | 2.940 | 3.000 | 3.040 | 3.060 | 3.060 | 3.030 | 2.980 | 2.900 | 2.790 | 2.650 | 2.490 | 2.320 | 2.160 | 2.000 | 1.840 | 1.660 |
| 177 | 1.550 | 1.640 | 1.730 | 1.820 | 1.910 | 1.990 | 2.060 | 2.120 | 2.160 | 2.180 | 2.180 | 2.160 | 2.120 | 2.080 | 2.020 | 1.960 | 1.900 | 1.840 | 1.780 | 1.730 | 1.670 | 1.630 | 1.610 | 1.620 | 1.660 | 1.720 |
| 178 | 1.630 | 1.720 | 1.820 | 1.920 | 2.030 | 2.130 | 2.230 | 2.310 | 2.380 | 2.420 | 2.450 | 2.450 | 2.430 | 2.400 | 2.350 | 2.300 | 2.240 | 2.170 | 2.100 | 2.020 | 1.940 | 1.870 | 1.820 | 1.790 | 1.770 | 1.760 |
| 179 | 2.130 | 2.250 | 2.380 | 2.510 | 2.630 | 2.740 | 2.840 | 2.910 | 2.960 | 2.980 | 2.980 | 2.950 | 2.890 | 2.810 | 2.720 | 2.620 | 2.500 | 2.380 | 2.250 | 2.110 | 1.980 | 1.860 | 1.760 | 1.670 | 1.580 | 1.470 |
| 180 | 1.620 | 1.710 | 1.800 | 1.890 | 1.980 | 2.070 | 2.140 | 2.200 | 2.240 | 2.260 | 2.270 | 2.250 | 2.220 | 2.170 | 2.120 | 2.060 | 1.990 | 1.930 | 1.860 | 1.800 | 1.740 | 1.700 | 1.750 | 1.810 | 1.890 | |
| 181 | 1.840 | 1.920 | 2.010 | 2.100 | 2.180 | 2.260 | 2.320 | 2.370 | 2.400 | 2.410 | 2.400 | 2.380 | 2.330 | 2.270 | 2.210 | 2.140 | 2.070 | 2.000 | 1.930 | 1.860 | 1.810 | 1.780 | 1.790 | 1.810 | 1.800 | |
| 182 | 1.780 | 1.860 | 1.940 | 2.020 | 2.100 | 2.160 | 2.210 | 2.240 | 2.260 | 2.250 | 2.210 | 2.160 | 2.100 | 2.030 | 1.950 | 1.890 | 1.830 | 1.770 | 1.720 | 1.670 | 1.630 | 1.580 | 1.550 | 1.530 | 1.550 | |
| 183 | 2.450 | 2.580 | 2.710 | 2.830 | 2.930 | 3.020 | 3.090 | 3.120 | 3.130 | 3.090 | 3.030 | 2.940 | 2.820 | 2.690 | 2.540 | 2.400 | 2.260 | 2.130 | 2.000 | 1.880 | 1.770 | 1.670 | 1.600 | 1.550 | 1.520 | 1.500 |
| 184 | 1.560 | 1.650 | 1.750 | 1.850 | 1.950 | 2.060 | 2.150 | 2.230 | 2.310 | 2.360 | 2.390 | 2.410 | 2.420 | 2.400 | 2.380 | 2.340 | 2.300 | 2.240 | 2.180 | 2.120 | 2.050 | 2.000 | 1.970 | 1.960 | 1.950 | 1.940 |
| 185 | 1.400 | 1.480 | 1.560 | 1.660 | 1.750 | 1.840 | 1.930 | 2.020 | 2.090 | 2.160 | 2.200 | 2.240 | 2.270 | 2.280 | 2.290 | 2.290 | 2.280 | 2.270 | 2.250 | 2.220 | 2.200 | 2.190 | 2.170 | 2.140 | | |
| 186 | 1.420 | 1.500 | 1.590 | 1.680 | 1.780 | 1.870 | 1.970 | 2.060 | 2.140 | 2.220 | 2.280 | 2.330 | 2.370 | 2.390 | 2.410 | 2.430 | 2.430 | 2.420 | 2.410 | 2.380 | 2.340 | 2.300 | 2.270 | 2.250 | 2.220 | 2.180 |
| 187 | 1.670 | 1.760 | 1.860 | 1.960 | 2.060 | 2.160 | 2.250 | 2.330 | 2.400 | 2.460 | 2.500 | 2.520 | 2.530 | 2.520 | 2.510 | 2.490 | 2.460 | 2.420 | 2.380 | 2.320 | 2.260 | 2.210 | 2.160 | 2.130 | 2.090 | 2.050 |
| 188 | 1.460 | 1.550 | 1.640 | 1.740 | 1.840 | 1.950 | 2.060 | 2.160 | 2.270 | 2.360 | 2.440 | 2.520 | 2.580 | 2.640 | 2.680 | 2.710 | 2.730 | 2.740 | 2.720 | 2.690 | 2.630 | 2.560 | 2.490 | 2.430 | 2.360 | 2.300 |
| 189 | 1.880 | 1.970 | 2.060 | 2.150 | 2.230 | 2.310 | 2.370 | 2.420 | 2.460 | 2.470 | 2.470 | 2.450 | 2.420 | 2.390 | 2.350 | 2.310 | 2.270 | 2.230 | 2.180 | 2.120 | 2.040 | 1.950 | 1.870 | 1.800 | 1.740 | 1.690 |
| 190 | 1.670 | 1.750 | 1.840 | 1.920 | 2.010 | 2.080 | 2.150 | 2.210 | 2.250 | 2.270 | 2.280 | 2.270 | 2.250 | 2.220 | 2.200 | 2.170 | 2.150 | 2.130 | 2.100 | 2.080 | 2.040 | 2.000 | 1.970 | 1.940 | 1.910 | 1.870 |
| 191 | 1.730 | 1.850 | 1.980 | 2.130 | 2.280 | 2.430 | 2.580 | 2.730 | 2.860 | 2.970 | 3.060 | 3.130 | 3.180 | 3.210 | 3.200 | 3.180 | 3.130 | 3.050 | 2.940 | 2.800 | 2.640 | 2.480 | 2.330 | 2.190 | 2.040 | 1.880 |
| 192 | 1.800 | 1.900 | 2.000 | 2.110 | 2.220 | 2.320 | 2.400 | 2.480 | 2.540 | 2.580 | 2.600 | 2.600 | 2.590 | 2.560 | 2.520 | 2.480 | 2.430 | 2.380 | 2.320 | 2.240 | 2.160 | 2.080 | 2.000 | 1.920 | 1.830 | 1.740 |
| 193 | 1.650 | 1.750 | 1.880 | 2.010 | 2.150 | 2.300 | 2.450 | 2.590 | 2.730 | 2.850 | 2.950 | 3.040 | 3.110 | 3.150 | 3.170 | 3.170 | 3.140 | 3.070 | 2.970 | 2.840 | 2.680 | 2.510 | 2.340 | 2.180 | 2.040 | 1.900 |
| 194 | 3.150 | 3.370 | 3.560 | 3.710 | 3.820 | 3.870 | 3.860 | 3.800 | 3.670 | 3.500 | 3.270 | 3.020 | 2.740 | 2.460 | 2.190 | 1.940 | 1.720 | 1.540 | 1.400 | 1.290 | 1.190 | 1.090 | 1.010 | 0.950 | 0.900 | 0.860 |
| 195 | 1.470 | 1.570 | 1.670 | 1.790 | 1.900 | 2.020 | 2.140 | 2.250 | 2.360 | 2.460 | 2.540 | 2.610 | 2.670 | 2.720 | 2.750 | 2.770 | 2.770 | 2.750 | 2.720 | 2.660 | 2.590 | 2.510 | 2.430 | 2.350 | 2.260 | 2.170 |
| 196 | 0.900 | 0.940 | 0.990 | 1.040 | 1.100 | 1.150 | 1.210 | 1.270 | 1.320 | 1.370 | 1.420 | 1.460 | 1.500 | 1.540 | 1.580 | 1.620 | 1.660 | 1.710 | 1.760 | 1.830 | 1.910 | 2.020 | 2.160 | 2.330 | 2.510 | 2.690 |
| 197 | 0.710 | 0.730 | 0.770 | 0.820 | 0.870 | 0.930 | 0.990 | 1.070 | 1.150 | 1.230 | 1.310 | 1.400 | 1.490 | 1.580 | 1.670 | 1.770 | 1.870 | 1.980 | 2.100 | 2.230 | 2.370 | 2.530 | 2.720 | 2.930 | 3.170 | 3.400 |
| 198 | 0.940 | 0.990 | 1.040 | 1.090 | 1.150 | 1.210 | 1.260 | 1.310 | 1.360 | 1.400 | 1.430 | 1.460 | 1.480 | 1.490 | 1.500 | 1.510 | 1.520 | 1.530 | 1.540 | 1.560 | 1.590 | 1.640 | 1.700 | 1.780 | 1.860 | |
| 199 | 2.090 | 2.220 | 2.340 | 2.470 | 2.600 | 2.720 | 2.830 | 2.910 | 2.980 | 3.020 | 3.030 | 3.010 | 2.970 | 2.910 | 2.830 | 2.740 | 2.640 | 2.520 | 2.390 | 2.250 | 2.110 | 1.980 | 1.850 | 1.740 | 1.610 | 1.460 |
| 200 | 2.010 | 2.130 | 2.260 | 2.390 | 2.520 | 2.650 | 2.760 | 2.850 | 2.920 | 2.970 | 3.000 | 3.000 | 2.970 | 2.920 | 2.860 | 2.780 | 2.680 | 2.570 | 2.440 | 2.300 | 2.160 | 2.030 | 1.910 | 1.810 | 1.720 | 1.610 |
| 201 | 1.810 | 1.940 | 2.080 | 2.230 | 2.380 | 2.530 | 2.670 | 2.790 | 2.900 | 2.990 | 3.050 | 3.090 | 3.100 | 3.080 | 3.040 | 2.970 | 2.880 | 2.770 | 2.640 | 2.500 | 2.350 | 2.200 | 2.080 | 1.990 | 1.900 | 1.820 |
| 202 | 1.120 | 1.180 | 1.250 | 1.330 | 1.410 | 1.480 | 1.560 | 1.620 | 1.680 | 1.720 | 1.750 | 1.770 | 1.770 | 1.770 | 1.750 | 1.730 | 1.700 | 1.670 | 1.640 | 1.600 | 1.570 | 1.560 | 1.580 | 1.620 | 1.670 | 1.720 |
| 203 | 0.990 | 1.040 | 1.100 | 1.160 | 1.220 | 1.280 | 1.340 | 1.400 | 1.450 | 1.490 | 1.530 | 1.550 | 1.570 | 1.590 | 1.600 | 1.610 | 1.620 | 1.630 | 1.640 | 1.650 | 1.670 | 1.700 | 1.750 | 1.800 | 1.840 | |
| 204 | 0.620 | 0.650 | 0.690 | 0.730 | 0.770 | 0.810 | 0.850 | 0.890 | 0.930 | 0.970 | 0.990 | 1.020 | 1.040 | 1.050 | 1.070 | 1.070 | 1.080 | 1.080 | 1.080 | 1.080 | 1.090 | 1.110 | 1.150 | 1.210 | 1.270 | |
| 205 | 0.500 | 0.510 | 0.530 | 0.540 | 0.570 | 0.590 | 0.620 | 0.640 | 0.680 | 0.710 | 0.740 | 0.770 | 0.810 | 0.840 | 0.890 | 0.930 | 0.980 | 1.040 | 1.120 | 1.200 | 1.300 | 1.430 | 1.580 | 1.760 | 1.960 | 2.180 |
| 206 | 0.510 | 0.530 | 0.550 | 0.580 | 0.600 | 0.630 | 0.660 | 0.690 | 0.720 | 0.740 | 0.770 | 0.790 | 0.810 | 0.840 | 0.850 | 0.870 | 0.890 | 0.910 | 0.940 | 0.970 | 1.010 | 1.070 | 1.140 | 1.250 | 1.370 | 1.520 |
| 207 | 0.310 | 0.310 | 0.320 | 0.330 | 0.340 | 0.350 | 0.360 | 0.380 | 0.390 | 0.400 | 0.410 | 0.430 | 0.440 | 0.450 | 0.450 | 0.460 | 0.470 | 0.480 | 0.490 | 0.500 | 0.520 | 0.540 | 0.580 | 0.630 | 0.710 | 0.800 |
| 208 | 0.710 | 0.740 | 0.780 | 0.830 | 0.870 | 0.920 | 0.970 | 1.010 | 1.060 | 1.090 | 1.120 | 1.140 | 1.160 | 1.170 | 1.180 | 1.190 | 1.190 | 1.190 | 1.190 | 1.190 | 1.190 | 1.180 | 1.190 | 1.210 | 1.240 | 1.280 |
| 209 | 0.600 | 0.620 | 0.650 | 0.690 | 0.720 | 0.760 | 0.800 | 0.830 | 0.870 | 0.900 | 0.930 | 0.950 | 0.970 | 0.990 | 1.010 | 1.020 | 1.030 | 1.040 | 1.050 | 1.060 | 1.060 | 1.070 | 1.090 | 1.120 | 1.160 | 1.210 |
| 210 | 0.760 | 0.790 | 0.830 | 0.880 | 0.920 | 0.970 | 1.020 | 1.060 | 1.110 | 1.140 | 1.180 | 1.210 | 1.230 | 1.250 | 1.270 | 1.280 | 1.300 | 1.320 | 1.330 | 1.350 | 1.370 | 1.390 | 1.430 | 1.470 | 1.510 | 1.530 |
| 211 | 0.660 | 0.690 | 0.725 | 0.765 | 0.805 | 0.850 | 0.895 | 0.930 | 0.970 | 1.000 | 1.030 | 1.055 | 1.070 | 1.085 | 1.09 | | | | | | | | | | | |

| ID | 8.824 | 8.689 | 8.554 | 8.420 | 8.285 | 8.151 | 8.016 | 7.881 | 7.747 | 7.612 | 7.478 | 7.343 | 7.209 | 7.074 | 6.940 | 6.805 | 6.670 | 6.535 | 6.401 | 6.266 | 6.132 | 5.998 | 5.863 | 5.729 | 5.594 | 5.459 |
|-----|-------|-------|-------|-------|-------|-------|-------|-------|-------|-------|-------|-------|-------|-------|-------|-------|-------|-------|-------|-------|-------|-------|-------|-------|-------|-------|
| | 218 | 0.380 | 0.380 | 0.400 | 0.410 | 0.430 | 0.440 | 0.460 | 0.480 | 0.490 | 0.510 | 0.520 | 0.530 | 0.540 | 0.550 | 0.560 | 0.560 | 0.570 | 0.570 | 0.570 | 0.580 | 0.590 | 0.610 | 0.640 | 0.690 | 0.770 |
| 219 | 0.360 | 0.360 | 0.380 | 0.390 | 0.400 | 0.420 | 0.440 | 0.450 | 0.470 | 0.490 | 0.510 | 0.520 | 0.540 | 0.550 | 0.570 | 0.580 | 0.590 | 0.600 | 0.620 | 0.640 | 0.660 | 0.680 | 0.730 | 0.790 | 0.870 | 0.980 |
| 220 | 0.290 | 0.290 | 0.290 | 0.300 | 0.310 | 0.310 | 0.320 | 0.330 | 0.340 | 0.350 | 0.350 | 0.360 | 0.370 | 0.370 | 0.380 | 0.380 | 0.390 | 0.400 | 0.410 | 0.420 | 0.440 | 0.470 | 0.520 | 0.580 | 0.670 | 0.770 |
| 221 | 0.510 | 0.520 | 0.540 | 0.560 | 0.590 | 0.620 | 0.650 | 0.680 | 0.710 | 0.740 | 0.770 | 0.800 | 0.830 | 0.860 | 0.880 | 0.910 | 0.940 | 0.970 | 1.000 | 1.040 | 1.080 | 1.130 | 1.200 | 1.280 | 1.390 | 1.500 |
| 222 | 0.410 | 0.420 | 0.430 | 0.450 | 0.460 | 0.480 | 0.500 | 0.520 | 0.550 | 0.570 | 0.590 | 0.610 | 0.640 | 0.660 | 0.690 | 0.710 | 0.740 | 0.780 | 0.820 | 0.870 | 0.940 | 1.020 | 1.130 | 1.280 | 1.450 | 1.660 |
| 223 | 0.510 | 0.520 | 0.530 | 0.550 | 0.560 | 0.580 | 0.610 | 0.630 | 0.660 | 0.680 | 0.710 | 0.740 | 0.770 | 0.810 | 0.840 | 0.880 | 0.930 | 0.990 | 1.070 | 1.160 | 1.280 | 1.440 | 1.640 | 1.890 | 2.200 | 2.570 |
| 224 | 0.520 | 0.530 | 0.550 | 0.570 | 0.590 | 0.620 | 0.650 | 0.680 | 0.710 | 0.750 | 0.790 | 0.830 | 0.880 | 0.930 | 0.980 | 1.040 | 1.100 | 1.180 | 1.260 | 1.360 | 1.480 | 1.620 | 1.790 | 2.000 | 2.230 | 2.490 |
| 225 | 0.510 | 0.530 | 0.550 | 0.570 | 0.600 | 0.630 | 0.660 | 0.700 | 0.740 | 0.790 | 0.830 | 0.880 | 0.930 | 0.990 | 1.050 | 1.110 | 1.180 | 1.260 | 1.350 | 1.440 | 1.550 | 1.680 | 1.820 | 1.990 | 2.180 | 2.380 |
| 226 | 0.460 | 0.470 | 0.480 | 0.500 | 0.520 | 0.550 | 0.570 | 0.600 | 0.630 | 0.660 | 0.690 | 0.710 | 0.740 | 0.770 | 0.810 | 0.840 | 0.880 | 0.920 | 0.970 | 1.030 | 1.100 | 1.190 | 1.300 | 1.430 | 1.570 | 1.740 |
| 227 | 0.600 | 0.620 | 0.640 | 0.670 | 0.700 | 0.740 | 0.780 | 0.830 | 0.870 | 0.920 | 0.970 | 1.020 | 1.080 | 1.130 | 1.190 | 1.260 | 1.330 | 1.410 | 1.500 | 1.600 | 1.710 | 1.840 | 1.990 | 2.160 | 2.360 | 2.560 |
| 228 | 0.590 | 0.610 | 0.630 | 0.660 | 0.690 | 0.720 | 0.760 | 0.800 | 0.840 | 0.880 | 0.930 | 0.980 | 1.030 | 1.090 | 1.150 | 1.210 | 1.280 | 1.370 | 1.460 | 1.560 | 1.690 | 1.830 | 1.990 | 2.180 | 2.390 | 2.620 |
| 229 | 0.750 | 0.780 | 0.820 | 0.870 | 0.920 | 0.970 | 1.030 | 1.090 | 1.160 | 1.220 | 1.280 | 1.340 | 1.410 | 1.470 | 1.530 | 1.600 | 1.670 | 1.740 | 1.820 | 1.900 | 1.990 | 2.090 | 2.210 | 2.340 | 2.490 | 2.640 |
| 230 | 0.770 | 0.810 | 0.850 | 0.890 | 0.940 | 1.000 | 1.050 | 1.110 | 1.180 | 1.240 | 1.300 | 1.370 | 1.430 | 1.500 | 1.570 | 1.640 | 1.720 | 1.800 | 1.900 | 2.010 | 2.130 | 2.270 | 2.430 | 2.610 | 2.810 | 2.990 |
| 231 | 0.600 | 0.620 | 0.650 | 0.680 | 0.720 | 0.760 | 0.800 | 0.840 | 0.890 | 0.940 | 0.990 | 1.040 | 1.100 | 1.150 | 1.210 | 1.270 | 1.340 | 1.410 | 1.500 | 1.590 | 1.700 | 1.820 | 1.970 | 2.140 | 2.330 | 2.530 |
| 232 | 0.410 | 0.420 | 0.430 | 0.450 | 0.470 | 0.490 | 0.520 | 0.550 | 0.580 | 0.610 | 0.650 | 0.690 | 0.730 | 0.770 | 0.810 | 0.860 | 0.920 | 0.980 | 1.060 | 1.140 | 1.250 | 1.380 | 1.530 | 1.710 | 1.920 | 2.150 |
| 233 | 0.490 | 0.500 | 0.520 | 0.540 | 0.560 | 0.590 | 0.620 | 0.650 | 0.680 | 0.710 | 0.750 | 0.790 | 0.820 | 0.860 | 0.910 | 0.960 | 1.010 | 1.080 | 1.150 | 1.240 | 1.350 | 1.480 | 1.640 | 1.830 | 2.040 | 2.280 |
| 234 | 0.590 | 0.610 | 0.640 | 0.670 | 0.700 | 0.740 | 0.780 | 0.830 | 0.880 | 0.920 | 0.970 | 1.020 | 1.070 | 1.120 | 1.170 | 1.230 | 1.290 | 1.360 | 1.440 | 1.520 | 1.630 | 1.750 | 1.890 | 2.050 | 2.230 | 2.420 |
| 235 | 0.500 | 0.510 | 0.530 | 0.550 | 0.570 | 0.590 | 0.620 | 0.650 | 0.680 | 0.720 | 0.750 | 0.790 | 0.830 | 0.870 | 0.910 | 0.960 | 1.020 | 1.090 | 1.170 | 1.270 | 1.390 | 1.530 | 1.700 | 1.900 | 2.120 | 2.370 |
| 236 | 0.620 | 0.640 | 0.670 | 0.690 | 0.730 | 0.760 | 0.800 | 0.840 | 0.880 | 0.920 | 0.960 | 1.010 | 1.050 | 1.100 | 1.150 | 1.210 | 1.280 | 1.360 | 1.450 | 1.550 | 1.680 | 1.830 | 2.020 | 2.230 | 2.460 | 2.690 |
| 237 | 0.520 | 0.530 | 0.550 | 0.570 | 0.600 | 0.620 | 0.660 | 0.690 | 0.730 | 0.770 | 0.810 | 0.850 | 0.890 | 0.940 | 0.990 | 1.050 | 1.120 | 1.200 | 1.290 | 1.400 | 1.530 | 1.680 | 1.870 | 2.080 | 2.310 | 2.550 |
| 238 | 0.500 | 0.510 | 0.530 | 0.550 | 0.570 | 0.600 | 0.620 | 0.650 | 0.680 | 0.710 | 0.740 | 0.780 | 0.810 | 0.840 | 0.880 | 0.920 | 0.970 | 1.030 | 1.100 | 1.180 | 1.280 | 1.400 | 1.550 | 1.730 | 1.930 | 2.140 |
| 239 | 0.470 | 0.480 | 0.500 | 0.520 | 0.540 | 0.560 | 0.590 | 0.610 | 0.640 | 0.670 | 0.700 | 0.730 | 0.760 | 0.790 | 0.830 | 0.860 | 0.910 | 0.960 | 1.010 | 1.080 | 1.160 | 1.260 | 1.390 | 1.530 | 1.710 | 1.900 |
| 240 | 0.660 | 0.690 | 0.720 | 0.760 | 0.810 | 0.860 | 0.910 | 0.970 | 1.020 | 1.070 | 1.120 | 1.170 | 1.220 | 1.270 | 1.310 | 1.350 | 1.390 | 1.440 | 1.480 | 1.530 | 1.590 | 1.660 | 1.750 | 1.860 | 2.000 | 2.140 |
| 241 | 1.810 | 1.880 | 1.970 | 2.050 | 2.140 | 2.220 | 2.300 | 2.370 | 2.430 | 2.490 | 2.520 | 2.550 | 2.570 | 2.580 | 2.590 | 2.590 | 2.580 | 2.570 | 2.530 | 2.460 | 2.360 | 2.240 | 2.110 | 1.980 | 1.870 | 1.770 |
| 242 | 1.240 | 1.310 | 1.390 | 1.470 | 1.560 | 1.660 | 1.750 | 1.850 | 1.940 | 2.020 | 2.100 | 2.170 | 2.230 | 2.280 | 2.330 | 2.370 | 2.400 | 2.430 | 2.450 | 2.450 | 2.460 | 2.480 | 2.510 | 2.540 | 2.560 | |
| 243 | 0.940 | 0.990 | 1.050 | 1.110 | 1.190 | 1.260 | 1.340 | 1.410 | 1.490 | 1.560 | 1.630 | 1.690 | 1.750 | 1.810 | 1.860 | 1.910 | 1.960 | 2.010 | 2.050 | 2.080 | 2.120 | 2.160 | 2.200 | 2.250 | 2.340 | |
| 244 | 0.920 | 0.970 | 1.030 | 1.090 | 1.150 | 1.220 | 1.290 | 1.350 | 1.420 | 1.480 | 1.540 | 1.590 | 1.630 | 1.680 | 1.710 | 1.750 | 1.780 | 1.820 | 1.850 | 1.890 | 1.930 | 1.990 | 2.060 | 2.160 | 2.250 | 2.350 |
| 245 | 0.990 | 1.040 | 1.100 | 1.170 | 1.240 | 1.310 | 1.390 | 1.470 | 1.550 | 1.620 | 1.690 | 1.760 | 1.830 | 1.890 | 1.940 | 2.000 | 2.050 | 2.110 | 2.150 | 2.190 | 2.230 | 2.280 | 2.330 | 2.390 | 2.450 | 2.480 |
| 246 | 1.060 | 1.130 | 1.210 | 1.300 | 1.390 | 1.490 | 1.590 | 1.700 | 1.800 | 1.900 | 2.000 | 2.090 | 2.170 | 2.260 | 2.330 | 2.390 | 2.450 | 2.500 | 2.540 | 2.570 | 2.590 | 2.610 | 2.630 | 2.650 | 2.660 | 2.650 |
| 247 | 1.050 | 1.110 | 1.180 | 1.250 | 1.330 | 1.420 | 1.500 | 1.590 | 1.670 | 1.750 | 1.820 | 1.890 | 1.950 | 2.000 | 2.050 | 2.090 | 2.130 | 2.160 | 2.180 | 2.190 | 2.200 | 2.220 | 2.250 | 2.290 | 2.310 | 2.320 |
| 248 | 0.980 | 1.030 | 1.090 | 1.160 | 1.230 | 1.300 | 1.380 | 1.450 | 1.530 | 1.590 | 1.650 | 1.710 | 1.760 | 1.810 | 1.850 | 1.890 | 1.920 | 1.960 | 2.020 | 2.050 | 2.080 | 2.130 | 2.180 | 2.240 | 2.280 | |
| 249 | 0.940 | 0.990 | 1.040 | 1.100 | 1.160 | 1.220 | 1.290 | 1.360 | 1.420 | 1.480 | 1.540 | 1.600 | 1.650 | 1.700 | 1.750 | 1.790 | 1.840 | 1.880 | 1.920 | 1.960 | 2.000 | 2.040 | 2.100 | 2.170 | 2.250 | 2.330 |
| 250 | 0.860 | 0.900 | 0.950 | 1.010 | 1.070 | 1.140 | 1.200 | 1.270 | 1.340 | 1.410 | 1.480 | 1.540 | 1.600 | 1.660 | 1.720 | 1.770 | 1.830 | 1.890 | 1.940 | 1.990 | 2.040 | 2.100 | 2.170 | 2.260 | 2.340 | 2.400 |
| 251 | 1.000 | 1.060 | 1.130 | 1.210 | 1.290 | 1.380 | 1.480 | 1.580 | 1.670 | 1.770 | 1.860 | 1.950 | 2.030 | 2.110 | 2.180 | 2.240 | 2.300 | 2.350 | 2.400 | 2.430 | 2.460 | 2.480 | 2.520 | 2.570 | 2.630 | 2.660 |
| 252 | 1.080 | 1.140 | 1.220 | 1.300 | 1.380 | 1.470 | 1.560 | 1.650 | 1.730 | 1.810 | 1.890 | 1.950 | 2.010 | 2.070 | 2.110 | 2.150 | 2.190 | 2.210 | 2.240 | 2.260 | 2.270 | 2.300 | 2.330 | 2.370 | 2.420 | 2.440 |
| 253 | 0.820 | 0.850 | 0.900 | 0.950 | 1.000 | 1.060 | 1.120 | 1.180 | 1.240 | 1.300 | 1.360 | 1.410 | 1.460 | 1.510 | 1.550 | 1.590 | 1.630 | 1.670 | 1.710 | 1.740 | 1.780 | 1.830 | 1.900 | 1.990 | 2.110 | 2.220 |
| 254 | 0.830 | 0.870 | 0.910 | 0.970 | 1.020 | 1.080 | 1.140 | 1.200 | 1.260 | 1.320 | 1.380 | 1.430 | 1.480 | 1.530 | 1.580 | 1.620 | 1.670 | 1.720 | 1.760 | 1.810 | 1.870 | 1.930 | 2.000 | 2.080 | 2.170 | 2.240 |
| 255 | 0.810 | 0.850 | 0.900 | 0.950 | 1.010 | 1.070 | 1.130 | 1.200 | | | | | | | | | | | | | | | | | | |

| ID | 8.824 | 8.689 | 8.554 | 8.420 | 8.285 | 8.151 | 8.016 | 7.881 | 7.747 | 7.612 | 7.478 | 7.343 | 7.209 | 7.074 | 6.940 | 6.805 | 6.670 | 6.535 | 6.401 | 6.266 | 6.132 | 5.998 | 5.863 | 5.729 | 5.594 | 5.459 |
|-----|-------|-------|-------|-------|-------|-------|-------|-------|-------|-------|-------|-------|-------|-------|-------|-------|-------|-------|-------|-------|-------|-------|-------|-------|-------|-------|
| 263 | 0.780 | 0.820 | 0.870 | 0.920 | 0.980 | 1.050 | 1.130 | 1.210 | 1.300 | 1.390 | 1.480 | 1.580 | 1.670 | 1.770 | 1.870 | 1.970 | 2.070 | 2.160 | 2.250 | 2.330 | 2.410 | 2.470 | 2.530 | 2.590 | 2.640 | 2.680 |
| 264 | 0.660 | 0.690 | 0.730 | 0.770 | 0.820 | 0.880 | 0.950 | 1.020 | 1.100 | 1.180 | 1.260 | 1.350 | 1.450 | 1.540 | 1.640 | 1.750 | 1.850 | 1.970 | 2.080 | 2.190 | 2.310 | 2.420 | 2.540 | 2.670 | 2.780 | 2.880 |
| 265 | 0.720 | 0.750 | 0.790 | 0.830 | 0.880 | 0.940 | 1.000 | 1.060 | 1.130 | 1.200 | 1.280 | 1.360 | 1.440 | 1.520 | 1.610 | 1.700 | 1.800 | 1.910 | 2.010 | 2.130 | 2.240 | 2.360 | 2.490 | 2.620 | 2.760 | 2.890 |
| 266 | 2.670 | 2.800 | 2.920 | 3.000 | 3.040 | 3.050 | 3.020 | 2.950 | 2.850 | 2.720 | 2.570 | 2.410 | 2.240 | 2.080 | 1.930 | 1.810 | 1.720 | 1.660 | 1.620 | 1.580 | 1.550 | 1.530 | 1.520 | 1.530 | 1.540 | 1.540 |
| 267 | 0.530 | 0.540 | 0.560 | 0.580 | 0.610 | 0.640 | 0.670 | 0.710 | 0.750 | 0.790 | 0.820 | 0.860 | 0.900 | 0.940 | 0.990 | 1.030 | 1.080 | 1.140 | 1.200 | 1.270 | 1.340 | 1.420 | 1.520 | 1.620 | 1.730 | 1.850 |
| 268 | 0.690 | 0.710 | 0.740 | 0.780 | 0.820 | 0.860 | 0.920 | 0.970 | 1.030 | 1.090 | 1.160 | 1.230 | 1.300 | 1.380 | 1.460 | 1.540 | 1.640 | 1.740 | 1.850 | 1.970 | 2.090 | 2.220 | 2.360 | 2.510 | 2.650 | 2.770 |
| 269 | 0.740 | 0.760 | 0.790 | 0.820 | 0.850 | 0.890 | 0.930 | 0.970 | 1.010 | 1.060 | 1.110 | 1.160 | 1.210 | 1.270 | 1.340 | 1.410 | 1.500 | 1.600 | 1.710 | 1.830 | 1.970 | 2.120 | 2.290 | 2.460 | 2.640 | 2.800 |
| 270 | 1.170 | 1.200 | 1.230 | 1.260 | 1.280 | 1.300 | 1.310 | 1.310 | 1.310 | 1.310 | 1.310 | 1.310 | 1.320 | 1.340 | 1.380 | 1.440 | 1.520 | 1.620 | 1.730 | 1.840 | 1.970 | 2.110 | 2.260 | 2.400 | 2.540 | |
| 271 | 1.170 | 1.220 | 1.280 | 1.340 | 1.400 | 1.460 | 1.510 | 1.560 | 1.600 | 1.640 | 1.680 | 1.700 | 1.730 | 1.760 | 1.790 | 1.820 | 1.870 | 1.930 | 2.010 | 2.090 | 2.190 | 2.300 | 2.420 | 2.540 | 2.630 | 2.700 |
| 272 | 1.280 | 1.340 | 1.410 | 1.470 | 1.540 | 1.600 | 1.650 | 1.700 | 1.740 | 1.760 | 1.770 | 1.780 | 1.770 | 1.770 | 1.760 | 1.750 | 1.760 | 1.770 | 1.790 | 1.830 | 1.880 | 1.950 | 2.040 | 2.150 | 2.270 | 2.360 |
| 273 | 2.930 | 3.070 | 3.180 | 3.240 | 3.260 | 3.240 | 3.160 | 3.030 | 2.870 | 2.660 | 2.430 | 2.190 | 1.940 | 1.710 | 1.510 | 1.360 | 1.250 | 1.200 | 1.180 | 1.180 | 1.200 | 1.240 | 1.310 | 1.380 | 1.460 | 1.500 |
| 274 | 1.600 | 1.690 | 1.770 | 1.860 | 1.940 | 2.020 | 2.080 | 2.130 | 2.160 | 2.170 | 2.160 | 2.140 | 2.100 | 2.060 | 2.010 | 1.960 | 1.920 | 1.890 | 1.870 | 1.860 | 1.890 | 1.940 | 2.020 | 2.100 | 2.160 | |
| 275 | 1.660 | 1.740 | 1.820 | 1.910 | 1.980 | 2.050 | 2.100 | 2.140 | 2.160 | 2.160 | 2.140 | 2.110 | 2.060 | 2.000 | 1.940 | 1.880 | 1.830 | 1.780 | 1.750 | 1.740 | 1.770 | 1.830 | 1.910 | 1.990 | 2.050 | |
| 276 | 1.570 | 1.650 | 1.740 | 1.820 | 1.910 | 1.980 | 2.040 | 2.090 | 2.120 | 2.130 | 2.120 | 2.100 | 2.060 | 2.010 | 1.960 | 1.910 | 1.870 | 1.830 | 1.810 | 1.790 | 1.790 | 1.820 | 1.870 | 1.930 | 1.990 | 2.040 |
| 277 | 1.610 | 1.690 | 1.770 | 1.860 | 1.940 | 2.010 | 2.080 | 2.130 | 2.160 | 2.170 | 2.170 | 2.140 | 2.110 | 2.060 | 2.010 | 1.950 | 1.900 | 1.860 | 1.830 | 1.800 | 1.790 | 1.810 | 1.850 | 1.910 | 1.970 | |
| 278 | 1.690 | 1.770 | 1.860 | 1.950 | 2.030 | 2.100 | 2.160 | 2.210 | 2.230 | 2.230 | 2.210 | 2.180 | 2.130 | 2.070 | 2.000 | 1.940 | 1.890 | 1.840 | 1.810 | 1.790 | 1.790 | 1.800 | 1.830 | 1.860 | 1.900 | 1.930 |
| 279 | 1.720 | 1.810 | 1.900 | 1.990 | 2.080 | 2.150 | 2.210 | 2.250 | 2.280 | 2.280 | 2.260 | 2.230 | 2.180 | 2.120 | 2.060 | 2.000 | 1.950 | 1.910 | 1.880 | 1.850 | 1.830 | 1.820 | 1.840 | 1.890 | 1.950 | |
| 280 | 1.640 | 1.720 | 1.800 | 1.890 | 1.970 | 2.040 | 2.100 | 2.140 | 2.170 | 2.170 | 2.160 | 2.130 | 2.080 | 2.030 | 1.970 | 1.910 | 1.850 | 1.810 | 1.770 | 1.740 | 1.720 | 1.710 | 1.720 | 1.750 | 1.790 | 1.850 |
| 281 | 1.520 | 1.590 | 1.670 | 1.760 | 1.840 | 1.910 | 1.970 | 2.020 | 2.050 | 2.060 | 2.060 | 2.040 | 2.000 | 1.960 | 1.920 | 1.880 | 1.840 | 1.810 | 1.790 | 1.770 | 1.770 | 1.780 | 1.800 | 1.830 | 1.880 | 1.930 |
| 282 | 1.570 | 1.650 | 1.740 | 1.830 | 1.920 | 1.990 | 2.060 | 2.100 | 2.130 | 2.140 | 2.130 | 2.100 | 2.060 | 2.010 | 1.960 | 1.910 | 1.860 | 1.820 | 1.790 | 1.770 | 1.760 | 1.790 | 1.840 | 1.910 | 1.990 | |
| 283 | 1.740 | 1.820 | 1.890 | 1.960 | 2.020 | 2.060 | 2.090 | 2.080 | 2.050 | 2.000 | 1.940 | 1.870 | 1.800 | 1.730 | 1.680 | 1.640 | 1.620 | 1.610 | 1.610 | 1.630 | 1.660 | 1.700 | 1.770 | 1.850 | 1.930 | |
| 284 | 1.390 | 1.460 | 1.540 | 1.620 | 1.700 | 1.780 | 1.850 | 1.910 | 1.960 | 1.990 | 2.020 | 2.020 | 2.020 | 2.010 | 1.990 | 1.970 | 1.950 | 1.940 | 1.920 | 1.920 | 1.920 | 1.950 | 2.000 | 2.060 | 2.120 | 2.160 |
| 285 | 1.600 | 1.680 | 1.770 | 1.860 | 1.940 | 2.030 | 2.100 | 2.170 | 2.220 | 2.260 | 2.280 | 2.280 | 2.270 | 2.260 | 2.230 | 2.200 | 2.170 | 2.150 | 2.120 | 2.090 | 2.080 | 2.100 | 2.120 | 2.130 | 2.120 | |
| 286 | 1.360 | 1.420 | 1.480 | 1.540 | 1.610 | 1.660 | 1.710 | 1.750 | 1.780 | 1.790 | 1.790 | 1.770 | 1.740 | 1.710 | 1.680 | 1.660 | 1.640 | 1.630 | 1.630 | 1.640 | 1.660 | 1.700 | 1.780 | 1.880 | 2.020 | 2.180 |
| 287 | 1.740 | 1.820 | 1.910 | 2.000 | 2.080 | 2.160 | 2.220 | 2.270 | 2.300 | 2.320 | 2.310 | 2.280 | 2.240 | 2.200 | 2.140 | 2.100 | 2.050 | 2.010 | 1.960 | 1.920 | 1.870 | 1.830 | 1.810 | 1.810 | 1.820 | |
| 288 | 1.940 | 2.030 | 2.120 | 2.200 | 2.270 | 2.320 | 2.360 | 2.380 | 2.370 | 2.340 | 2.290 | 2.220 | 2.130 | 2.040 | 1.950 | 1.870 | 1.800 | 1.750 | 1.710 | 1.680 | 1.660 | 1.670 | 1.710 | 1.760 | 1.810 | 1.830 |
| 289 | 2.260 | 2.370 | 2.470 | 2.570 | 2.650 | 2.710 | 2.750 | 2.760 | 2.740 | 2.690 | 2.620 | 2.510 | 2.390 | 2.270 | 2.140 | 2.020 | 1.910 | 1.820 | 1.740 | 1.670 | 1.610 | 1.560 | 1.530 | 1.500 | 1.470 | 1.420 |
| 290 | 3.660 | 3.850 | 4.010 | 4.110 | 4.160 | 4.140 | 4.050 | 3.890 | 3.670 | 3.380 | 3.050 | 2.690 | 2.310 | 1.940 | 1.610 | 1.340 | 1.130 | 0.990 | 0.890 | 0.830 | 0.790 | 0.770 | 0.780 | 0.800 | 0.840 | 0.850 |
| 291 | 2.190 | 2.280 | 2.380 | 2.460 | 2.540 | 2.590 | 2.610 | 2.610 | 2.580 | 2.510 | 2.410 | 2.290 | 2.160 | 2.020 | 1.880 | 1.760 | 1.660 | 1.580 | 1.520 | 1.470 | 1.430 | 1.420 | 1.440 | 1.500 | 1.560 | 1.610 |
| 292 | 2.060 | 2.160 | 2.250 | 2.340 | 2.420 | 2.480 | 2.520 | 2.530 | 2.510 | 2.460 | 2.380 | 2.270 | 2.150 | 2.020 | 1.890 | 1.780 | 1.670 | 1.590 | 1.520 | 1.460 | 1.430 | 1.430 | 1.460 | 1.530 | 1.610 | 1.670 |
| 293 | 2.100 | 2.210 | 2.310 | 2.400 | 2.480 | 2.540 | 2.580 | 2.580 | 2.550 | 2.490 | 2.400 | 2.280 | 2.150 | 2.010 | 1.870 | 1.740 | 1.620 | 1.530 | 1.450 | 1.390 | 1.340 | 1.330 | 1.350 | 1.400 | 1.470 | 1.520 |
| 294 | 2.130 | 2.240 | 2.350 | 2.450 | 2.530 | 2.590 | 2.630 | 2.630 | 2.610 | 2.540 | 2.450 | 2.330 | 2.190 | 2.040 | 1.900 | 1.770 | 1.660 | 1.560 | 1.490 | 1.430 | 1.390 | 1.400 | 1.440 | 1.470 | 1.490 | |
| 295 | 2.250 | 2.360 | 2.460 | 2.550 | 2.620 | 2.670 | 2.700 | 2.690 | 2.650 | 2.580 | 2.470 | 2.340 | 2.200 | 2.050 | 1.900 | 1.770 | 1.650 | 1.560 | 1.490 | 1.420 | 1.370 | 1.340 | 1.330 | 1.350 | 1.410 | 1.480 |
| 296 | 1.880 | 1.960 | 2.040 | 2.120 | 2.180 | 2.220 | 2.250 | 2.240 | 2.210 | 2.160 | 2.080 | 1.970 | 1.860 | 1.750 | 1.640 | 1.550 | 1.490 | 1.450 | 1.430 | 1.430 | 1.460 | 1.510 | 1.590 | 1.690 | 1.790 | 1.880 |
| 297 | 1.920 | 2.000 | 2.070 | 2.130 | 2.180 | 2.220 | 2.230 | 2.220 | 2.180 | 2.120 | 2.030 | 1.930 | 1.820 | 1.710 | 1.600 | 1.510 | 1.440 | 1.390 | 1.370 | 1.360 | 1.370 | 1.420 | 1.500 | 1.620 | 1.760 | 1.880 |
| 298 | 3.350 | 3.570 | 3.760 | 3.890 | 3.970 | 3.990 | 3.930 | 3.800 | 3.600 | 3.330 | 3.010 | 2.660 | 2.290 | 1.910 | 1.570 | 1.270 | 1.030 | 0.860 | 0.750 | 0.680 | 0.660 | 0.670 | 0.710 | 0.770 | 0.830 | 0.860 |
| 299 | 1.860 | 1.940 | 2.020 | 2.090 | 2.150 | 2.190 | 2.210 | 2.210 | 2.120 | 2.040 | 1.940 | 1.820 | 1.700 | 1.590 | 1.490 | 1.410 | 1.360 | 1.330 | 1.310 | 1.330 | 1.380 | 1.470 | 1.600 | 1.730 | 1.840 | |
| 300 | 2.010 | 2.140 | 2.270 | 2.400 | 2.530 | 2.640 | 2.720 | 2.790 | 2.820 | 2.810 | 2.770 | 2.700 | 2.600 | 2.480 | 2.350 | 2.210 | 2.080 | 1.950 | 1.820 | 1.700 | 1.600 | 1.520 | 1.460 | 1.430 | 1.420 | 1.410 |
| 301 | 1.870 | 1.960 | 2.060 | 2.160 | 2.250 | 2.330 | 2.400 | 2.450 | 2.480 | 2.490 | 2.470 | 2.430 | 2.380 | 2.300 | 2.220 | 2.140 | 2.060 | 1.980 | | | | | | | | |

| ID | 8.824 | 8.689 | 8.554 | 8.420 | 8.285 | 8.151 | 8.016 | 7.881 | 7.747 | 7.612 | 7.478 | 7.343 | 7.209 | 7.074 | 6.940 | 6.805 | 6.670 | 6.535 | 6.401 | 6.266 | 6.132 | 5.998 | 5.863 | 5.729 | 5.594 | 5.459 | |
|-------|-------|-------|-------|-------|-------|-------|-------|-------|-------|-------|-------|-------|-------|-------|-------|-------|-------|-------|-------|-------|-------|-------|-------|-------|-------|-------|-------|
| 308 | 1.910 | 2.020 | 2.130 | 2.240 | 2.340 | 2.440 | 2.520 | 2.580 | 2.610 | 2.620 | 2.610 | 2.570 | 2.500 | 2.420 | 2.330 | 2.240 | 2.150 | 2.050 | 1.950 | 1.850 | 1.760 | 1.710 | 1.680 | 1.690 | 1.680 | 1.650 | |
| 309 | 1.650 | 1.740 | 1.840 | 1.930 | 2.030 | 2.110 | 2.180 | 2.240 | 2.280 | 2.290 | 2.290 | 2.260 | 2.220 | 2.170 | 2.110 | 2.040 | 1.980 | 1.920 | 1.850 | 1.800 | 1.750 | 1.730 | 1.740 | 1.770 | 1.790 | 1.790 | |
| 310 | 1.760 | 1.850 | 1.950 | 2.050 | 2.140 | 2.220 | 2.290 | 2.340 | 2.370 | 2.380 | 2.360 | 2.320 | 2.260 | 2.190 | 2.120 | 2.040 | 1.960 | 1.890 | 1.830 | 1.770 | 1.730 | 1.700 | 1.710 | 1.740 | 1.790 | 1.820 | |
| 311 | 1.170 | 1.230 | 1.290 | 1.360 | 1.430 | 1.500 | 1.570 | 1.640 | 1.700 | 1.750 | 1.790 | 1.820 | 1.840 | 1.860 | 1.870 | 1.890 | 1.900 | 1.920 | 1.940 | 1.970 | 2.010 | 2.060 | 2.140 | 2.240 | 2.330 | 2.410 | |
| 312 | 1.140 | 1.200 | 1.270 | 1.340 | 1.410 | 1.480 | 1.550 | 1.610 | 1.670 | 1.720 | 1.760 | 1.800 | 1.820 | 1.840 | 1.860 | 1.880 | 1.910 | 1.940 | 1.970 | 2.010 | 2.070 | 2.160 | 2.260 | 2.390 | 2.510 | | |
| P15 | | | | | | | | | | | | | | | | | | | | | | | | | | | |
| 324 | 0.990 | 1.060 | 1.120 | 1.170 | 1.210 | 1.230 | 1.240 | 1.220 | 1.190 | 1.150 | 1.090 | 1.020 | 0.940 | 0.870 | 0.800 | 0.740 | 0.690 | 0.660 | 0.650 | 0.660 | 0.690 | 0.730 | 0.790 | 0.860 | 0.940 | 1.030 | |
| 325 | 0.800 | 0.830 | 0.850 | 0.860 | 0.870 | 0.860 | 0.840 | 0.820 | 0.790 | 0.750 | 0.710 | 0.670 | 0.630 | 0.590 | 0.560 | 0.540 | 0.530 | 0.540 | 0.560 | 0.600 | 0.650 | 0.710 | 0.800 | 0.910 | 1.040 | 1.180 | |
| 326 | 0.540 | 0.570 | 0.590 | 0.600 | 0.620 | 0.620 | 0.620 | 0.610 | 0.600 | 0.580 | 0.550 | 0.530 | 0.500 | 0.470 | 0.440 | 0.410 | 0.390 | 0.380 | 0.380 | 0.390 | 0.410 | 0.440 | 0.490 | 0.550 | 0.630 | 0.720 | |
| 327 | 0.830 | 0.870 | 0.920 | 0.950 | 0.970 | 0.980 | 0.980 | 0.960 | 0.930 | 0.890 | 0.840 | 0.790 | 0.730 | 0.660 | 0.600 | 0.550 | 0.510 | 0.480 | 0.480 | 0.500 | 0.550 | 0.630 | 0.750 | 0.900 | 1.090 | 1.320 | |
| 332 | 0.780 | 0.810 | 0.850 | 0.870 | 0.890 | 0.900 | 0.890 | 0.880 | 0.860 | 0.830 | 0.790 | 0.750 | 0.700 | 0.660 | 0.610 | 0.580 | 0.550 | 0.550 | 0.560 | 0.590 | 0.640 | 0.730 | 0.860 | 1.020 | 1.220 | 1.470 | |
| 333 | 0.940 | 0.990 | 1.030 | 1.070 | 1.090 | 1.110 | 1.110 | 1.100 | 1.080 | 1.050 | 1.020 | 0.980 | 0.930 | 0.890 | 0.850 | 0.820 | 0.800 | 0.800 | 0.820 | 0.870 | 0.960 | 1.090 | 1.260 | 1.470 | 1.740 | 2.080 | |
| 334 | 0.790 | 0.820 | 0.840 | 0.860 | 0.870 | 0.880 | 0.880 | 0.890 | 0.880 | 0.880 | 0.870 | 0.870 | 0.860 | 0.860 | 0.870 | 0.890 | 0.930 | 0.980 | 1.060 | 1.170 | 1.320 | 1.520 | 1.780 | 2.090 | 2.470 | 2.920 | |
| 335 | 1.040 | 1.090 | 1.130 | 1.170 | 1.190 | 1.210 | 1.210 | 1.210 | 1.190 | 1.170 | 1.150 | 1.120 | 1.090 | 1.060 | 1.040 | 1.030 | 1.040 | 1.080 | 1.140 | 1.230 | 1.360 | 1.530 | 1.730 | 1.980 | 2.260 | 2.580 | |
| 336 | 1.320 | 1.380 | 1.440 | 1.490 | 1.530 | 1.560 | 1.580 | 1.600 | 1.600 | 1.600 | 1.590 | 1.580 | 1.560 | 1.560 | 1.570 | 1.590 | 1.630 | 1.700 | 1.800 | 1.940 | 2.110 | 2.310 | 2.540 | 2.810 | 3.080 | 3.340 | |
| 337 | 1.050 | 1.100 | 1.140 | 1.170 | 1.200 | 1.210 | 1.220 | 1.210 | 1.200 | 1.180 | 1.160 | 1.130 | 1.110 | 1.090 | 1.080 | 1.090 | 1.120 | 1.170 | 1.270 | 1.420 | 1.620 | 1.890 | 2.230 | 2.630 | 3.080 | 3.560 | |
| 338 | 1.270 | 1.330 | 1.390 | 1.440 | 1.480 | 1.520 | 1.550 | 1.560 | 1.580 | 1.580 | 1.580 | 1.580 | 1.590 | 1.600 | 1.620 | 1.650 | 1.720 | 1.810 | 1.930 | 2.100 | 2.300 | 2.540 | 2.820 | 3.120 | 3.420 | 3.680 | |
| 339 | 1.260 | 1.310 | 1.370 | 1.420 | 1.460 | 1.510 | 1.540 | 1.570 | 1.600 | 1.610 | 1.630 | 1.640 | 1.660 | 1.670 | 1.700 | 1.740 | 1.790 | 1.870 | 1.970 | 2.110 | 2.270 | 2.460 | 2.680 | 2.910 | 3.140 | 3.340 | |
| 340 | 1.250 | 1.310 | 1.360 | 1.410 | 1.460 | 1.500 | 1.530 | 1.560 | 1.580 | 1.600 | 1.620 | 1.640 | 1.660 | 1.690 | 1.730 | 1.780 | 1.850 | 1.940 | 2.060 | 2.190 | 2.360 | 2.550 | 2.760 | 3.000 | 3.240 | 3.460 | |
| 341 | 1.060 | 1.100 | 1.140 | 1.170 | 1.200 | 1.220 | 1.230 | 1.240 | 1.240 | 1.230 | 1.220 | 1.220 | 1.210 | 1.210 | 1.210 | 1.230 | 1.250 | 1.300 | 1.380 | 1.490 | 1.640 | 1.840 | 2.080 | 2.360 | 2.690 | 3.050 | 3.410 |
| 342 | 1.070 | 1.110 | 1.150 | 1.180 | 1.220 | 1.240 | 1.270 | 1.290 | 1.310 | 1.330 | 1.350 | 1.370 | 1.400 | 1.440 | 1.500 | 1.570 | 1.670 | 1.800 | 1.950 | 2.140 | 2.350 | 2.590 | 2.840 | 3.080 | 3.320 | 3.530 | |
| 343 | 1.110 | 1.140 | 1.180 | 1.220 | 1.270 | 1.320 | 1.370 | 1.420 | 1.480 | 1.540 | 1.600 | 1.660 | 1.730 | 1.800 | 1.890 | 1.980 | 2.100 | 2.220 | 2.370 | 2.530 | 2.700 | 2.890 | 3.070 | 3.250 | 3.400 | 3.510 | |
| 344 | 1.140 | 1.190 | 1.230 | 1.270 | 1.310 | 1.340 | 1.380 | 1.410 | 1.440 | 1.470 | 1.500 | 1.540 | 1.590 | 1.650 | 1.720 | 1.820 | 1.940 | 2.090 | 2.270 | 2.480 | 2.710 | 2.950 | 3.200 | 3.420 | 3.610 | 3.720 | |
| 345 | 0.870 | 0.900 | 0.930 | 0.960 | 0.980 | 0.990 | 1.000 | 1.000 | 1.000 | 1.000 | 0.990 | 0.990 | 0.990 | 1.000 | 1.020 | 1.050 | 1.100 | 1.190 | 1.300 | 1.450 | 1.650 | 1.890 | 2.180 | 2.510 | 2.870 | 3.230 | |
| 346 | 0.900 | 0.930 | 0.970 | 0.990 | 1.010 | 1.020 | 1.020 | 1.010 | 0.990 | 0.970 | 0.940 | 0.910 | 0.880 | 0.860 | 0.840 | 0.830 | 0.850 | 0.880 | 0.950 | 1.050 | 1.190 | 1.380 | 1.620 | 1.910 | 2.260 | 2.660 | |
| P21-H | | | | | | | | | | | | | | | | | | | | | | | | | | | |
| 397 | 0.900 | 0.940 | 0.990 | 1.050 | 1.120 | 1.190 | 1.260 | 1.340 | 1.410 | 1.480 | 1.550 | 1.610 | 1.670 | 1.730 | 1.790 | 1.840 | 1.900 | 1.960 | 2.020 | 2.080 | 2.140 | 2.220 | 2.300 | 2.400 | 2.500 | 2.590 | |
| 398 | 1.050 | 1.110 | 1.180 | 1.260 | 1.350 | 1.440 | 1.530 | 1.620 | 1.710 | 1.800 | 1.880 | 1.950 | 2.020 | 2.090 | 2.150 | 2.210 | 2.270 | 2.330 | 2.380 | 2.430 | 2.470 | 2.520 | 2.570 | 2.630 | 2.670 | 2.700 | |
| 399 | 0.920 | 0.970 | 1.020 | 1.090 | 1.150 | 1.230 | 1.300 | 1.380 | 1.460 | 1.540 | 1.610 | 1.690 | 1.760 | 1.830 | 1.900 | 1.970 | 2.040 | 2.120 | 2.210 | 2.300 | 2.400 | 2.520 | 2.650 | 2.800 | 2.950 | 3.090 | |
| 400 | 0.780 | 0.820 | 0.860 | 0.900 | 0.950 | 1.000 | 1.050 | 1.110 | 1.170 | 1.230 | 1.290 | 1.350 | 1.410 | 1.470 | 1.530 | 1.600 | 1.670 | 1.750 | 1.840 | 1.940 | 2.070 | 2.220 | 2.400 | 2.620 | 2.860 | 3.110 | |
| 405 | 0.410 | 0.420 | 0.430 | 0.450 | 0.470 | 0.490 | 0.510 | 0.530 | 0.550 | 0.570 | 0.590 | 0.610 | 0.630 | 0.650 | 0.670 | 0.690 | 0.720 | 0.750 | 0.790 | 0.850 | 0.920 | 1.020 | 1.150 | 1.330 | 1.550 | 1.800 | |
| 406 | 0.330 | 0.340 | 0.340 | 0.350 | 0.360 | 0.370 | 0.380 | 0.390 | 0.400 | 0.420 | 0.430 | 0.440 | 0.460 | 0.470 | 0.480 | 0.500 | 0.520 | 0.550 | 0.580 | 0.630 | 0.690 | 0.780 | 0.890 | 1.040 | 1.220 | 1.450 | |
| 407 | 0.600 | 0.620 | 0.640 | 0.670 | 0.700 | 0.730 | 0.760 | 0.800 | 0.830 | 0.860 | 0.890 | 0.930 | 0.960 | 0.990 | 1.030 | 1.060 | 1.110 | 1.160 | 1.220 | 1.300 | 1.400 | 1.520 | 1.680 | 1.880 | 2.100 | 2.350 | |
| 408 | 2.040 | 2.170 | 2.270 | 2.360 | 2.420 | 2.440 | 2.430 | 2.390 | 2.310 | 2.210 | 2.090 | 1.950 | 1.810 | 1.680 | 1.560 | 1.460 | 1.400 | 1.380 | 1.390 | 1.440 | 1.520 | 1.630 | 1.760 | 1.910 | 2.080 | 2.260 | |
| 409 | 2.050 | 2.210 | 2.350 | 2.480 | 2.590 | 2.680 | 2.730 | 2.760 | 2.760 | 2.730 | 2.670 | 2.600 | 2.510 | 2.410 | 2.310 | 2.220 | 2.150 | 2.090 | 2.060 | 2.050 | 2.060 | 2.080 | 2.120 | 2.160 | 2.180 | 2.150 | |
| 410 | 1.880 | 2.000 | 2.100 | 2.180 | 2.230 | 2.260 | 2.250 | 2.210 | 2.140 | 2.050 | 1.940 | 1.810 | 1.680 | 1.550 | 1.430 | 1.340 | 1.280 | 1.250 | 1.270 | 1.320 | 1.400 | 1.520 | 1.670 | 1.840 | 2.040 | 2.230 | |
| 411 | 0.670 | 0.700 | 0.740 | 0.780 | 0.830 | 0.880 | 0.930 | 0.980 | 1.030 | 1.080 | 1.120 | 1.160 | 1.200 | 1.240 | 1.270 | 1.300 | 1.340 | 1.370 | 1.410 | 1.460 | 1.510 | 1.580 | 1.670 | 1.780 | 1.920 | 2.080 | |
| 412 | 0.650 | 0.710 | 0.780 | 0.850 | 0.920 | 1.000 | 1.090 | 1.170 | 1.250 | 1.320 | 1.390 | 1.450 | 1.510 | 1.560 | 1.600 | 1.630 | 1.650 | 1.660 | 1.650 | 1.660 | 1.630 | 1.600 | 1.570 | 1.550 | 1.540 | 1.530 | |
| 413 | 0.270 | 0.280 | 0.290 | 0.300 | 0.310 | 0.320 | 0.330 | 0.340 | 0.360 | 0.370 | 0.380 | 0.390 | 0.400 | 0.410 | 0.420 | 0.430 | 0.430 | 0.440 | 0.450 | 0.460 | 0.470 | 0.490 | 0.520 | 0.550 | 0.600 | 0.660 | |
| 414 | 0.170 | 0.170 | 0.180 | 0.190 | 0.200 | 0.210 | 0.230 | 0.240 | 0.250 | 0.260 | 0 | | | | | | | | | | | | | | | | |

| ID | 5.325 | 5.191 | 5.056 | 4.921 | 4.786 | 4.652 | 4.518 | 4.383 | 4.248 | 4.114 | 3.979 | 3.844 | 3.710 | 3.575 | 3.441 | 3.306 | 3.171 | 3.037 | 2.903 | 2.768 | 2.633 | 2.500 | 2.364 | 2.230 | 2.095 | 1.961 |
|------------|-------|-------|-------|-------|-------|-------|-------|-------|-------|-------|-------|-------|-------|-------|-------|-------|-------|-------|-------|-------|-------|-------|-------|---------|-------|-------|
| P02 | | | | | | | | | | | | | | | | | | | | | | | | | | |
| 512 | 0.910 | 0.990 | 1.100 | 1.240 | 1.440 | 1.690 | 1.990 | 2.290 | 2.590 | 2.830 | 3.000 | 3.080 | 3.060 | 2.950 | 2.740 | 2.470 | 2.160 | 1.860 | 1.620 | 1.460 | 1.380 | 1.370 | 1.370 | 1.340 | 1.300 | |
| 514 | 1.360 | 1.530 | 1.740 | 2.000 | 2.320 | 2.730 | 3.190 | 3.690 | 4.160 | 4.540 | 4.790 | 4.850 | 4.740 | 4.460 | 4.050 | 3.570 | 3.070 | 2.590 | 2.170 | 1.840 | 1.580 | 1.380 | 1.230 | 1.100 | 0.990 | 0.890 |
| 516 | 0.610 | 0.660 | 0.720 | 0.800 | 0.910 | 1.040 | 1.220 | 1.440 | 1.670 | 1.920 | 2.140 | 2.320 | 2.430 | 2.480 | 2.480 | 2.430 | 2.360 | 2.290 | 2.240 | 2.230 | 2.250 | 2.330 | 2.470 | 2.650 | 2.850 | 3.030 |
| 518 | 1.900 | 2.150 | 2.470 | 2.870 | 3.370 | 3.930 | 4.500 | 4.990 | 5.310 | 5.370 | 5.150 | 4.680 | 4.050 | 3.340 | 2.660 | 2.050 | 1.540 | 1.130 | 0.830 | 0.630 | 0.500 | 0.420 | 0.370 | 0.310 | 0.240 | 0.170 |
| 520 | 2.580 | 2.690 | 2.780 | 2.870 | 2.940 | 2.970 | 2.970 | 2.910 | 2.790 | 2.620 | 2.400 | 2.150 | 1.880 | 1.590 | 1.310 | 1.040 | 0.800 | 0.610 | 0.470 | 0.400 | 0.380 | 0.400 | 0.430 | 0.430 | 0.380 | 0.280 |
| 522 | 2.160 | 2.200 | 2.240 | 2.280 | 2.330 | 2.380 | 2.400 | 2.350 | 2.220 | 2.010 | 1.770 | 1.530 | 1.310 | 1.120 | 0.950 | 0.770 | 0.560 | 0.370 | 0.220 | 0.150 | 0.140 | 0.170 | 0.190 | 0.170 | 0.110 | 0.051 |
| 524 | 2.510 | 2.770 | 3.050 | 3.350 | 3.690 | 4.030 | 4.340 | 4.570 | 4.660 | 4.580 | 4.320 | 3.930 | 3.450 | 2.930 | 2.420 | 1.930 | 1.490 | 1.120 | 0.850 | 0.660 | 0.550 | 0.440 | 0.350 | 0.260 | 0.180 | 0.091 |
| 526 | 3.370 | 3.580 | 3.800 | 4.020 | 4.220 | 4.370 | 4.420 | 4.330 | 4.070 | 3.660 | 3.150 | 2.580 | 2.040 | 1.570 | 1.200 | 0.920 | 0.710 | 0.550 | 0.410 | 0.300 | 0.210 | 0.160 | 0.130 | 0.120 | 0.110 | 0.078 |
| 528 | 2.410 | 2.390 | 2.340 | 2.260 | 2.150 | 2.020 | 1.860 | 1.680 | 1.480 | 1.280 | 1.080 | 0.890 | 0.690 | 0.490 | 0.300 | 0.150 | 0.053 | 0.010 | 0.001 | 0.000 | 0.000 | 0.000 | 0.000 | 0.000 | 0.000 | |
| 530 | 2.280 | 2.230 | 2.150 | 2.050 | 1.970 | 1.880 | 1.780 | 1.660 | 1.490 | 1.280 | 1.050 | 0.820 | 0.630 | 0.490 | 0.400 | 0.340 | 0.300 | 0.250 | 0.190 | 0.120 | 0.063 | 0.033 | 0.028 | 0.033 | 0.037 | 0.034 |
| 532 | 2.750 | 2.700 | 2.610 | 2.500 | 2.370 | 2.230 | 2.060 | 1.870 | 1.670 | 1.450 | 1.230 | 1.040 | 0.890 | 0.770 | 0.690 | 0.640 | 0.590 | 0.540 | 0.470 | 0.380 | 0.290 | 0.220 | 0.180 | 0.160 | 0.140 | 0.120 |
| 534 | 3.030 | 3.130 | 3.190 | 3.220 | 3.200 | 3.130 | 3.010 | 2.840 | 2.610 | 2.340 | 2.050 | 1.750 | 1.460 | 1.220 | 1.030 | 0.890 | 0.810 | 0.760 | 0.710 | 0.640 | 0.550 | 0.440 | 0.320 | 0.210 | 0.110 | 0.040 |
| 536 | 2.930 | 2.780 | 2.590 | 2.370 | 2.150 | 1.930 | 1.710 | 1.500 | 1.280 | 1.050 | 0.840 | 0.660 | 0.510 | 0.390 | 0.310 | 0.240 | 0.190 | 0.140 | 0.110 | 0.064 | 0.027 | 0.006 | 0.000 | 0.000 | 0.000 | |
| 538 | 2.120 | 1.940 | 1.760 | 1.580 | 1.430 | 1.290 | 1.170 | 1.060 | 0.950 | 0.850 | 0.750 | 0.680 | 0.610 | 0.560 | 0.510 | 0.460 | 0.420 | 0.370 | 0.310 | 0.240 | 0.190 | 0.160 | 0.150 | 0.150 | 0.140 | |
| 567 | 2.720 | 2.680 | 2.580 | 2.440 | 2.280 | 2.100 | 1.920 | 1.740 | 1.560 | 1.360 | 1.160 | 0.950 | 0.750 | 0.580 | 0.430 | 0.330 | 0.280 | 0.270 | 0.270 | 0.260 | 0.230 | 0.170 | 0.110 | 0.050 | 0.015 | 0.002 |
| P06 | | | | | | | | | | | | | | | | | | | | | | | | | | |
| 49 | 1.600 | 1.730 | 1.850 | 1.990 | 2.180 | 2.420 | 2.720 | 3.060 | 3.400 | 3.700 | 3.910 | 4.000 | 3.960 | 3.790 | 3.530 | 3.200 | 2.850 | 2.490 | 2.160 | 1.870 | 1.620 | 1.420 | 1.260 | 1.120 | 0.970 | 0.840 |
| 51 | 0.290 | 0.300 | 0.300 | 0.310 | 0.330 | 0.360 | 0.400 | 0.450 | 0.500 | 0.560 | 0.600 | 0.640 | 0.680 | 0.720 | 0.750 | 0.800 | 0.850 | 0.920 | 0.990 | 1.080 | 1.160 | 1.240 | 1.330 | 1.420 | 1.530 | 1.650 |
| 53 | 0.290 | 0.300 | 0.300 | 0.320 | 0.340 | 0.380 | 0.440 | 0.500 | 0.580 | 0.660 | 0.740 | 0.820 | 0.890 | 0.960 | 1.030 | 1.090 | 1.170 | 1.260 | 1.360 | 1.480 | 1.600 | 1.730 | 1.870 | 2.020 | 2.180 | 2.350 |
| 55 | 0.710 | 0.780 | 0.870 | 0.990 | 1.130 | 1.310 | 1.510 | 1.720 | 1.910 | 2.080 | 2.190 | 2.230 | 2.220 | 2.150 | 2.040 | 1.940 | 1.850 | 1.800 | 1.780 | 1.790 | 1.840 | 1.900 | 1.980 | 2.090 | 2.200 | 2.320 |
| 57 | 1.420 | 1.540 | 1.670 | 1.830 | 2.010 | 2.220 | 2.450 | 2.670 | 2.850 | 2.970 | 3.000 | 2.940 | 2.790 | 2.560 | 2.260 | 1.920 | 1.580 | 1.290 | 1.100 | 1.050 | 1.130 | 1.270 | 1.370 | 1.330 | 1.140 | 0.920 |
| 59 | 1.330 | 1.380 | 1.420 | 1.480 | 1.580 | 1.730 | 1.940 | 2.160 | 2.360 | 2.480 | 2.480 | 2.360 | 2.160 | 1.940 | 1.780 | 1.710 | 1.710 | 1.720 | 1.660 | 1.500 | 1.300 | 1.160 | 1.150 | 1.230 | 1.310 | 1.360 |
| 61 | 1.290 | 1.340 | 1.410 | 1.490 | 1.590 | 1.720 | 1.870 | 2.040 | 2.250 | 2.460 | 2.640 | 2.750 | 2.750 | 2.600 | 2.330 | 1.970 | 1.600 | 1.290 | 1.110 | 1.080 | 1.170 | 1.340 | 1.470 | 1.470 | 1.300 | 1.000 |
| 63 | 1.200 | 1.220 | 1.240 | 1.290 | 1.380 | 1.520 | 1.680 | 1.830 | 1.930 | 1.970 | 1.950 | 1.890 | 1.820 | 1.760 | 1.720 | 1.670 | 1.580 | 1.420 | 1.200 | 0.990 | 0.880 | 0.920 | 1.070 | 1.250 | 1.310 | 1.160 |
| 65 | 0.910 | 0.850 | 0.830 | 0.860 | 0.950 | 1.090 | 1.210 | 1.290 | 1.230 | 1.120 | 1.000 | 0.920 | 0.890 | 0.880 | 0.850 | 0.780 | 0.670 | 0.530 | 0.410 | 0.340 | 0.320 | 0.330 | 0.320 | 0.250 | 0.150 | |
| 67 | 1.390 | 1.410 | 1.440 | 1.460 | 1.490 | 1.510 | 1.560 | 1.630 | 1.740 | 1.880 | 2.010 | 2.100 | 2.090 | 1.970 | 1.730 | 1.420 | 1.100 | 0.850 | 0.700 | 0.680 | 0.790 | 1.000 | 1.230 | 1.370 | 1.310 | 1.060 |
| 69 | 1.850 | 1.790 | 1.710 | 1.650 | 1.590 | 1.550 | 1.510 | 1.480 | 1.430 | 1.390 | 1.330 | 1.270 | 1.190 | 1.090 | 0.980 | 0.870 | 0.750 | 0.640 | 0.550 | 0.480 | 0.450 | 0.460 | 0.480 | 0.480 | 0.440 | 0.340 |
| 71 | 2.050 | 1.870 | 1.670 | 1.490 | 1.370 | 1.320 | 1.330 | 1.370 | 1.400 | 1.370 | 1.290 | 1.180 | 1.070 | 1.000 | 0.990 | 0.990 | 0.960 | 0.840 | 0.630 | 0.390 | 0.240 | 0.190 | 0.210 | 0.280 | 0.350 | 0.360 |
| 73 | 1.770 | 1.710 | 1.630 | 1.550 | 1.490 | 1.460 | 1.470 | 1.500 | 1.520 | 1.510 | 1.450 | 1.350 | 1.250 | 1.180 | 1.130 | 1.090 | 1.010 | 0.860 | 0.660 | 0.480 | 0.390 | 0.390 | 0.470 | 0.580 | 0.620 | 0.550 |
| 75 | 1.730 | 1.590 | 1.430 | 1.280 | 1.160 | 1.090 | 1.050 | 1.040 | 1.000 | 0.930 | 0.820 | 0.700 | 0.610 | 0.570 | 0.600 | 0.660 | 0.690 | 0.640 | 0.500 | 0.330 | 0.210 | 0.160 | 0.160 | 0.170 | 0.150 | 0.100 |
| 77 | 1.520 | 1.400 | 1.280 | 1.180 | 1.110 | 1.070 | 1.060 | 1.050 | 1.030 | 0.980 | 0.910 | 0.810 | 0.700 | 0.580 | 0.430 | 0.280 | 0.160 | 0.095 | 0.087 | 0.120 | 0.170 | 0.190 | 0.170 | 0.110 | 0.042 | 0.008 |
| 79 | 2.140 | 1.960 | 1.760 | 1.540 | 1.330 | 1.130 | 0.940 | 0.760 | 0.610 | 0.480 | 0.380 | 0.310 | 0.260 | 0.230 | 0.200 | 0.180 | 0.160 | 0.150 | 0.160 | 0.160 | 0.150 | 0.130 | 0.100 | 0.071 | 0.041 | 0.018 |
| 81 | 0.980 | 0.880 | 0.780 | 0.700 | 0.630 | 0.570 | 0.530 | 0.490 | 0.450 | 0.410 | 0.380 | 0.350 | 0.330 | 0.320 | 0.300 | 0.280 | 0.280 | 0.270 | 0.270 | 0.250 | 0.200 | 0.130 | 0.066 | 0.022 | 0.004 | |
| 83 | 1.690 | 1.640 | 1.580 | 1.550 | 1.540 | 1.550 | 1.590 | 1.620 | 1.640 | 1.630 | 1.580 | 1.490 | 1.380 | 1.250 | 1.120 | 0.990 | 0.870 | 0.750 | 0.640 | 0.540 | 0.460 | 0.420 | 0.410 | 0.400 | 0.360 | 0.280 |
| 85 | 1.350 | 1.230 | 1.110 | 1.000 | 0.920 | 0.870 | 0.850 | 0.870 | 0.900 | 0.930 | 0.960 | 0.960 | 0.930 | 0.870 | 0.770 | 0.650 | 0.530 | 0.410 | 0.320 | 0.290 | 0.340 | 0.390 | 0.340 | 0.210 | 0.099 | |
| 87 | 0.990 | 0.900 | 0.820 | 0.770 | 0.760 | 0.790 | 0.850 | 0.940 | 1.030 | 1.120 | 1.180 | 1.220 | 1.230 | 1.230 | 1.210 | 1.160 | 1.070 | 0.970 | 0.880 | 0.840 | 0.870 | 0.940 | 1.000 | 0.980 | 0.850 | 0.610 |
| 89 | 2.040 | 1.810 | 1.610 | 1.460 | 1.360 | 1.310 | 1.310 | 1.340 | 1.380 | 1.420 | 1.440 | 1.420 | 1.370 | 1.280 | 1.140 | 0.990 | 0.840 | 0.710 | 0.600 | 0.530 | 0.470 | 0.400 | 0.320 | 0.220 | 0.120 | 0.046 |
| 91 | 1.840 | 1.660 | 1.490 | 1.340 | 1.230 | 1.160 | 1.110 | 1.070 | 1.050 | 1.020 | 0.980 | 0.940 | 0.890 | 0.830 | 0.760 | 0.680 | 0.600 | 0.530 | 0.470 | 0.420 | 0.390 | 0.350 | 0.310 | 0.240</ | | |

| ID | 5.325 | 5.191 | 5.056 | 4.921 | 4.786 | 4.652 | 4.518 | 4.383 | 4.248 | 4.114 | 3.979 | 3.844 | 3.710 | 3.575 | 3.441 | 3.306 | 3.171 | 3.037 | 2.903 | 2.768 | 2.633 | 2.500 | 2.364 | 2.230 | 2.095 | 1.961 |
|-----|-------|-------|-------|-------|-------|-------|-------|-------|-------|-------|-------|-------|-------|-------|-------|-------|-------|-------|-------|-------|-------|-------|-------|-------|-------|-------|
| 103 | 1.760 | 1.670 | 1.580 | 1.500 | 1.450 | 1.410 | 1.380 | 1.370 | 1.360 | 1.340 | 1.310 | 1.260 | 1.190 | 1.100 | 0.990 | 0.860 | 0.730 | 0.610 | 0.530 | 0.480 | 0.470 | 0.470 | 0.450 | 0.380 | 0.270 | 0.140 |
| 105 | 1.840 | 1.760 | 1.680 | 1.600 | 1.540 | 1.510 | 1.510 | 1.530 | 1.540 | 1.520 | 1.480 | 1.410 | 1.320 | 1.230 | 1.130 | 1.030 | 0.910 | 0.760 | 0.600 | 0.470 | 0.400 | 0.390 | 0.420 | 0.440 | 0.420 | 0.330 |
| 107 | 2.300 | 2.300 | 2.270 | 2.240 | 2.230 | 2.270 | 2.370 | 2.500 | 2.640 | 2.720 | 2.730 | 2.650 | 2.520 | 2.350 | 2.170 | 1.980 | 1.730 | 1.440 | 1.120 | 0.860 | 0.680 | 0.600 | 0.570 | 0.520 | 0.420 | 0.260 |
| 109 | 2.960 | 3.100 | 3.220 | 3.300 | 3.340 | 3.320 | 3.250 | 3.120 | 2.940 | 2.720 | 2.460 | 2.160 | 1.850 | 1.510 | 1.170 | 0.860 | 0.620 | 0.480 | 0.400 | 0.380 | 0.380 | 0.360 | 0.280 | 0.170 | 0.066 | 0.014 |
| 111 | 2.550 | 2.620 | 2.670 | 2.720 | 2.770 | 2.820 | 2.850 | 2.850 | 2.810 | 2.730 | 2.590 | 2.410 | 2.200 | 1.960 | 1.710 | 1.460 | 1.230 | 1.020 | 0.860 | 0.730 | 0.640 | 0.580 | 0.510 | 0.410 | 0.290 | 0.160 |
| 113 | 2.210 | 2.320 | 2.440 | 2.570 | 2.720 | 2.880 | 3.040 | 3.170 | 3.250 | 3.260 | 3.190 | 3.030 | 2.810 | 2.530 | 2.220 | 1.910 | 1.630 | 1.380 | 1.170 | 1.000 | 0.860 | 0.710 | 0.560 | 0.400 | 0.230 | 0.100 |
| 115 | 1.870 | 1.940 | 2.020 | 2.120 | 2.240 | 2.370 | 2.500 | 2.620 | 2.710 | 2.740 | 2.710 | 2.600 | 2.410 | 2.160 | 1.870 | 1.560 | 1.260 | 0.990 | 0.750 | 0.570 | 0.450 | 0.380 | 0.310 | 0.240 | 0.170 | 0.089 |
| 117 | 1.800 | 1.860 | 1.940 | 2.040 | 2.160 | 2.310 | 2.470 | 2.610 | 2.720 | 2.770 | 2.750 | 2.650 | 2.480 | 2.260 | 2.010 | 1.750 | 1.500 | 1.270 | 1.070 | 0.920 | 0.820 | 0.770 | 0.730 | 0.660 | 0.540 | 0.370 |
| 119 | 1.600 | 1.650 | 1.710 | 1.790 | 1.890 | 1.990 | 2.100 | 2.180 | 2.240 | 2.260 | 2.230 | 2.170 | 2.050 | 1.890 | 1.700 | 1.480 | 1.250 | 1.040 | 0.870 | 0.760 | 0.700 | 0.700 | 0.690 | 0.650 | 0.530 | 0.350 |
| 121 | 1.590 | 1.690 | 1.800 | 1.890 | 1.960 | 2.020 | 2.070 | 2.150 | 2.260 | 2.390 | 2.500 | 2.530 | 2.440 | 2.200 | 1.830 | 1.410 | 1.020 | 0.740 | 0.610 | 0.600 | 0.700 | 0.820 | 0.890 | 0.830 | 0.650 | 0.400 |
| 123 | 1.710 | 1.760 | 1.820 | 1.920 | 2.040 | 2.170 | 2.310 | 2.420 | 2.490 | 2.500 | 2.450 | 2.350 | 2.180 | 1.980 | 1.740 | 1.500 | 1.270 | 1.050 | 0.870 | 0.740 | 0.650 | 0.610 | 0.600 | 0.570 | 0.500 | 0.370 |
| 125 | 1.740 | 1.810 | 1.890 | 1.990 | 2.120 | 2.260 | 2.410 | 2.540 | 2.630 | 2.660 | 2.630 | 2.520 | 2.350 | 2.120 | 1.860 | 1.590 | 1.320 | 1.070 | 0.860 | 0.720 | 0.660 | 0.660 | 0.680 | 0.670 | 0.580 | 0.410 |
| 127 | 1.720 | 1.790 | 1.880 | 1.990 | 2.140 | 2.300 | 2.470 | 2.620 | 2.730 | 2.780 | 2.760 | 2.650 | 2.460 | 2.210 | 1.920 | 1.620 | 1.310 | 1.030 | 0.810 | 0.670 | 0.610 | 0.610 | 0.630 | 0.610 | 0.510 | 0.340 |
| 129 | 1.570 | 1.510 | 1.460 | 1.430 | 1.430 | 1.460 | 1.510 | 1.560 | 1.610 | 1.630 | 1.600 | 1.520 | 1.390 | 1.230 | 1.060 | 0.910 | 0.810 | 0.740 | 0.690 | 0.660 | 0.610 | 0.540 | 0.440 | 0.320 | 0.200 | 0.097 |
| 131 | 2.320 | 2.540 | 2.800 | 3.100 | 3.430 | 3.770 | 4.070 | 4.260 | 4.320 | 4.220 | 3.980 | 3.640 | 3.240 | 2.810 | 2.380 | 1.960 | 1.570 | 1.230 | 0.970 | 0.790 | 0.660 | 0.550 | 0.420 | 0.270 | 0.130 | 0.044 |
| 133 | 3.200 | 3.110 | 3.000 | 2.880 | 2.760 | 2.640 | 2.500 | 2.310 | 2.060 | 1.780 | 1.490 | 1.240 | 1.030 | 0.850 | 0.680 | 0.500 | 0.320 | 0.190 | 0.130 | 0.120 | 0.130 | 0.150 | 0.140 | 0.098 | 0.044 | 0.010 |
| 135 | 2.290 | 1.960 | 1.640 | 1.370 | 1.160 | 1.000 | 0.890 | 0.800 | 0.710 | 0.610 | 0.500 | 0.400 | 0.320 | 0.280 | 0.270 | 0.270 | 0.250 | 0.190 | 0.110 | 0.038 | 0.009 | 0.006 | 0.009 | 0.009 | 0.003 | 0.000 |
| 137 | 3.520 | 3.170 | 2.660 | 2.080 | 1.550 | 1.180 | 0.960 | 0.830 | 0.720 | 0.610 | 0.520 | 0.440 | 0.370 | 0.330 | 0.290 | 0.260 | 0.240 | 0.220 | 0.190 | 0.170 | 0.140 | 0.110 | 0.077 | 0.048 | 0.025 | 0.011 |
| 139 | 2.220 | 1.930 | 1.660 | 1.430 | 1.260 | 1.110 | 0.980 | 0.830 | 0.650 | 0.450 | 0.270 | 0.160 | 0.110 | 0.100 | 0.110 | 0.130 | 0.140 | 0.130 | 0.120 | 0.096 | 0.079 | 0.067 | 0.057 | 0.045 | 0.028 | 0.013 |
| 141 | 2.140 | 1.870 | 1.630 | 1.430 | 1.290 | 1.180 | 1.080 | 0.960 | 0.810 | 0.650 | 0.500 | 0.400 | 0.340 | 0.310 | 0.280 | 0.230 | 0.170 | 0.100 | 0.065 | 0.053 | 0.063 | 0.083 | 0.093 | 0.078 | 0.045 | 0.016 |
| 143 | 2.820 | 2.710 | 2.580 | 2.440 | 2.310 | 2.190 | 2.070 | 1.930 | 1.760 | 1.560 | 1.350 | 1.130 | 0.930 | 0.740 | 0.560 | 0.380 | 0.240 | 0.150 | 0.120 | 0.140 | 0.180 | 0.210 | 0.190 | 0.120 | 0.052 | 0.011 |
| 145 | 2.780 | 3.250 | 3.770 | 4.300 | 4.820 | 5.260 | 5.550 | 5.640 | 5.480 | 5.090 | 4.510 | 3.830 | 3.140 | 2.510 | 1.980 | 1.550 | 1.210 | 0.950 | 0.760 | 0.630 | 0.530 | 0.440 | 0.340 | 0.230 | 0.130 | 0.060 |
| 147 | 2.830 | 3.180 | 3.550 | 3.930 | 4.310 | 4.650 | 4.920 | 5.060 | 5.030 | 4.790 | 4.360 | 3.790 | 3.170 | 2.570 | 2.050 | 1.620 | 1.280 | 1.000 | 0.770 | 0.590 | 0.460 | 0.380 | 0.310 | 0.240 | 0.150 | 0.061 |
| 149 | 3.150 | 2.940 | 2.680 | 2.400 | 2.120 | 1.860 | 1.610 | 1.380 | 1.170 | 0.970 | 0.800 | 0.650 | 0.530 | 0.450 | 0.390 | 0.350 | 0.320 | 0.290 | 0.260 | 0.220 | 0.170 | 0.120 | 0.072 | 0.038 | 0.019 | 0.008 |
| 151 | 2.810 | 2.660 | 2.620 | 2.670 | 2.740 | 2.680 | 2.380 | 1.830 | 1.120 | 0.500 | 0.140 | 0.020 | 0.001 | 0.000 | 0.000 | 0.000 | 0.000 | 0.000 | 0.000 | 0.000 | 0.000 | 0.000 | 0.000 | 0.000 | 0.000 | 0.000 |
| 153 | 3.490 | 3.600 | 3.660 | 3.660 | 3.590 | 3.460 | 3.260 | 2.990 | 2.670 | 2.320 | 1.960 | 1.610 | 1.310 | 1.060 | 0.870 | 0.720 | 0.610 | 0.530 | 0.460 | 0.380 | 0.290 | 0.190 | 0.110 | 0.051 | 0.019 | 0.005 |
| 155 | 3.000 | 2.900 | 2.750 | 2.580 | 2.390 | 2.190 | 2.000 | 1.800 | 1.590 | 1.380 | 1.180 | 0.990 | 0.840 | 0.710 | 0.610 | 0.530 | 0.470 | 0.410 | 0.350 | 0.290 | 0.250 | 0.210 | 0.190 | 0.170 | 0.150 | 0.120 |
| 157 | 2.940 | 3.040 | 3.130 | 3.220 | 3.290 | 3.340 | 3.340 | 3.280 | 3.120 | 2.880 | 2.560 | 2.200 | 1.830 | 1.490 | 1.200 | 0.970 | 0.800 | 0.660 | 0.540 | 0.440 | 0.350 | 0.280 | 0.220 | 0.170 | 0.120 | 0.062 |

P14

| | | | | | | | | | | | | | | | | | | | | | | | | | | |
|-----|-------|-------|-------|-------|-------|-------|-------|-------|-------|-------|-------|-------|-------|-------|-------|-------|-------|-------|-------|-------|-------|-------|-------|-------|-------|-------|
| 159 | 1.570 | 1.720 | 1.900 | 2.120 | 2.390 | 2.730 | 3.120 | 3.540 | 3.940 | 4.270 | 4.480 | 4.540 | 4.420 | 4.150 | 3.760 | 3.300 | 2.830 | 2.370 | 1.950 | 1.580 | 1.270 | 1.040 | 0.880 | 0.810 | 0.800 | 0.820 |
| 160 | 0.830 | 0.920 | 1.040 | 1.220 | 1.490 | 1.880 | 2.400 | 3.030 | 3.720 | 4.400 | 4.970 | 5.350 | 5.460 | 5.290 | 4.870 | 4.270 | 3.590 | 2.900 | 2.270 | 1.750 | 1.350 | 1.100 | 0.970 | 0.940 | 1.000 | 1.090 |
| 161 | 2.010 | 2.180 | 2.390 | 2.630 | 2.910 | 3.230 | 3.550 | 3.840 | 4.070 | 4.200 | 4.210 | 4.090 | 3.840 | 3.510 | 3.120 | 2.720 | 2.330 | 1.970 | 1.630 | 1.320 | 1.040 | 0.800 | 0.620 | 0.500 | 0.420 | 0.370 |
| 162 | 1.790 | 1.960 | 2.170 | 2.440 | 2.780 | 3.200 | 3.660 | 4.140 | 4.560 | 4.870 | 5.010 | 4.950 | 4.690 | 4.270 | 3.730 | 3.140 | 2.570 | 2.050 | 1.590 | 1.210 | 0.880 | 0.630 | 0.450 | 0.350 | 0.300 | 0.280 |
| 163 | 2.190 | 2.350 | 2.530 | 2.740 | 3.000 | 3.300 | 3.620 | 3.910 | 4.140 | 4.260 | 4.240 | 4.070 | 3.780 | 3.380 | 2.920 | 2.450 | 2.000 | 1.590 | 1.240 | 0.930 | 0.690 | 0.520 | 0.430 | 0.390 | 0.380 | 0.370 |
| 164 | 2.210 | 2.370 | 2.540 | 2.740 | 2.960 | 3.220 | 3.470 | 3.700 | 3.860 | 3.920 | 3.860 | 3.680 | 3.400 | 3.050 | 2.670 | 2.300 | 1.960 | 1.650 | 1.380 | 1.120 | 0.880 | 0.660 | 0.480 | 0.360 | 0.290 | 0.270 |
| 165 | 2.460 | 2.560 | 2.670 | 2.780 | 2.900 | 3.020 | 3.130 | 3.200 | 3.210 | 3.150 | 3.020 | 2.810 | 2.550 | 2.260 | 1.970 | 1.700 | 1.450 | 1.230 | 1.020 | 0.820 | 0.620 | 0.450 | 0.330 | 0.250 | 0.210 | 0.200 |
| 166 | 2.540 | 2.600 | 2.670 | 2.760 | 2.860 | 2.960 | 3.060 | 3.120 | 3.110 | 3.040 | 2.890 | 2.680 | 2.430 | 2.150 | 1.860 | 1.580 | 1.310 | 1.090 | 0.910 | 0.790 | 0.710 | 0.630 | 0.530 | 0.400 | 0.250 | 0.120 |
| 167 | 2.660 | 2.830 | 3.000 | 3.150 | 3.290 | 3.420 | 3.550 | 3.640 | | | | | | | | | | | | | | | | | | |

| ID | 5.325 | 5.191 | 5.056 | 4.921 | 4.786 | 4.652 | 4.518 | 4.383 | 4.248 | 4.114 | 3.979 | 3.844 | 3.710 | 3.575 | 3.441 | 3.306 | 3.171 | 3.037 | 2.903 | 2.768 | 2.633 | 2.500 | 2.364 | 2.230 | 2.095 | 1.961 |
|---------|-------|-------|-------|-------|-------|-------|-------|-------|-------|-------|-------|-------|-------|-------|-------|-------|-------|-------|-------|-------|-------|-------|-------|-------|-------|-------|
| 174 | 2.720 | 3.030 | 3.330 | 3.640 | 3.930 | 4.190 | 4.390 | 4.500 | 4.480 | 4.310 | 4.000 | 3.570 | 3.070 | 2.550 | 2.060 | 1.630 | 1.290 | 1.030 | 0.820 | 0.660 | 0.520 | 0.400 | 0.310 | 0.240 | 0.180 | 0.130 |
| 175 (1) | 1.650 | 1.610 | 1.550 | 1.480 | 1.410 | 1.340 | 1.270 | 1.200 | 1.130 | 1.040 | 0.950 | 0.860 | 0.770 | 0.680 | 0.610 | 0.570 | 0.560 | 0.570 | 0.620 | 0.660 | 0.650 | 0.590 | 0.460 | 0.290 | 0.140 | 0.043 |
| 175 (2) | 1.520 | 1.320 | 1.120 | 0.930 | 0.770 | 0.630 | 0.510 | 0.410 | 0.320 | 0.250 | 0.190 | 0.160 | 0.160 | 0.190 | 0.250 | 0.330 | 0.410 | 0.460 | 0.440 | 0.340 | 0.200 | 0.074 | 0.014 | 0.001 | 0.000 | 0.000 |
| 176 | 1.470 | 1.270 | 1.090 | 0.930 | 0.810 | 0.710 | 0.620 | 0.540 | 0.450 | 0.360 | 0.290 | 0.260 | 0.260 | 0.280 | 0.330 | 0.380 | 0.450 | 0.520 | 0.580 | 0.620 | 0.600 | 0.520 | 0.380 | 0.220 | 0.092 | 0.023 |
| 177 | 1.780 | 1.840 | 1.880 | 1.900 | 1.920 | 1.930 | 1.940 | 1.940 | 1.930 | 1.880 | 1.790 | 1.670 | 1.510 | 1.350 | 1.200 | 1.080 | 0.990 | 0.910 | 0.820 | 0.710 | 0.580 | 0.440 | 0.310 | 0.200 | 0.110 | 0.051 |
| 178 | 1.740 | 1.680 | 1.610 | 1.510 | 1.420 | 1.340 | 1.270 | 1.230 | 1.190 | 1.150 | 1.110 | 1.060 | 0.990 | 0.920 | 0.850 | 0.800 | 0.780 | 0.760 | 0.740 | 0.690 | 0.600 | 0.470 | 0.320 | 0.180 | 0.078 | 0.023 |
| 179 | 1.340 | 1.190 | 1.040 | 0.900 | 0.790 | 0.700 | 0.620 | 0.550 | 0.470 | 0.390 | 0.330 | 0.300 | 0.290 | 0.320 | 0.370 | 0.440 | 0.530 | 0.630 | 0.720 | 0.770 | 0.730 | 0.610 | 0.420 | 0.230 | 0.086 | 0.020 |
| 180 | 1.930 | 1.930 | 1.880 | 1.810 | 1.730 | 1.670 | 1.640 | 1.610 | 1.580 | 1.540 | 1.460 | 1.360 | 1.260 | 1.150 | 1.060 | 0.970 | 0.890 | 0.810 | 0.730 | 0.640 | 0.560 | 0.470 | 0.380 | 0.290 | 0.190 | 0.096 |
| 181 | 1.750 | 1.680 | 1.600 | 1.510 | 1.450 | 1.390 | 1.340 | 1.270 | 1.180 | 1.080 | 0.970 | 0.880 | 0.820 | 0.770 | 0.740 | 0.720 | 0.710 | 0.700 | 0.690 | 0.690 | 0.670 | 0.610 | 0.500 | 0.360 | 0.200 | 0.083 |
| 182 | 1.570 | 1.600 | 1.620 | 1.630 | 1.620 | 1.610 | 1.580 | 1.550 | 1.500 | 1.440 | 1.370 | 1.290 | 1.190 | 1.080 | 0.980 | 0.900 | 0.850 | 0.800 | 0.750 | 0.680 | 0.580 | 0.460 | 0.320 | 0.190 | 0.091 | 0.030 |
| 183 | 1.450 | 1.380 | 1.260 | 1.110 | 0.950 | 0.790 | 0.650 | 0.530 | 0.430 | 0.350 | 0.280 | 0.230 | 0.190 | 0.160 | 0.140 | 0.120 | 0.100 | 0.072 | 0.039 | 0.014 | 0.003 | 0.000 | 0.000 | 0.000 | 0.000 | 0.000 |
| 184 | 1.910 | 1.860 | 1.800 | 1.720 | 1.650 | 1.570 | 1.490 | 1.410 | 1.310 | 1.220 | 1.130 | 1.050 | 0.990 | 0.930 | 0.890 | 0.860 | 0.840 | 0.820 | 0.810 | 0.780 | 0.720 | 0.620 | 0.480 | 0.320 | 0.170 | 0.068 |
| 185 | 2.080 | 1.990 | 1.900 | 1.810 | 1.720 | 1.650 | 1.580 | 1.510 | 1.420 | 1.330 | 1.240 | 1.170 | 1.110 | 1.060 | 1.020 | 0.980 | 0.940 | 0.880 | 0.820 | 0.740 | 0.640 | 0.530 | 0.390 | 0.260 | 0.130 | 0.047 |
| 186 | 2.120 | 2.020 | 1.890 | 1.750 | 1.630 | 1.510 | 1.410 | 1.330 | 1.250 | 1.170 | 1.090 | 1.020 | 0.950 | 0.890 | 0.840 | 0.800 | 0.770 | 0.760 | 0.770 | 0.790 | 0.780 | 0.720 | 0.600 | 0.430 | 0.240 | 0.094 |
| 187 | 1.980 | 1.890 | 1.790 | 1.690 | 1.600 | 1.500 | 1.400 | 1.260 | 1.080 | 0.890 | 0.700 | 0.560 | 0.480 | 0.420 | 0.390 | 0.370 | 0.380 | 0.410 | 0.470 | 0.530 | 0.560 | 0.530 | 0.430 | 0.280 | 0.140 | 0.050 |
| 188 | 2.210 | 2.100 | 1.960 | 1.800 | 1.630 | 1.470 | 1.320 | 1.180 | 1.050 | 0.940 | 0.830 | 0.740 | 0.660 | 0.590 | 0.540 | 0.510 | 0.480 | 0.460 | 0.430 | 0.380 | 0.330 | 0.270 | 0.200 | 0.140 | 0.086 | 0.041 |
| 189 | 1.610 | 1.500 | 1.350 | 1.180 | 1.020 | 0.890 | 0.800 | 0.750 | 0.740 | 0.730 | 0.720 | 0.700 | 0.680 | 0.670 | 0.690 | 0.730 | 0.790 | 0.830 | 0.770 | 0.660 | 0.510 | 0.360 | 0.230 | 0.120 | 0.048 | |
| 190 | 1.810 | 1.730 | 1.630 | 1.530 | 1.440 | 1.360 | 1.300 | 1.240 | 1.170 | 1.110 | 1.040 | 0.980 | 0.920 | 0.890 | 0.870 | 0.870 | 0.870 | 0.870 | 0.840 | 0.770 | 0.660 | 0.510 | 0.360 | 0.210 | 0.095 | 0.031 |
| 191 | 1.700 | 1.500 | 1.310 | 1.130 | 0.990 | 0.880 | 0.780 | 0.680 | 0.570 | 0.470 | 0.370 | 0.300 | 0.250 | 0.220 | 0.210 | 0.220 | 0.220 | 0.230 | 0.210 | 0.190 | 0.140 | 0.087 | 0.035 | 0.007 | 0.001 | 0.000 |
| 192 | 1.620 | 1.500 | 1.360 | 1.230 | 1.110 | 1.000 | 0.900 | 0.800 | 0.720 | 0.650 | 0.600 | 0.570 | 0.580 | 0.600 | 0.650 | 0.690 | 0.730 | 0.750 | 0.740 | 0.690 | 0.600 | 0.470 | 0.330 | 0.190 | 0.088 | 0.027 |
| 193 | 1.740 | 1.560 | 1.360 | 1.160 | 0.970 | 0.810 | 0.670 | 0.560 | 0.470 | 0.390 | 0.330 | 0.290 | 0.260 | 0.240 | 0.240 | 0.250 | 0.290 | 0.360 | 0.440 | 0.500 | 0.510 | 0.440 | 0.310 | 0.160 | 0.056 | 0.010 |
| 194 | 0.820 | 0.760 | 0.680 | 0.590 | 0.490 | 0.400 | 0.350 | 0.330 | 0.330 | 0.360 | 0.400 | 0.430 | 0.450 | 0.490 | 0.530 | 0.600 | 0.670 | 0.730 | 0.760 | 0.710 | 0.610 | 0.460 | 0.310 | 0.190 | 0.038 | |
| 195 | 2.050 | 1.910 | 1.760 | 1.600 | 1.450 | 1.310 | 1.190 | 1.070 | 0.950 | 0.840 | 0.750 | 0.680 | 0.640 | 0.620 | 0.610 | 0.610 | 0.620 | 0.640 | 0.670 | 0.700 | 0.700 | 0.650 | 0.540 | 0.380 | 0.200 | 0.075 |
| 196 | 2.850 | 2.980 | 3.070 | 3.130 | 3.170 | 3.170 | 3.130 | 3.030 | 2.870 | 2.640 | 2.380 | 2.100 | 1.850 | 1.630 | 1.450 | 1.300 | 1.180 | 1.070 | 0.970 | 0.880 | 0.770 | 0.650 | 0.500 | 0.340 | 0.180 | 0.067 |
| 197 | 3.610 | 3.770 | 3.860 | 3.870 | 3.800 | 3.640 | 3.400 | 3.090 | 2.730 | 2.350 | 1.970 | 1.620 | 1.340 | 1.120 | 0.970 | 0.880 | 0.830 | 0.800 | 0.770 | 0.720 | 0.630 | 0.500 | 0.350 | 0.200 | 0.087 | 0.025 |
| 198 | 1.970 | 2.110 | 2.280 | 2.500 | 2.750 | 3.030 | 3.320 | 3.610 | 3.870 | 4.070 | 4.130 | 3.970 | 3.560 | 2.910 | 2.150 | 1.440 | 0.940 | 0.660 | 0.510 | 0.410 | 0.340 | 0.290 | 0.250 | 0.210 | 0.160 | 0.100 |
| 199 | 1.280 | 1.090 | 0.920 | 0.790 | 0.700 | 0.640 | 0.590 | 0.540 | 0.470 | 0.400 | 0.350 | 0.320 | 0.330 | 0.360 | 0.400 | 0.440 | 0.460 | 0.450 | 0.430 | 0.380 | 0.310 | 0.230 | 0.150 | 0.082 | 0.041 | 0.018 |
| 200 | 1.480 | 1.330 | 1.180 | 1.040 | 0.930 | 0.830 | 0.740 | 0.650 | 0.560 | 0.470 | 0.410 | 0.380 | 0.350 | 0.340 | 0.320 | 0.310 | 0.310 | 0.340 | 0.380 | 0.420 | 0.430 | 0.410 | 0.330 | 0.230 | 0.120 | 0.041 |
| 201 | 1.720 | 1.600 | 1.450 | 1.300 | 1.160 | 1.030 | 0.920 | 0.830 | 0.760 | 0.710 | 0.660 | 0.610 | 0.550 | 0.470 | 0.380 | 0.280 | 0.190 | 0.110 | 0.040 | 0.008 | 0.001 | 0.000 | 0.000 | 0.000 | 0.000 | 0.000 |
| 202 | 1.760 | 1.780 | 1.800 | 1.840 | 1.910 | 2.010 | 2.150 | 2.290 | 2.410 | 2.510 | 2.560 | 2.570 | 2.520 | 2.420 | 2.280 | 2.090 | 1.870 | 1.640 | 1.440 | 1.260 | 1.120 | 0.970 | 0.800 | 0.580 | 0.340 | 0.150 |
| 203 | 1.860 | 1.850 | 1.840 | 1.830 | 1.850 | 1.900 | 2.000 | 2.140 | 2.290 | 2.450 | 2.600 | 2.710 | 2.770 | 2.770 | 2.680 | 2.520 | 2.280 | 1.990 | 1.700 | 1.440 | 1.270 | 1.140 | 1.030 | 0.880 | 0.660 | 0.400 |
| 204 | 1.350 | 1.420 | 1.520 | 1.660 | 1.860 | 2.150 | 2.540 | 3.020 | 3.550 | 4.070 | 4.510 | 4.770 | 4.820 | 4.640 | 4.270 | 3.770 | 3.230 | 2.700 | 2.230 | 1.830 | 1.500 | 1.220 | 1.000 | 0.820 | 0.680 | 0.560 |
| 205 | 2.400 | 2.630 | 2.870 | 3.130 | 3.420 | 3.740 | 4.050 | 4.320 | 4.510 | 4.570 | 4.470 | 4.230 | 3.860 | 3.410 | 2.940 | 2.490 | 2.090 | 1.760 | 1.480 | 1.230 | 1.010 | 0.800 | 0.620 | 0.480 | 0.380 | 0.320 |
| 206 | 1.690 | 1.870 | 2.090 | 2.360 | 2.710 | 3.160 | 3.670 | 4.230 | 4.740 | 5.140 | 5.340 | 5.280 | 4.940 | 4.390 | 3.710 | 3.010 | 2.380 | 1.880 | 1.520 | 1.250 | 1.040 | 0.870 | 0.740 | 0.630 | 0.560 | 0.510 |
| 207 | 0.920 | 1.050 | 1.210 | 1.430 | 1.740 | 2.210 | 2.850 | 3.700 | 4.700 | 5.760 | 6.740 | 7.460 | 7.760 | 7.570 | 6.910 | 5.890 | 4.690 | 3.480 | 2.410 | 1.580 | 1.020 | 0.680 | 0.520 | 0.450 | 0.420 | 0.370 |
| 208 | 1.310 | 1.330 | 1.360 | 1.420 | 1.530 | 1.710 | 2.000 | 2.400 | 2.900 | 3.470 | 4.030 | 4.520 | 4.820 | 4.880 | 4.680 | 4.230 | 3.620 | 2.920 | 2.250 | 1.660 | 1.200 | 0.890 | 0.710 | 0.610 | 0.560 | 0.520 |
| 209 | 1.260 | 1.300 | 1.350 | 1.430 | 1.570 | 1.800 | 2.160 | 2.640 | 3.240 | 3.900 | 4.550 | 5.070 | 5.380 | 5.400 | 5.120 | 4.590 | 3.880 | 3.120 | 2.390 | 1.770 | 1.280 | 0.950 | 0.750 | 0.650 | 0.600 | 0.570 |
| 210 | 1.550 | 1.550 | 1.550 | 1.590 | 1.690 | 1.860 | 2.110 | 2.440 | 2.840 | 3.280 | 3.720 | 4.080 | 4.300 | 4.330 | 4.140 | 3.750 | 3.210 | 2.590 | 1.990 | 1.480 | 1.110 | 0.890 | 0.770 | 0.710 | 0.650 | 0.550 |
| 211 | 1.275 | 1.300 | 1.330 | 1.395 | 1.515 | 1.700 | 1.965 | 2.320 | 2.7 | | | | | | | | | | | | | | | | | |

| ID | Performance Metrics | | | | | | | | | | | | | | | | | | | | | | | | | |
|-----|---------------------|-------|-------|-------|-------|-------|-------|-------|-------|-------|-------|-------|-------|-------|-------|-------|-------|-------|-------|-------|-------|-------|-------|-------|-------|-------|
| | 5.325 | 5.191 | 5.056 | 4.921 | 4.786 | 4.652 | 4.518 | 4.383 | 4.248 | 4.114 | 3.979 | 3.844 | 3.710 | 3.575 | 3.441 | 3.306 | 3.171 | 3.037 | 2.903 | 2.768 | 2.633 | 2.500 | 2.364 | 2.230 | 2.095 | 1.961 |
| 218 | 0.980 | 1.100 | 1.280 | 1.540 | 1.940 | 2.540 | 3.370 | 4.390 | 5.490 | 6.520 | 7.270 | 7.570 | 7.340 | 6.610 | 5.530 | 4.310 | 3.150 | 2.220 | 1.550 | 1.120 | 0.850 | 0.690 | 0.580 | 0.520 | 0.480 | 0.450 |
| 219 | 1.100 | 1.260 | 1.460 | 1.760 | 2.210 | 2.840 | 3.660 | 4.630 | 5.660 | 6.590 | 7.250 | 7.490 | 7.230 | 6.510 | 5.450 | 4.250 | 3.100 | 2.140 | 1.430 | 0.960 | 0.670 | 0.520 | 0.440 | 0.410 | 0.390 | 0.360 |
| 220 | 0.890 | 1.030 | 1.230 | 1.530 | 1.980 | 2.620 | 3.490 | 4.530 | 5.670 | 6.750 | 7.590 | 8.020 | 7.950 | 7.370 | 6.380 | 5.150 | 3.890 | 2.760 | 1.850 | 1.200 | 0.780 | 0.530 | 0.400 | 0.350 | 0.350 | 0.350 |
| 221 | 1.620 | 1.750 | 1.920 | 2.140 | 2.480 | 2.930 | 3.510 | 4.170 | 4.840 | 5.400 | 5.740 | 5.780 | 5.490 | 4.900 | 4.120 | 3.280 | 2.500 | 1.840 | 1.350 | 1.000 | 0.760 | 0.600 | 0.490 | 0.420 | 0.380 | 0.330 |
| 222 | 1.900 | 2.170 | 2.490 | 2.880 | 3.350 | 3.880 | 4.460 | 5.030 | 5.510 | 5.820 | 5.890 | 5.680 | 5.200 | 4.520 | 3.720 | 2.930 | 2.230 | 1.670 | 1.250 | 0.940 | 0.700 | 0.530 | 0.410 | 0.350 | 0.320 | 0.310 |
| 223 | 2.990 | 3.450 | 3.930 | 4.410 | 4.830 | 5.170 | 5.380 | 5.420 | 5.260 | 4.900 | 4.370 | 3.730 | 3.050 | 2.390 | 1.830 | 1.390 | 1.070 | 0.850 | 0.700 | 0.570 | 0.460 | 0.360 | 0.270 | 0.210 | 0.170 | 0.140 |
| 224 | 2.780 | 3.110 | 3.460 | 3.840 | 4.220 | 4.540 | 4.770 | 4.840 | 4.740 | 4.450 | 4.020 | 3.510 | 2.980 | 2.490 | 2.080 | 1.750 | 1.490 | 1.280 | 1.080 | 0.890 | 0.710 | 0.540 | 0.400 | 0.310 | 0.240 | 0.190 |
| 225 | 2.600 | 2.820 | 3.080 | 3.370 | 3.690 | 4.050 | 4.390 | 4.670 | 4.840 | 4.830 | 4.620 | 4.220 | 3.670 | 3.040 | 2.420 | 1.870 | 1.430 | 1.100 | 0.860 | 0.670 | 0.510 | 0.380 | 0.280 | 0.210 | 0.160 | 0.130 |
| 226 | 1.910 | 2.090 | 2.290 | 2.510 | 2.780 | 3.090 | 3.450 | 3.860 | 4.280 | 4.670 | 4.990 | 5.170 | 5.150 | 4.920 | 4.490 | 3.890 | 3.200 | 2.490 | 1.840 | 1.290 | 0.870 | 0.600 | 0.430 | 0.350 | 0.310 | 0.280 |
| 227 | 2.770 | 2.970 | 3.170 | 3.360 | 3.540 | 3.700 | 3.830 | 3.930 | 3.950 | 3.880 | 3.700 | 3.410 | 3.040 | 2.630 | 2.230 | 1.880 | 1.600 | 1.380 | 1.180 | 0.990 | 0.780 | 0.560 | 0.380 | 0.240 | 0.160 | 0.110 |
| 228 | 2.850 | 3.080 | 3.320 | 3.540 | 3.750 | 3.940 | 4.070 | 4.140 | 4.110 | 3.970 | 3.730 | 3.390 | 2.990 | 2.570 | 2.180 | 1.820 | 1.530 | 1.270 | 1.050 | 0.830 | 0.620 | 0.420 | 0.280 | 0.190 | 0.140 | 0.130 |
| 229 | 2.770 | 2.880 | 2.980 | 3.060 | 3.140 | 3.200 | 3.250 | 3.270 | 3.250 | 3.170 | 3.030 | 2.830 | 2.590 | 2.300 | 2.000 | 1.700 | 1.420 | 1.160 | 0.940 | 0.740 | 0.580 | 0.430 | 0.300 | 0.190 | 0.100 | 0.042 |
| 230 | 3.140 | 3.250 | 3.330 | 3.360 | 3.370 | 3.340 | 3.290 | 3.180 | 3.030 | 2.830 | 2.580 | 2.310 | 2.030 | 1.770 | 1.520 | 1.310 | 1.130 | 0.980 | 0.840 | 0.720 | 0.580 | 0.440 | 0.290 | 0.160 | 0.066 | 0.016 |
| 231 | 2.730 | 2.920 | 3.110 | 3.310 | 3.520 | 3.730 | 3.920 | 4.080 | 4.170 | 4.160 | 4.030 | 3.790 | 3.440 | 3.010 | 2.540 | 2.050 | 1.580 | 1.150 | 0.780 | 0.480 | 0.280 | 0.160 | 0.100 | 0.080 | 0.071 | 0.064 |
| 232 | 2.380 | 2.630 | 2.880 | 3.140 | 3.410 | 3.710 | 4.010 | 4.300 | 4.550 | 4.730 | 4.810 | 4.750 | 4.540 | 4.180 | 3.700 | 3.150 | 2.570 | 2.010 | 1.500 | 1.080 | 0.750 | 0.510 | 0.360 | 0.280 | 0.240 | 0.210 |
| 233 | 2.520 | 2.760 | 3.000 | 3.240 | 3.480 | 3.730 | 3.970 | 4.200 | 4.390 | 4.500 | 4.500 | 4.380 | 4.120 | 3.740 | 3.280 | 2.780 | 2.270 | 1.800 | 1.390 | 1.020 | 0.720 | 0.490 | 0.340 | 0.240 | 0.180 | 0.140 |
| 234 | 2.610 | 2.800 | 2.980 | 3.170 | 3.360 | 3.570 | 3.770 | 3.940 | 4.050 | 4.080 | 3.990 | 3.790 | 3.480 | 3.080 | 2.650 | 2.200 | 1.790 | 1.420 | 1.090 | 0.810 | 0.570 | 0.390 | 0.270 | 0.210 | 0.170 | 0.150 |
| 235 | 2.620 | 2.870 | 3.110 | 3.340 | 3.570 | 3.810 | 4.040 | 4.250 | 4.410 | 4.490 | 4.470 | 4.310 | 4.020 | 3.620 | 3.130 | 2.620 | 2.130 | 1.680 | 1.280 | 0.940 | 0.640 | 0.410 | 0.240 | 0.150 | 0.110 | 0.110 |
| 236 | 2.910 | 3.100 | 3.270 | 3.410 | 3.550 | 3.670 | 3.770 | 3.850 | 3.870 | 3.830 | 3.710 | 3.530 | 3.270 | 2.950 | 2.570 | 2.150 | 1.710 | 1.280 | 0.900 | 0.620 | 0.420 | 0.290 | 0.200 | 0.140 | 0.100 | 0.078 |
| 237 | 2.800 | 3.040 | 3.270 | 3.490 | 3.710 | 3.920 | 4.100 | 4.250 | 4.330 | 4.320 | 4.210 | 3.980 | 3.660 | 3.250 | 2.790 | 2.310 | 1.860 | 1.450 | 1.100 | 0.790 | 0.540 | 0.340 | 0.210 | 0.130 | 0.100 | 0.100 |
| 238 | 2.340 | 2.550 | 2.760 | 2.980 | 3.220 | 3.490 | 3.780 | 4.070 | 4.330 | 4.530 | 4.630 | 4.610 | 4.440 | 4.120 | 3.670 | 3.130 | 2.560 | 1.990 | 1.470 | 1.020 | 0.670 | 0.430 | 0.290 | 0.220 | 0.190 | 0.170 |
| 239 | 2.100 | 2.320 | 2.540 | 2.790 | 3.070 | 3.380 | 3.720 | 4.070 | 4.410 | 4.700 | 4.890 | 4.930 | 4.800 | 4.500 | 4.040 | 3.480 | 2.860 | 2.250 | 1.690 | 1.200 | 0.810 | 0.530 | 0.360 | 0.270 | 0.230 | 0.200 |
| 240 | 2.280 | 2.430 | 2.580 | 2.740 | 2.930 | 3.160 | 3.410 | 3.660 | 3.890 | 4.040 | 4.090 | 4.000 | 3.770 | 3.400 | 2.950 | 2.450 | 1.950 | 1.490 | 1.090 | 0.770 | 0.530 | 0.360 | 0.250 | 0.190 | 0.140 | 0.100 |
| 241 | 1.660 | 1.530 | 1.390 | 1.230 | 1.080 | 0.940 | 0.820 | 0.740 | 0.680 | 0.640 | 0.610 | 0.580 | 0.560 | 0.540 | 0.530 | 0.550 | 0.570 | 0.580 | 0.570 | 0.530 | 0.440 | 0.340 | 0.230 | 0.140 | 0.069 | 0.027 |
| 242 | 2.530 | 2.470 | 2.360 | 2.250 | 2.170 | 2.120 | 2.100 | 2.080 | 2.020 | 1.870 | 1.630 | 1.330 | 1.050 | 0.840 | 0.700 | 0.610 | 0.540 | 0.490 | 0.450 | 0.430 | 0.400 | 0.350 | 0.270 | 0.180 | 0.095 | 0.034 |
| 243 | 2.380 | 2.400 | 2.420 | 2.440 | 2.460 | 2.500 | 2.540 | 2.560 | 2.530 | 2.530 | 2.450 | 2.320 | 2.150 | 1.950 | 1.740 | 1.540 | 1.360 | 1.210 | 1.070 | 0.940 | 0.790 | 0.610 | 0.430 | 0.250 | 0.110 | 0.033 |
| 244 | 2.430 | 2.480 | 2.520 | 2.570 | 2.660 | 2.760 | 2.880 | 2.980 | 3.030 | 3.000 | 2.900 | 2.710 | 2.450 | 2.160 | 1.850 | 1.540 | 1.270 | 1.050 | 0.880 | 0.750 | 0.650 | 0.560 | 0.460 | 0.350 | 0.220 | 0.110 |
| 245 | 2.480 | 2.470 | 2.460 | 2.470 | 2.510 | 2.580 | 2.650 | 2.700 | 2.690 | 2.620 | 2.490 | 2.310 | 2.100 | 1.860 | 1.600 | 1.320 | 1.050 | 0.800 | 0.600 | 0.460 | 0.370 | 0.310 | 0.250 | 0.190 | 0.043 | |
| 246 | 2.610 | 2.550 | 2.470 | 2.400 | 2.350 | 2.320 | 2.310 | 2.280 | 2.220 | 2.130 | 1.990 | 1.830 | 1.630 | 1.410 | 1.170 | 0.930 | 0.680 | 0.470 | 0.300 | 0.210 | 0.160 | 0.140 | 0.120 | 0.088 | 0.051 | 0.020 |
| 247 | 2.290 | 2.230 | 2.170 | 2.120 | 2.100 | 2.100 | 2.100 | 2.060 | 2.000 | 1.910 | 1.810 | 1.700 | 1.600 | 1.510 | 1.410 | 1.330 | 1.250 | 1.190 | 1.140 | 1.060 | 0.920 | 0.720 | 0.490 | 0.250 | 0.091 | |
| 248 | 2.300 | 2.300 | 2.300 | 2.340 | 2.410 | 2.530 | 2.680 | 2.820 | 2.920 | 2.950 | 2.870 | 2.710 | 2.450 | 2.140 | 1.790 | 1.440 | 1.120 | 0.850 | 0.660 | 0.530 | 0.450 | 0.390 | 0.330 | 0.260 | 0.170 | 0.085 |
| 249 | 2.380 | 2.430 | 2.470 | 2.530 | 2.610 | 2.730 | 2.870 | 2.990 | 3.080 | 3.080 | 2.990 | 2.800 | 2.510 | 2.170 | 1.800 | 1.440 | 1.120 | 0.860 | 0.650 | 0.510 | 0.420 | 0.370 | 0.340 | 0.300 | 0.240 | 0.160 |
| 250 | 2.450 | 2.470 | 2.490 | 2.520 | 2.590 | 2.700 | 2.830 | 2.960 | 3.060 | 3.100 | 3.060 | 2.930 | 2.720 | 2.430 | 2.090 | 1.730 | 1.380 | 1.070 | 0.820 | 0.630 | 0.480 | 0.360 | 0.260 | 0.170 | 0.090 | 0.036 |
| 251 | 2.670 | 2.620 | 2.540 | 2.430 | 2.330 | 2.240 | 2.160 | 2.080 | 1.990 | 1.870 | 1.730 | 1.570 | 1.410 | 1.270 | 1.150 | 1.060 | 0.990 | 0.940 | 0.890 | 0.840 | 0.770 | 0.660 | 0.520 | 0.350 | 0.190 | 0.076 |
| 252 | 2.440 | 2.410 | 2.360 | 2.310 | 2.280 | 2.260 | 2.250 | 2.230 | 2.180 | 2.090 | 1.950 | 1.780 | 1.600 | 1.410 | 1.240 | 1.100 | 0.990 | 0.930 | 0.890 | 0.850 | 0.790 | 0.670 | 0.500 | 0.320 | 0.150 | 0.050 |
| 253 | 2.340 | 2.450 | 2.560 | 2.700 | 2.860 | 3.060 | 3.270 | 3.480 | 3.630 | 3.690 | 3.620 | 3.420 | 3.100 | 2.690 | 2.250 | 1.800 | 1.390 | 1.040 | 0.760 | 0.560 | 0.420 | 0.310 | 0.230 | 0.150 | 0.083 | 0.032 |
| 254 | 2.310 | 2.380 | 2.470 | 2.600 | 2.770 | 2.960 | 3.160 | 3.330 | 3.440 | 3.470 | 3.390 | 3.200 | 2.910 | 2.550 | 2.150 | 1.750 | 1.390 | 1.090 | 0.860 | 0.690 | 0.570 | 0.470 | 0.370 | 0.260 | 0.150 | 0.065 |
| 255 | 2.600 | 2.690 | 2.770 | 2.840 | 2.930 | 3.020 | 3.110 | 3.190 | 3.220 | 3.170 | 3.040 | 2.820 | 2.510 | 2.160 | 1.790 | 1. | | | | | | | | | | |

| ID | 5.325 | 5.191 | 5.056 | 4.921 | 4.786 | 4.652 | 4.518 | 4.383 | 4.248 | 4.114 | 3.979 | 3.844 | 3.710 | 3.575 | 3.441 | 3.306 | 3.171 | 3.037 | 2.903 | 2.768 | 2.633 | 2.500 | 2.364 | 2.230 | 2.095 | 1.961 |
|-----|-------|-------|-------|-------|-------|-------|-----------|-------|-------|-------|-------|-------|-------|-------|-------|-------|-------|-------|-------|-------|-------|-------|-------|-------|-------|-------|
| 263 | 2.700 | 2.710 | 2.710 | 2.710 | 2.710 | 2.720 | 2.730 | 2.730 | 2.710 | 2.640 | 2.520 | 2.350 | 2.140 | 1.920 | 1.690 | 1.480 | 1.270 | 1.070 | 0.890 | 0.720 | 0.580 | 0.450 | 0.330 | 0.200 | 0.096 | 0.030 |
| 264 | 2.960 | 3.010 | 3.060 | 3.100 | 3.150 | 3.210 | 3.270 | 3.290 | 3.260 | 3.140 | 2.940 | 2.680 | 2.370 | 2.040 | 1.730 | 1.450 | 1.200 | 1.000 | 0.830 | 0.680 | 0.560 | 0.440 | 0.330 | 0.230 | 0.130 | 0.059 |
| 265 | 3.000 | 3.090 | 3.150 | 3.200 | 3.230 | 3.260 | 3.290 | 3.290 | 3.250 | 3.160 | 2.980 | 2.730 | 2.410 | 2.050 | 1.690 | 1.370 | 1.090 | 0.860 | 0.680 | 0.530 | 0.400 | 0.290 | 0.200 | 0.140 | 0.092 | 0.052 |
| 266 | 1.520 | 1.470 | 1.410 | 1.340 | 1.290 | 1.250 | 1.220 | 1.190 | 1.150 | 1.090 | 1.010 | 0.910 | 0.810 | 0.710 | 0.620 | 0.540 | 0.470 | 0.410 | 0.350 | 0.290 | 0.240 | 0.180 | 0.130 | 0.090 | 0.053 | 0.025 |
| 267 | 1.960 | 2.100 | 2.260 | 2.470 | 2.740 | 3.090 | 3.510 | 3.950 | 4.380 | 4.740 | 4.960 | 4.980 | 4.770 | 4.360 | 3.790 | 3.140 | 2.490 | 1.900 | 1.410 | 1.010 | 0.700 | 0.470 | 0.320 | 0.230 | 0.180 | 0.160 |
| 268 | 2.860 | 2.920 | 2.970 | 3.010 | 3.080 | 3.160 | 3.250 | 3.330 | 3.370 | 3.330 | 3.200 | 2.980 | 2.680 | 2.340 | 1.990 | 1.660 | 1.380 | 1.140 | 0.940 | 0.780 | 0.630 | 0.510 | 0.400 | 0.310 | 0.230 | 0.150 |
| 269 | 2.940 | 3.050 | 3.150 | 3.250 | 3.360 | 3.490 | 3.600 | 3.680 | 3.700 | 3.610 | 3.410 | 3.110 | 2.710 | 2.270 | 1.820 | 1.420 | 1.080 | 0.840 | 0.670 | 0.560 | 0.480 | 0.400 | 0.310 | 0.210 | 0.110 | 0.039 |
| 270 | 2.670 | 2.760 | 2.830 | 2.880 | 2.920 | 2.950 | 2.970 | 2.970 | 2.930 | 2.840 | 2.670 | 2.440 | 2.160 | 1.850 | 1.570 | 1.320 | 1.130 | 0.970 | 0.840 | 0.710 | 0.590 | 0.470 | 0.350 | 0.250 | 0.160 | 0.082 |
| 271 | 2.730 | 2.740 | 2.720 | 2.710 | 2.690 | 2.650 | 2.590 | 2.490 | 2.350 | 2.160 | 1.950 | 1.730 | 1.520 | 1.320 | 1.140 | 0.980 | 0.840 | 0.730 | 0.640 | 0.580 | 0.520 | 0.470 | 0.390 | 0.290 | 0.180 | 0.082 |
| 272 | 2.420 | 2.440 | 2.420 | 2.380 | 2.340 | 2.290 | 2.240 | 2.180 | 2.100 | 2.000 | 1.870 | 1.730 | 1.580 | 1.440 | 1.320 | 1.230 | 1.150 | 1.100 | 1.050 | 0.990 | 0.880 | 0.720 | 0.530 | 0.330 | 0.160 | 0.055 |
| 273 | 1.490 | 1.440 | 1.350 | 1.260 | 1.190 | 1.150 | 1.120 | 1.090 | 1.050 | 0.980 | 0.910 | 0.840 | 0.780 | 0.740 | 0.720 | 0.700 | 0.670 | 0.630 | 0.570 | 0.500 | 0.430 | 0.350 | 0.270 | 0.190 | 0.110 | 0.049 |
| 274 | 2.190 | 2.160 | 2.100 | 2.010 | 1.930 | 1.860 | 1.800 | 1.740 | 1.660 | 1.560 | 1.440 | 1.310 | 1.170 | 1.050 | 0.940 | 0.840 | 0.760 | 0.690 | 0.620 | 0.540 | 0.470 | 0.390 | 0.300 | 0.210 | 0.130 | 0.064 |
| 275 | 2.080 | 2.070 | 2.030 | 1.980 | 1.930 | 1.880 | 1.810 | 1.730 | 1.620 | 1.490 | 1.350 | 1.210 | 1.080 | 0.970 | 0.890 | 0.820 | 0.770 | 0.760 | 0.760 | 0.750 | 0.710 | 0.610 | 0.460 | 0.280 | 0.130 | 0.041 |
| 276 | 2.060 | 2.050 | 2.030 | 2.000 | 1.960 | 1.920 | 1.860 | 1.770 | 1.670 | 1.560 | 1.440 | 1.330 | 1.230 | 1.130 | 1.050 | 0.980 | 0.910 | 0.860 | 0.810 | 0.750 | 0.660 | 0.540 | 0.390 | 0.230 | 0.100 | 0.029 |
| 277 | 2.010 | 2.010 | 1.980 | 1.920 | 1.850 | 1.770 | 1.700 | 1.620 | 1.540 | 1.440 | 1.330 | 1.200 | 1.080 | 0.970 | 0.890 | 0.830 | 0.810 | 0.820 | 0.860 | 0.880 | 0.860 | 0.770 | 0.610 | 0.410 | 0.210 | 0.074 |
| 278 | 1.950 | 1.960 | 1.950 | 1.930 | 1.890 | 1.840 | 1.770 | 1.700 | 1.610 | 1.520 | 1.390 | 1.230 | 1.030 | 0.820 | 0.650 | 0.550 | 0.540 | 0.570 | 0.610 | 0.650 | 0.670 | 0.630 | 0.520 | 0.380 | 0.210 | 0.086 |
| 279 | 2.000 | 2.040 | 2.040 | 2.010 | 1.950 | 1.860 | 1.770 | 1.680 | 1.580 | 1.470 | 1.350 | 1.210 | 1.060 | 0.910 | 0.780 | 0.670 | 0.590 | 0.530 | 0.480 | 0.410 | 0.340 | 0.260 | 0.180 | 0.120 | 0.071 | 0.035 |
| 280 | 1.890 | 1.910 | 1.900 | 1.870 | 1.820 | 1.770 | 1.710 | 1.640 | 1.560 | 1.450 | 1.330 | 1.200 | 1.080 | 0.980 | 0.920 | 0.890 | 0.890 | 0.920 | 0.940 | 0.950 | 0.910 | 0.810 | 0.660 | 0.460 | 0.270 | 0.120 |
| 281 | 1.960 | 1.980 | 1.980 | 1.970 | 1.950 | 1.910 | 1.860 | 1.790 | 1.690 | 1.580 | 1.460 | 1.330 | 1.190 | 1.060 | 0.960 | 0.900 | 0.890 | 0.930 | 1.020 | 1.100 | 1.110 | 1.020 | 0.820 | 0.540 | 0.270 | 0.093 |
| 282 | 2.070 | 2.130 | 2.160 | 2.150 | 2.110 | 2.050 | 1.970 | 1.880 | 1.780 | 1.660 | 1.530 | 1.390 | 1.240 | 1.100 | 0.980 | 0.880 | 0.800 | 0.720 | 0.640 | 0.530 | 0.410 | 0.300 | 0.220 | 0.170 | 0.140 | 0.100 |
| 283 | 1.980 | 2.000 | 1.980 | 1.950 | 1.900 | 1.840 | 1.790 | 1.730 | 1.650 | 1.570 | 1.470 | 1.360 | 1.250 | 1.160 | 1.090 | 1.040 | 1.020 | 1.000 | 0.960 | 0.890 | 0.760 | 0.600 | 0.430 | 0.260 | 0.140 | 0.057 |
| 284 | 2.170 | 2.160 | 2.130 | 2.110 | 2.090 | 2.070 | 2.030 | 1.950 | 1.830 | 1.680 | 1.510 | 1.360 | 1.230 | 1.130 | 1.060 | 1.020 | 1.010 | 1.000 | 1.000 | 0.970 | 0.890 | 0.750 | 0.560 | 0.350 | 0.170 | 0.056 |
| 285 | 2.090 | 2.040 | 1.990 | 1.960 | 1.940 | 1.910 | 1.860 | 1.770 | 1.640 | 1.480 | 1.310 | 1.150 | 1.010 | 0.890 | 0.780 | 0.680 | 0.590 | 0.510 | 0.450 | 0.380 | 0.310 | 0.230 | 0.150 | 0.077 | 0.028 | 0.005 |
| 286 | 2.340 | 2.490 | 2.620 | 2.700 | 2.740 | 2.730 | 2.680 | 2.580 | 2.430 | 2.230 | 1.990 | 1.720 | 1.440 | 1.180 | 0.960 | 0.790 | 0.680 | 0.620 | 0.580 | 0.550 | 0.500 | 0.430 | 0.340 | 0.230 | 0.120 | 0.043 |
| 287 | 1.810 | 1.770 | 1.710 | 1.630 | 1.540 | 1.450 | 1.370 | 1.280 | 1.190 | 1.100 | 1.010 | 0.920 | 0.840 | 0.790 | 0.750 | 0.740 | 0.750 | 0.760 | 0.740 | 0.690 | 0.590 | 0.450 | 0.300 | 0.170 | 0.070 | 0.020 |
| 288 | 1.810 | 1.750 | 1.680 | 1.600 | 1.540 | 1.490 | 1.440 | 1.360 | 1.250 | 1.120 | 0.970 | 0.850 | 0.760 | 0.700 | 0.670 | 0.660 | 0.670 | 0.690 | 0.720 | 0.750 | 0.750 | 0.690 | 0.560 | 0.380 | 0.200 | 0.071 |
| 289 | 1.360 | 1.300 | 1.250 | 1.220 | 1.190 | 1.160 | 1.110 | 1.030 | 0.920 | 0.790 | 0.680 | 0.600 | 0.560 | 0.540 | 0.540 | 0.550 | 0.540 | 0.500 | 0.450 | 0.390 | 0.320 | 0.260 | 0.200 | 0.140 | 0.083 | 0.037 |
| 290 | 0.820 | 0.760 | 0.660 | 0.580 | 0.510 | 0.470 | 0.440 | 0.410 | 0.360 | 0.300 | 0.240 | 0.200 | 0.180 | 0.200 | 0.230 | 0.270 | 0.290 | 0.290 | 0.250 | 0.190 | 0.130 | 0.079 | 0.040 | 0.014 | 0.002 | 0.000 |
| 291 | 1.620 | 1.580 | 1.490 | 1.390 | 1.290 | 1.210 | 1.130 | 1.060 | 0.960 | 0.850 | 0.730 | 0.630 | 0.560 | 0.530 | 0.550 | 0.570 | 0.590 | 0.590 | 0.570 | 0.530 | 0.460 | 0.380 | 0.280 | 0.180 | 0.093 | 0.032 |
| 292 | 1.690 | 1.650 | 1.560 | 1.450 | 1.330 | 1.230 | 1.130 | 1.040 | 0.950 | 0.860 | 0.760 | 0.690 | 0.640 | 0.620 | 0.640 | 0.680 | 0.760 | 0.860 | 0.980 | 1.070 | 1.080 | 0.960 | 0.730 | 0.450 | 0.200 | 0.053 |
| 293 | 1.530 | 1.490 | 1.410 | 1.310 | 1.220 | 1.130 | 1.070 | 1.010 | 0.960 | 0.900 | 0.860 | 0.830 | 0.830 | 0.870 | 0.920 | 0.980 | 1.020 | 1.030 | 1.020 | 0.960 | 0.870 | 0.740 | 0.570 | 0.380 | 0.200 | 0.075 |
| 294 | 1.480 | 1.450 | 1.400 | 1.350 | 1.300 | 1.250 | 1.180 | 1.100 | 1.000 | 0.900 | 0.810 | 0.740 | 0.720 | 0.730 | 0.760 | 0.790 | 0.810 | 0.800 | 0.760 | 0.700 | 0.610 | 0.490 | 0.360 | 0.230 | 0.120 | 0.041 |
| 295 | 1.530 | 1.560 | 1.540 | 1.480 | 1.400 | 1.310 | 1.220 | 1.130 | 1.050 | 0.960 | 0.870 | 0.790 | 0.720 | 0.660 | 0.630 | 0.610 | 0.600 | 0.570 | 0.540 | 0.480 | 0.410 | 0.330 | 0.250 | 0.170 | 0.099 | 0.042 |
| 296 | 1.930 | 1.950 | 1.950 | 1.930 | 1.890 | 1.840 | 1.750 | 1.610 | 1.450 | 1.270 | 1.100 | 0.970 | 0.890 | 0.840 | 0.820 | 0.810 | 0.800 | 0.780 | 0.740 | 0.690 | 0.610 | 0.520 | 0.400 | 0.270 | 0.140 | 0.052 |
| 297 | 1.980 | 2.030 | 2.040 | 2.010 | 1.970 | 1.910 | 1.820 | 1.720 | 1.580 | 1.420 | 1.260 | 1.110 | 0.990 | 0.910 | 0.860 | 0.830 | 0.820 | 0.800 | 0.770 | 0.710 | 0.620 | 0.490 | 0.350 | 0.210 | 0.096 | 0.030 |
| 298 | 0.860 | 0.840 | 0.800 | 0.760 | 0.750 | 0.740 | 0.740 | 0.720 | 0.680 | 0.630 | 0.590 | 0.570 | 0.580 | 0.610 | 0.660 | 0.710 | 0.750 | 0.780 | 0.790 | 0.750 | 0.660 | 0.520 | 0.340 | 0.170 | 0.059 | 0.011 |
| 299 | 1.910 | 1.920 | 1.890 | 1.840 | 1.790 | 1.740 | 1.670 | 1.570 | 1.430 | 1.270 | 1.100 | 0.960 | 0.870 | 0.820 | 0.820 | 0.850 | 0.900 | 0.980 | 1.060 | 1.130 | 1.150 | 1.070 | 0.870 | 0.590 | 0.310 | 0.110 |
| 300 | 1.390 | 1.360 | 1.300 | 1.240 | 1.160 | 1.090 | 1.020 | 0.940 | 0.860 | 0.790 | 0.720 | 0.670 | 0.640 | 0.630 | 0.650 | 0.680 | 0.710 | 0.720 | 0.700 | 0.630 | 0.530 | 0.410 | 0.300 | 0.190 | 0.110 | 0.047 |
| 301 | 1.630 | 1.550 | 1.450 | 1.360 | 1.280 | 1.210 | 1.140</td | | | | | | | | | | | | | | | | | | | |

| ID | 5.325 | 5.191 | 5.056 | 4.921 | 4.786 | 4.652 | 4.518 | 4.383 | 4.248 | 4.114 | 3.979 | 3.844 | 3.710 | 3.575 | 3.441 | 3.306 | 3.171 | 3.037 | 2.903 | 2.768 | 2.633 | 2.500 | 2.364 | 2.230 | 2.095 | 1.961 | |
|--------------|-------|-------|-------|-------|-------|-------|-------|-------|-------|-------|-------|-------|-------|-----------|-------|-------|-------|-------|-------|-------|-------|-------|-------|-------|-------|-------|--|
| 308 | 1.580 | 1.480 | 1.380 | 1.320 | 1.310 | 1.330 | 1.340 | 1.320 | 1.230 | 1.100 | 0.950 | 0.820 | 0.720 | 0.660 | 0.620 | 0.590 | 0.550 | 0.510 | 0.460 | 0.410 | 0.350 | 0.300 | 0.250 | 0.200 | 0.160 | 0.110 | |
| 309 | 1.800 | 1.800 | 1.790 | 1.780 | 1.780 | 1.770 | 1.740 | 1.690 | 1.610 | 1.500 | 1.390 | 1.270 | 1.160 | 1.060 | 0.980 | 0.900 | 0.840 | 0.780 | 0.730 | 0.680 | 0.610 | 0.510 | 0.390 | 0.250 | 0.130 | 0.043 | |
| 310 | 1.830 | 1.810 | 1.780 | 1.730 | 1.690 | 1.650 | 1.600 | 1.530 | 1.430 | 1.310 | 1.180 | 1.060 | 0.940 | 0.840 | 0.760 | 0.690 | 0.640 | 0.610 | 0.600 | 0.610 | 0.580 | 0.490 | 0.360 | 0.210 | 0.085 | | |
| 311 | 2.470 | 2.490 | 2.510 | 2.520 | 2.530 | 2.520 | 2.480 | 2.390 | 2.240 | 2.050 | 1.850 | 1.660 | 1.490 | 1.360 | 1.240 | 1.130 | 1.020 | 0.910 | 0.810 | 0.720 | 0.650 | 0.590 | 0.510 | 0.400 | 0.270 | 0.140 | |
| 312 | 2.630 | 2.720 | 2.780 | 2.800 | 2.800 | 2.770 | 2.690 | 2.570 | 2.400 | 2.190 | 1.950 | 1.690 | 1.440 | 1.230 | 1.050 | 0.910 | 0.810 | 0.740 | 0.670 | 0.600 | 0.530 | 0.450 | 0.360 | 0.280 | 0.190 | 0.110 | |
| P15 | | | | | | | | | | | | | | | | | | | | | | | | | | | |
| 324 | 1.120 | 1.230 | 1.370 | 1.580 | 1.890 | 2.330 | 2.910 | 3.580 | 4.290 | 4.930 | 5.370 | 5.520 | 5.360 | 4.920 | 4.300 | 3.620 | 2.980 | 2.410 | 1.910 | 1.450 | 1.020 | 0.680 | 0.450 | 0.340 | 0.330 | 0.380 | |
| 325 | 1.330 | 1.500 | 1.700 | 1.960 | 2.310 | 2.780 | 3.360 | 4.030 | 4.720 | 5.330 | 5.760 | 5.920 | 5.760 | 5.320 | 4.650 | 3.890 | 3.130 | 2.450 | 1.900 | 1.460 | 1.100 | 0.820 | 0.590 | 0.430 | 0.320 | 0.240 | |
| 326 | 0.820 | 0.950 | 1.120 | 1.370 | 1.720 | 2.180 | 2.760 | 3.410 | 4.090 | 4.720 | 5.230 | 5.540 | 5.650 | 5.540 | 5.260 | 4.870 | 4.430 | 3.970 | 3.520 | 3.060 | 2.610 | 2.180 | 1.780 | 1.440 | 1.140 | 0.880 | |
| 327 | 1.610 | 1.990 | 2.480 | 3.100 | 3.830 | 4.620 | 5.370 | 5.980 | 6.330 | 6.350 | 6.010 | 5.360 | 4.500 | 3.580 | 2.740 | 2.070 | 1.610 | 1.290 | 1.060 | 0.840 | 0.600 | 0.380 | 0.220 | 0.150 | 0.140 | 0.160 | |
| 332 | 1.800 | 2.210 | 2.740 | 3.380 | 4.100 | 4.840 | 5.510 | 6.010 | 6.260 | 6.200 | 5.830 | 5.170 | 4.340 | 3.440 | 2.610 | 1.950 | 1.490 | 1.190 | 0.980 | 0.780 | 0.560 | 0.330 | 0.160 | 0.080 | 0.062 | 0.078 | |
| 333 | 2.480 | 2.970 | 3.540 | 4.140 | 4.720 | 5.210 | 5.510 | 5.580 | 5.380 | 4.940 | 4.310 | 3.560 | 2.800 | 2.110 | 1.560 | 1.160 | 0.910 | 0.760 | 0.650 | 0.530 | 0.380 | 0.230 | 0.110 | 0.044 | 0.028 | 0.030 | |
| 334 | 3.400 | 3.900 | 4.370 | 4.780 | 5.070 | 5.200 | 5.150 | 4.900 | 4.480 | 3.920 | 3.300 | 2.680 | 2.120 | 1.680 | 1.350 | 1.120 | 0.970 | 0.850 | 0.740 | 0.610 | 0.480 | 0.340 | 0.230 | 0.150 | 0.085 | 0.046 | |
| 335 | 2.940 | 3.330 | 3.730 | 4.100 | 4.400 | 4.590 | 4.650 | 4.560 | 4.310 | 3.930 | 3.440 | 2.890 | 2.320 | 1.770 | 1.320 | 0.980 | 0.770 | 0.650 | 0.560 | 0.470 | 0.340 | 0.200 | 0.082 | 0.021 | 0.003 | 0.000 | |
| 336 | 3.560 | 3.690 | 3.710 | 3.620 | 3.420 | 3.150 | 2.820 | 2.480 | 2.150 | 1.840 | 1.560 | 1.310 | 1.080 | 0.880 | 0.710 | 0.600 | 0.530 | 0.500 | 0.470 | 0.410 | 0.320 | 0.210 | 0.110 | 0.045 | 0.016 | 0.005 | |
| 337 | 4.010 | 4.380 | 4.620 | 4.690 | 4.590 | 4.350 | 4.000 | 3.600 | 3.170 | 2.750 | 2.350 | 1.960 | 1.590 | 1.260 | 0.980 | 0.780 | 0.650 | 0.570 | 0.500 | 0.410 | 0.290 | 0.160 | 0.059 | 0.011 | 0.001 | 0.000 | |
| 338 | 3.840 | 3.880 | 3.780 | 3.550 | 3.240 | 2.880 | 2.520 | 2.180 | 1.880 | 1.620 | 1.390 | 1.190 | 1.010 | 0.850 | 0.710 | 0.610 | 0.540 | 0.480 | 0.430 | 0.360 | 0.270 | 0.180 | 0.110 | 0.056 | 0.027 | 0.010 | |
| 339 | 3.480 | 3.530 | 3.490 | 3.360 | 3.140 | 2.860 | 2.560 | 2.260 | 1.990 | 1.750 | 1.540 | 1.340 | 1.150 | 0.960 | 0.790 | 0.650 | 0.570 | 0.520 | 0.480 | 0.410 | 0.310 | 0.180 | 0.080 | 0.022 | 0.003 | 0.000 | |
| 340 | 3.610 | 3.670 | 3.620 | 3.460 | 3.210 | 2.900 | 2.560 | 2.220 | 1.880 | 1.580 | 1.320 | 1.100 | 0.920 | 0.770 | 0.660 | 0.590 | 0.540 | 0.510 | 0.470 | 0.420 | 0.340 | 0.260 | 0.180 | 0.110 | 0.057 | 0.026 | |
| 341 | 3.750 | 4.020 | 4.220 | 4.310 | 4.290 | 4.170 | 3.950 | 3.640 | 3.250 | 2.820 | 2.360 | 1.900 | 1.480 | 1.120 | 0.850 | 0.670 | 0.560 | 0.490 | 0.430 | 0.340 | 0.230 | 0.120 | 0.041 | 0.008 | 0.001 | 0.000 | |
| 342 | 3.700 | 3.830 | 3.880 | 3.860 | 3.750 | 3.560 | 3.290 | 2.960 | 2.600 | 2.230 | 1.850 | 1.490 | 1.160 | 0.890 | 0.690 | 0.580 | 0.540 | 0.530 | 0.500 | 0.420 | 0.280 | 0.140 | 0.048 | 0.011 | 0.002 | 0.000 | |
| 343 | 3.560 | 3.520 | 3.410 | 3.220 | 2.980 | 2.710 | 2.420 | 2.130 | 1.850 | 1.590 | 1.350 | 1.130 | 0.930 | 0.750 | 0.600 | 0.500 | 0.440 | 0.410 | 0.370 | 0.310 | 0.220 | 0.120 | 0.049 | 0.013 | 0.002 | 0.000 | |
| 344 | 3.750 | 3.690 | 3.570 | 3.390 | 3.190 | 2.950 | 2.690 | 2.390 | 2.070 | 1.740 | 1.420 | 1.140 | 0.910 | 0.730 | 0.590 | 0.480 | 0.400 | 0.330 | 0.270 | 0.230 | 0.180 | 0.140 | 0.100 | 0.065 | 0.031 | 0.009 | |
| 345 | 3.570 | 3.850 | 4.070 | 4.200 | 4.250 | 4.220 | 4.110 | 3.900 | 3.620 | 3.250 | 2.830 | 2.400 | 1.980 | 1.620 | 1.340 | 1.140 | 1.000 | 0.890 | 0.780 | 0.680 | 0.600 | 0.540 | 0.480 | 0.420 | 0.320 | 0.190 | |
| 346 | 3.090 | 3.560 | 4.020 | 4.460 | 4.830 | 5.100 | 5.220 | 5.160 | 4.890 | 4.430 | 3.830 | 3.140 | 2.460 | 1.870 | 1.420 | 1.110 | 0.910 | 0.770 | 0.630 | 0.450 | 0.260 | 0.120 | 0.048 | 0.027 | 0.020 | 0.014 | |
| P21-H | | | | | | | | | | | | | | | | | | | | | | | | | | | |
| 397 | 2.680 | 2.760 | 2.820 | 2.870 | 2.910 | 2.930 | 2.920 | 2.870 | 2.770 | 2.610 | 2.410 | 2.170 | 1.920 | 1.670 | 1.430 | 1.220 | 1.030 | 0.880 | 0.740 | 0.620 | 0.510 | 0.410 | 0.320 | 0.230 | 0.140 | 0.071 | |
| 398 | 2.710 | 2.690 | 2.640 | 2.570 | 2.490 | 2.380 | 2.250 | 2.090 | 1.900 | 1.700 | 1.500 | 1.320 | 1.170 | 1.040 | 0.950 | 0.880 | 0.830 | 0.790 | 0.740 | 0.670 | 0.570 | 0.440 | 0.310 | 0.180 | 0.083 | 0.026 | |
| 399 | 3.200 | 3.270 | 3.300 | 3.280 | 3.220 | 3.120 | 2.960 | 2.750 | 2.480 | 2.170 | 1.840 | 1.530 | 1.260 | 1.040 | 0.880 | 0.760 | 0.670 | 0.590 | 0.520 | 0.440 | 0.360 | 0.270 | 0.190 | 0.120 | 0.066 | 0.028 | |
| 400 | 3.340 | 3.550 | 3.720 | 3.830 | 3.890 | 3.870 | 3.760 | 3.570 | 3.290 | 2.930 | 2.530 | 2.120 | 1.740 | 1.400 | 1.130 | 0.930 | 0.770 | 0.650 | 0.550 | 0.450 | 0.350 | 0.260 | 0.180 | 0.120 | 0.073 | 0.042 | |
| 405 | 2.100 | 2.420 | 2.760 | 3.130 | 3.520 | 3.920 | 4.300 | 4.640 | 4.900 | 5.030 | 4.990 | 4.790 | 4.440 | 3.980 | 3.480 | 2.990 | 2.550 | 2.170 | 1.850 | 1.560 | 1.290 | 1.040 | 0.830 | 0.670 | 0.540 | 0.440 | |
| 406 | 1.710 | 2.020 | 2.400 | 2.840 | 3.360 | 3.940 | 4.550 | 5.150 | 5.650 | 5.990 | 6.090 | 5.930 | 5.520 | 4.920 | 4.200 | 3.470 | 2.790 | 2.220 | 1.760 | 1.380 | 1.070 | 0.800 | 0.590 | 0.450 | 0.360 | 0.320 | |
| 407 | 2.610 | 2.900 | 3.220 | 3.570 | 3.930 | 4.280 | 4.580 | 4.760 | 4.790 | 4.640 | 4.310 | 3.840 | 3.280 | 2.700 | 2.160 | 1.700 | 1.330 | 1.050 | 0.840 | 0.660 | 0.510 | 0.390 | 0.290 | 0.230 | 0.200 | 0.170 | |
| 408 | 2.430 | 2.590 | 2.710 | 2.800 | 2.830 | 2.790 | 2.680 | 2.510 | 2.260 | 1.970 | 1.650 | 1.330 | 1.040 | 0.800 | 0.630 | 0.510 | 0.440 | 0.400 | 0.370 | 0.320 | 0.270 | 0.200 | 0.140 | 0.087 | 0.044 | 0.017 | |
| 409 | 2.070 | 1.920 | 1.720 | 1.510 | 1.320 | 1.150 | 1.010 | 0.900 | 0.810 | 0.740 | 0.690 | 0.660 | 0.670 | 0.700 | 0.730 | 0.770 | 0.800 | 0.810 | 0.810 | 0.780 | 0.710 | 0.600 | 0.440 | 0.280 | 0.130 | 0.044 | |
| 410 | 2.410 | 2.560 | 2.690 | 2.770 | 2.830 | 2.840 | 2.800 | 2.720 | 2.570 | 2.370 | 2.110 | 1.820 | 1.530 | 1.260 | 1.030 | 0.840 | 0.710 | 0.620 | 0.540 | 0.470 | 0.380 | 0.290 | 0.190 | 0.110 | 0.047 | 0.014 | |
| 411 | 2.240 | 2.390 | 2.530 | 2.670 | 2.810 | 2.970 | 3.140 | 3.320 | 3.480 | 3.590 | 3.630 | 3.570 | 3.400 | 3.150 | 2.830 | 2.490 | 2.160 | 1.840 | 1.550 | 1.270 | 1.010 | 0.770 | 0.570 | 0.430 | 0.350 | 0.300 | |
| 412 | 1.520 | 1.500 | 1.500 | 1.520 | 1.570 | 1.680 | 1.840 | 2.050 | 2.300 | 2.570 | 2.830 | 3.040 | 3.170 | 3.180 | 3.080 | 2.870 | 2.580 | 2.240 | 1.900 | 1.570 | 1.300 | 1.090 | 0.940 | 0.850 | 0.780 | 0.720 | |
| 413 | 0.730 | 0.810 | 0.920 | 1.100 | 1.380 | 1.800 | 2.410 | 3.190 | 4.120 | 5.100 | 5.990 | 6.670 | 7.020 | 6.980</td | | | | | | | | | | | | | |

P14

